POLITECNICO DI TORINO

DEGREE COURSE IN MECHANICAL ENGINEER

Master Thesis in ACTUATION SYSTEMS and SMART MAT

Investigation of magneto-mechanical coupling phenom for novel actuator designs.

Supervisor: Prof. Dr. CHAMONINE MIKHAIL

Advisor: Prof. Ing. TONOLI ANDREA

FA

ACADEMIC YEAR 2017 – 2018

Stay hungry, Stay foolish

Steve Jobs

INDEX

INTRODUCTION

Smart Materials are materials which react to environmental inputs by modifying one or more of their properties: thanks to the help of chemistry it is possible to produce materials with different shape, properties and aspects. For these reasons, this branch deals with materials designed to fulfill precise functions and their features to react to specific stresses are obtained by the addition of substances capable of modifying some of their physicochemical characteristics. This aspect categorizes materials as smart and it is an innovative process to produce them, aimed at getting the best performance in every field.

The purpose of this work is to investigate the behavior of smart material with specific setups because it is a magnetostrictive material which changes its shape and dimensions, when outer magnetic fields are applied. The study focused on it, considers two different setups: first it is took into account a wire with two Helmholtz coils and secondly a wire with two permanent magnets. Smart material is fixed around the wire between coils or permanent magnets and it is important to examine the torsion of the material when Wiedmann's effect acts on it, because it could be useful in many engineering applications. Even though twisting is the main parameter to study, the aim of this investigation is to find a relation between smart material properties and setups parameters through the evaluation of displacements, stress, torsion and its angle, magnetic fields.

The work considers three important steps: theory, simulations on software Comsol Multiphysics and experimentation. Theory is linked to magnetism and it is the main point at the base of this study. Simulations, which are useful to predict the action of smart materials when there are magnetic fields, are fundamental steps because they are a valuable way to reproduce the reality in short time. Experimentation, which is the last point, allows to proof the concept and to evaluate errors. Working setting and in particular safety are topics explained at the end of the work.

It is reasonable that final results include errors due to simulations and measurements, obtained during the experimentation. Simulations cause errors linked mostly to mesh, to measurements and to precision of instrumentations. It has been attempted to minimize error values but it is inevitable to obtain the same theoretical result because a mathematical model has its hypothesis to evaluate.

1.0 Magnetism

The main theoretical topic of this work is Magnetism and it is closely fundamental the study of how a magnetic field can produce a magnetic force on a moving charged particle or on a magnetic object. [1]

The science of the magnetic field is physics and its applications are studied by engineering. Both the science and the application begin with the investigation about the effects which a magnetic field generates.

A magnetic field $\vec{B}$ is produced by a magnetic charge (magnetic monopoles), which are predicted by certain theories but their existence has not been confirmed. It is reasonable to produce a magnetic field in two different ways; the first is to use moving electrically charged particles, such as a current in a wire, to make an electromagnet. In this work, it is examined how ***Helmholtz Coils*** produce a magnetic field when the current flows inside them. This research is important because we want to control a component, which is prepared with ***Smart Materials***, the study object of this work. It is described in detail Helmholtz coils performances in the next chapter.
The second way to produce a magnetic field is by means of elementary particles such us electrons because these particles have an intrinsic magnetic field around them. The magnetic field of electrons in certain materials add together to give a net magnetic field around the material. Such addiction is the reason why permanent magnet has a permanent magnetic field. In the other magnetic field of electrons cancel out, giving no net field surrounding the material. ***Permanent Magnets*** are studied and compared with the investigation on Helmholtz coils, concerning effects that magnetic field produces on smart materials, which have magnetic properties.

Surely, we can underline how material properties are relevant because they are linked to magnetic field which acts on the smart material and moves it. Its behavior references to ***Wiedmann's Effect***, which is verified when there is the composition of two magnetic fields. In this thesis it is explained how the smart material twists when we assembly these two different setups:
- ***Wire and Helmholtz Coils***;
- ***Wire and Permanent Magnets***.

1.1 Definition of Magnetic Field

The vector $\vec{B}$ come from this equation:

$$\overrightarrow{F_B} = q\vec{v} \times \vec{B} \tag{1.0}$$

Where the force on the particle $\overrightarrow{F_B}$ is equal to the charge q times the cross product of its velocity $\vec{v}$ and the field $\vec{B}$, all measured in the same reference frame. The direction of the vector $\overrightarrow{F_B}$ is perpendicular to $\vec{v}$ and $\vec{B}$ defined by the right-hand rule.

We can write the magnitude of $\overrightarrow{F_B}$ as:

$$F_B = |q|vB \sin\theta \tag{1.1}$$

where θ is the angle between the directions of velocity $\vec{v}$ and magnetic field $\vec{B}$.

The equation (1.1) tell us the magnitude of the force F_B action on a particle in a magnetic field B is proportional to the charge q and the speed v of the particle. Thus, the force is equal to zero if the charge is zero or if the particle is stationary. The equation (1.1) also explains that the magnitude of the force is zero if $\vec{v}$ and $\vec{B}$ are either parallel ($\theta = 0$) or antiparallel ($\theta = 180$), and the force is at its maximum when $\vec{v}$ and $\vec{B}$ are perpendicular to each other.

The SI for $\vec{B}$ that follow from the equation (1.0) is the Tesla T:

$$1\,T = 1\,Tesla = 1\,\frac{Newton}{(Coulomb)\left({}^{meter}/_{second}\right)}$$

$$1\,T = 1\,\frac{N}{A \cdot m}$$

The magnetic field $\vec{B}$ can also written as:

$$1\,T = 10^4 G$$

Earth's magnetic field near the planet's surface is about $1G = 10^{-4}T$.

We can represent magnetic field lines following these rules:

- the direction of the tangent to a magnetic field line at any point gives the direction of $\vec{B}$ at that point;

- the spacing of the lines represents the magnitude of $\vec{B}$, the magnetic field is stronger where the lines are closer together, and conversely.

The Figure 1 shows how the magnetic field near a permanent magnet in the shape of a bar, can be represented by magnetic field lines.

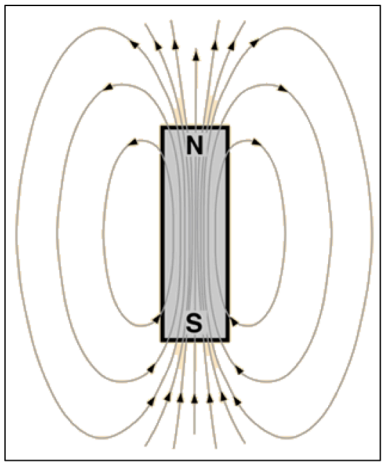

Figure 1: Magnetic field lines

The lines all pass through the magnet and they all form closed loops. The external magnetic effects of a bar magnet are strongest near its end, where the field lines are most closely spaced. The closed field lines enter one end of a magnet and exit to another end. The end of a magnet from which the field lines emerge is called the *north pole* of the magnet; the other end, where the field lines enter, is called the *south pole*. Because the magnet has two poles, it is said to be a magnetic dipole. Opposite magnetic poles attract each other and like magnets poles repel each other.

In this thesis it will be used two permanent magnets with the shape of a ring and they are placed side by side along the same main axis and opposite poles. In the first time it will be useful to investigate the magnetic field between them, because secondly we analyze the behavior of the component, prepared with smart materials, which is putted in that field.

1.2 Magnetic Force on a Current-Carrying Wire

A magnetic field exerts a sideways force on electrons moving in a wire. This force must be transmitted to the wire itself because the conduction electron cannot escape sideways out of the wire.
Consider a length L of the wire (Figure 2), all the conduction electrons in this section of wire will drift past plane XX in a time $t = {}^{L}/_{v_d}$.

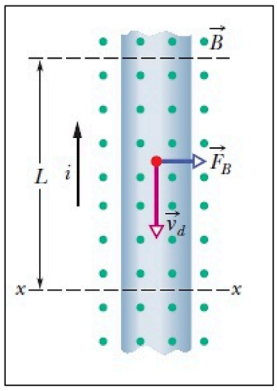

Figure 2: Section of wire

Thus, in that time a charge given by

$$q = it = i\frac{L}{v_d} \tag{1.2}$$

will pass through that plane. Substituting this into Equation 1.0 yields:

$$\overrightarrow{F_B} = q\vec{v} \times \vec{B} = i\vec{L} \times \vec{B} \tag{1.3}$$

The magnitude of $\overrightarrow{F_B}$ is:

$$F_B = qv_dB \sin\theta = iLB \sin\theta \tag{1.4}$$

where θ is the angle between $\vec{L}$ and $\vec{B}$ (Figure 3).

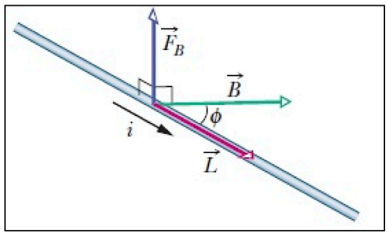

Figure 3: Angle between $\vec{L}$ and $\vec{B}$

If the magnetic force acts on a length $\vec{L}$ of straight wire carrying a current i and if it is immersed in a uniform magnetic field $\vec{B}$ that is perpendicular to the wire, we obtain:

$$F_B = qv_dB = iLB \tag{1.5}$$

because $\sin\theta = \sin 90 = 1$.

1.3 Magnetic Field due to a Current; Biot-Savart's Law

Our first step in this chapter is to find the magnetic field due to the current in a very small section of current-carrying wire. Then we shall find the magnetic field owing to the entire wire for several different arrangements of the wire.

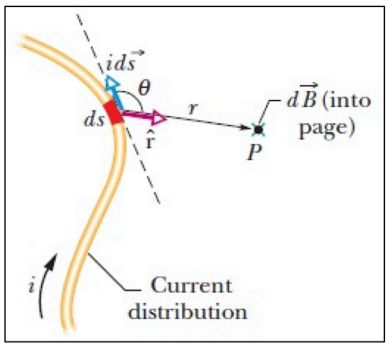

Figure 4: Magnetic field due to a current

The Figure 4 shows, a wire of arbitrary shape carries a current i. We want to find the magnetic field $\vec{B}$ at a nearby point P. We first mentally divide the wire into differential elements ds and then define

for each element a length vector that has length $d\vec{s}$ and whose direction is the same of the current in ds.Then we can define as a differential current-length element i; we try to calculate the field produced at P by a typical current-length element. From experiment results, we find that magnetic fields can be superimposed to find a net field. Thus, we can calculate the net field at P by summing, via integration, the contributions from all the current-length elements. However, this summation is more challenging than the process associated with electric fields because of a complexity; whereas a charge element dq producing an electric field is a scalar, a current-length element i producing a magnetic field is a vector, being the product of a scalar and a vector. The magnitude of the field produced at point P at distance r by a current-length element i turns out to be:

$$\overrightarrow{dB} = \frac{\mu_0}{4\pi} \frac{id\vec{s} \times \vec{r}}{r^2} \tag{1.6}$$

where μ_0 is the permeability constant ($4\pi \cdot 10^{-7}$ H/m). This is Biot-Savart's law, used to prove that the magnitude of the magnetic field at a perpendicular distance R from a long (infinite) straight wire (Figure 5) carrying a current i is given by:

$$B = \frac{\mu_0 i}{2\pi R} \tag{1.7}$$

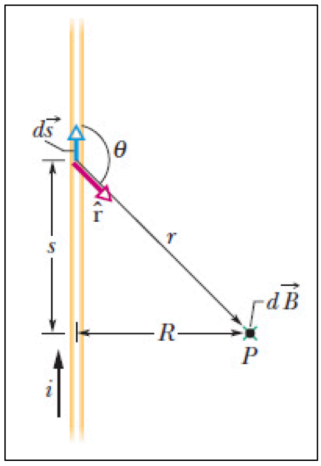

Figure 5: Straight wire

The field magnitude B depends only on the current and the perpendicular distance R of the point from the wire. We shall show in our derivation that the field lines of $\vec{B}$ form concentric circles around the

wire, as simulation shows. The increase in the spacing of the lines (Figure 6) with increasing distance from the wire represents the $1/R$ decrease in the magnitude of $\vec{B}$ predicted by previous equation. The lengths of the two vectors in the figure also show the $1/R$ decrease.

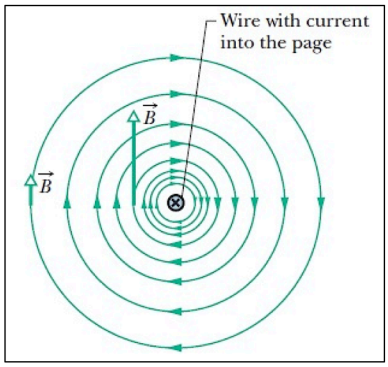

Figure 6: Magnetic field lines

Plugging values into previous equation to find the field magnitude B at a given radius is easy. The field lines form circles around a long straight wire, and the field vector at any point on a circle must be tangent to the circle and obviously perpendicular to a radial line extending to the point from the wire. To determine the direction of the magnetic field set up at any particular point by this current, mentally wrap your right-hand around the wire with your thumb in the direction of the current. Let your fingertips pass through the point; their direction is then the direction of the magnetic field at that point.

1.4 Ampere's Law

We can find the net magnetic field due to any distribution of currents by first writing the differential magnetic field (Equation 1.6) due to current-length element and then summing the contributions of from all the elements. If the distribution has some symmetry, we may be able to apply Ampere's law to find the magnetic field with considerably less effort. This law is:

$$\oint \vec{B} \cdot d\vec{s} = \mu_0 i_{enc} \tag{1.8}$$

The loop on the integral sign means that the scalar product is to be integrated around a closed loop, called an Amperian loop. The current i is the net current encircled by that closed loop. To apply Ampere's law, we mentally divide the loop into differential vector elements $d\vec{s}$ that are everywhere directed along the tangent to the loop in the direction of integration. Assume that at the location of the element $d\vec{s}$ the net magnetic field due to the currents is $\vec{B}$. Because the wires are perpendicular to the page, we know that the magnetic field at $d\vec{s}$ due to each current is in the plane of Figure 7: thus, their net magnetic field $\vec{B}$ at $d\vec{s}$ must also be in that plane.

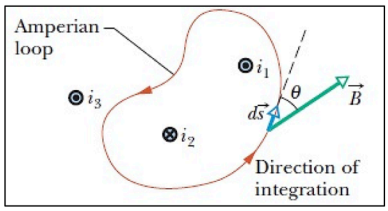

Figure 7: Ampere's law

However, we do not know the orientation of $\vec{B}$ within the plane, thus the Ampere's law can be written as:

$$\oint \vec{B} \cdot d\vec{s} = \oint B \cos\vartheta \, ds = \mu_0 i_{enc} \tag{1.9}$$

We can interpret the scalar product $\vec{B} \cdot d\vec{s}$ as being the product of a length ds of the Amperian loop and the field component $B \cos\vartheta$ tangent to the loop. Then we can interpret the integration as being the summation of all such products around the entire loop. We arbitrary assume $\vec{B}$ to be generally in the direction of integration, then we use the following curled-straight right-hand rule to assign a plus or a minus sign to each of the current that make up net encircled current i_{enc}.

1.5 Ampere's Law: Magnetic Field Outside a Long Straight Wire with Current

We consider a long straight wire that carries current i directly out of the page (Figure). The Biot-Savart's law (Equation 1.7) tell us that the magnetic field $\vec{B}$ produced by the current has the same magnitude at all points that are the same distance r from the wire; that is, the field $\vec{B}$ has cylindrical symmetry about the wire (Figure 8).

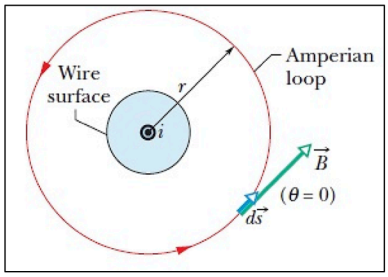

Figure 8: Ampere's law, magnetic field outside the wire

We can take advantage of that symmetry to simplify the integral in Ampere's law (Equation 1.9) if we encircle the wire with a concentric circular Amperian loop of radius r. The magnetic field has the same magnitude $\vec{B}$ at every point on the loop, thus $\vec{B}$ and $d\vec{s}$ are either parallel or antiparallel at each point of the loop. The integral becomes:

$$\oint \vec{B} \cdot d\vec{s} = \oint B \cos\vartheta \, ds = B \oint ds = B(2\pi r) \tag{1.10}$$

The $\oint ds$ is the summation of all the line segment lengths ds around the circular loop; that is, it simply gives the circumference $2\pi r$ of the loop. Our right-hand rule gives us a plus sign for the current, and then we have:

$$B(2\pi r) = \mu_0 i \tag{1.11}$$

which is the Biot-Savart's law.

1.6 Ampere's Law: Magnetic Field Inside a Long Straight Wire with Current

We consider the cross section of a long straight wire of radius R that carries a uniformly distributed current i directly out of the page. Because the current is uniformly distributed over a cross section of the wire, the magnetic field $\vec{B}$ produced by current must be cylindrically symmetrical. Thus, to find the magnetic field at points inside the wire, we can again use an Amperian loop of radius $r < R$.

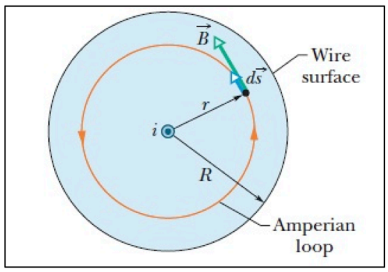

Figure 9: Ampere's law, magnetic field inside the wire

Symmetry again suggests that $\vec{B}$ is tangent to the loop, as shown in figure and we obtain:

$$\oint \vec{B} \cdot d\vec{s} = \oint B \cos\vartheta \, ds = B \oint ds = B(2\pi r) \tag{1.11}$$

Because the current is uniformly distributed, the current i encircled by the loop is proportional to the area encircled by the loop; that is:

$$i_{enc} = i\frac{\pi r^2}{\pi R^2} \tag{1.12}$$

The Ampere's law gives us:

$$B(2\pi r) = \mu_0 i\frac{\pi r^2}{\pi R^2} \tag{1.13}$$

Thus, inside the wire, the magnitude B of the magnetic field is proportional to r, is zero at the center, and its maximum at $r = R$.

1.7 Magnetic Field of a Solenoid

We now turn our attention to another situation in which Ampere's law proves use
magnetic field produced by the current in a long, tightly wound helical coil of wi
We assume that the length of the solenoid is much greater than the diameter.
Figure 10 shows a section through a portion of a "stretched-out" solenoid whose n
vector sum of the fields produced by the individual *turns* (windings) that make up

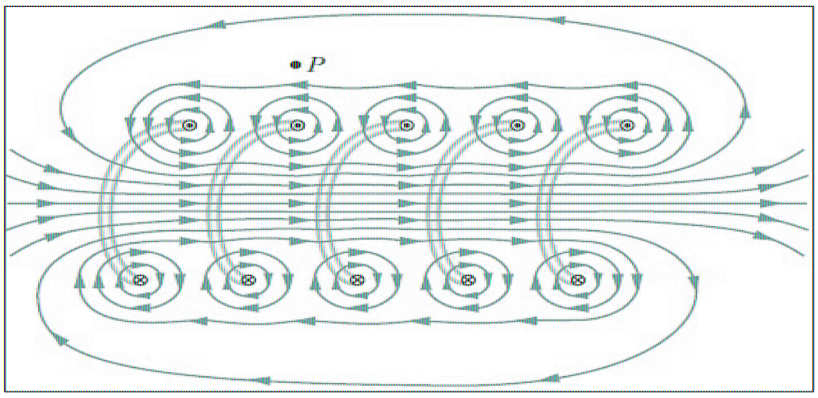

Figure 10: Magnetic field of a solenoid

In the figure is represented a vertical cross section through the central axis o
solenoid. The back portions of five turns are shown, as are the magnetic field l
through the solenoid. Each turn produces circular magnetic field lines near itself.
axis the field lines combine into a net magnetic field that is directed along the a
closely spaced field lines is stronger. Instead, outside the solenoid the field is very
lines are widely spaced.

For points very close to a turn, the wire behaves magnetically almost like a long
the lines of $\vec{B}$ there are almost concentric circles. Figure suggests that the field tend
adjacent turns. It also suggests that, at points inside the solenoid and reasonably f
is approximately parallel to the central solenoid axis. In the limiting case of an id
is infinitely long and consists of tightly packed turns of square wire, the field inside
and parallel to the solenoid axis.

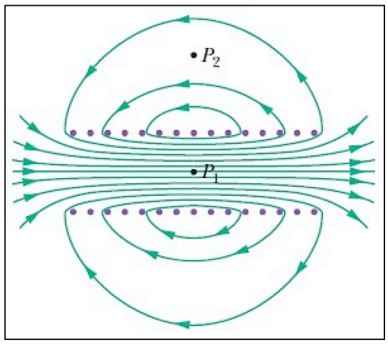

Figure 11: Magnetic field lines

At points above the solenoid, such as P in Figure 10, the magnetic field set up by the upper parts of the solenoid turns and tends to cancel the field set up at P by the lower parts of the turns. In the limiting case of an ideal solenoid, the magnetic field outside the solenoid is zero. Taking the external field to be zero is an excellent assumption for a real solenoid if its length is much greater than its diameter and if we consider external points such as point P that at either end of the solenoid. The direction of the magnetic field along the solenoid axis is given by a curled-straight right-hand rule.

Figure 11 shows the lines of $\vec{B}$ for a real solenoid. The spacing of these lines in the central region shows that the field inside the coil is fairly strong and uniform over the cross section of the coil. The external field, however, is relatively weak.

Now we apply Ampere's law (Equation 1.8) to the ideal solenoid of figure, where $\vec{B}$ is uniform within the solenoid and zero outside it, using the rectangular Amperian loop. We have:

$$\oint \vec{B} \cdot d\vec{s} = \int_a^b \vec{B} \cdot d\vec{s} + \int_b^c \vec{B} \cdot d\vec{s} + \int_c^d \vec{B} \cdot d\vec{s} + \int_d^e \vec{B} \cdot d\vec{s} \tag{1.14}$$

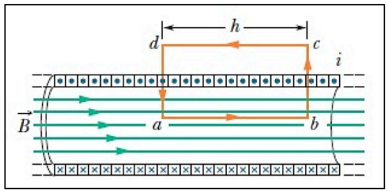

Figure 12: Ampere's law application

The first integral on the right of the Equation 1.14 is Bh, where B is the magnitude of the uniform field $\vec{B}$ inside the solenoid and h is the arbitrary length of the segment from a to b. The second and the fourth integrals are zero because for every element ds of these segments, $\vec{B}$ either is perpendicular to ds or is zero, and thus the product $\vec{B} \cdot d\vec{s}$ is zero. The third integral, which is taken along a segment that lies outside the solenoid, is zero because $B = 0$ at all external points. Thus, the $\oint \vec{B} \cdot d\vec{s}$ for the entire rectangular loop has the value Bh. The current i_{enc} encircled by the rectangular Amperian loop is not the same as the current i in the solenoid windings because the windings pass more than once through this loop. Let n be the number of turns per unit length of the solenoid; then the loop encloses nh turns and $i_{enc} = i(nh)$. Ampere's law gives us:

$$Bh = \mu_0 inh \tag{1.15}$$

For an infinitely long ideal solenoid:

$$Bh = \mu_0 in \tag{1.16}$$

The equation is consistent with the experimental fact that the magnetic field magnitude B within a solenoid does not depend on the diameter or the length of the solenoid and that B is uniform over the solenoidal cross section.

1.8 Current-Currying Coil as a Magnetic Dipole

A torque acts to rotate a current-carrying coil placed in a magnetic field. In that sense, the coil behaves like a bar magnet placed in the magnetic field. Thus, like a bar magnet, a current-carrying coil is said to be a magnetic dipole. Moreover, to account for the torque on the coil due to magnetic field, we assign a magnetic dipole moment $\vec{\mu}$ to the coil. The direction of $\vec{\mu}$ is that of the normal vector $\vec{n}$ to the plane of the coil and thus is given by the same right-hand rule. The magnitude is given by:

$$\mu = NiA \tag{1.17}$$

in which N is the number of turns in the coil, i the current through the coil, and A is the area enclosed by each turn of the coil.

We can generalize to the vector relation:

$$\vec{\tau} = \vec{\mu} \times \vec{B} \tag{1.18}$$

A magnetic dipole in an external magnetic field has an energy that depends on the dipole's orientation in the field.

$$U(\vartheta) = -\vec{\mu} \cdot \vec{B} \tag{1.19}$$

In each case the energy due to the field is equal to the negative of the scalar product of the corresponding dipole moment and the field vector. A magnetic dipole has its lowest energy when its dipole moment $\vec{\mu}$ is lined up with the magnetic field $\vec{B}$. It has its highest energy when $\vec{\mu}$ is directed opposite field (Figure 13).

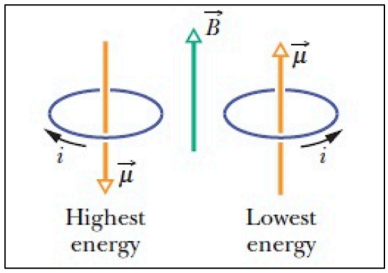

Figure 13: Dipole moment

1.9 Magnetic Field of a Coil

We turn now to the other aspect of a current-carrying coils as a magnetic dipole. We consider a coil with a single circular loop and only points on its perpendicular central axis, which we take to be a z axis. We shall show that the magnitude of the magnetic field at such points is:

$$B(z) = \frac{\mu_0 i R^2}{2(R^2 + z^2)^{3/2}} \tag{1.20}$$

In which R is the radius of the circular loop and z is the distance of the point in question from the center of the loop. Furthermore, the direction of the magnetic field $\vec{B}$ is the same as the direction of

the magnetic dipole moment $\vec{\mu}$ of the loop. For axial points far from the loop, we have $z \gg R$ in Equation 1.20. with the approximation, the equation reduces to:

$$B(z) = \frac{\mu_0 i R^2}{2z^3} \tag{1.21}$$

Recalling that πR^2 is the area A of the loop and extending our result to include a coil of N turns, we can write this equation as:

$$B(z) = \frac{\mu_0}{2\pi}\frac{NiA}{z^3} \tag{1.21}$$

Further $\vec{B}$ and $\vec{\mu}$ have the same direction, we can write the equation in vector form:

$$B(z) = \frac{\mu_0}{2\pi}\frac{\vec{\mu}}{z^3} \tag{1.21}$$

Thus, we have two ways in which we can regard a current-carrying coil as a magnetic dipole:
- it experiences a torque when we place it in an external magnetic field;
- it generates its own intrinsic magnetic field, given, for distant point along its axis.

Figure 14 shows the magnetic field of a current loop; one side of the loop acts as a north pole (in the direction of $\vec{\mu}$) and the other side as a south pole, as suggested by the lightly drawn magnet in the figure. If we were to place a current-carrying coil in an external magnetic field, it would tend to rotate just like a bar magnet would.

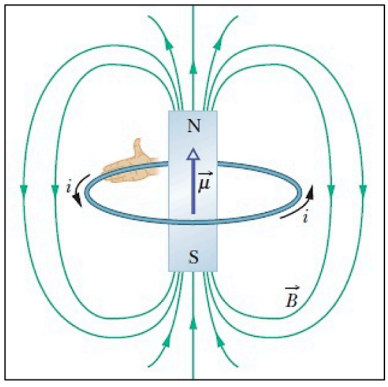

Figure 14: Magnetic field of a current loop

1.10 Magnetic Field of Helmholtz Coils

A Helmholtz coil is a parallel pair of identical circular coils (solenoid electromagnets) spaced one radius apart and wound so that the current flows through both coils in the same direction. This winding results in a uniform magnetic field between the coils with the primary component parallel to the axis of the two coils. The uniform field is the result of the sum of the two field components parallel to the axis of the coils and the difference between the components perpendicular to the same axis. [2] (Figure 15)

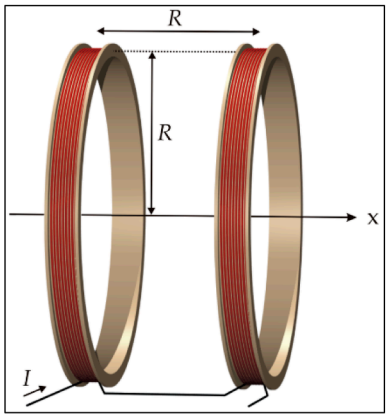

Figure 15: Helmholtz coils

Setting the distance between the two coils $D = R$ minimizes the no uniformity of the field at the center of the coils. It is reasonable to use slightly larger value of D because it reduces the difference between the center and the planes of the coils. [3]

The magnetic field is calculated with the Equation 1.20 and in particular in the point halfway between the two loops. In this case we know $z = R/2$, so we obtain:

$$B_1(R/2) = \frac{\mu_0 i R^2}{2(R^2 + (R/2)^2)^{3/2}} \tag{1.22}$$

For two coils, we have:

$$B_2\left({}^{R}/_{2}\right) = \frac{2\mu_0 i R^2}{2\left(R^2 + \left({}^{R}/_{2}\right)^2\right)^{3/2}} = \frac{8}{5\sqrt{5}}\frac{\mu_0 n i}{R} \tag{1.22}$$

where R is the radius of the coil.

It is useful to calculates the current i necessary if we know the magnetic field B:

$$i = \frac{5\sqrt{5}}{8}\frac{BR}{\mu_0 n} \tag{1.23}$$

1.11 Magnetic Field of Permanent Magnets

In this chapter, it is showed which equation is used for calculating the magnetic field B when it is known the remancence field B_r [4]. In our case we will consider permanent magnets with a ring shape, thus it will be:

$$B = \frac{B_r}{2}\left[\frac{D+z}{\sqrt{{R_a}^2 + (D+z)^2}} - \frac{z}{\sqrt{{R_a}^2 + z^2}} - \left(\frac{D+z}{\sqrt{{R_i}^2 + (D+z)^2}} - \frac{z}{\sqrt{{R_i}^2 + z^2}}\right)\right] \tag{1.24}$$

where:

B_r is the remanence field;

z is the distance from a pole face on the symmetry axis;

D is the thickness (or height) of the ring;

R_a is the outer radius of the ring;

R_i is the inner radius of the ring.

The Figure 16 clarify the parameters explained before. In chapters before, it is discussed about permanent magnets, which have the same behavior of the coil, thus every consideration had already been pointed out.

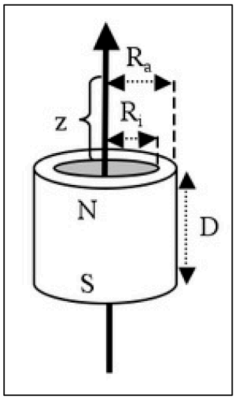

Figure 16: Permanent magnets (ring shape)

2.0 Materials properties

In this chapter is illustrated the interaction of magnetic fields and materials. The way in which matter responds to magnetic fields is totally determined by quantum mechanical nature of their molecular structure, particularly their electrons. [5]

The electrons in a molecule exist in orbits (as a simple loop of current). In most materials there are an enormous number of orbits, randomly oriented so that they produce no net field. Suppose an external magnetic field is applied to some substance that contains many orbitals. The net tendency can be understood in terms of Lenz's law: the orbits rearrange themselves in order to oppose the change in magnetic flux. This tendency for Lenz's law to work on the microscopic scale ends up opposing the magnetic field from the material.

One other quantum mechanical property of electrons plays an extremely important role in this discussion: electrons have a built-in, intrinsic magnetic moment. This means that each electron all on its own acts as a source of magnetic field, producing dipole-type very similar to that of current loop. Because this field is associated with the electron itself, it does not exhibit the Lenz's law type behavior of the field that we see from the orbits. Instead, the most important behavior in this context is the fact that a magnetic moment placed in an external field feels a torque. In this case, the action of this torque tends to line up the electrons magnetic moments with the external field.

The quantum mechanical nature of electrons in molecules leads to two behaviors:
- Lenz's law on the scale of electron orbitals opposes magnetic fields from entering a material;
- magnetic torque acting on the individual electrons augments magnetic fields in a material.

Both of these behaviors could be important and it varies from material to material, depending upon its detailed electronic orbital structure. The first property plays some role in all materials. Such materials are called ***diamagnetic***. A diamagnetic material is one whose magnetization (to be defined precisely in a moment) opposes an external magnetic field. Even though almost materials are diamagnetic, the effect is so puny that it is very difficult to see. A consequence of this is that a diamagnetic substance will be expelled from a magnetic field.

For some materials, the second property – alignment of electron magnetic moments – wins out. Such materials typically have several electron orbits that contain unpaired electrons; the orbit thus has a net magnetic moment. (In most diamagnetic materials, the orbits are filled with paired electrons, so

that the orbit has no net moment). Such materials are called ***paramagnetic***. A paramagnetic material has a magnetization that augments an external field. Paramagnetic substances are pulled into magnetic field. In the vast majority of cases, paramagnetic effects are also so puny that they can barely be seen.

One particular class of material acts essentially as paramagnetic materials do. However, they respond so strongly that they truly belong in a class of their own. These are the ***ferromagnetic*** materials.

2.1 Magnetization

As we discuss before, it is important to define magnetization as the magnetic dipole moment per unit volume of a material. Notice that magnetization $\vec{M}$ has the same dimensions as magnetic field $\vec{B}$.

It is important to define $\vec{H}$ in terms of the normal magnetic field $\vec{B}$ and the magnetization $\vec{M}$:

$$\vec{B} = \mu_0(\vec{H} + \vec{M}) \tag{2.0}$$

Where there is no magnetization, the normal magnetic field $\vec{B}$ is just this new field $\vec{H}$. This means that $\vec{H}$ is nothing more than the bit of the magnetic field that arises from normal electric currents, as opposed to those that are bound in matter.

The magnetization $\vec{M}$ makes a contribution to the current density $\vec{J}$, known as the magnetization current:

$$\overrightarrow{J_{bound}} = \vec{\nabla} \times \vec{M} \tag{2.1}$$

Where $\overrightarrow{J_{bound}}$ is the bound density current because the magnetization defines bound currents.

$$\overrightarrow{J_{free}} = \vec{\nabla} \times \vec{H} \tag{2.1}$$

Where $\overrightarrow{J_{free}}$ is the density current of free electrical current.

So it becomes:

$$\vec{\nabla} \times \vec{B} = \mu_0\left(\vec{\nabla} \times \vec{H} + \vec{\nabla} \times \vec{M}\right) = \mu_0\left(\overrightarrow{J_{bound}} + \overrightarrow{J_{free}}\right) = \mu_0\vec{J} \tag{2.2}$$

The total current density $\vec{J}$ is given by adding the free current density $\overrightarrow{J_{free}}$ (the current due to moving charges that we can imagine controlling) and the bound current density $\overrightarrow{J_{bound}}$ (the current that is bound up with electron orbits, and it is really a part of the material).

2.1 Magnetic Susceptibility

A wide variety of materials exhibit linear magnetization, meaning that the magnetization $\vec{M}$ depends linearly on the field $\vec{H}$:

$$\vec{M} = \chi_m \vec{H} \tag{2.3}$$

The quantity χ_m is the magnetic susceptibility. From this, we have:

$$\vec{B} = \mu_0(\vec{H} + \vec{M}) = \mu_0(\vec{H} + \chi_m \vec{H}) = \mu_0\mu_r\vec{H} = \mu\vec{H} \tag{2.0}$$

where $\mu_r = 1 + \chi_m$ is the relative permeability and μ the permeability.

If $\chi_m < 0$ the magnetic field is decreased by the material. This corresponds to diamagnetism.

If $\chi_m > 0$ the magnetic field is increased by the material. This corresponds to paramagnetism.

2.2 Ferromagnetism

Since ferromagnetism is conceptually a lot like paramagnetism, we expect that it will be explainable in terms of the alignment of many atomic scale magnetic moments. This is indeed the case. However, with ferromagnetism there is an important modification: one finds that moments of many atoms or molecules tend to be aligned in small regions. In normal paramagnetic materials, moments are randomly arranged until an external field comes along and aligns them. If you were to look at the magnetic moment layout of a typical ferromagnetic materials you would find something like in the Figure 17.

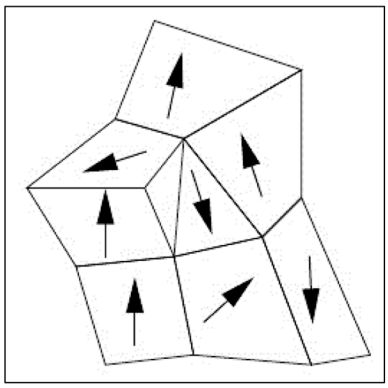

Figure 17: Ferromagnetic materials

Enough atomic scale moments are aligned that definite regions or domains of magnetization exist. Each domain is fairly small, and each is randomly oriented with respect to its neighbor; the material as a whole has no net magnetization. This is why a random piece of iron (a representative ferromagnetic material) is usually not magnetized. If this material is placed into a strong enough external magnetic field, the domains are re-aligned so that they all point in the same direction (Figure 18).

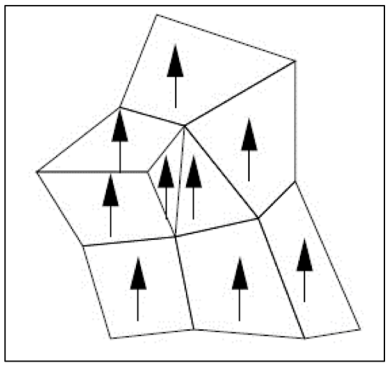

Figure 18: Alienation

Once the external magnetic field is removed, it turns out to be energetically favorable for these domains to remain pointing in this direction. The domains are fixed with this magnetization. This is how permanent magnets are made.

Ferromagnetism is important in this thesis because a smart material with ferromagnetic properties is investigated.

2.3 Hysteresis

The nonlinear relationship between $\vec{H}$ and $\vec{B}$ means that the magnetic field $\vec{B}$ in a ferromagnetic material has rather complicated dependence on the external applied field $\vec{H}$. As $\vec{H}$ is varied between a minimum and a maximum, one finds that $\vec{B}$ in the material traces out an interesting shape called a hysteresis curve (Figure 19).

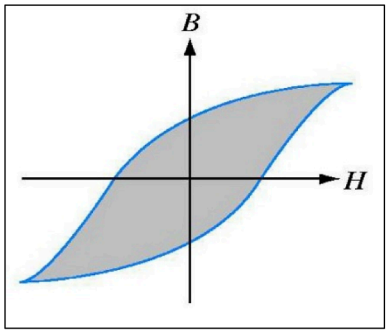

Figure 19: Hysteresis

Notice that when $B \neq 0,\ H = 0$ reflecting the fact that the material has been given a permanent magnetization. If H was large and positive most recently, B would go to the positive value when H is set to zero. If H was large and negative, B would go to the negative value. It turns out that it takes work to go around the hysteresis curve. As we go from $+H$ to $-H$, we have to flip lots of magnetic domains around (it takes energy to do that). The amount of done work goes from $+H \rightarrow -H \rightarrow +H$ is proportional to the area of the hysteresis curve. One consequence of this is that solenoids with an iron core can be very lost elements in AC circuits which are continually changing the direction of the flow of the current, and hence of the $\vec{H}$ field. If a portion of the circuit contains a ferromagnet, some of the power put into the circuit will be lost by continually changing the orientation of the ferromagnet's domains.

2.4 Curie Temperature

The Curie temperature T_c, is a temperature above which a material very suddenly ceases to act like ferromagnetic. If the temperature is above T_c, the random motion of the magnetic moments is so strong that they can never become aligned. For iron $T_c = 770^0$ Celsius.

3.0 Magnetostriction: Wiedmann's Effect

Magnetostriction is a property of ferromagnetic materials that causes them to change their shape or dimensions during the process of magnetization. The variation of materials' magnetization due to the applied magnetic field changes the magnetostrictive strain until reaching its saturation value λ_s. [6]

Internally, ferromagnetic materials have a structure that is divided into domains, each of which is a region of uniform magnetic polarization. When a magnetic field is applied, the boundaries between the domains shift and the domains rotate; both of these effects cause a change in the material's dimensions. The reason that a change in the magnetic domains of a material results in a change in the materials dimensions is a consequence of magneto crystalline anisotropy, that it takes more energy to magnetize a crystalline material in one direction than another. If a magnetic field is applied to the material at an angle to an easy axis of magnetization, the material will tend to rearrange its structure so that an easy axis is aligned with the field to minimize the free energy of the system. Since different crystal directions are associated with different lengths this effect induces a strain in the material. [7]

The order of the domains, and thus the magnitude of the effect, can be influenced by alloy selection, thermal annealing, cold working, and magnetic field strength.

The reciprocal effect, the change of the magnetic susceptibility (response to an applied field) of a material when subjected to a mechanical stress, is called Villari's effect. Two other effects are thus related to magnetostriction: Matteucci's effect is the creation of a helical anisotropy of the susceptibility of a magnetostrictive material when subjected to a torque and Wiedemann's effect is the twisting of these materials when a helical magnetic field is applied to them.

Since applying a magnetic field causes stress that changes the physical properties of a magnetostrictive material, it is interesting to note that the reverse is also true: applying stress to a magnetostrictive material changes its magnetic properties (e.g. magnetic permeability). This is called Villari's effect.

On magnetization, a magnetic material undergoes changes of volume which are small about the order of micrometers.

Wiedemann's effect describes the twisting owing to an axial magnetic field applied to a ferromagnetic wire or tube that is carrying an electric current. An important characteristic of a wire made of a magnetostrictive material is Wiedemann's effect. When an axial magnetic field is applied to a

magnetostrictive wire, and a current is passed through the wire, a twisting occurs at the location of the axial magnetic field. The twisting is caused by interaction of the axial magnetic field, usually from a permanent magnet, with the circular magnetic field along the magnetostrictive wire, which is present due to the current in the wire. The current is applied as a short-duration pulse, -1 or 2 μs; the minimum current density is along the center of the wire and the maximum at the wire surface. This is caused by the skin effect. The magnetic field intensity is also greatest at the wire surface. This aids in developing the waveguide twist. Since the current is applied as a pulse, the mechanical twisting travels in the wire as an ultrasonic wave.

This work considers known aspects of Wiedmann's effect on a magnetostrictive wire and it tries to introduce a smart magnetostrictive material fixed around a copper wire, taking into account how his behavior changes when an axial magnetic field is applied. The axial magnetic field comes from permanent magnets or Helmholtz coils and it is summed to the magnetic field of the wire.

In the next chapter it is possible to read in detail applications of magnetostrictive materials and it is clarified how the magneto-mechanical coupling is considered in our investigation.

3.1 Magnetostriction: Applications

Applications of magnetostriction can be divided into two modes. Either when magnetic energy is converted to mechanical energy it can be used for producing force as the case of ***actuators*** or can be used for detecting magnetic field as the case of ***sensors***. If mechanical energy is converted to magnetic energy it can be used for detecting force or motion. In early days, this device was used in applications like torque meters, sonar scanning devices, hydrophones, telephone receivers, and so on. Nowadays, with the invent of "giant" magnetostrictive alloys, it is being used in making devices like high force linear motors, positioners for adaptive optics, active vibration or noise control systems, medical and industrial ultrasonic, pumps, and so on. Ultrasonic magnetostrictive ***transducers*** have also been developed for making surgical tools, underwater sonar, and chemical and material processing. [8]

Ferromagnetic materials used in magnetostrictive position sensors are transition metals such as iron, nickel, and cobalt. In these metals, the 3rd electron shell is not completely filled, which allows the formation of a magnetic moment. (i.e., the shells closer to the nucleus than the 3d shell are complete,

and they do not contribute to the magnetic moment). As electron spins are rotated by a magnetic field, coupling between the electron spin and electron orbit causes electron energy to change. The crystal then strains so that electrons at the surface can relax to states of lower energy. When a material has positive magnetostriction, it enlarges when placed in a magnetic field; with negative magnetostriction, the material shrinks.

As we discussed before, applying a magnetic field causes stress that changes the physical properties of a magnetostrictive material. However, the reverse is also true: applying stress to a magnetostrictive material changes its magnetic properties. That is, a dimensional change in the material can lead to induced magnetic fields. Magnetostrictive sensors employ both properties to generate an ultrasonic strain wave from the location of an external marker magnet and detect its passage by a fixed reference point in a wave guide. By knowing the speed of sound in the material, marker magnet position can be determined using a time-of-flight measurement technique.

Firstly, the time-of-flight measurement is to apply an axial magnetic field to a magnetostrictive wire, and then pass a current through the wire. The magnetostrictive effect causes a twisting at the location of the axial magnetic field (Wiedmann's effect). The twisting is caused by interaction of the axial magnetic field, usually from a permanent marker magnet, with the magnetic field along the magnetostrictive wire, which is present due to the current in the wire. Because the current is applied as a pulse, the mechanical twisting travels in the wire as an ultrasonic wave. The magnetostrictive wire is, therefore, called the waveguide. Each magnetostrictive strain wave travels at the speed of sound in the waveguide material, approximately at 3000 m/s. The position magnet is attached to whatever is being measured, perhaps a piston in a cylinder. The waveguide wire is enclosed within a protective cover and is attached to the stationary part of the machine, perhaps a cylinder body. The location of the position magnet is determined by starting a counter timer when the current pulse is launched. The current pulse causes a sonic wave to be generated at the location of the position magnet. The sonic wave travels along the waveguide until it is detected by the pickup. A pickup makes use of the reverse magnetostrictive effect described earlier (Villari's effect). A small piece of magnetostrictive material, called the tape, is welded to the waveguide near one end of the waveguide. This tape passes through a coil and is magnetized by a small permanent magnet called the bias magnet. When a sonic wave propagates down the waveguide and then down the tape, the stress induced by the wave causes a permeability change in the tape. This in turn causes a change in the tape magnetic flux density, and thus a voltage output pulse is produced from the coil. At a defined output level of the coil output voltage, the counter timer is instructed to stop. The elapsed time indicated by the timer

then represents the distance between the position magnet and the pickup. The frequency of the counter determines the resolution of the measurement; a higher frequency lead to a finer resolution.

Today magnetostrictive sensors are used by many industries dominating approximately 10% of the entire long-linear sensors market. Traditionally, they have been used in a vast range of manufacturing equipment including injection molding machines, wood processing equipment, hydraulic cylinders, hundreds of specialty manufacturing machines, process level control in pharmaceuticals and petrochemical plants, off and on-road machinery for construction and agriculture as well as many others.

Magnetostrictive linear position sensors are well regarded for ruggedness and accuracy. Pavement machines, off-road machinery and saw mill machinery provide some of the most demanding environments and the sensors perform reliably. Some applications, such as high end injection molding machines, require micron-level resolutions. Recent advances in magnetostrictive electronics, including counter timers that have 150 picosecond periods or better, allow this depth of performance.

New, novel automated manufacturing processes reduce unit cost on some new models into a whole new realm compatible with the cost demands of high volume products. This technology advancement, which offers high reliability and high performance, is suddenly very attractive for high-volume use in medical, recreational, professional tool and other extremely cost sensitive commercial or light industrial applications. Standard products are available and customized units are possible in higher volumes.

3.2 Magnetostriction: Magneto-Mechanical Coupling

Actuation systems are another way of application of magnetostrictive materials. When the magnetic energy is converted into mechanical energy, it can be used to produce forces: in our study a magneto actuator, which moves a smart material, is considered. Particularly, it is noticeable to consider that it is composed of ferromagnetic materials that produce a twist caused by interaction of the axial magnetic field, usually produced by a permanent magnet or coil, with the magnetic field along the wire, caused by the current inside. It is important to understand how Wiedmann's effect takes part in the system and which values are considerable.

The magneto-mechanical coupling is the phenomena analyzed in this work and it is fundamental because it considers two aspects:

- magnetic;
- mechanical.

The last aspect is a consequence of the magnetic one, because the smart material twists when there is the composition of two magnetic fields. Therefore, mechanical of materials is useful to explain and to find a relation between smart material properties, which are figure out in the next chapter, and setups parameters (like intensity of current) through the investigation of torsion.

The link between two aspects listed before is the relative permeability, explained in the Chapter 2.1, because thanks to this property our material interacts with the surrounding magnetic space. Parameters are calculated because it is known that magnetic properties are linked to magnetism and this last one to mechanics. In this case, magnetic properties allow to control the smart material whose performances are established by chemistry in fact it is prepared to support our goals.

This work explains how it is possible to prepare a specific material which can perform as we want, thanks to its magnetic properties. As discussed before, the word actuator describes a device capable of converting an input energy, in our case magnetic, to output energy which is mechanical. Surely the value of input energy is linked to the output effect, in fact this work shows the influence of setup parameters on the torsion. The intensity of current is the main setup parameter which creates magnetic fields (wire and coils) and acts on the smart material, changing its shape and dimensions.

4.0 Smart Materials: MAE (Magneto-Active-Elastomer)

As we explained, Smart Materials are materials which react to environmental inputs by modifying one or more of their properties: thanks to the help of chemistry it is possible to produce materials with different shape, properties and aspects. For these reasons, this branch deals with materials designed to fulfill precise functions and their features to react to specific stresses are obtained by the addition of substances capable of modifying some of their physicochemical characteristics. This aspect categorizes materials as smart and it is an innovative process to produce them, aimed at getting the best performance in every field.

In this work it is prepared a sample with these substances [9]:
- Base polymer VS 100000(vinyl-functional polydimethylsiloxane) for addition curing silicone;
- Chain extenders Modifier 715 (SiH-terminated polydimethylsiloxane);
- Reactive diluent polymer MV 2000 (mono-vinyl functional polydimethylsiloxane);
- Cross linker 210 (dimethyl siloxanes-methyl hydrogen siloxanes copolymer);
- Pt-Catalyst 510;
- Inhibitor DVS;
- Silicone oil WACKER® AK 10 (linear, non-reactive polydimethylsiloxane)
- CIP (carbonyl iron powder) type SQ. (particles size of 4,5 μm)

This last material is as ferromagnetic filling for ***MAE (Magneto-Active-Elastomer)*** and it is important for our investigation because when there are two magnetic fields the component twists. This effect is linked to Wiedmann's theory, which could be useful to understand with more details the behaviour of our sample. However, the theory about magnetic material first discussed is the main step to this study.

In this research are considered two different setups:
- Helmholtz coils and wire;
- permanent magnets and wire.

The current flows inside the Helmholtz coils (or permanent magnets) and the wire. This last one is arranged along the main axis of the Helmholtz coils (or permanent magnets) which have a ring shape.

While, the sample MAE (with cylindrical shape) is fixed around the wire in the middle way and it behaves differently with different input parameters or setups, which they are illustrated in the consecutive chapters.

4.1 Smart Materials: Preparation, Properties and Sizes

The sample is prepared in this way:

- in the first step, the polymer VS 100000, the polymer MV 2000, the modifier 715 and the Silicone oil AK 10 are putted together and mixed with an electric mixer (Roti®-Speed-stirrer, Carl Roth GmbH, Germany) to form an elastomer mixture *MRE (Magneto-Rheological-Elastomer)*. The mixture ratio is shown in the following table:

Component	Quantity [g]
VS 100000	*14,00*
MV 2000	*2,50*
Modifier 715	*0,05*
AK 10	*33,00*

- in the second step, the elastomer mixture is mixed (6,00 g) with CIP (70 wt % or 80 wt %) and the cross linker 210 (0,03 g). The cross linking reaction is activated by the Pt-Catalyst 510 (0,02 g). For the control of the catalytic activity is used the inhibitor DVS (recommended dosage 0,01÷0,50 % from the total weight of all organosilicon compounds). The necessary amount of the inhibitor for this MAE mixture is 0,002 g.

- in the third step, the air bubbles in the MAE mixture are removed using a vacuum mixer (Twister evolution, Renfert GmbH, Germany).

- in the last step, the MAE samples is fixed to the Petri dishes (35 mm of height, Greiner Bio-One GmbH, Germany) and it is cured in the universal oven Memmert UF30 at 80°C for 1 hour and after at 60°C for 24 hours with air circulation (Figure 20).

For the test, the sample is synthesized and has the shear storage modulus, in the absence of a magnetic field, approximately around 10 kPa. Moreover, it has an isotropic distribution of the CIP and it is called *MAE70* (70 wt % of the CIP) or *MAE80* (80 wt % of the CIP).

Figure 20: Smart material in Petri dishes

Figure 21: Sample of smart material

The sample showed in the Figure 21 has these sizes:

SIZES [mm]	
Length	*60,00*
Inner Radius	*1,00*
Outer Radius	*2,00*

and these properties:

PROPERTIES	
Density ρ [kg/m³]	*6000,00*
Young's modulus E [Pa]	*40000,00*
Poisson's ratio v	*0,45*
Electric conductivity [S/m]	*0,00*
Relative permittivity ε_r	*10,00*
Permeability μ_0 [H/m]	*4π*10^(-7)*
Relative permeability μr [H/m]	*10,00*
Saturation magnetostriction λ_s	*0,10*
Saturation magnetization M_s [A/m]	*0,45*10^(6)*

The sample is fixed around a wire illustrated in Figure 22 and the aim of our work is to investigate:

- torsion (twisting) with its angle;
- stress;
- displacement;
- magnetic field;
- optimal sizes of the sample and relative permeability μ_r to obtain a visible displacement (values around millimeters).

It is important to underline that in general way the study must find a relationship between the input parameters (current is the main parameter) and the parameters listed above.

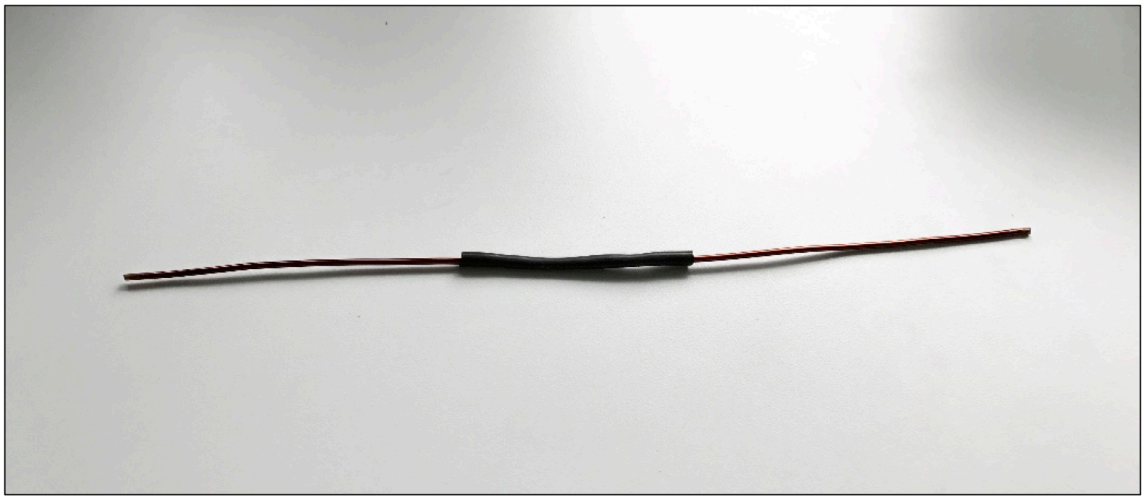

Figure 22: Sample of smart material fixed around the wire

In order to get valid results, it has changed the experimental setup, which is illustrated in the consecutive chapters. It is reasonable that final results include errors due to:

- simulations;
- measurements.

Simulations cause errors linked mostly to mesh and measurements to precision of instrumentations. It has been attempted to minimize this error values but it is inevitable to obtain the same result to the theoretical one. Later, it will be made numerically known of what has been mentioned at the moment.

5.0 Studying Components

In this chapter, it is studied the magnetic field of components which will be assembled to build a magneto-mechanical actuator. Before, it was discussed the theoretical part which is useful to understand and to give the right interpretation to the simulation data. Thanks to the software Comsol Multiphysics [10], it was possible to predict the performance of components with different setups and input parameters. Simulation is a valuable way to reproduce the reality in short time. It is the step before the experimentation and in our work it is examined these components:

- wire;
- Helmholtz Coils;
- permanent magnets.

In this thesis setup parameters, linked to reality and feasibility of the experiment, are considered. This last step will be useful to confirm what it is investigated.

5.1 Wire

Our first step in this chapter is to find the magnetic field owing to the current in a very small section of current-carrying wire. Then we shall find the magnetic field due to the entire wire for several different arrangements of the wire. It is supposed a straight wire and it is possible to compare the simulation data using Ampere's law (or Biot-Savart's law):

- outside the wire the theoretical reference is Equation 1.11;
- inside the wire the theoretical reference is Equation 1.13.

The simulation on the software Comsol Multiphysics shows how the magnetic field is around the wire when current flows inside of it. It is used these input parameters to simulate the wire:

Name	Expression	Unit	Description
i	*1,00*	*[A]*	*Current*
j	*i/(πR²)*	*[A/m²]*	*Density current*
R	*1,00*	*[mm]*	*Radius*
L	*250,00*	*[mm]*	*Length*

Materials used in the simulation are:

- Copper for the wire;

- Air around the wire.

The Figure 23 shows the wire in coordinate system space.

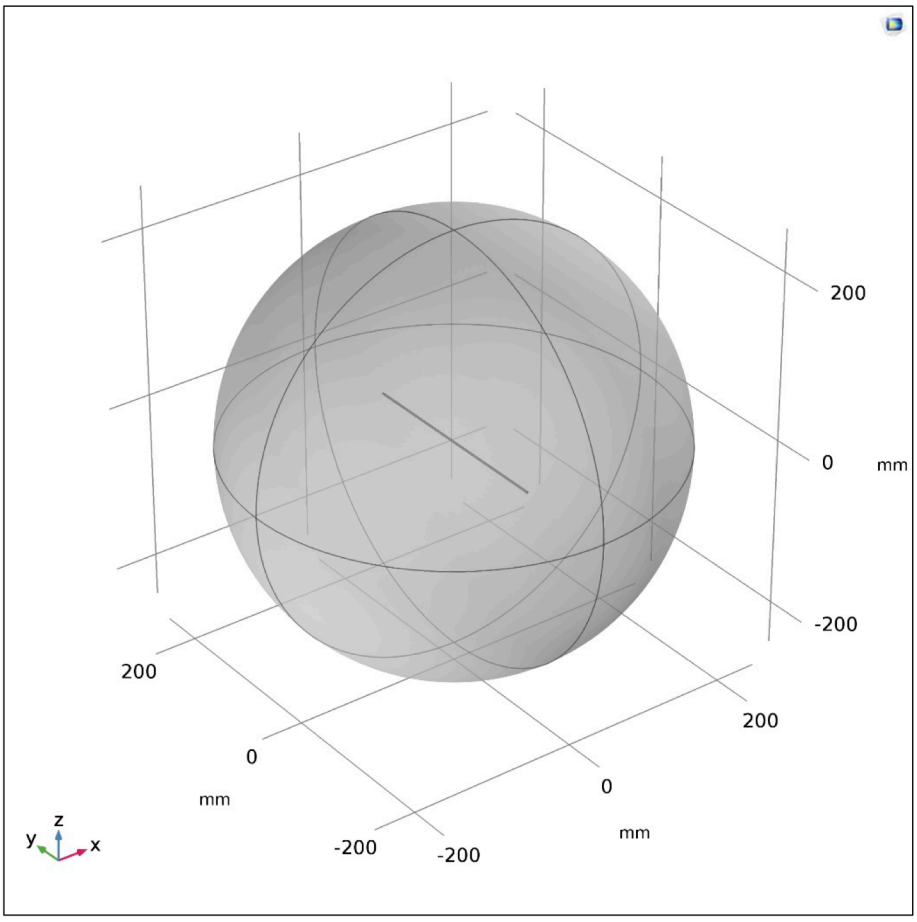

Figure 23: Setup of the wire

When the current flows into the wire, it is possible to evaluate how the magnetic field surrounds the wire. In this view, there is a global representation with the two cutting plane, which are considered for the evaluation of the magnetic field.

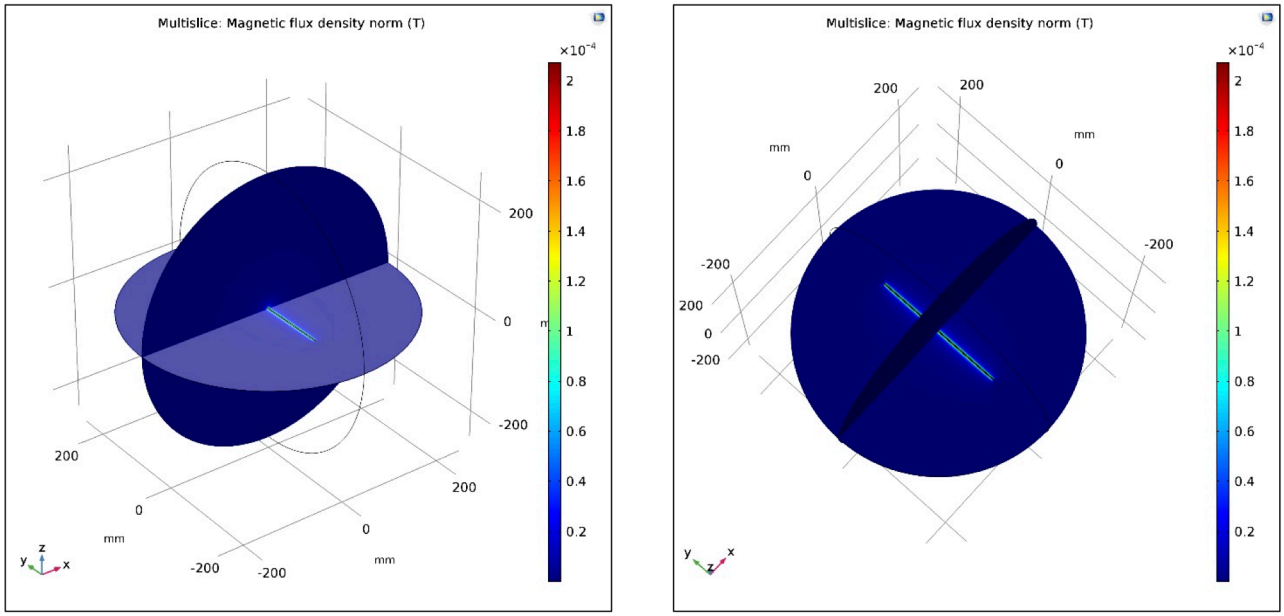

Figure 24: Magnetic Field

As discussed before, the magnetic field is studied with the application of two cutting planes shown in Figure 24:

- the first one is on ZX axis;
- the second one is on XY axis.

Cutting planes are considered because it is useful to compare results simulated with the theory. This is fundamental for achieve a right investigation and to explain with more details the work of thesis.

The first cutting plane is shown in Figure 25.

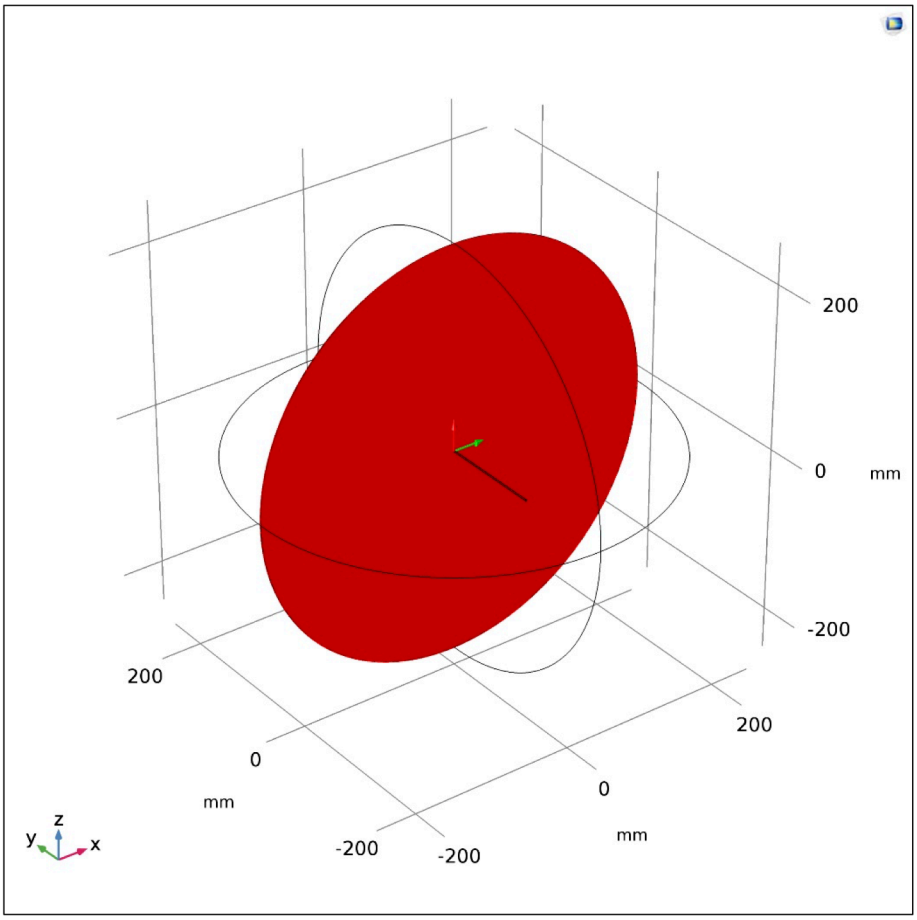

Figure 25: First cutting plane

In the following images (Figure 26, Figure 27), it is possible to focus on the evolution of magnetic field, which is represented by arrows and isolines (contour): in this plane arrows assume the circular shape around the wire and they became smaller with the distance. This trend is demonstrating in the previous paragraph when it is explained Ampere's law (or Biot-Savart's law).

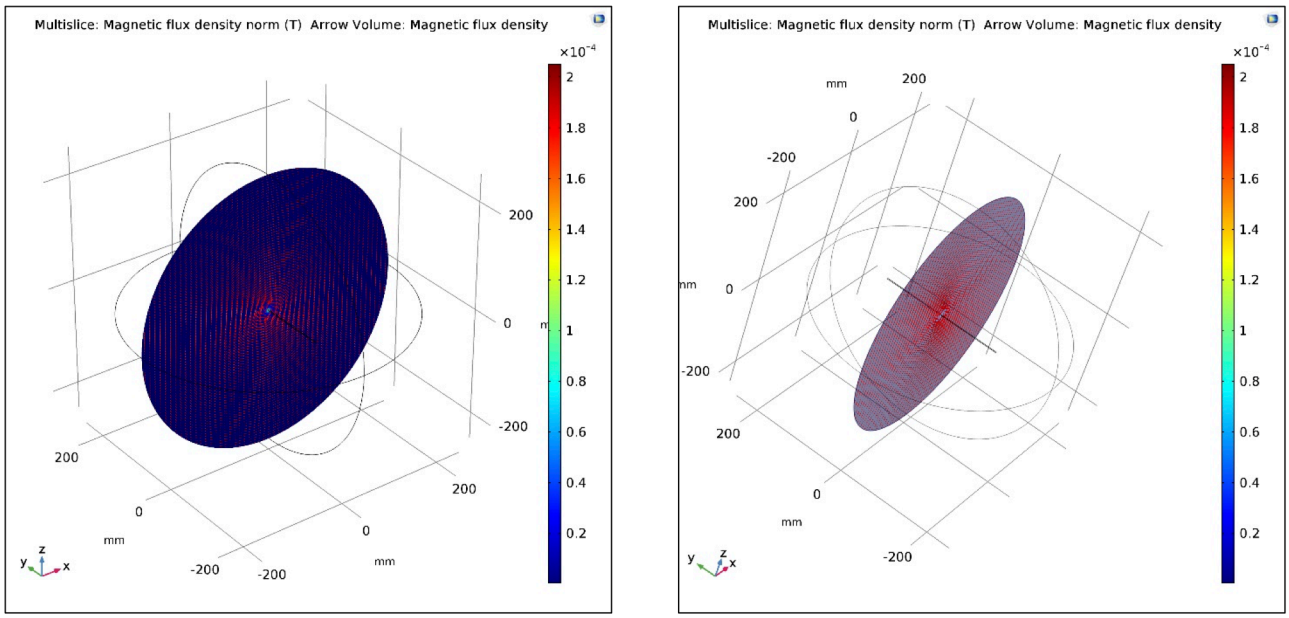

Figure 26: Magnetic flux density, first cutting plane

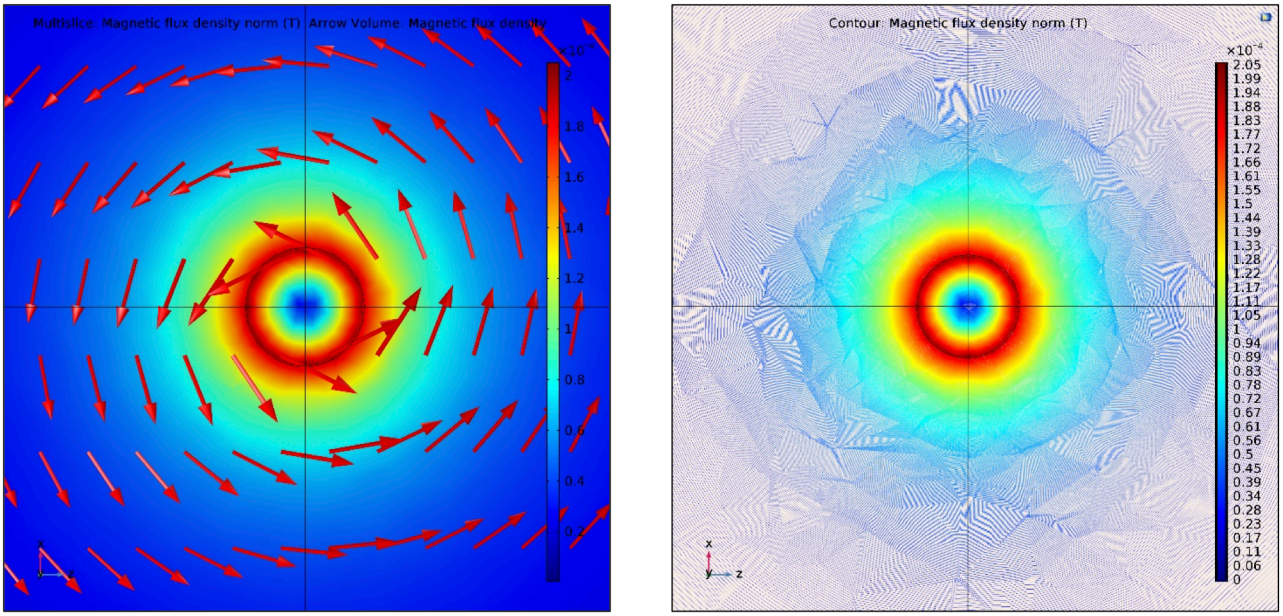

Figure 27: Magnetic flux density, arrows and contour

As it is explained in the previous paragraph, the magnetic field is calculated on first cut plane when the cut line is considered (Figure 28). Biot-Savart's law is demonstrated and compared with simulation data.

In this figure the cutting line on the plane is represented and it is necessary to underline that the coordinate system is in the center of the section wire.

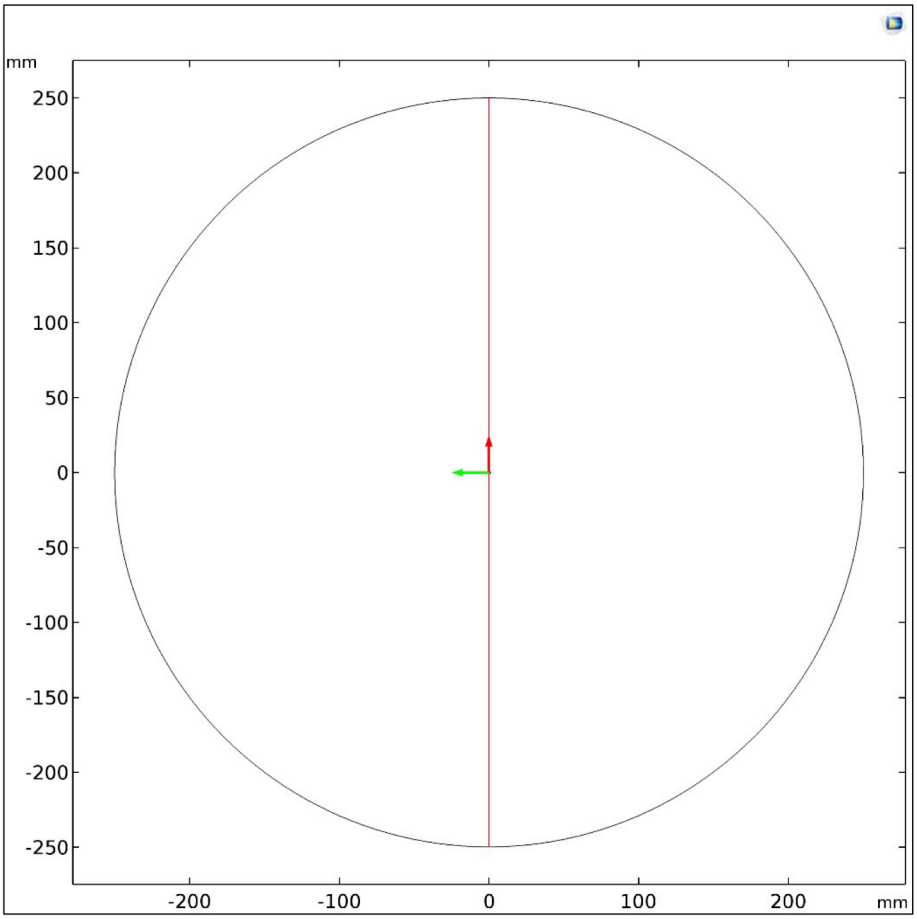

Figure 28: Cutting line, first cutting plane

Biot-Savart Law explains that you must obtain only a component value of magnetic field, which is the B_z in our case. Instead B_x and B_y should be null because it is the result of the vector product.

Following graphs, linked to simulation, show how trends are quite similar to theory. In our case:

$$r = \sqrt{(x-0)^2 + (y-0)^2 + (z-0)^2}$$

$$x \neq 0, \qquad y = 0, \qquad z = 0$$

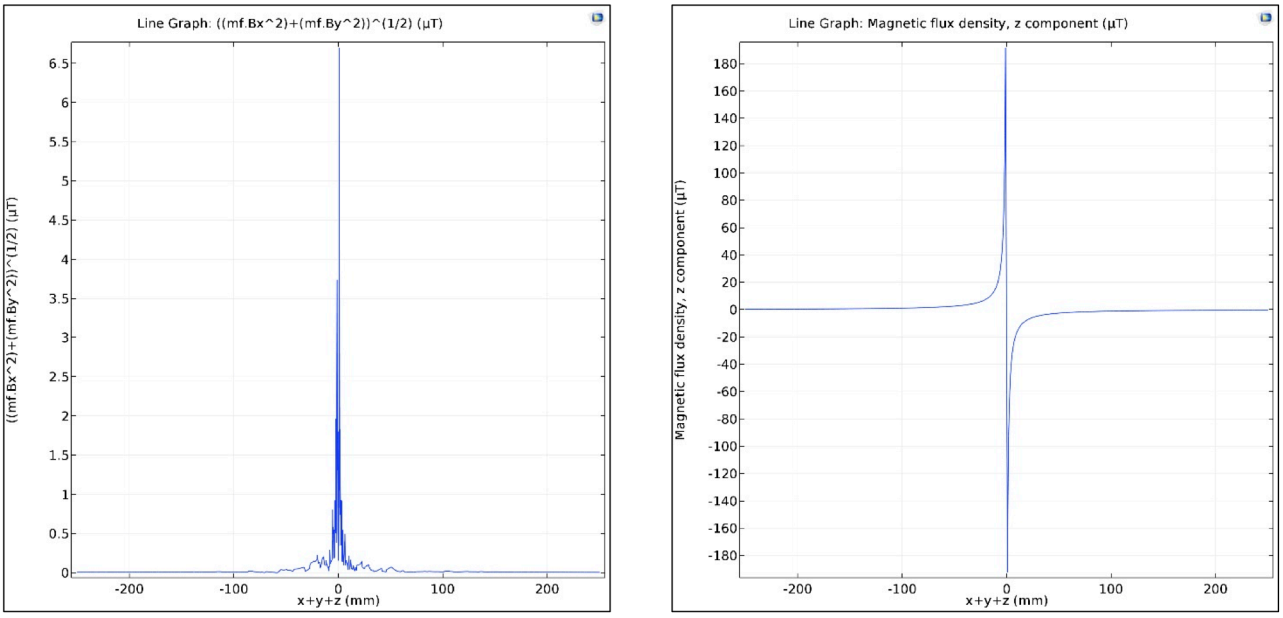

Figure 29: Magnetic field, first cutting plane

The magnetic field B_x and B_y (figure on the left) could be null for the theory data, instead the magnetic field B_z (figure on the right) gives us a margin of error approximately of 2% in correspondence to the maximum value.

The modulus of the magnetic field is illustrated in Figure 30 and in the end of the chapter it is demonstrated the same trend with the theory.

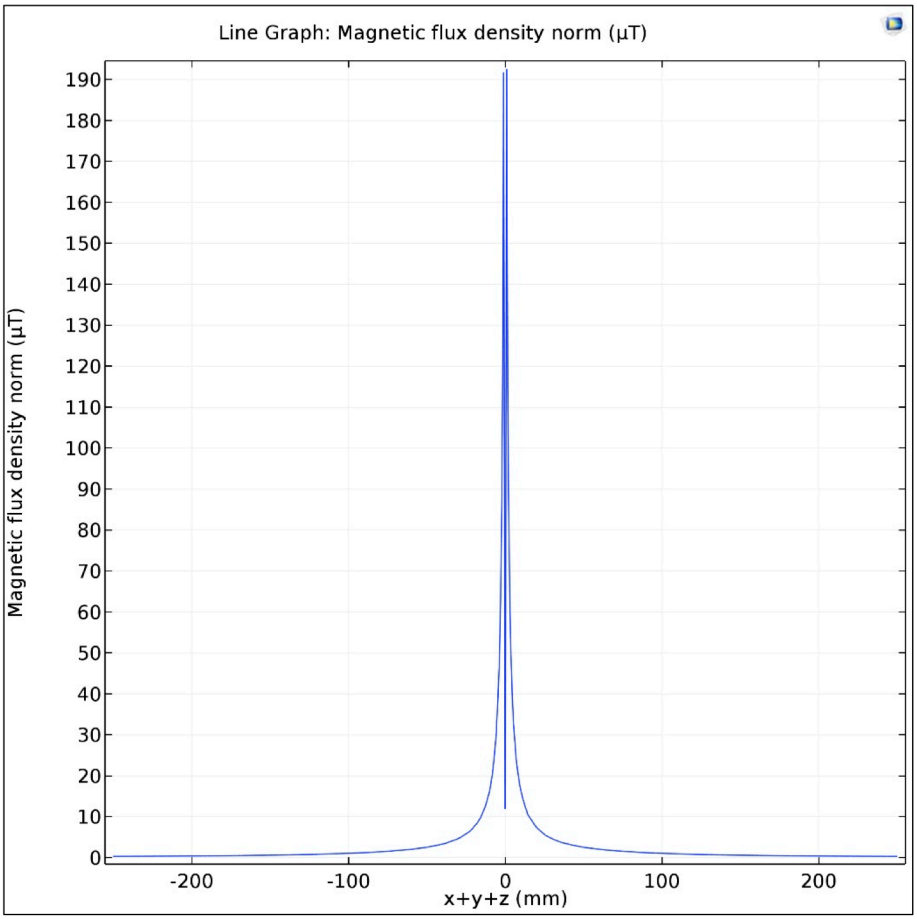

Figure 30: Modulus B

If a second cutting plane (Figure 31) is considered, we will obtain a theoretical null magnetic field. This result is linked to mesh error whose value is around 10%.

Figure 34, Figure 35, Figure 36 report results about the second cutting plane with the same cutting line and it is interesting to notice how the magnetic field is not null. Even if this last result could be wrong because calculator and simulation software introduce evaluated errors, there are margins of acceptability and in this study are widely respected.

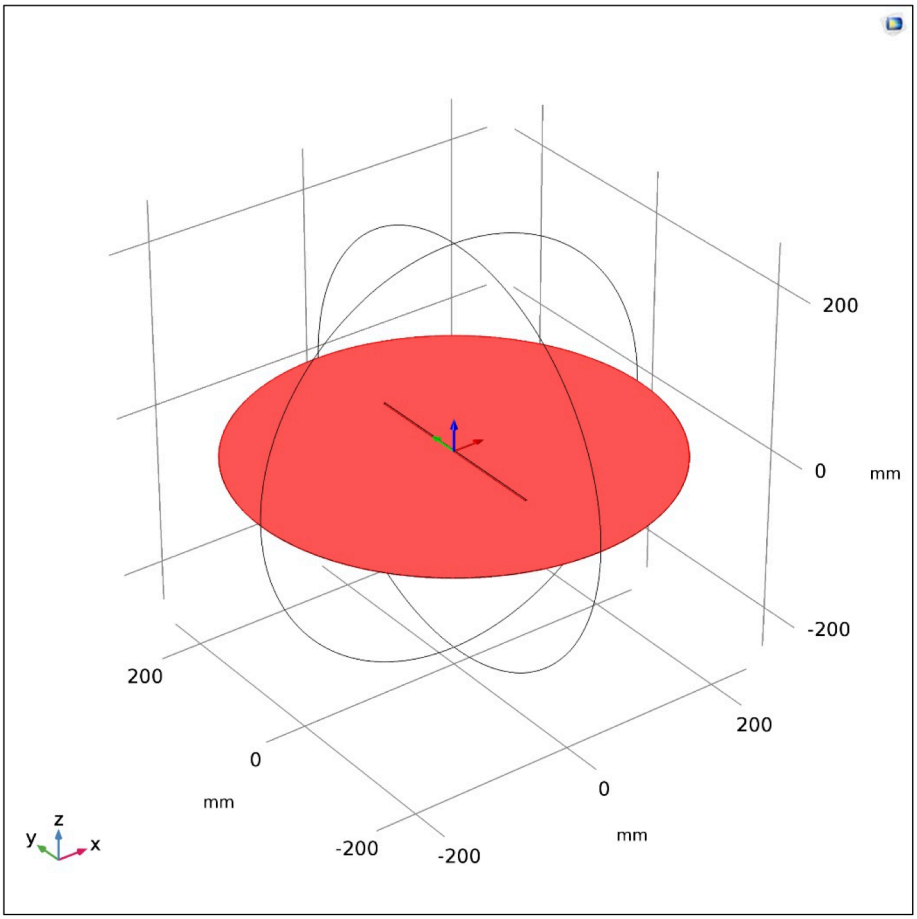

Figure 31: Second cutting plane

In these following images (Figure 32, Figure 33), it is possible to focus on the same results obtained before, but with the second cutting plane. Arrows go in the plane, if the first middle is considered, and go out from the plane in the other middle.

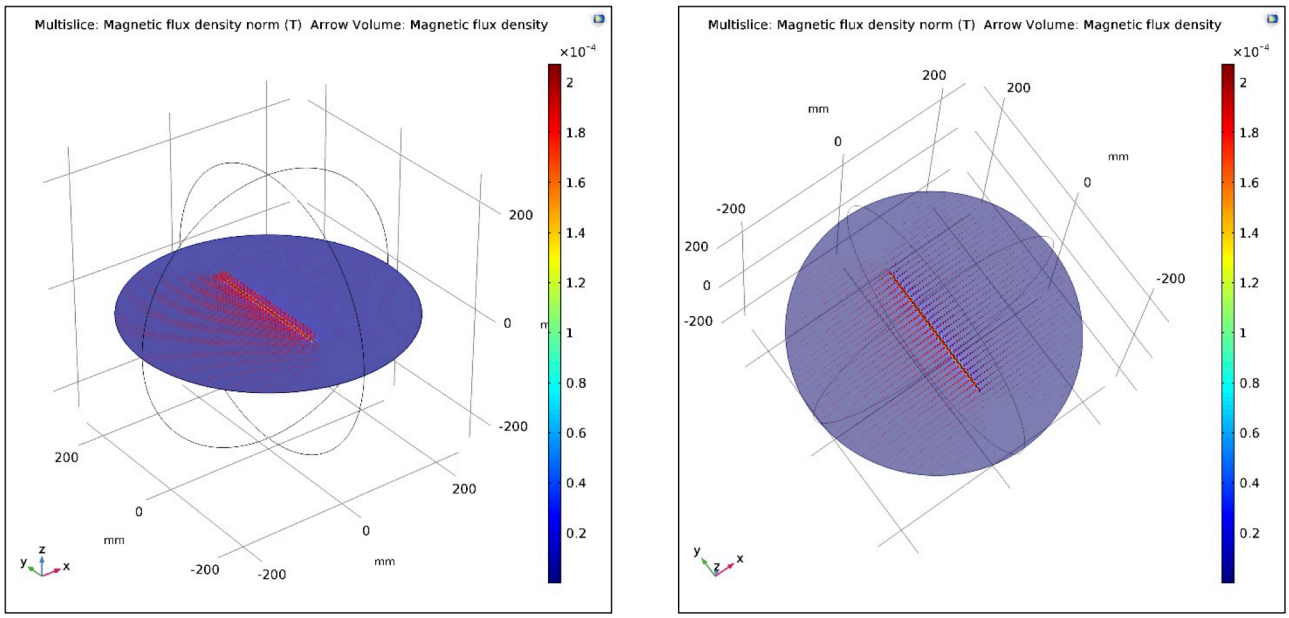

Figure 32: Magnetic flux density, second cutting plane

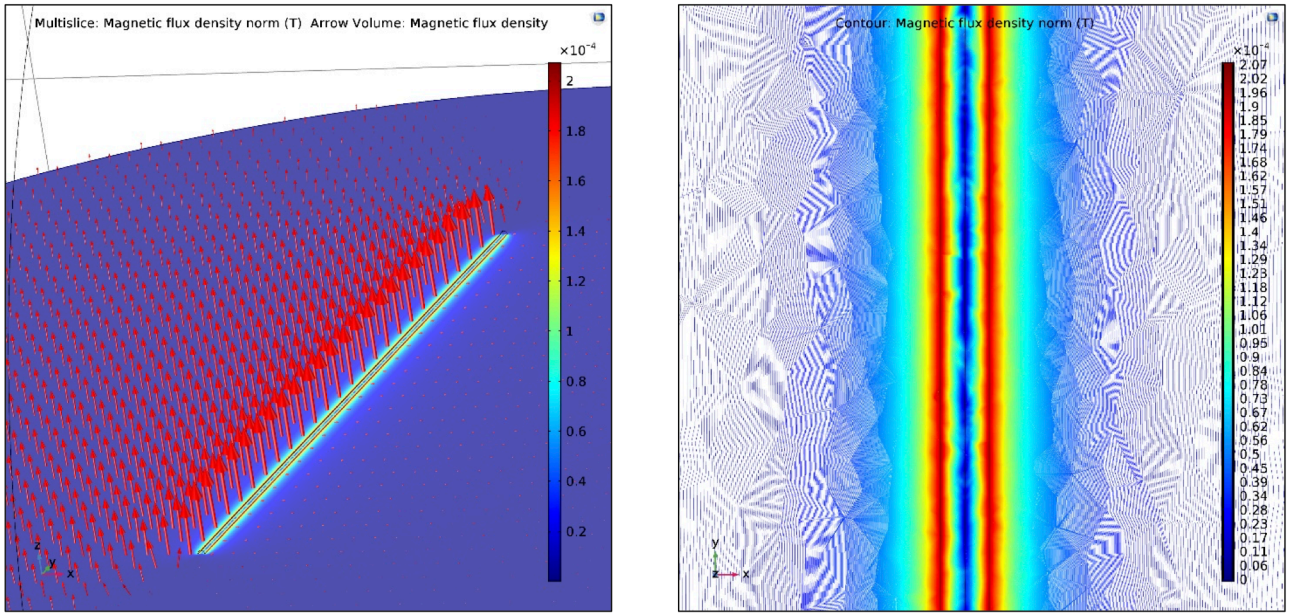

Figure 33: Magnetic flux density, arrows and contour

In this figure (Figure 33) it is showed that the greatest value of magnetic field is at the distance of 1 mm, which is the radius of the wire. Isolines (contour) are not homogeneous because the mesh is not extra-finer. This figure is a zoom of the wire, which has very small section. In the next figures there is the evaluation of the magnetic field values on the second cutting plane.

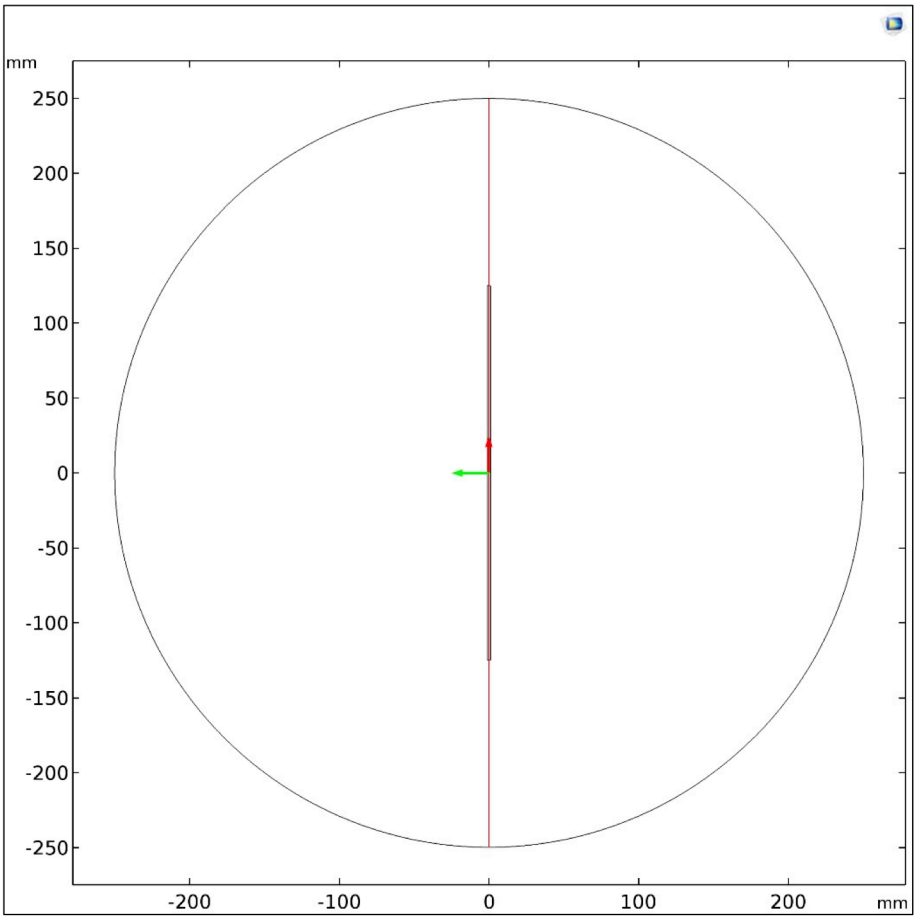

Figure 34: Cutting line, second cutting plane

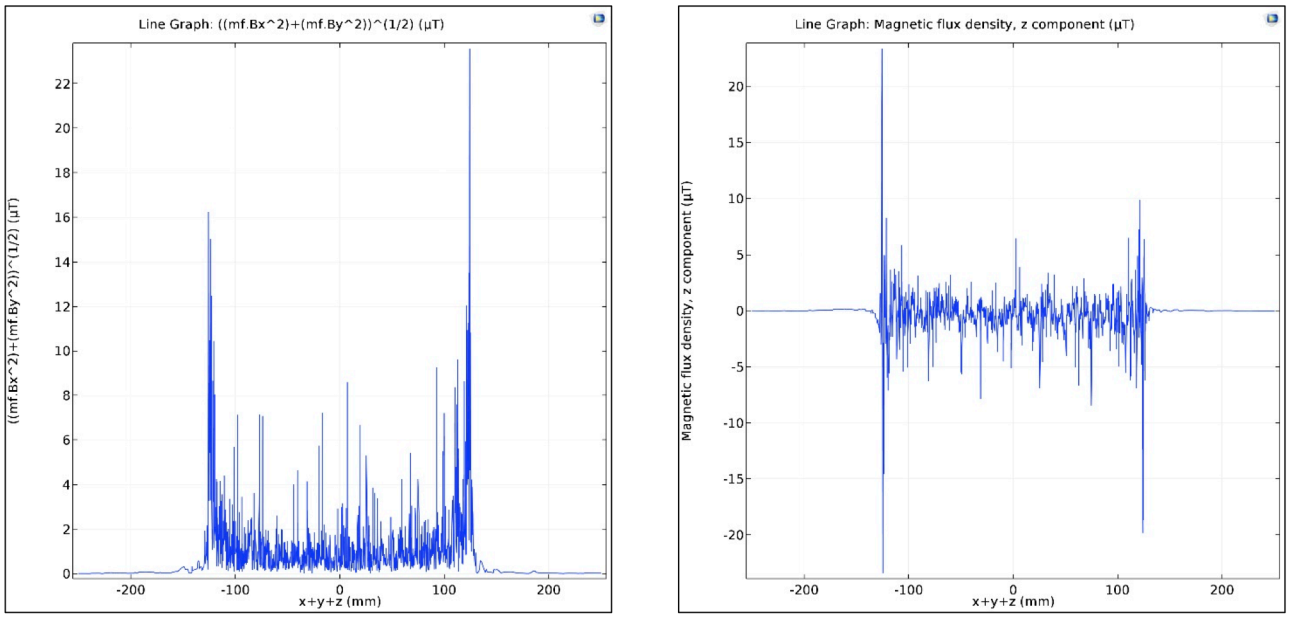

Figure 35: Magnetic Field, second cutting plane

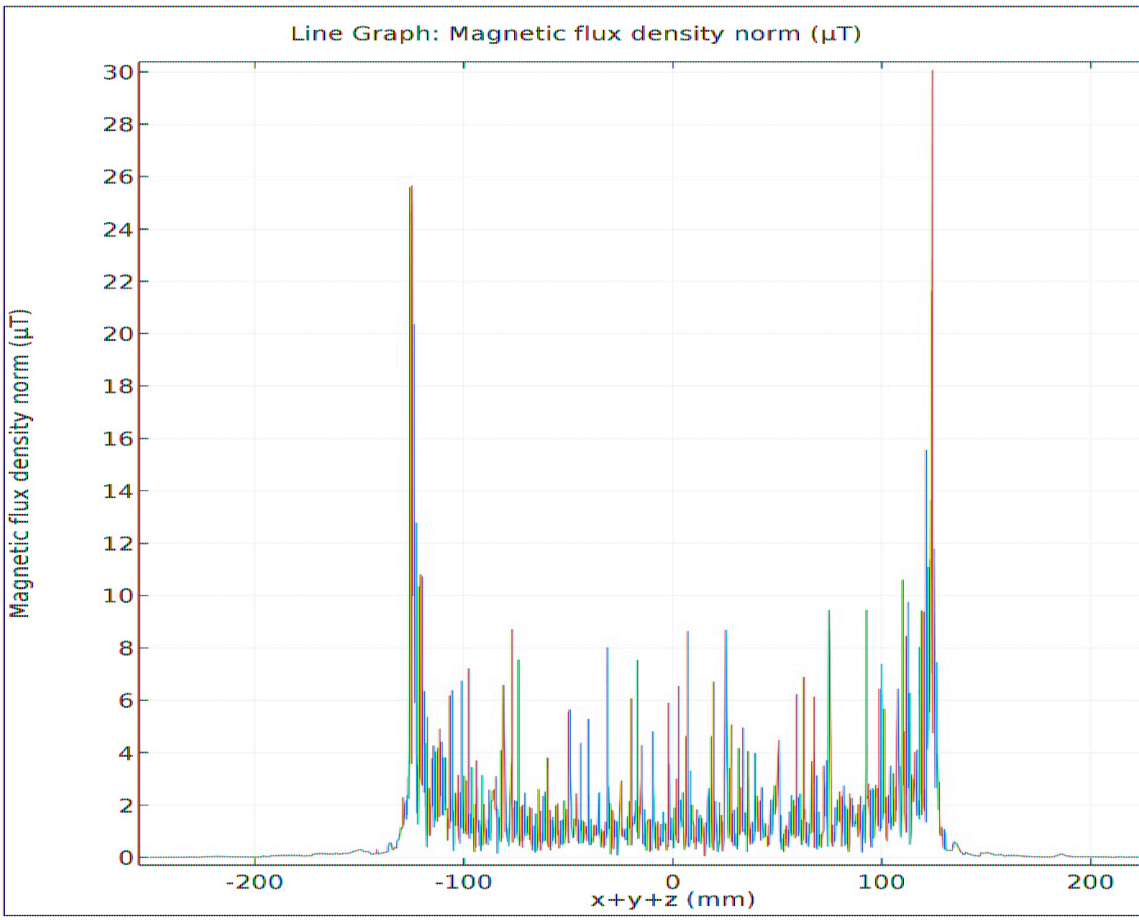

Figure 36: Modulus B

The graph below verifies how the trend simulation with the red line is quite simila
data with the yellow line. The greatest value of the magnetic field B is at the radi
value obtained from the simulation is 196,6 μT and the margin of the error is app
the distance of the radius.

Results underline that the value of magnetic field halves to double distance from
shown in Table 1 in the Appendix, comparing the error between the theory and s
they come to convergence after considering a distance superior of 10 mm.

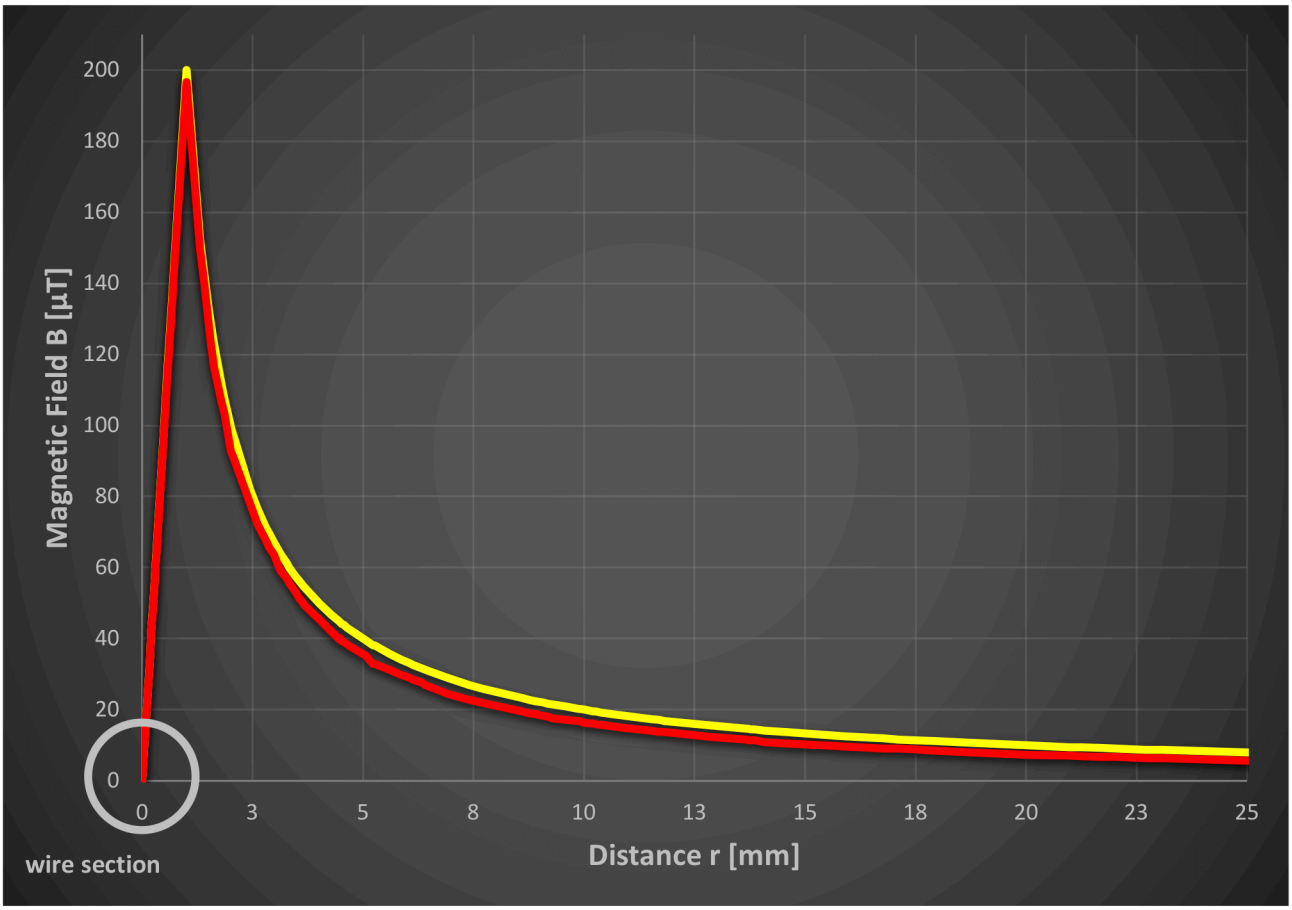

From this simulation, it is useful to establish the boundary condition when the magnetic field is null (Figure 37), thus the safety condition from the wire could be at the distance 200 mm.

Errors in the simulation are surely caused by the mesh. If it is extra-finer, errors will be smaller than a coarse mesh. In this simulation it is used a fine mesh (Figure 37) and it is avoided tetrahedral shape, which could invalidate results. Error obtained is around 2% as discussed before when it is illustrated the comparison between theory and simulation data. On the other plane where the theoretical magnetic field could be null it is obtained an error around 10%.

The error is calculated in this way:

$$\%Error = \left(\frac{simulation - theory}{theory}\right) \cdot 100 \tag{5.0}$$

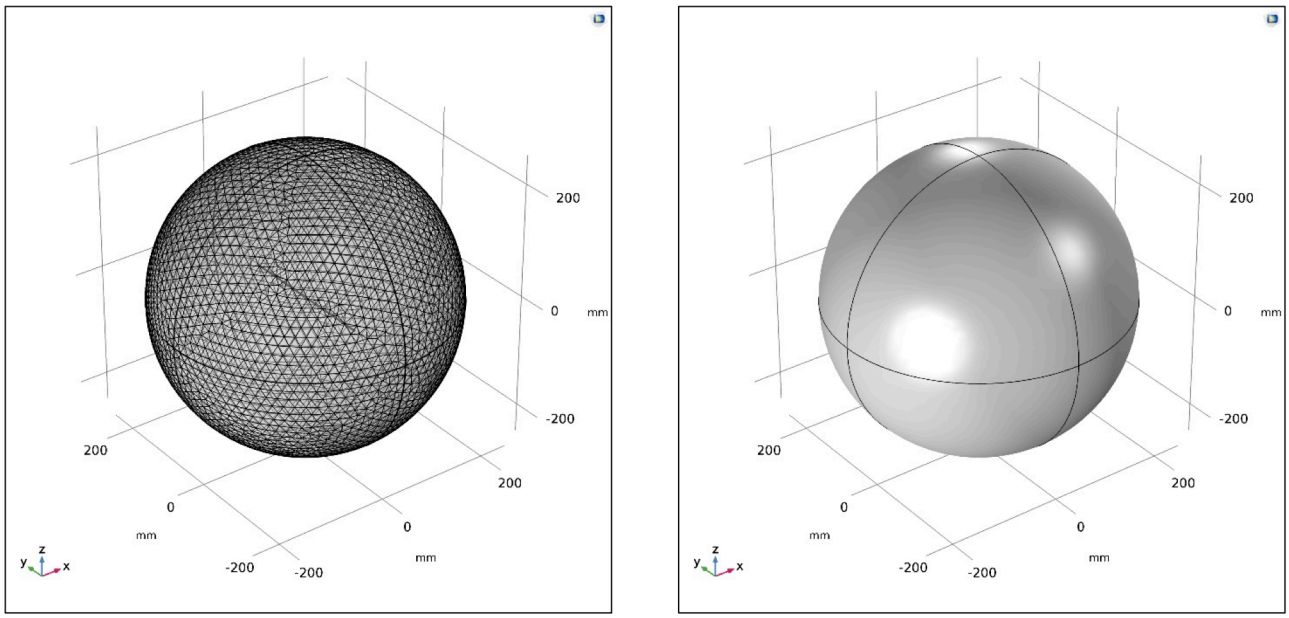

Figure 37: Mesh and boundary condition

5.2 Helmholtz Coils

Helmholtz coils are simulated because our investigation consider the same setup with a wire and a sample of smart material. As for the wire, it is reasonable to study how the behavior of these coils is: obviously the same way to prove the concept is followed. Input parameters for the simulation are:

Name	Expression	Unit	Description
i	*1,00*	*[A]*	*Current*
L	*5,00*	*[mm]*	*Length coil*
H	*10,00*	*[mm]*	*Height coil*
R	*100,00*	*[mm]*	*Radius coil*
D	*100,00*	*[mm]*	*Distance coils*
N	*10*	*/*	*Windings*
i_{tot}	*i*N*	*[A]*	*Current tot*

The Figure 38 shows the setup, and it is important to have the same distance of the radius if we want a uniform magnetic field between two coils.

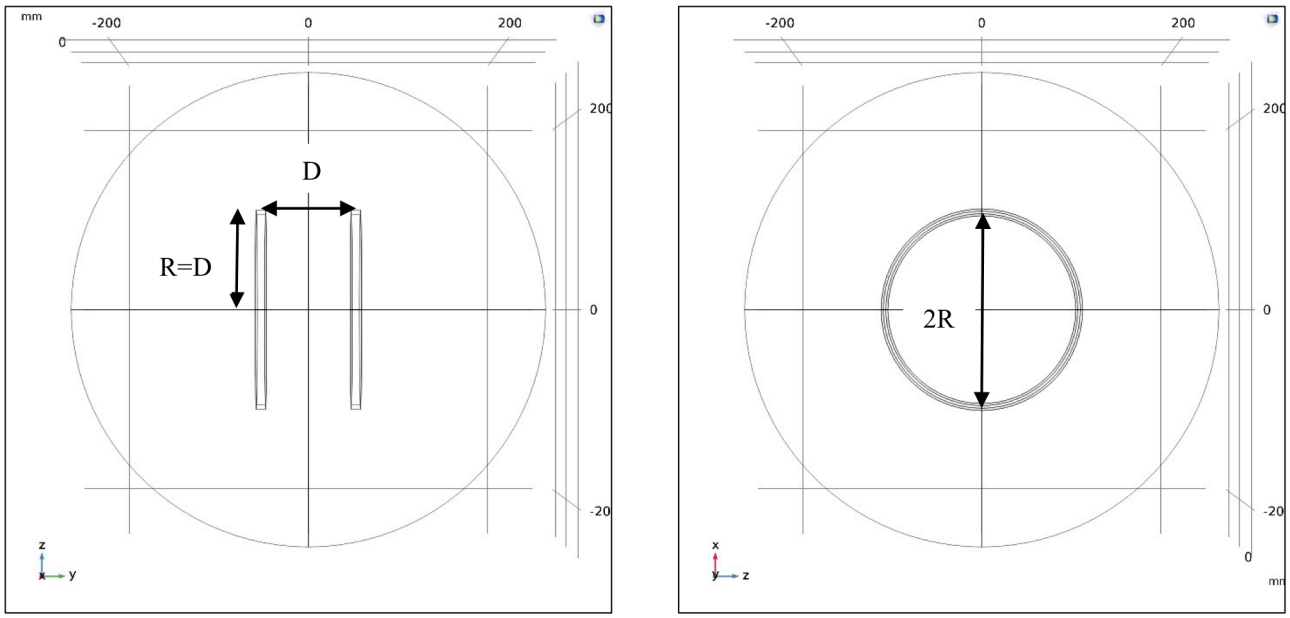

Figure 38: Geometry

Materials used in the simulation are:

- Iron Powder SMP1172 for coils ($\mu r = 1$ *H/m)*;
- Air around coils.

The uniformity of magnetic field between two coils will be fundamental when the smart material will be investigated and in particular the torsion, because it gives a homogenous behavior.

The Figure 39 shows Helmholtz coils in coordinate system space.

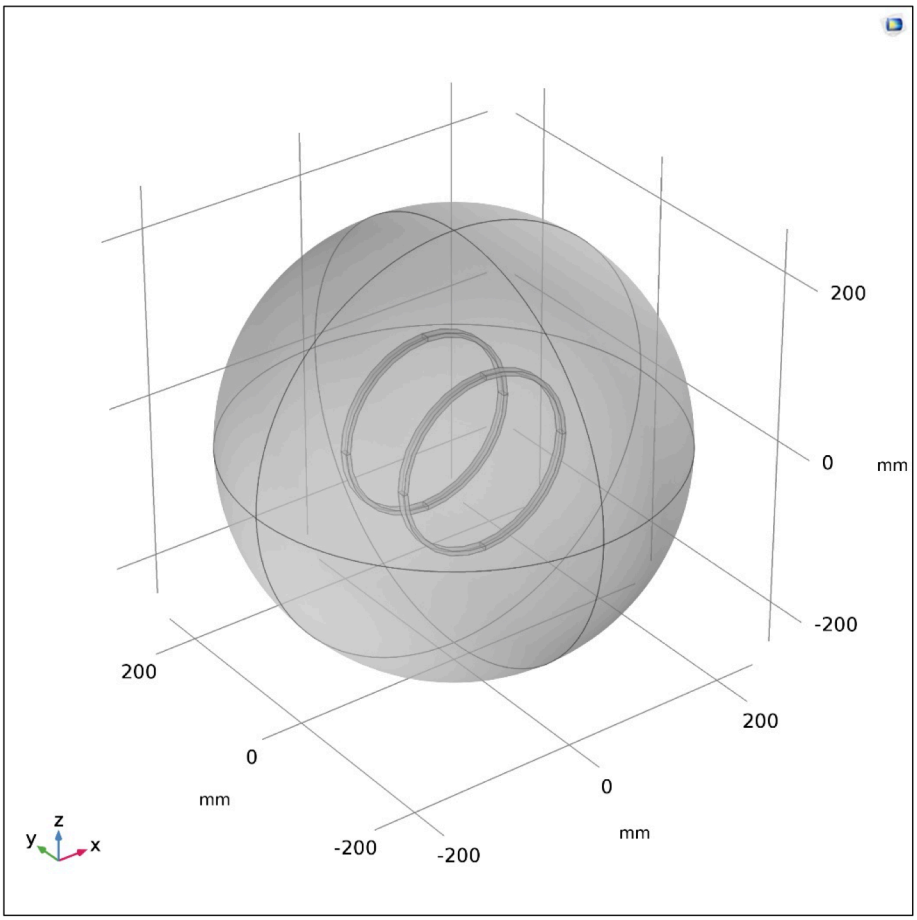

Figure 39: Setup of Helmholtz coils

Flowing the current into coils, the magnetic field, which surrounds coils, is represented in the figure below and could be investigated through arrows, isolines (contour) or numerical data.

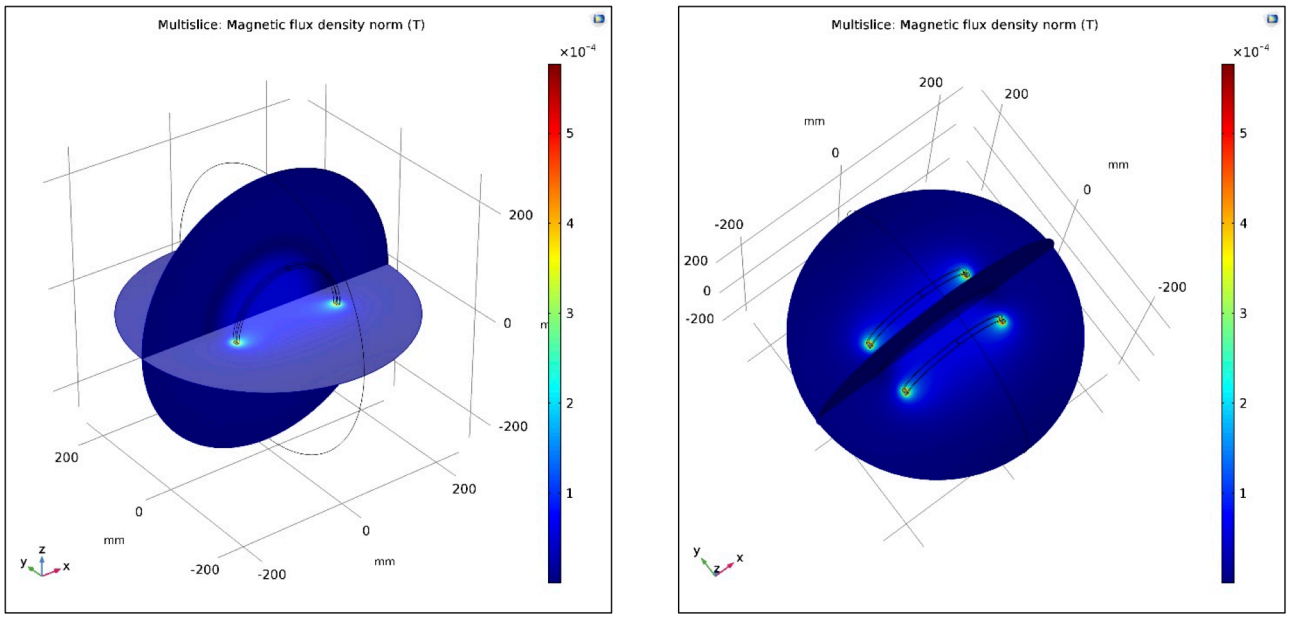

Figure 40: Magnetic Field

As it is illustrated in Figure 40, the magnetic field is studied with the application of two cutting planes:

- the first one is on ZX axis;
- the second one is on XY axis.

The first cut plane is shown in the Figure 41 instead in the Figure 42 and in the Figure 43 there are illustrations of the magnetic flux density with arrows and contour as explained before.

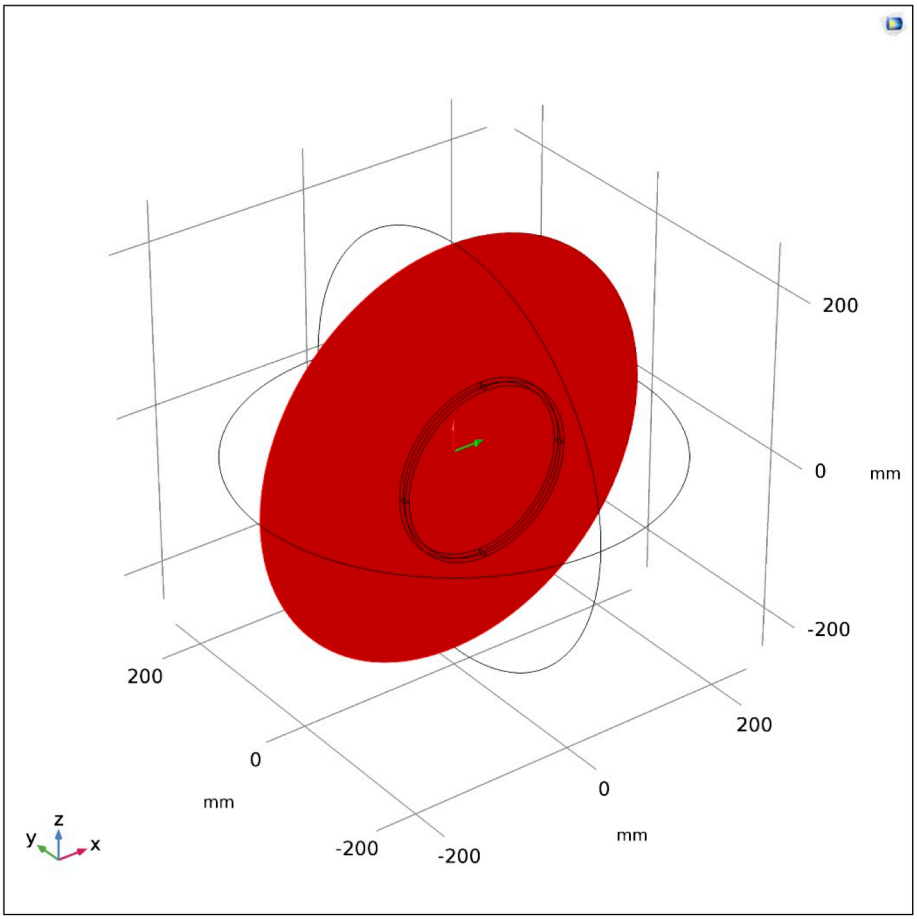

Figure 41: First cutting plane

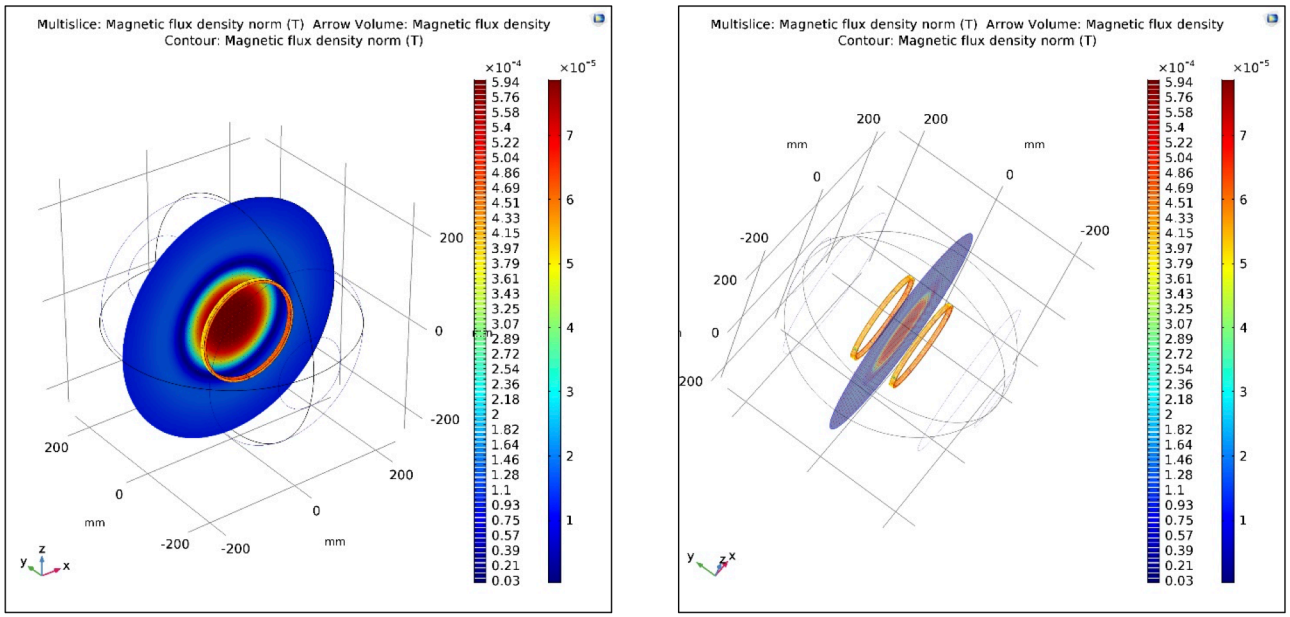

Figure 42: Magnetic flux density, first cutting plane

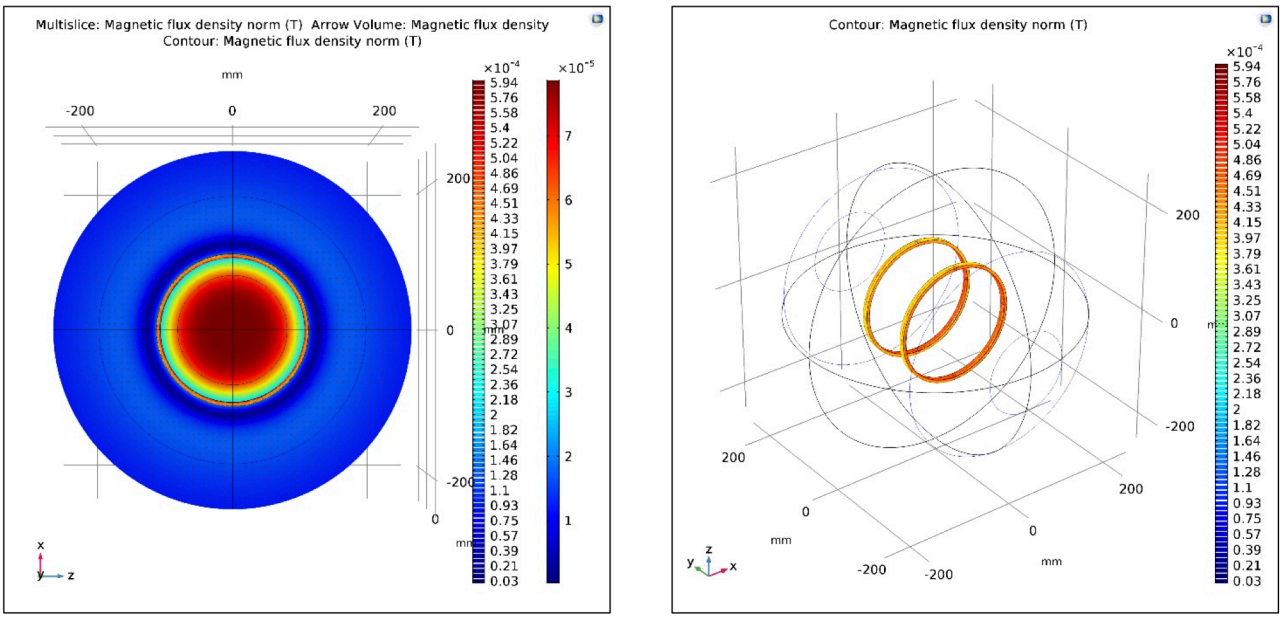

Figure 43: Magnetic flux density, first cutting plane

Figure 44 considers two cutting lines on the first cutting plane, while the Figure 45 below shows how the magnetic field trend is. Surely, it is more important to investigate the second cutting plane and compare obtained results with the theory.

For the first cutting line:

$$r = \sqrt{(x-0)^2 + (y-0)^2 + (z-0)^2}$$

$$x \neq 0, \qquad y = 0, \qquad z = 0$$

Instead for the second cutting line:

$$r = \sqrt{(x-0)^2 + (y-0)^2 + (z-0)^2}$$

$$x = 0, \qquad y = 0, \qquad z \neq 0$$

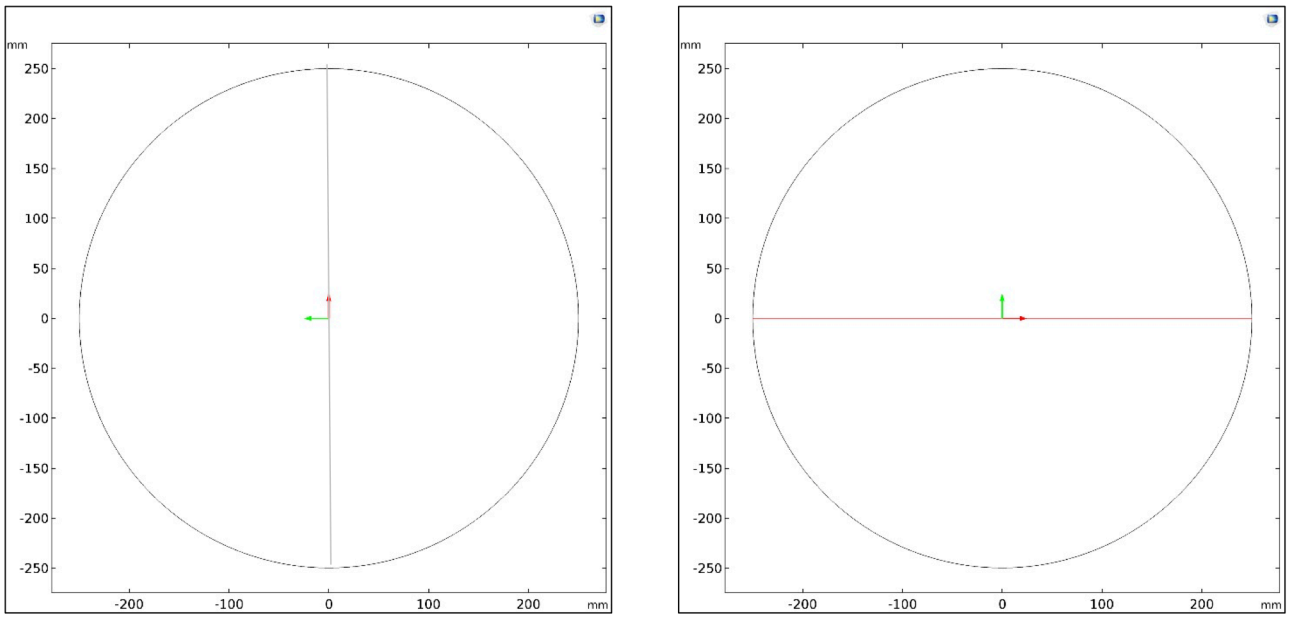

Figure 44: Cutting lines

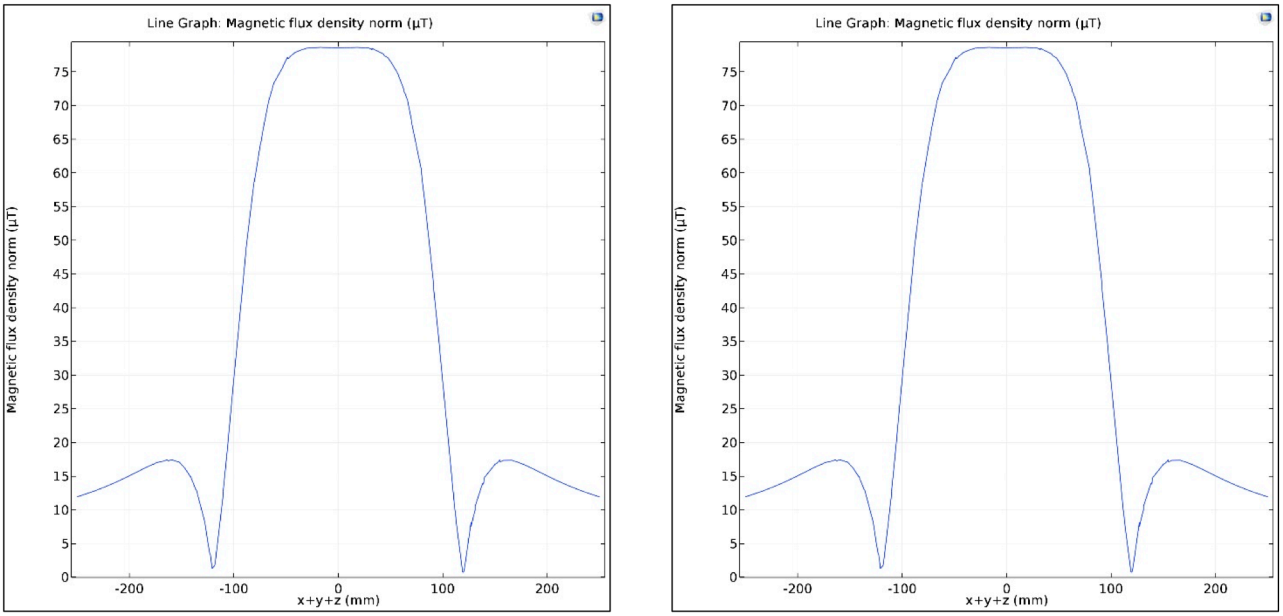

Figure 45: Magnetic Field, first cutting plane

The Figure 46 shows the second cutting plane with the representation of the magnetic flux density, using arrow and contour. This plane explains in clear way how the trend of the magnetic field is. It is also interesting to see that there is uniformity between the two coils, as the theory explains, and both the direction and side of the magnetic field are on the Y axis. In other chapters the composition of Helmholtz coils field with the magnetic field of the wire determines the Wiedmann's effect.

The Figure 49 and the Figure 50 illustrate how the trend of the magnetic field is, if two cutting lines are considered. Trends on the left of both figures demonstrate that it is approximately the same of the theory. The error is around 10% in the middle between two coils.

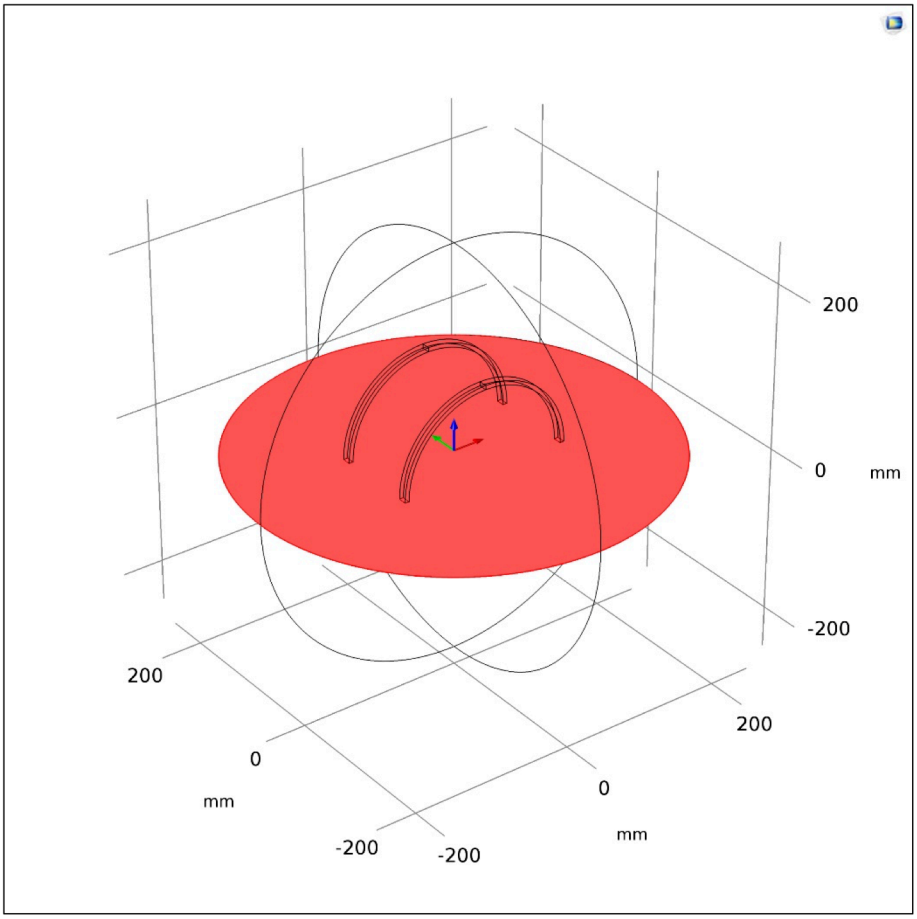

Figure 46: Second cutting plane

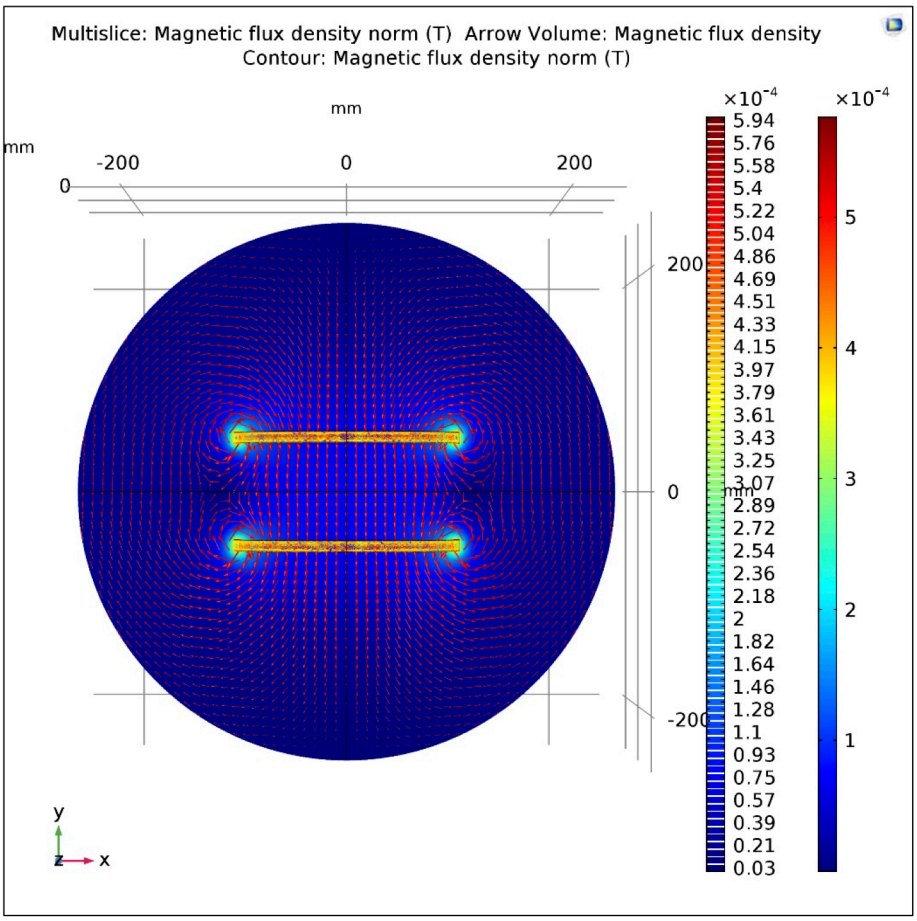

Figure 47: Magnetic flux density, second cutting plane

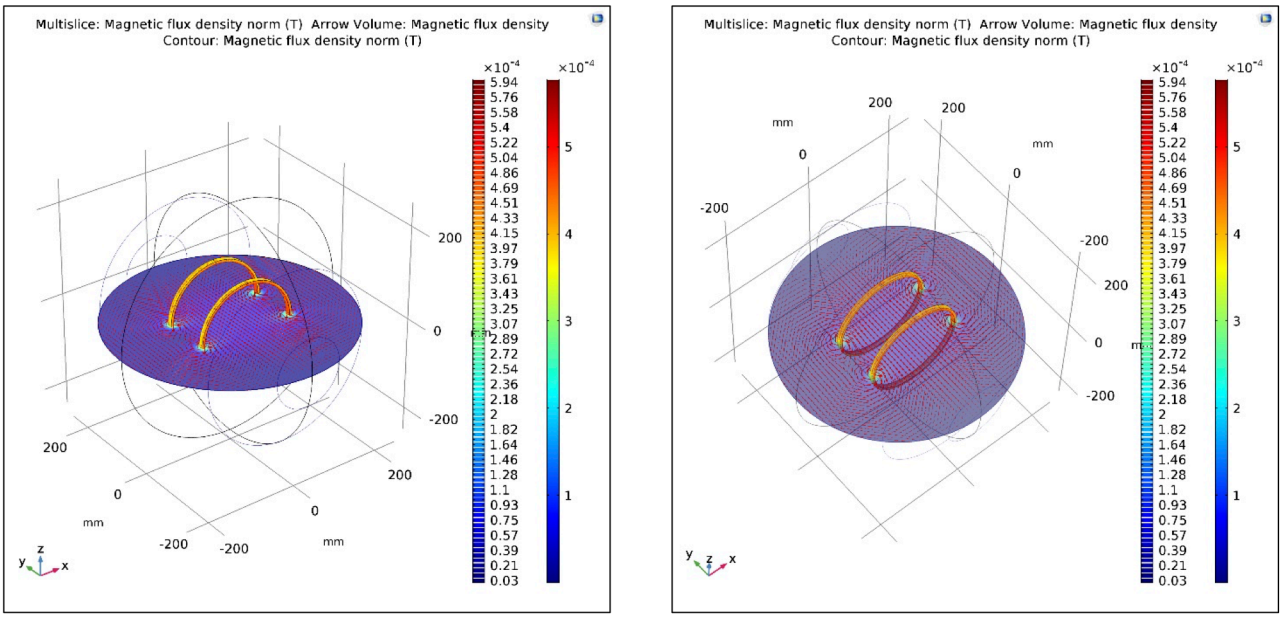

Figure 48: Magnetic flux density, second cutting plane

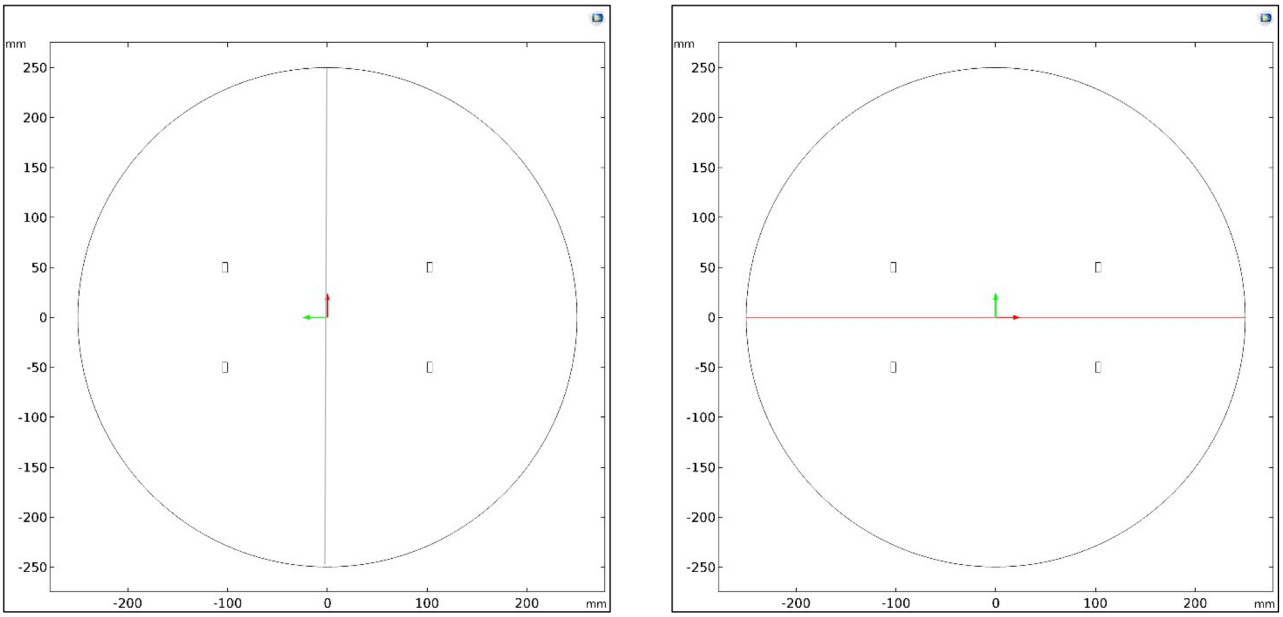

Figure 49: Cutting lines

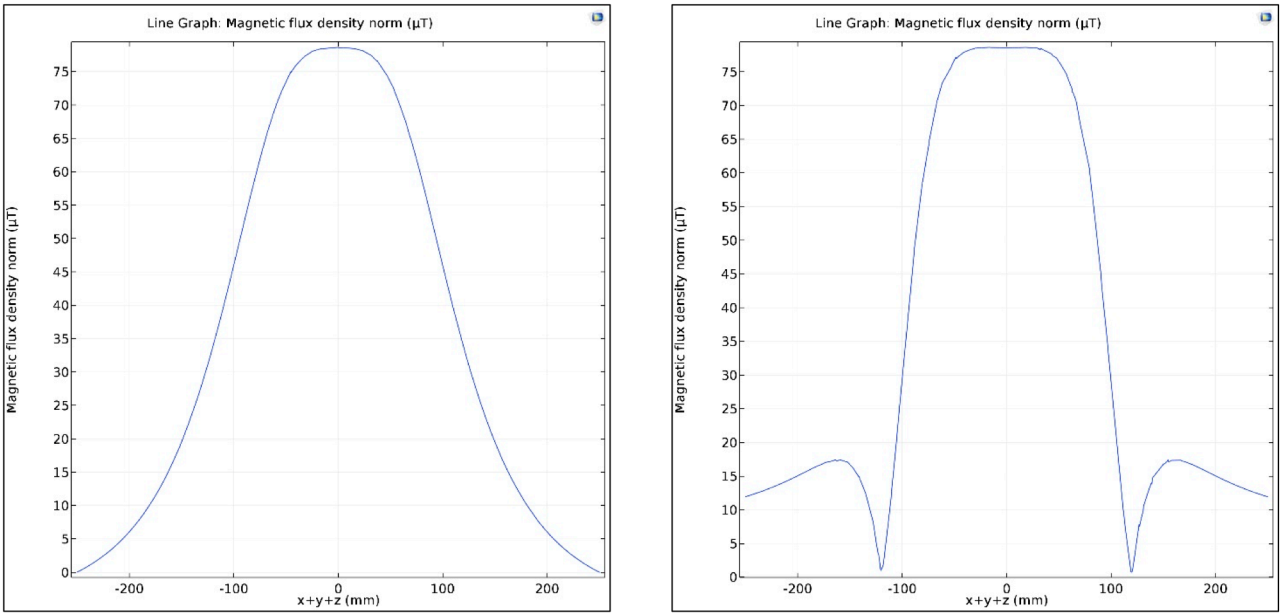

Figure 50: Magnetic field, second cutting plane

As discussed before, it is verified that the simulation data gives us the same results of the theory. The graph below compares the theory, expressed with yellow line, with the simulation data, represented with the red line. In this case results are quite similar and the error is 9,43% because it is due to the geometry, which considers rectangular shape for coils. Edges determine a non uniform magnetic field in the near space.

The table 2 in the Appendix reports the theory data, in which it is considered the Equation 1.20 demonstrated in the previous chapter. The distance along the cutting line is listed between -50 mm and 50 mm, because it is important to evaluate the part that gives the uniformity of the magnetic field.

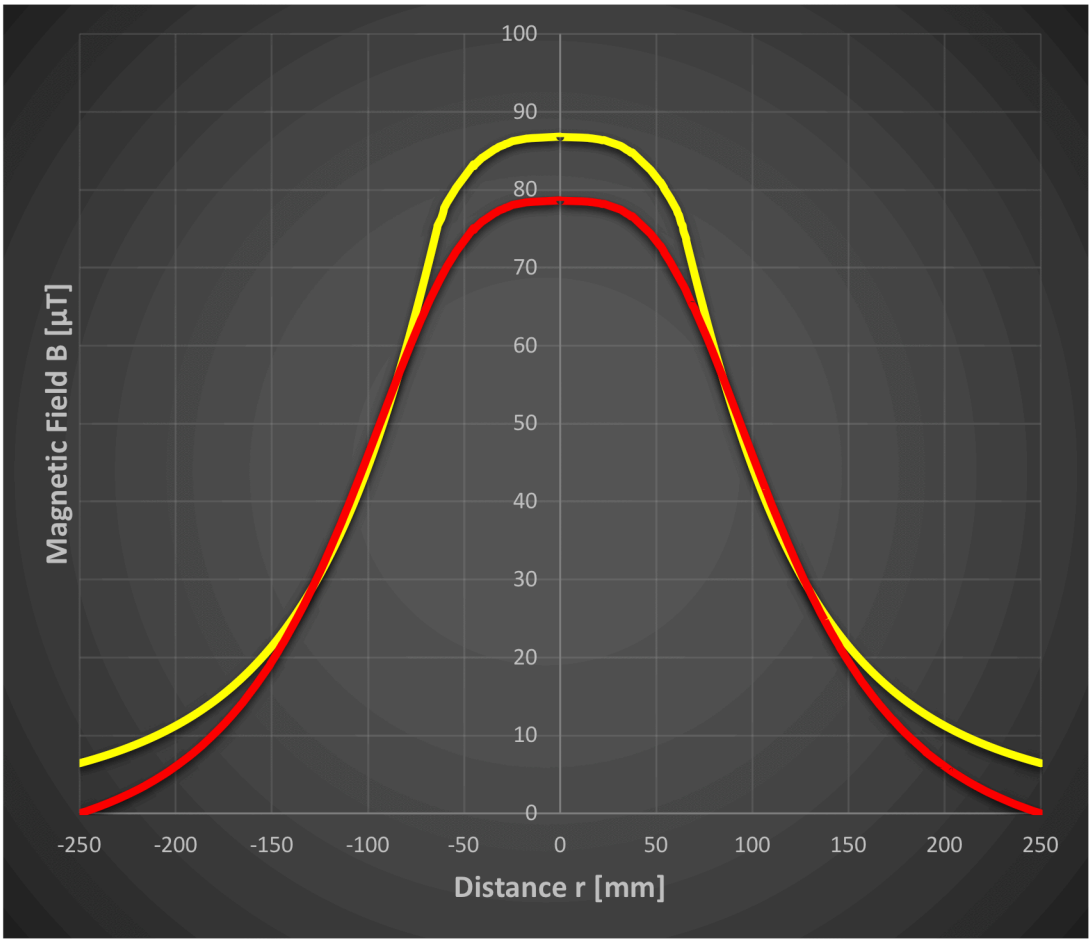

It is useful to establish the boundary condition and consequently the safety one, at the distance of 200 mm, where the magnetic field is null (Figure 51).

Errors in the simulation are surely due to mesh. In this simulation it is used a fine mesh (Figure 51) and it is avoided tetrahedral shape, which could invalidate results. The obtained error is around 10% as explained before when it is illustrated the comparison between theory and simulation data.

The error is calculated with the Equation 5.0

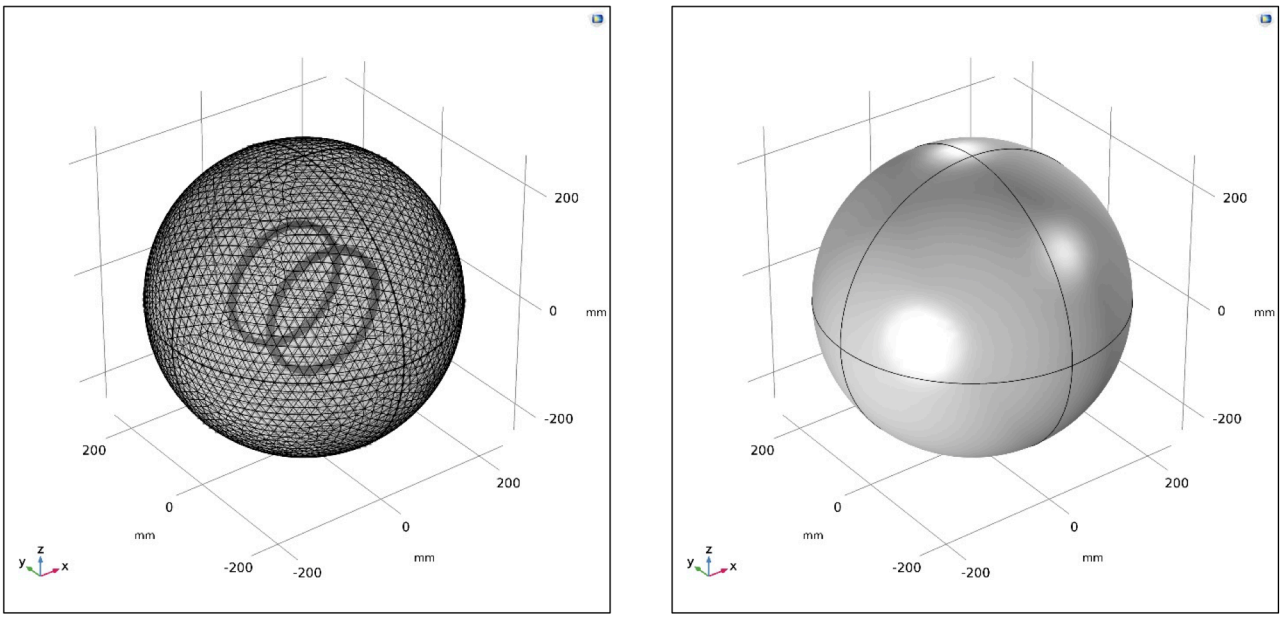

Figure 51: Mesh and boundary condition

5.3 Permanent Magnets

Permanent magnets could be considered an alternative to Helmholtz coils, because they produce the same effects. In this chapter the same setup of coils is simulated with these input parameters:

Name	Expression	Unit	Description
M	*10^6*	*[A/m]*	*Magnetization*
Br	*1,32*	*[T]*	*Remanence*
R	*30,00*	*[mm]*	*Outer Radius permanent magnet*
r	*3,00*	*[mm]*	*Inner Radius permanent magnet*
H	*30,00*	*[mm]*	*Height permanent magnet*
D	*100,00*	*[mm]*	*Distance permanent magnets*

Permanent magnets are fixed with different pole faces, thus the attraction is obtained. In the figure below the geometry of the permanent magnets is illustrated.

Sizes of magnets are the same used in the experimentation. In Chapter 9 there are more details about the experimental part.

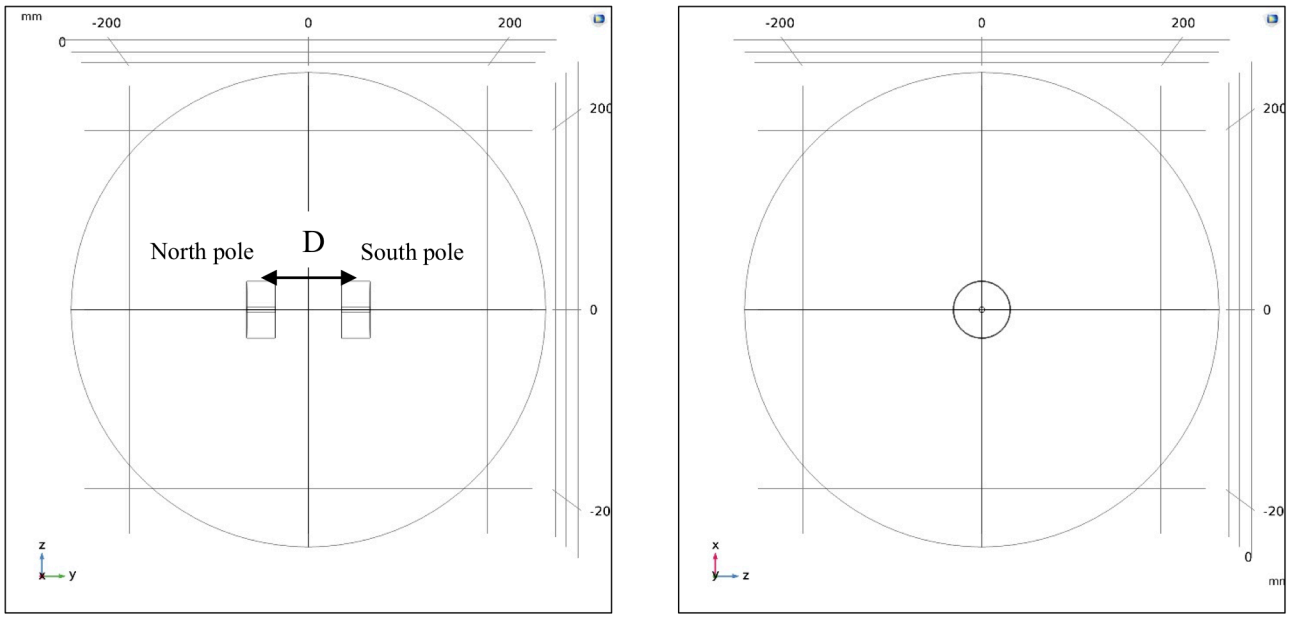

Figure 52: Geometry

Materials used in the simulation are:

- Neodymium for permanent magnets;
- Air around permanent magnets.

The figure shows the setup in coordinate system space.

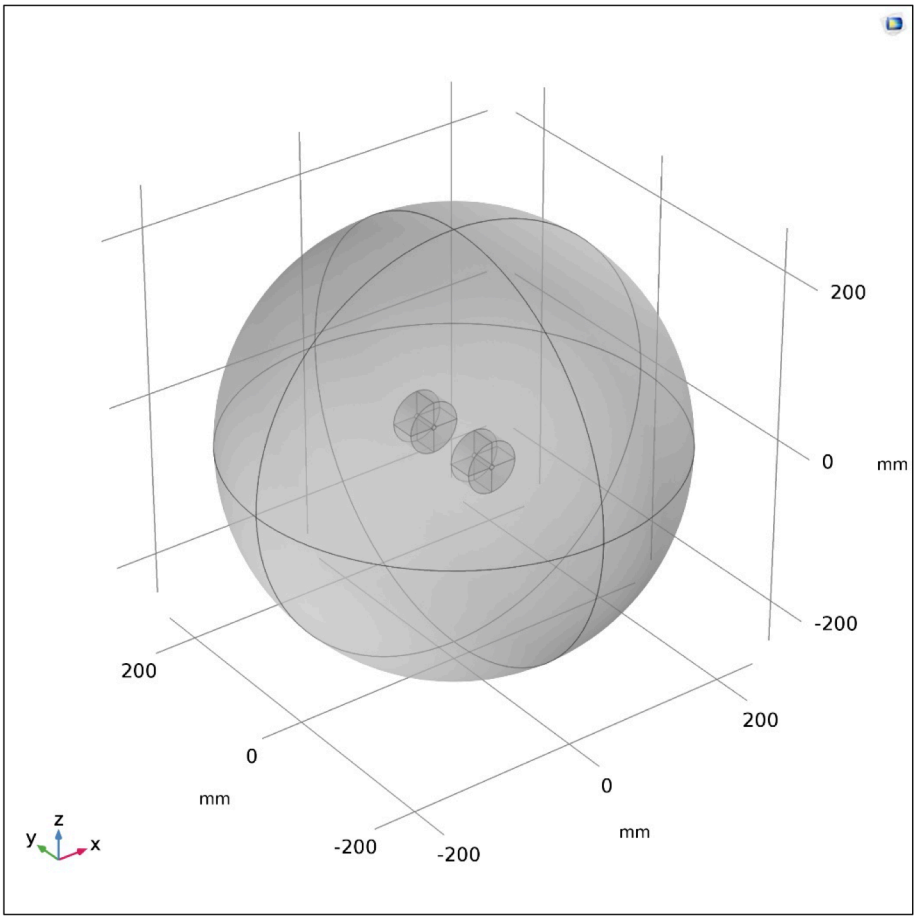

Figure 53: Setup of permanent magnets

When the current flows into the permanent magnets, it is possible to evaluate how the magnetic field is. In this view, there is a global representation with the two cutting planes, which are considered to evaluate the magnetic field.

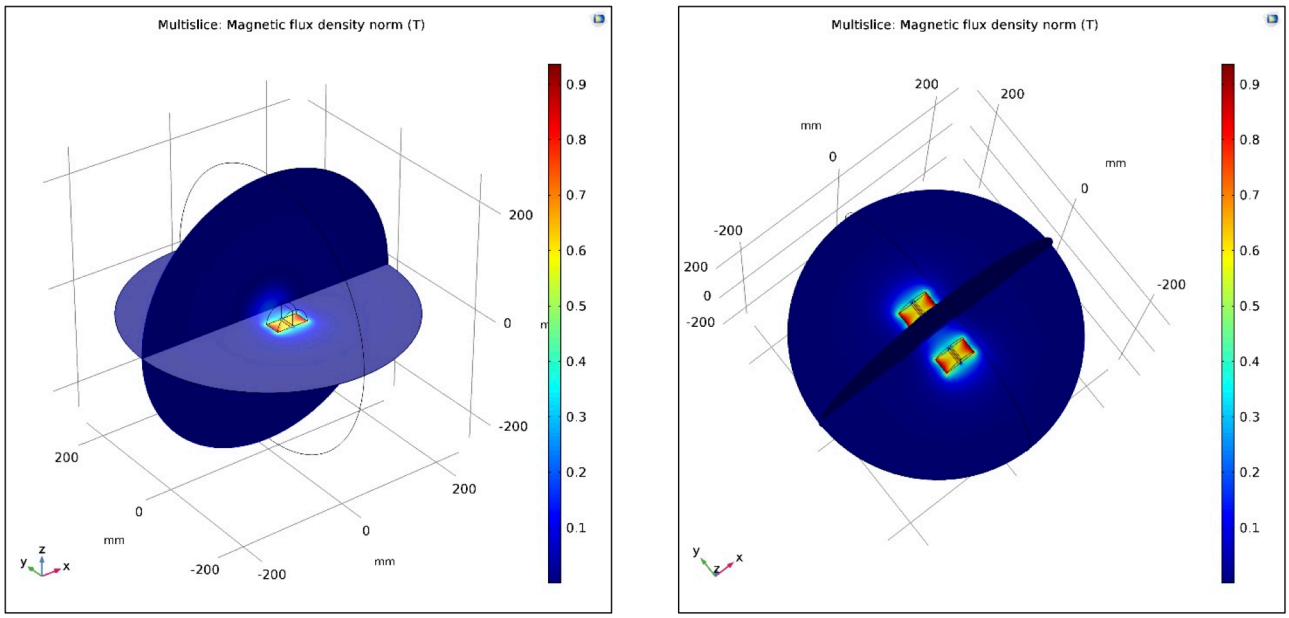

Figure 54: Magnetic field

The two cutting planes are:

- the first one is on ZX axis;
- the second one is on XY axis.

The first cutting plane is shown in Figure 55 rather arrows and contour, which represent the magnetic flux density, are illustrated in the Figure 56 and in the Figure 57.

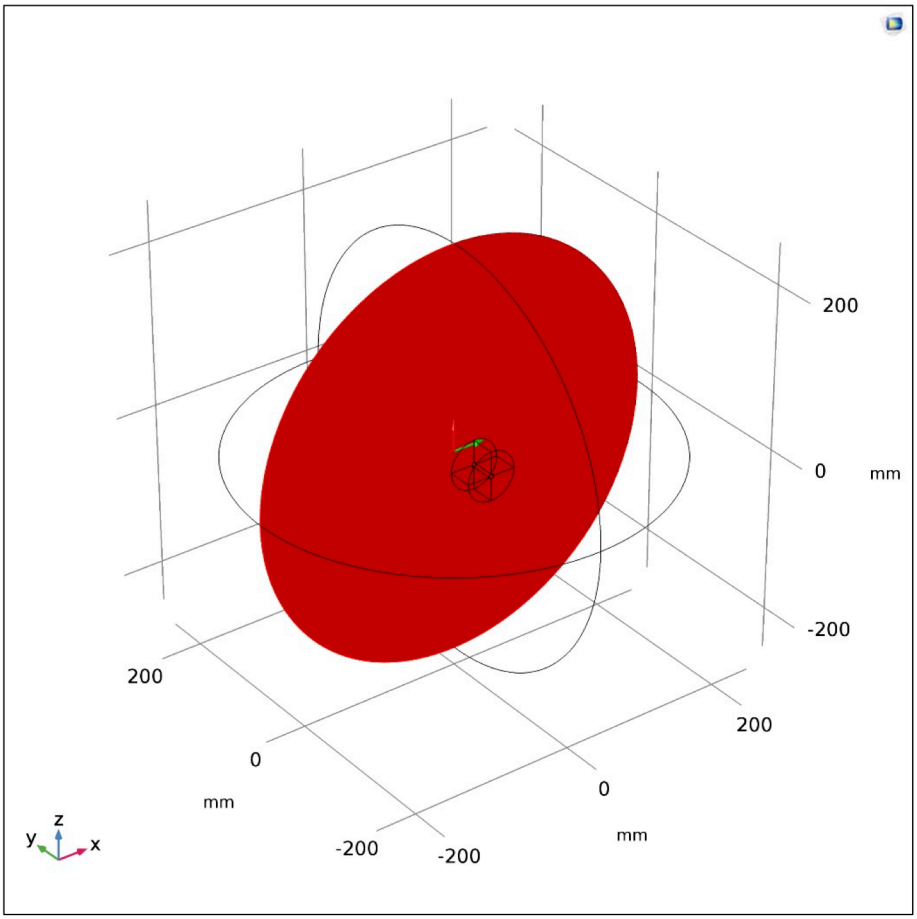

Figure 55: First cutting plane

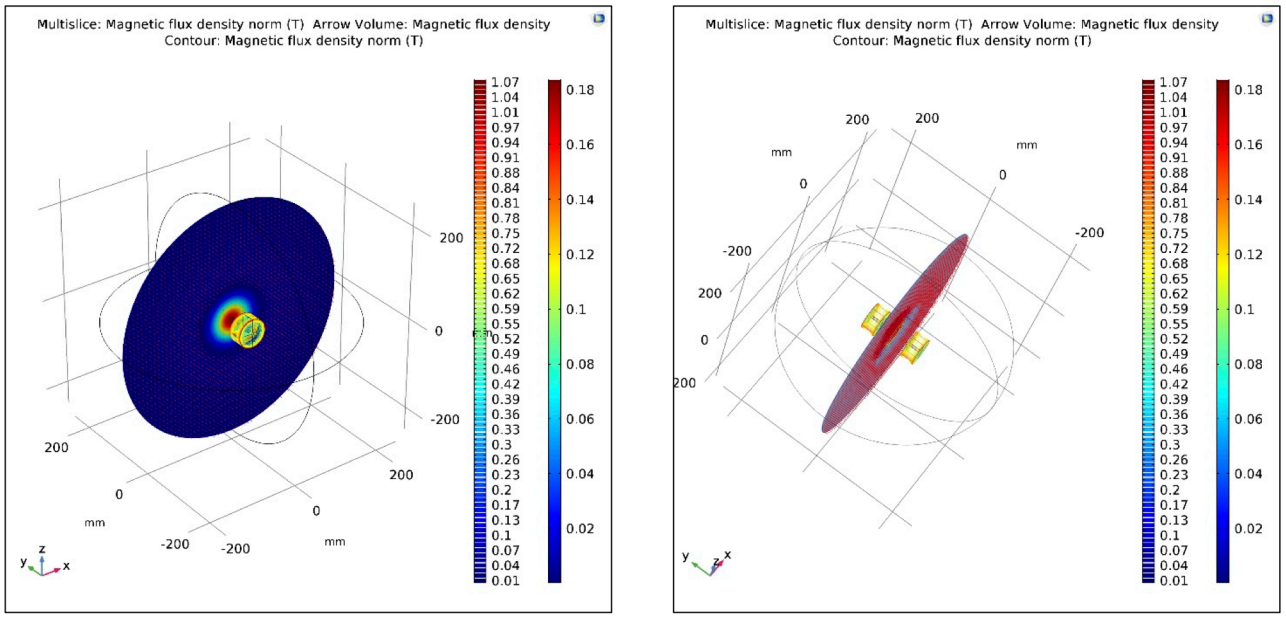

Figure 56: Magnetic flux density, first cutting plane

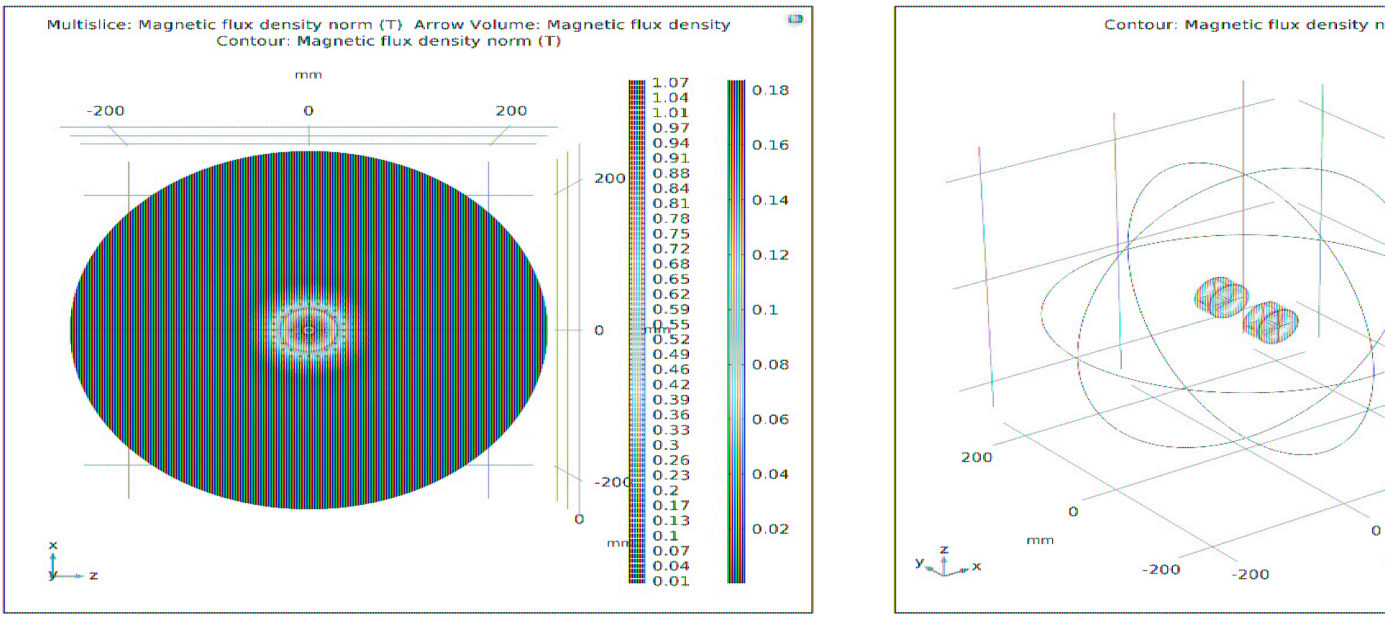

Figure 57: Magnetic flux density, first cutting plane

As investigated in the chapter before, two cutting lines are considered on the fir
the evaluation of the magnetic field. It is possible to note that if we compare the
Figure 59 the trend is quite similar. Surely, this last figure has a more acute line
because the geometry is different and the radius of the permanent magnets is smalle

Moreover here, it is reasonable to investigate the second cutting plane and to comp
with the theory, using the Equation 1.24.

For the first cutting line:

$$r = \sqrt{(x-0)^2 + (y-0)^2 + (z-0)^2}$$

$$x \neq 0, \qquad y = 0, \qquad z = 0$$

Instead for the second cutting line:

$$r = \sqrt{(x-0)^2 + (y-0)^2 + (z-0)^2}$$

$$x = 0, \qquad y = 0, \qquad z \neq 0$$

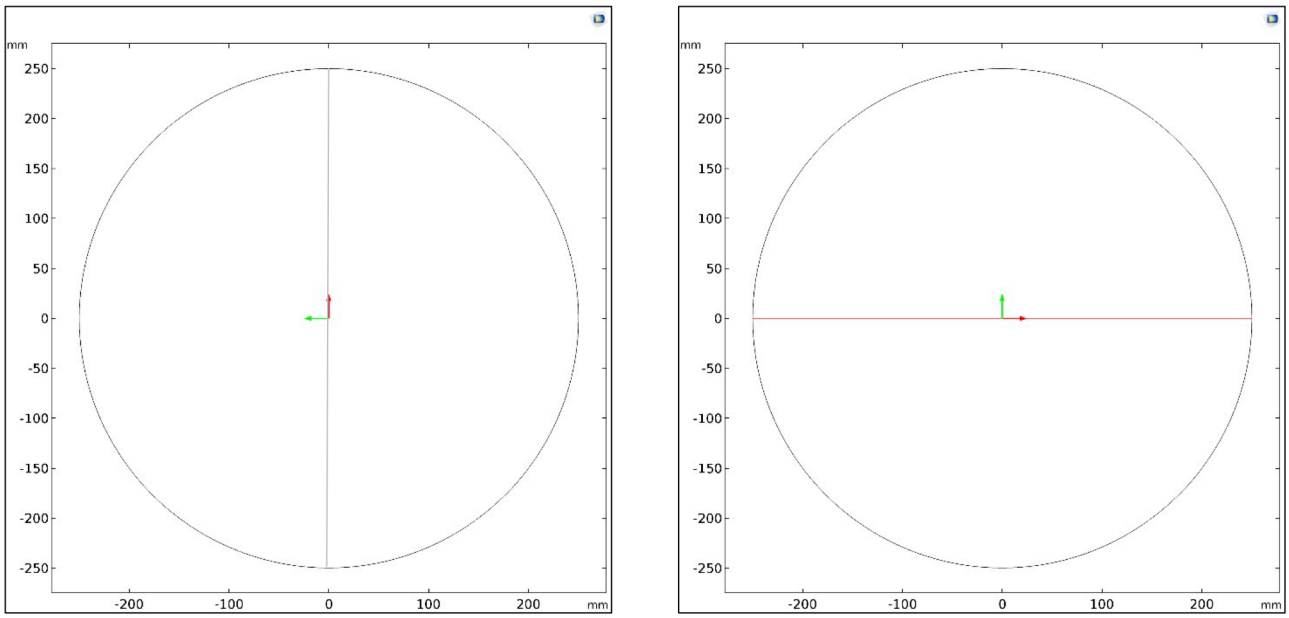

Figure 58: Cutting lines

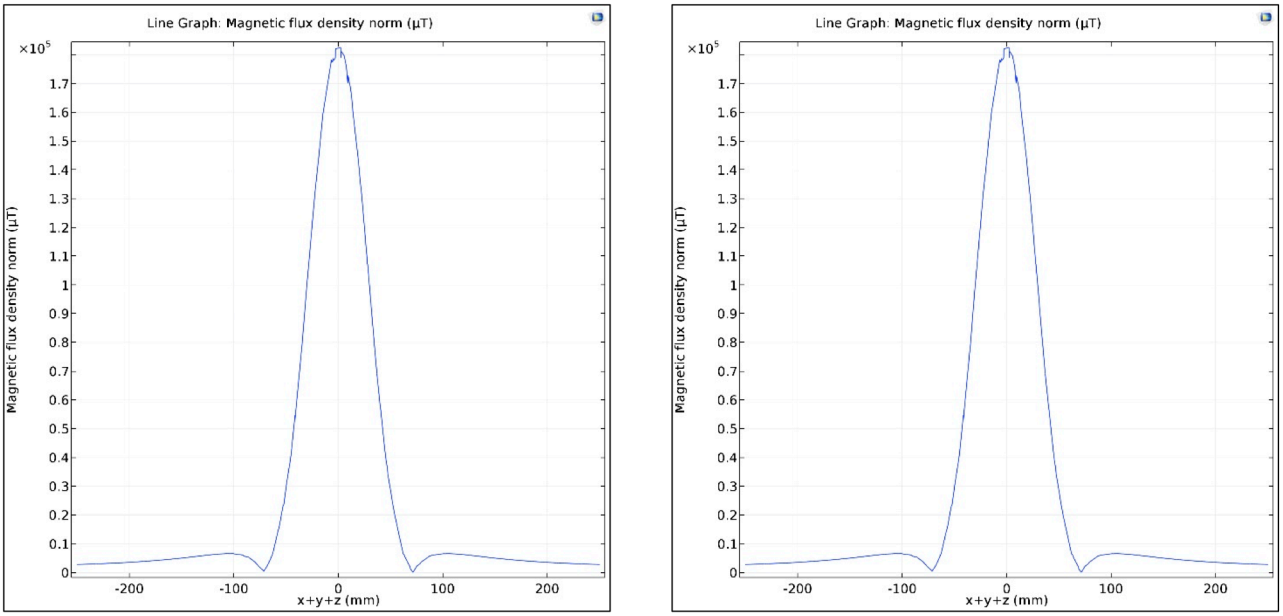

Figure 59: Magnetic field, first cutting plane

The Figure 60 shows the second cutting plane with the representation of the magnetic flux density using arrows and contour. This plane explains clearly how the magnetic field behaves. It is also interesting to see that there is not uniformity between two permanent magnets because their geometry is smaller than Helmholtz coils and the distance is bigger than the radius. To obtain a uniform magnetic field it is useful to find the right distance, investigated in the following chapters, between two components. Also here, it is possible to see that the direction and side of the magnetic field are on the Y axis. As explained for Helmholtz coils, the composition of this field with the magnetic one of the wire determines the Wiedmann's effect.

The Figure 61 and the Figure 62 illustrate how the trend of the magnetic field is, if two cutting lines are considered. The trend, reported on the left of figures mentioned before, demonstrates that it is approximately the same of the theory. The error is around 30% in the middle between two permanent magnets.

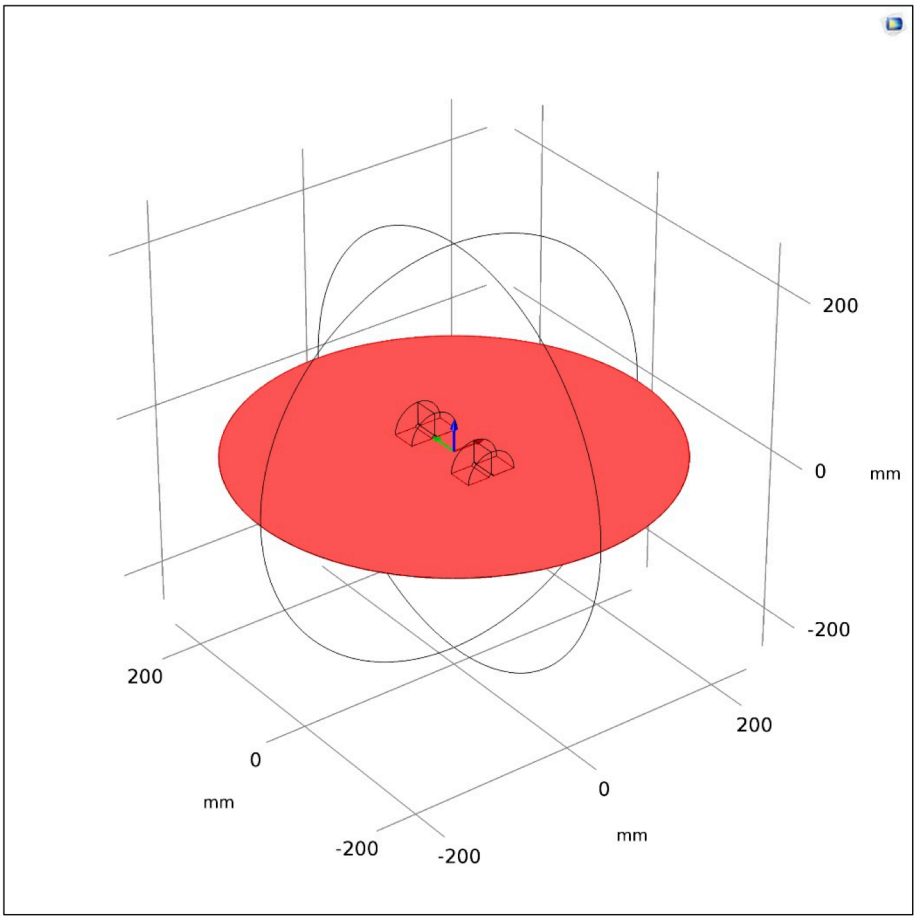

Figure 60: Second cutting plane

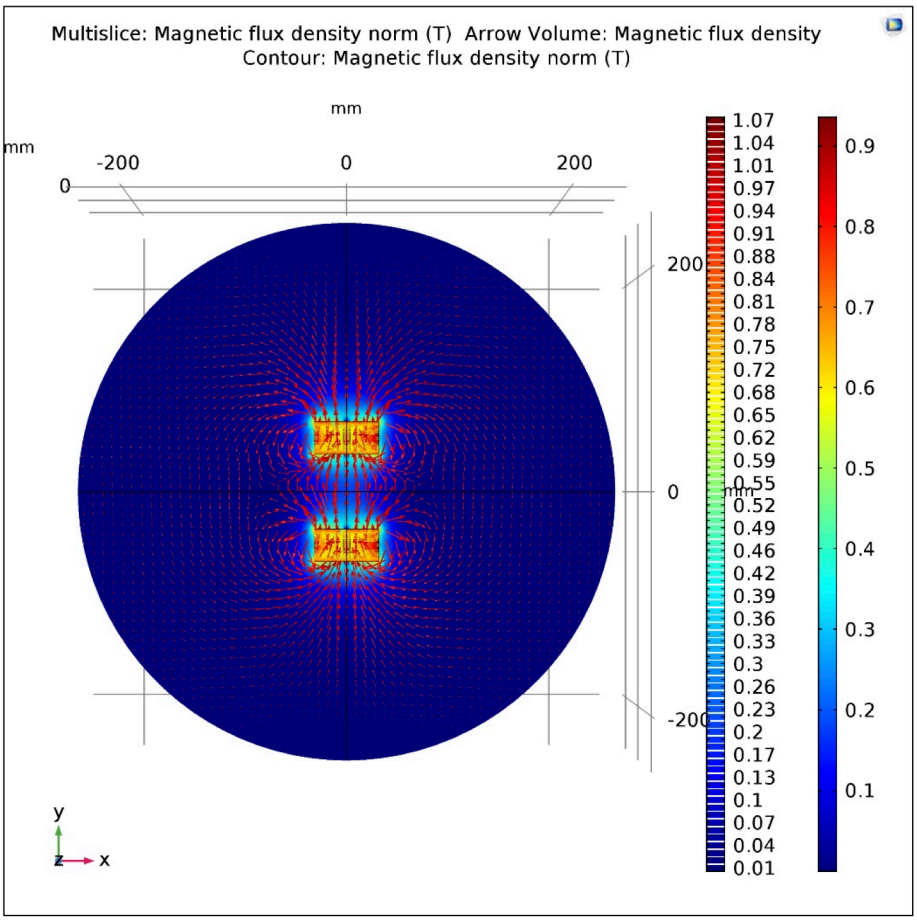

Figure 61: Magnetic flux density, second cutting plane

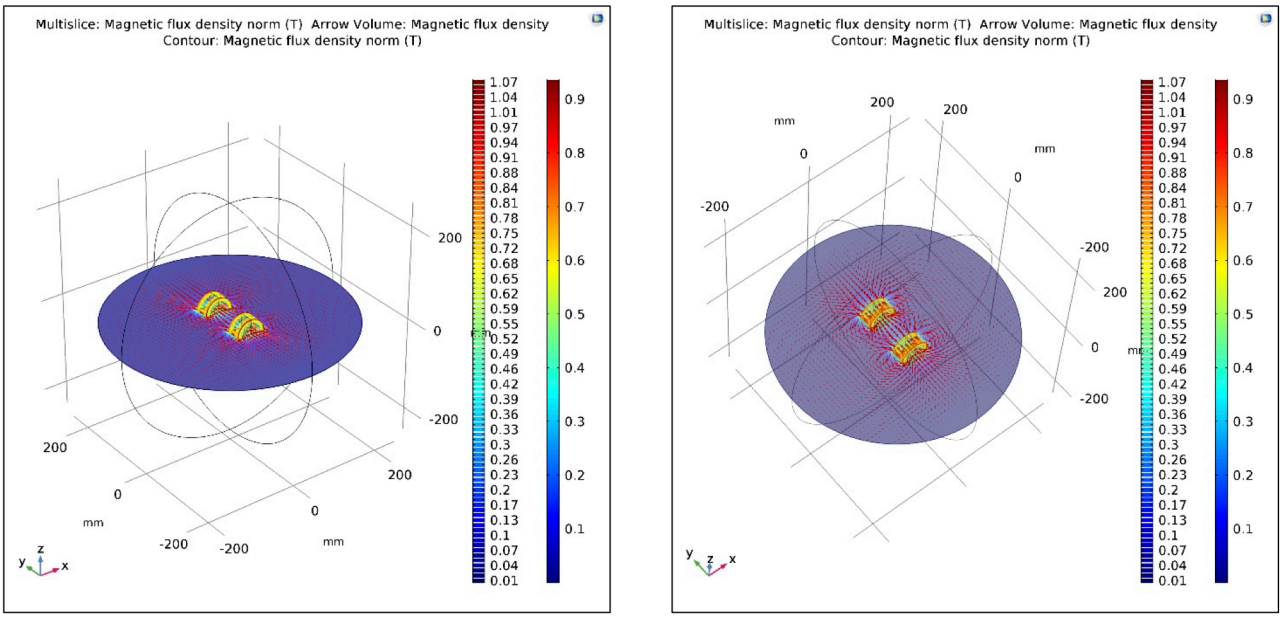

Figure 62: Magnetic flux density, second cutting plane

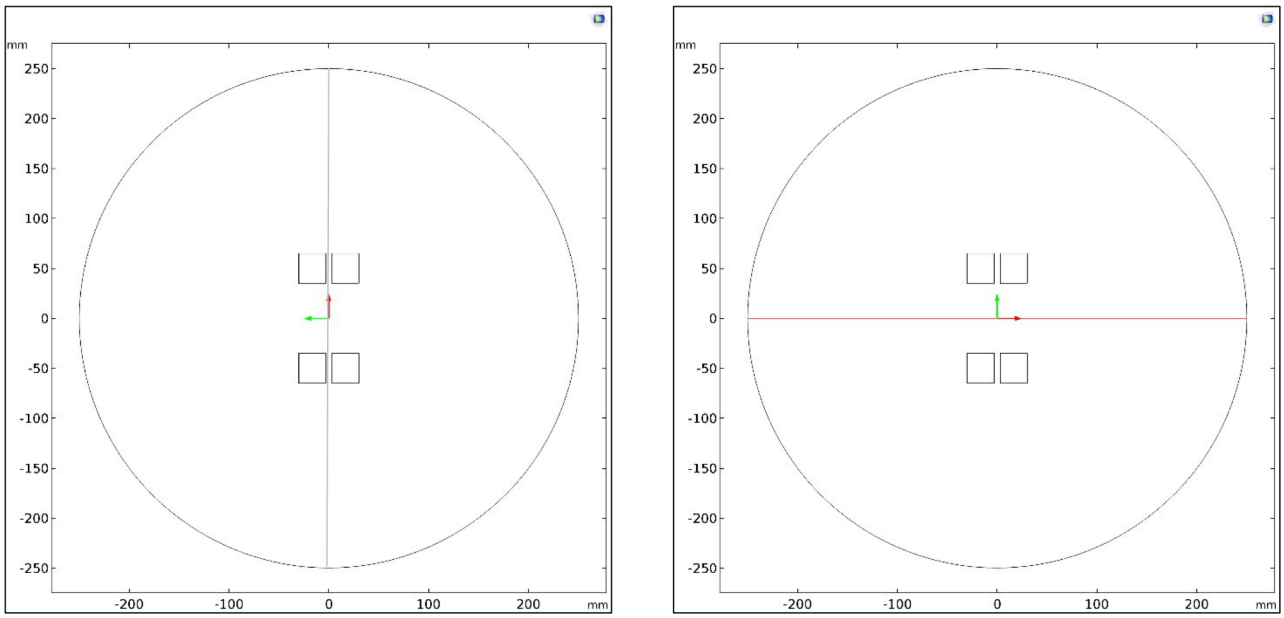

Figure 63: Cutting lines, second cutting plane

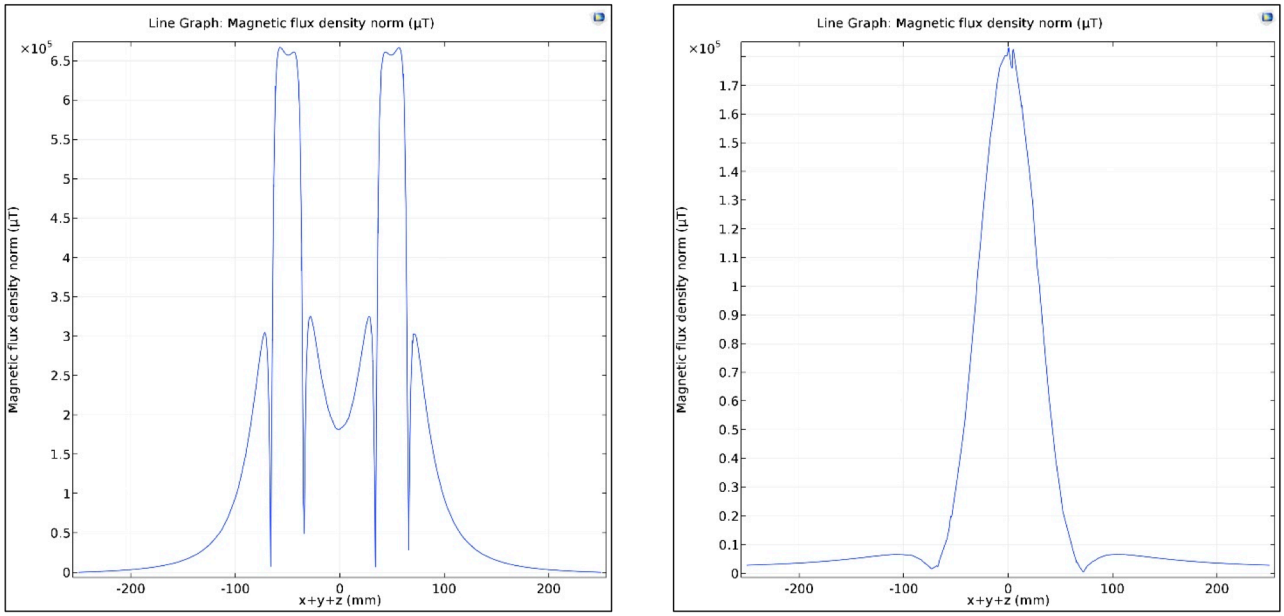

Figure 64: Magnetic field, second cutting plane

As discussed before, it is verified that the simulation data gives us the same results of the theory: the graph below compares the theory with the simulation data. The yellow line is associated with the theory instead the red line represents the simulation data. Results are quite similar and the error is approximately 30% because geometry considers small rectangular shape for the permanent magnets:

edges and distance between them determine a non uniform magnetic field in the near space, influencing so much the error.

The table 3 in the Appendix reports the theory data, in which it is considered the Equation 1.24 demonstrated in the previous chapter. It is possible to examine the distance between permanent magnets from -50 mm to 50 mm for coherence with results obtained by Helmholtz coils.

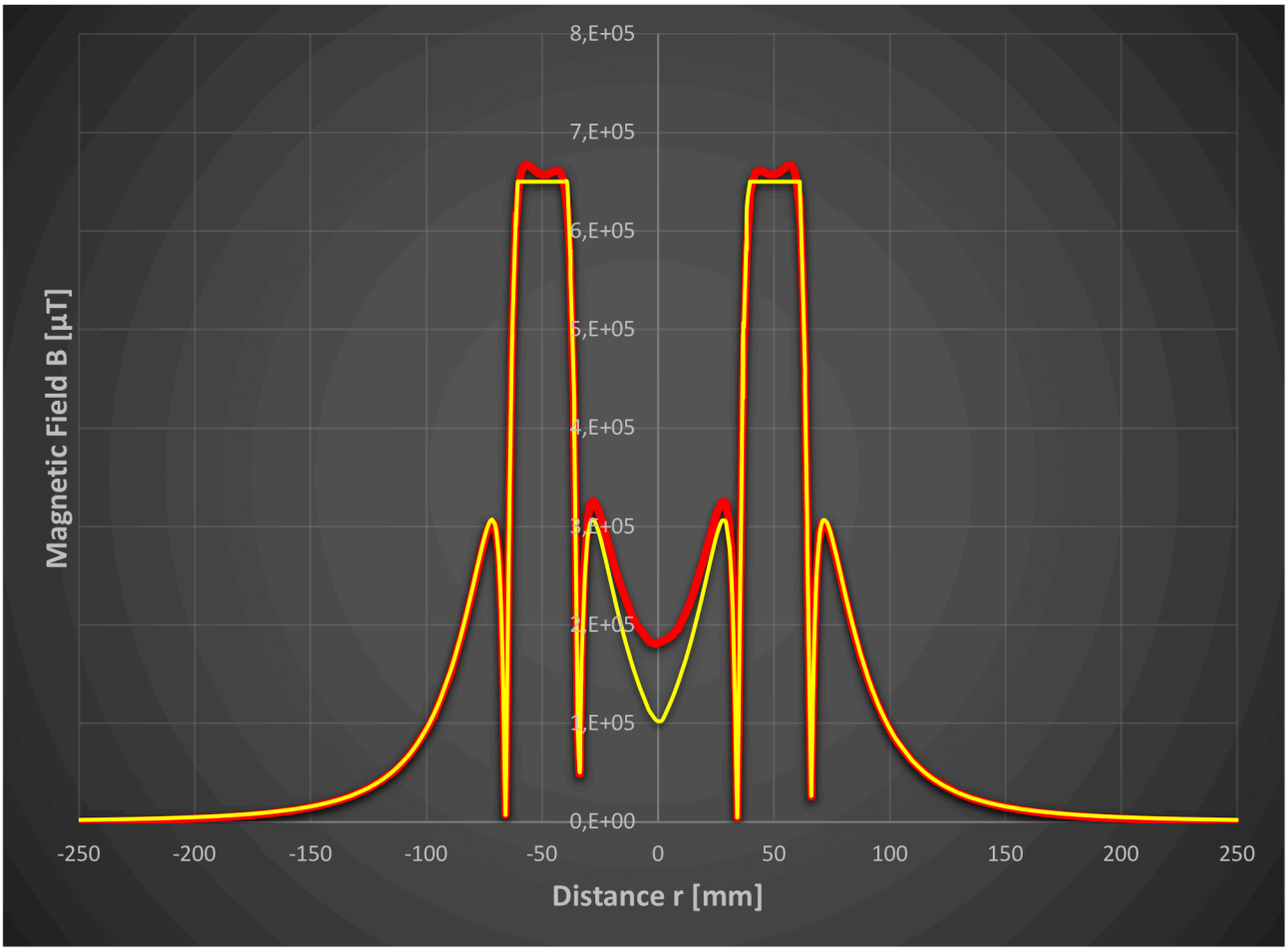

As considered in the chapter before, it is useful to establish the boundary condition when the magnetic field is null (Figure 65). The safety condition could be at the same distance of 200 mm, as considered for coils.

Errors in the simulation are surely due to mesh but in this case high values are caused by sizes and geometry of permanent magnets. In this simulation a fine mesh (Figure 65) is built and the tetrahedral shape, which could invalidate results, is avoided. Error obtained is around 30%, as discussed when

the comparison between theory and simulation data is illustrated, and it is possible to reduce it if we consider other geometries.

Error is calculated with the Equation 5.0 in the same way of coils.

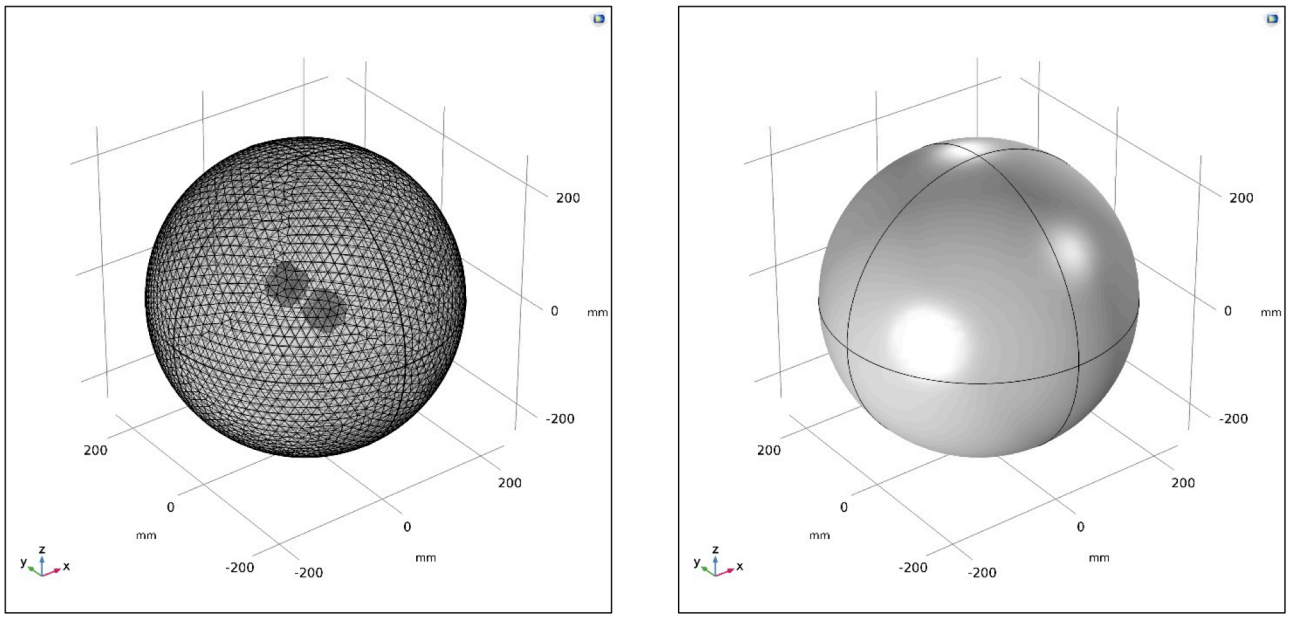

Figure 65: Mesh and boundary condition

6.0 Assembling Components: Magnetic Actuation Systems

In this chapter it is studied how a Magnetic Actuation System works, investigating two different setups:

- Helmholtz coils and wire;
- permanent magnets and wire.

It is discussed the work of the magnetic actuator and what is the aim of this study. The first step is to define the magnetic field behavior, because after we have to research how the sample of smart material twists. This last one is obtained with the sum of the magnetic field of the wire and the magnetic field of Helmholtz coils or permanent magnets. The relation is:

$$\overrightarrow{B_{sm}} = \overrightarrow{B_{Hc}} + \overrightarrow{B_w} \tag{6.0}$$

$$\overrightarrow{B_{sm}} = \overrightarrow{B_{pm}} + \overrightarrow{B_w} \tag{6.1}$$

where $\overrightarrow{B_{sm}}$ is the magnetic field of the smart material, $\overrightarrow{B_{Hc}}$ is the magnetic field of Helmholtz coils, $\overrightarrow{B_{pm}}$ is the magnetic field of permanent magnets and $\overrightarrow{B_w}$ the magnetic field of the wire.

If the second cut plane is considered, it is clear that the wire has only the $\overrightarrow{B_z}$ component not null and Helmholtz coils or permanent magnets have $\overrightarrow{B_y}$ component not null. The composition of these components define the Wiedmann's effect which causes the twist of the smart material. The torsion is considered with the reference to theory explanation and Maxwell tensor is useful to calculate forces which act on the smart material. The maximum angle of the torsion is determined in this way:

$$\vartheta = arctg\left(\frac{T_z}{T_y}\right) \tag{6.2}$$

where T_z is the torsion on Z axis and T_y is the torsion on Y axis.

The distance between two Helmholtz coils or permanent magnets, the density of the current, which flows inside the wire, and the remanence field are fundamental because they are linked to $\overrightarrow{B_{sm}}$ so that also values of torsion, which depends on relative permeability of the material, with its angle ϑ are noticeable. The stress of the smart material is calculated referring to Von Mises' law and it is an important parameter to evaluate a global behavior of the material.

6.1 Helmholtz Coils and Wire

In this chapter it is investigated how the magnetic field is, if we consider two Helmholtz coils and a wire currying current. Firstly, results about wire and Helmholtz coils are explained, but when these components work together it requires more attention, for this reason the next step is the evaluation of the smart material behavior. The geometry is in Figure 66 and the input parameters are:

Name	Expression	Unit	Description
Helmholtz Coils			
i	*1,00*	*[A]*	*Current*
L	*5,00*	*[mm]*	*Length coil*
H	*10,00*	*[mm]*	*Height coil*
R	*100,00*	*[mm]*	*Radius coil*
D	*100,00*	*[mm]*	*Distance coils*
N	*10*	*/*	*Windings*
i_{tot}	*i*N*	*[A]*	*Current tot*
Wire			
i	*1,00*	*[A]*	*Current*
j	$i/(\pi R^2)$	$[A/m^2]$	*Density current*
R	*1,00*	*[mm]*	*Radius wire*
L	*250,00*	*[mm]*	*Length wire*

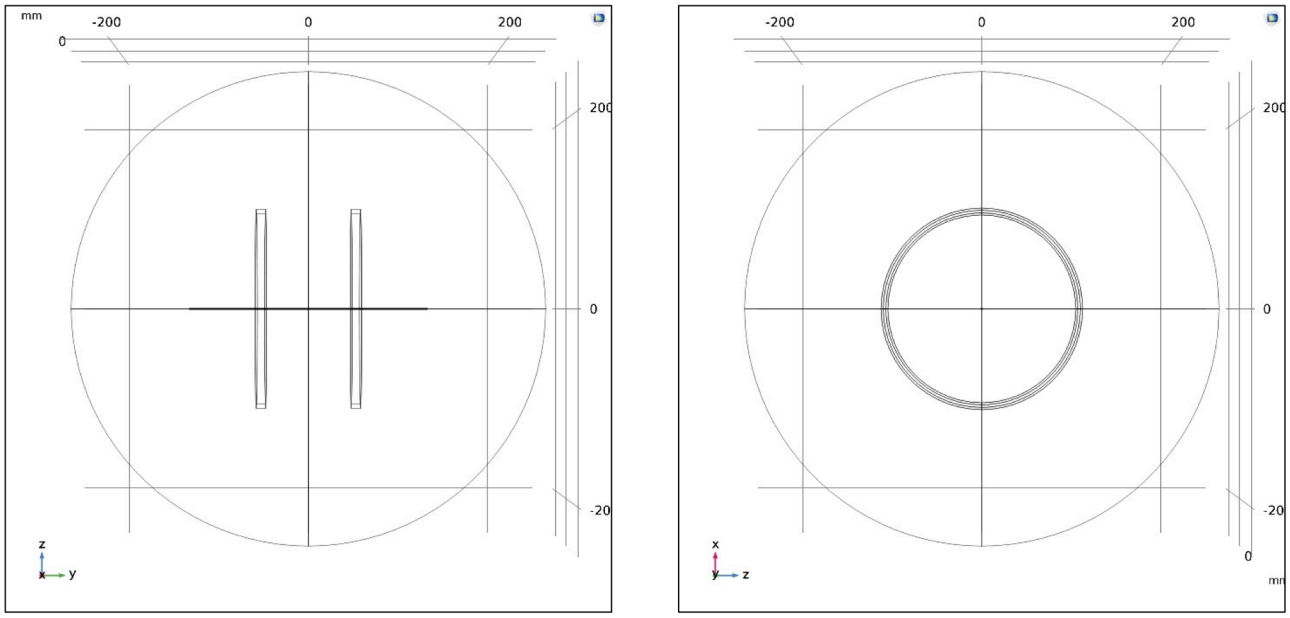

Figure 66: Geometry

Materials used in the simulation are:

- Iron Powder SMP1172 for the coils ($\mu r = 1\ H/m$);
- Copper for the wire;
- Air around the components.

The Figure 67 shows the setup in coordinate system space. In the Figure 68 there is a global representation with the two cutting planes considered.

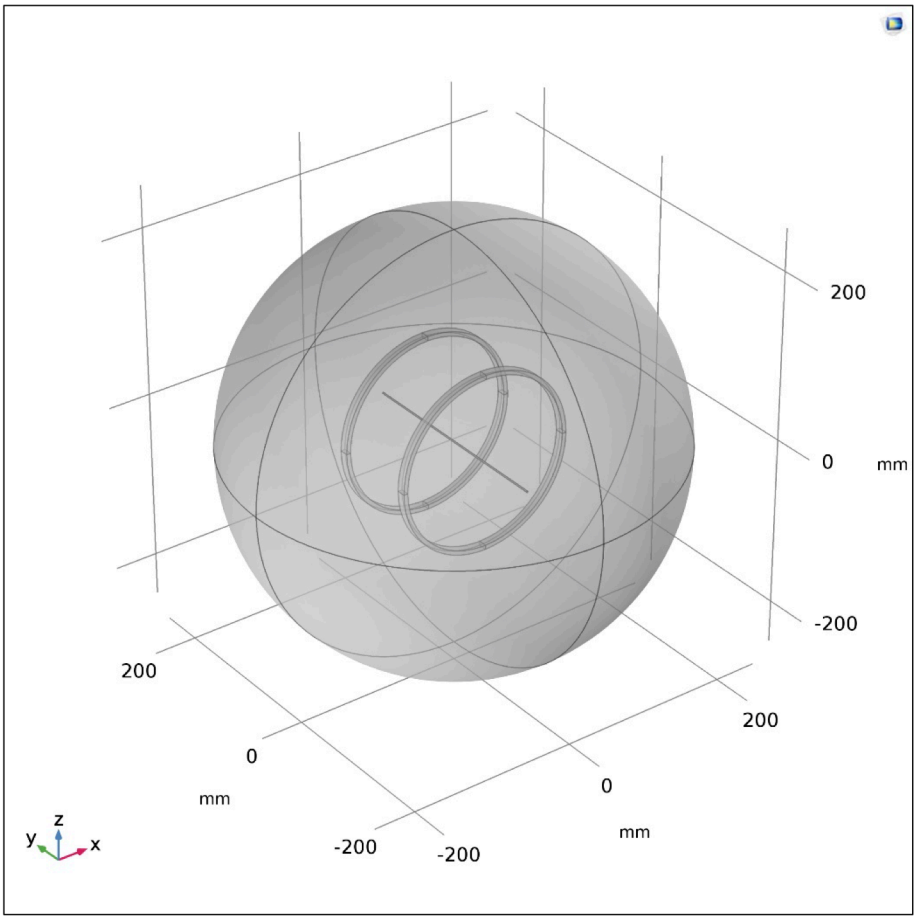

Figure 67: Setup of Helmholtz coils and wire

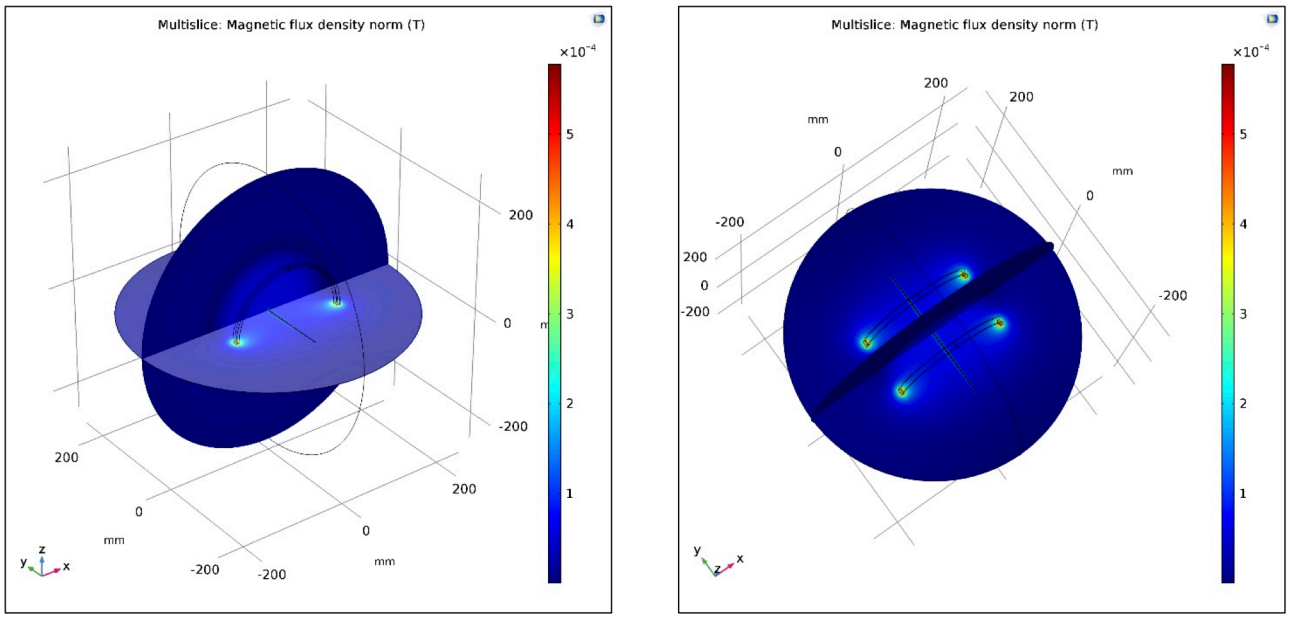

Figure 68: Magnetic field

The application of two cutting planes considers:

- the first one is on ZX axis;
- the second one is on XY axis.

The first cutting plane is shown in the figure below with the magnetic flux density in the Figure 70 and in the Figure 71.

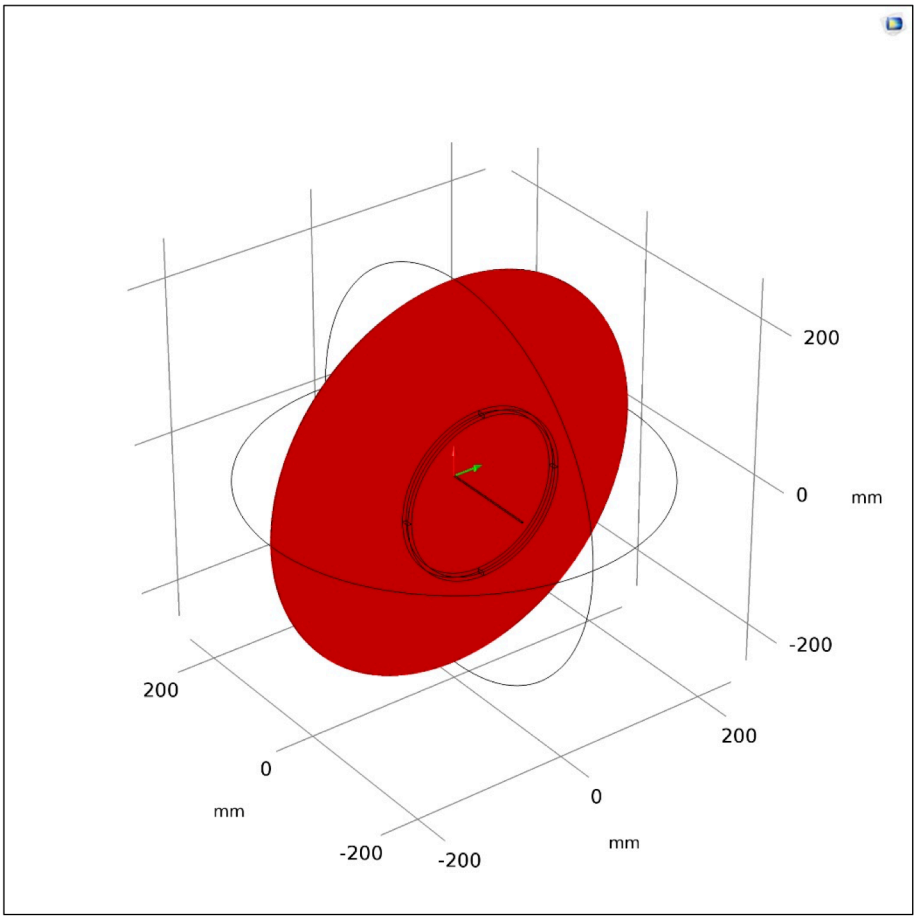

Figure 69: First cutting plane

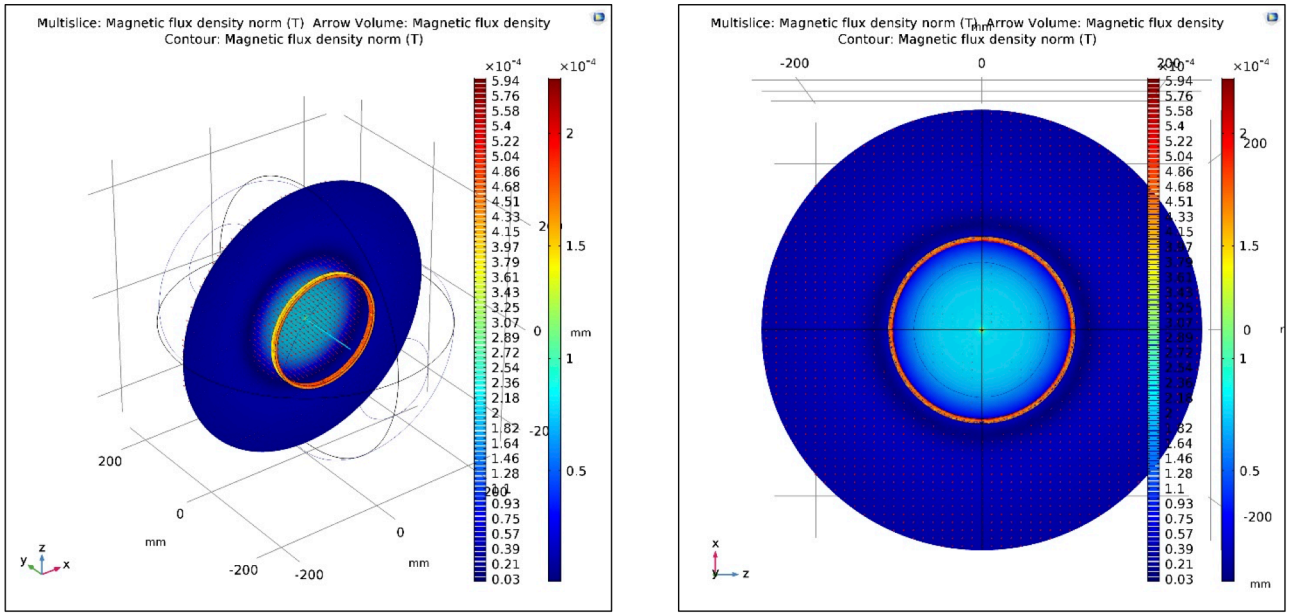

Figure 70: Magnetic flux density, first cutting plane

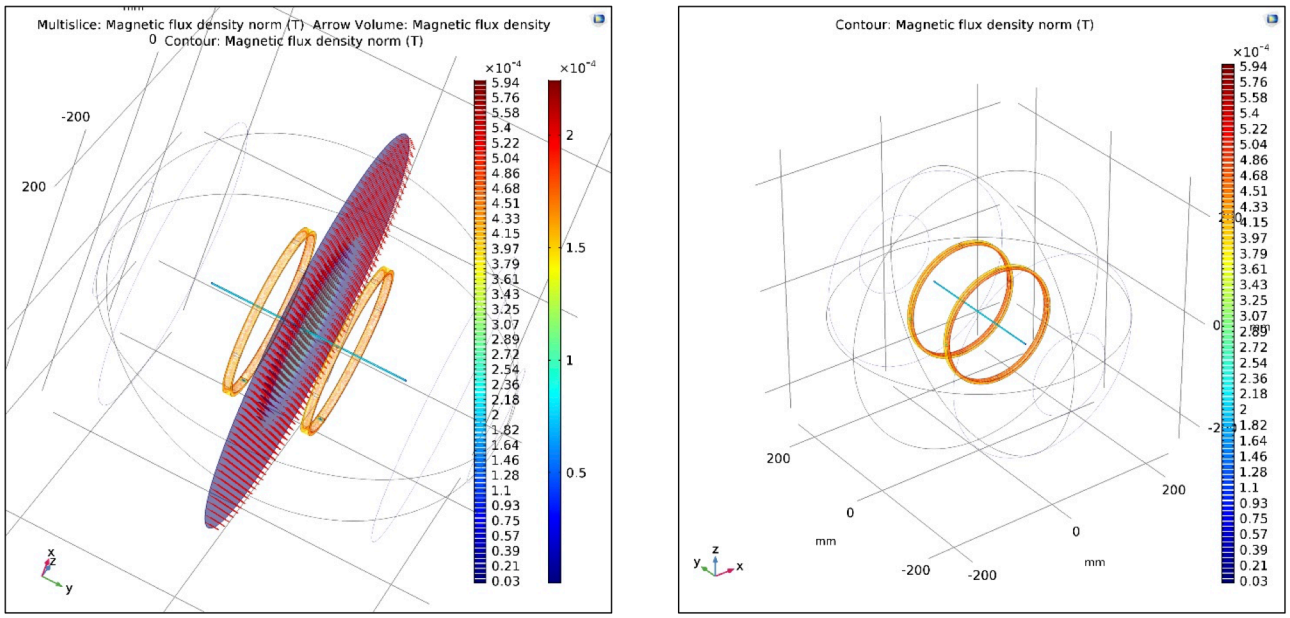

Figure 71: Magnetic flux density, first cutting plane

As investigated for Helmholtz coils, two cutting lines on the first cutting plane are considered for the evaluation of the magnetic field. It is possible to consider how the magnetic field of the wire with the magnetic field of coils is.

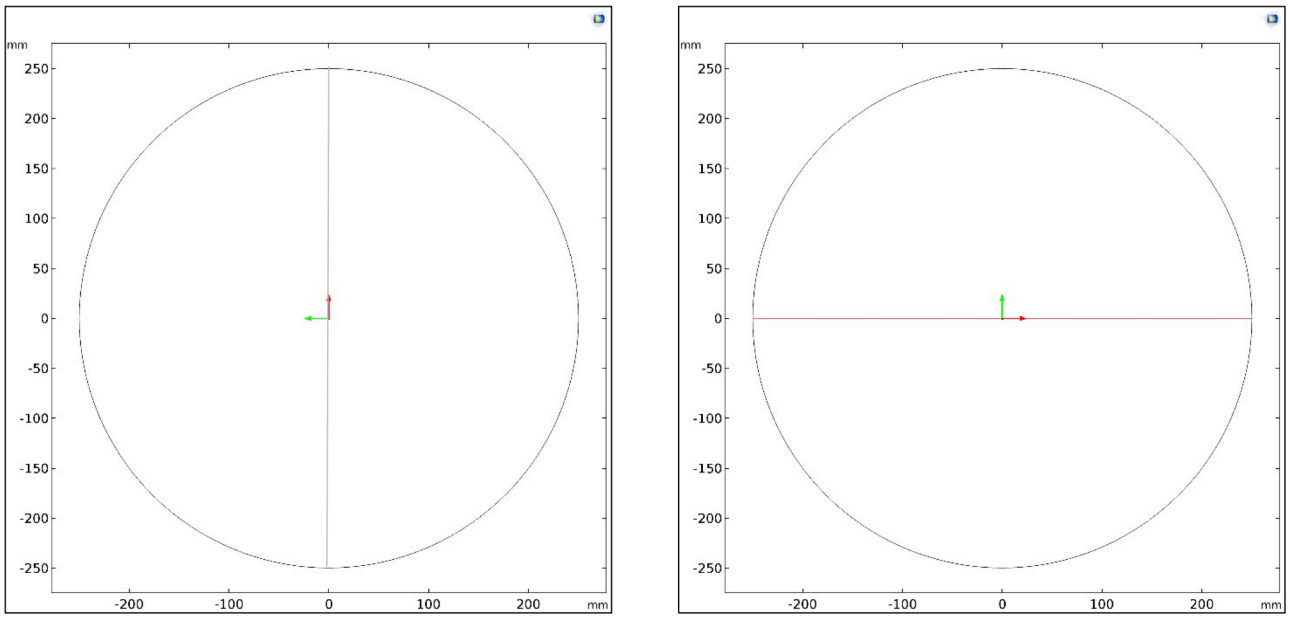

Figure 72: Cutting lines, first cutting plane

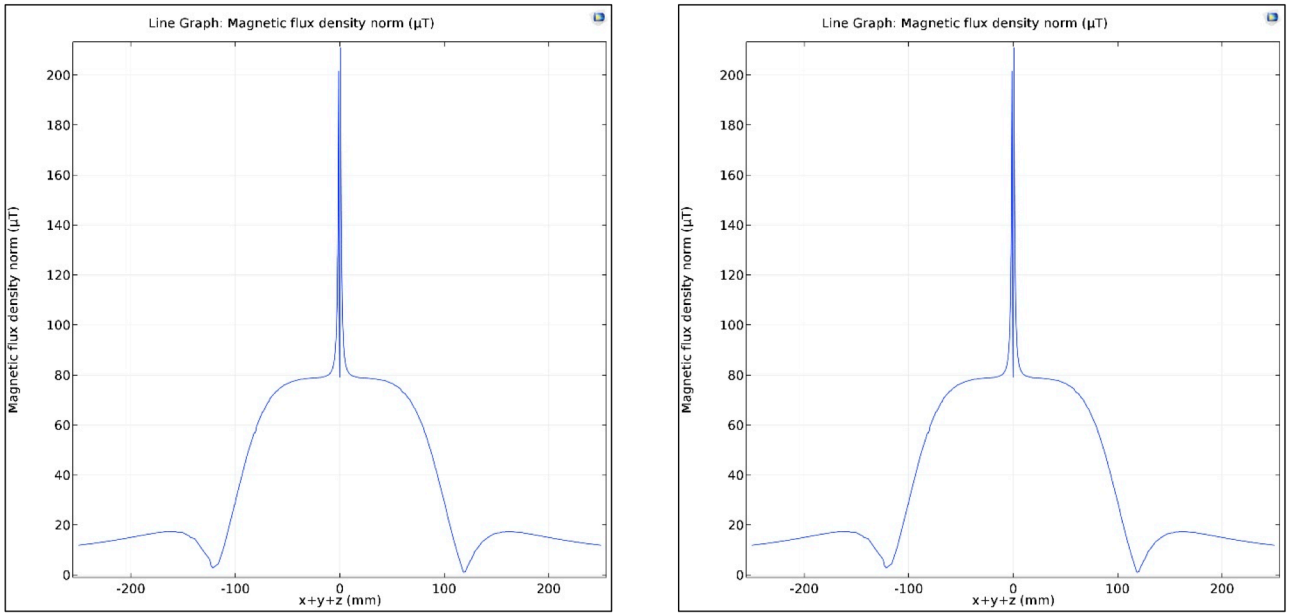

Figure 73: Magnetic field, first cutting plane

The Figure 74 shows the second cutting plane with the representation of the magnetic flux density, using arrows and contour: this plane explains in clear way how the trend of the magnetic field is. It is also interesting to see that there is uniformity between two coils, so that this demonstrates the coherence with the Helmholtz coils simulation, made before.

The Figure 76 illustrates that the composition of the magnetic field of coils with the magnetic field of wire creates Wiedmann's effect. If a sample of smart material around the wire is fixed we could see that it twists.

The Figure 77 and the Figure 78 illustrate how is the trend of the magnetic field if are considered two cutting lines.

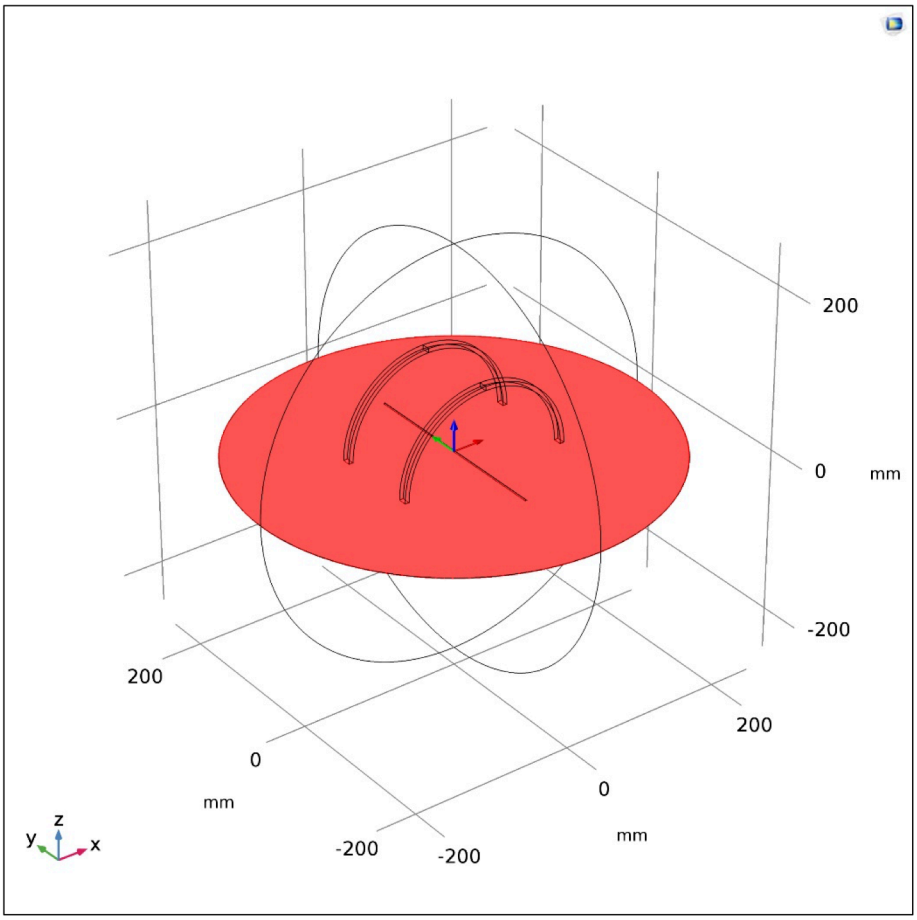

Figure 74: Second cutting plane

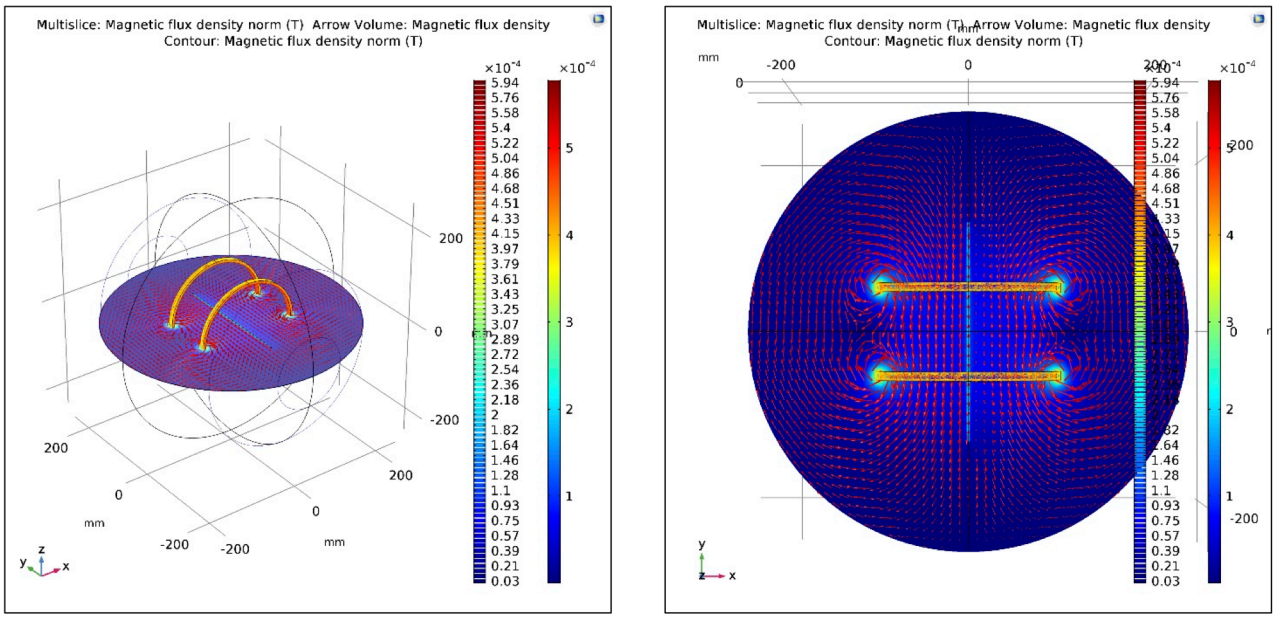

Figure 75: Magnetic flux density, second cutting plane

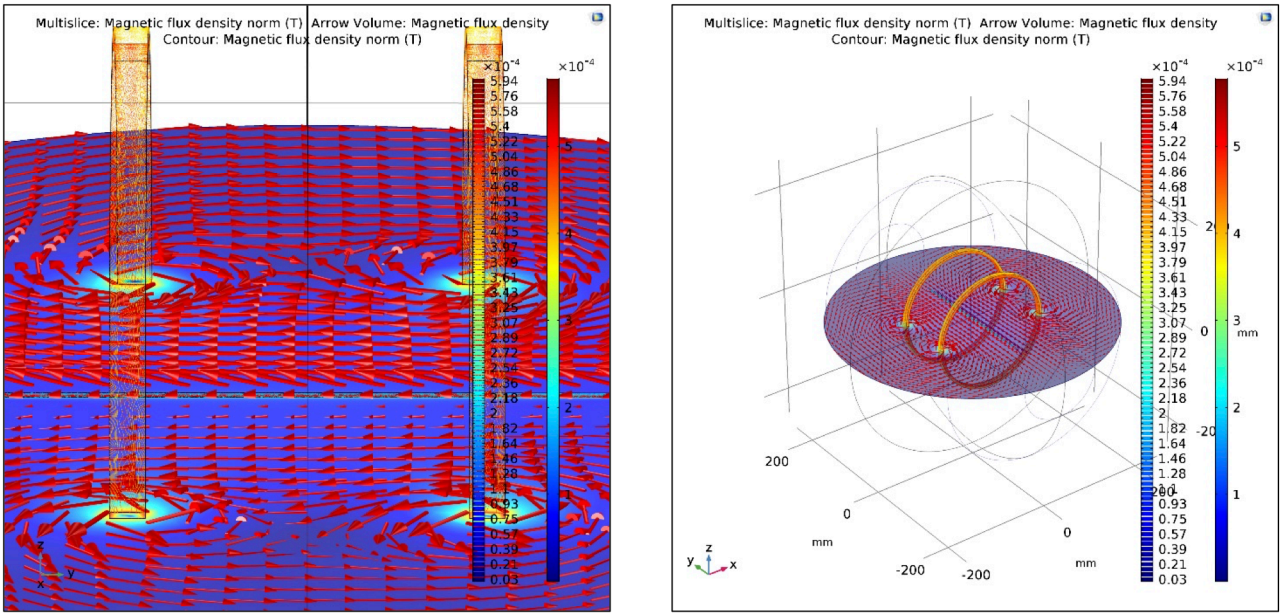

Figure 76: Magnetic flux density, second cutting plane

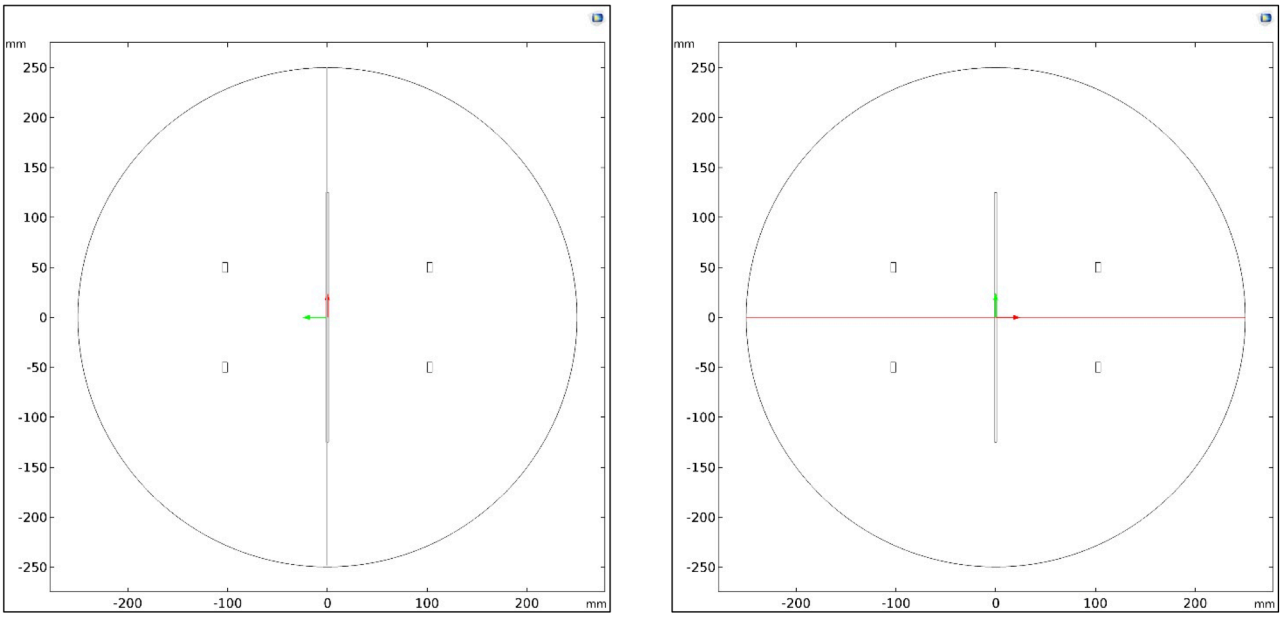

Figure 77: Cutting lines, second cutting plane

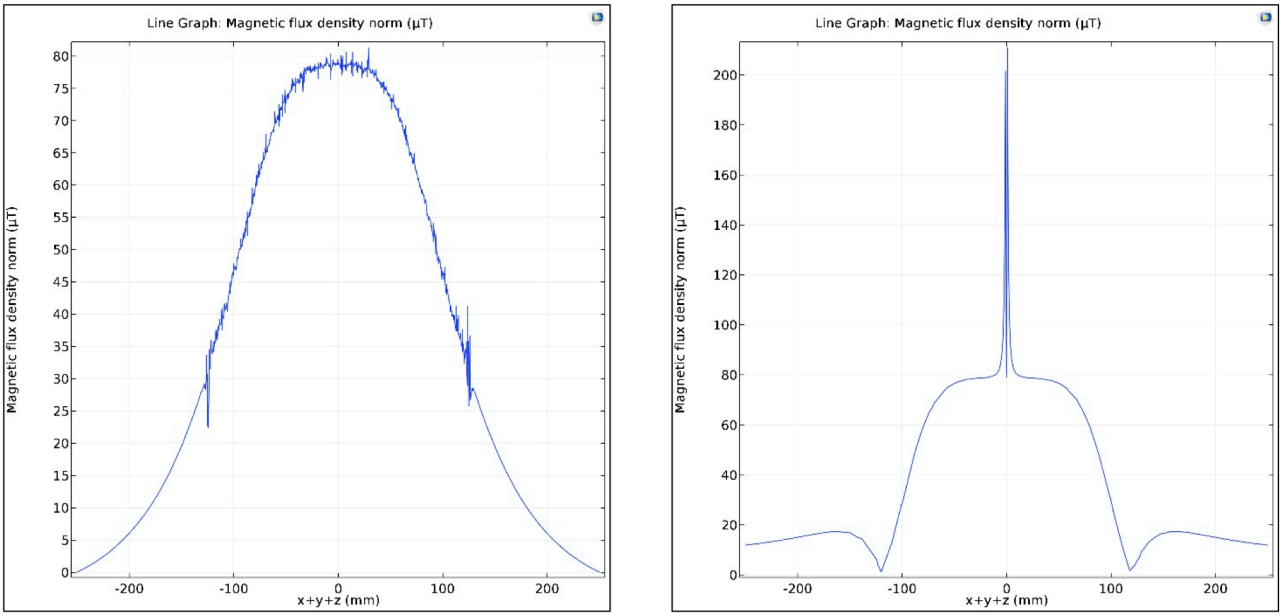

Figure 78: Magnetic field, second cutting plane

A good interpretation of the magnetic field trend, illustrated in the Figure 78, is given in the next figure where it is evaluated the composition. It is important to see that between coils, also with the wire, the magnetic field is uniform.

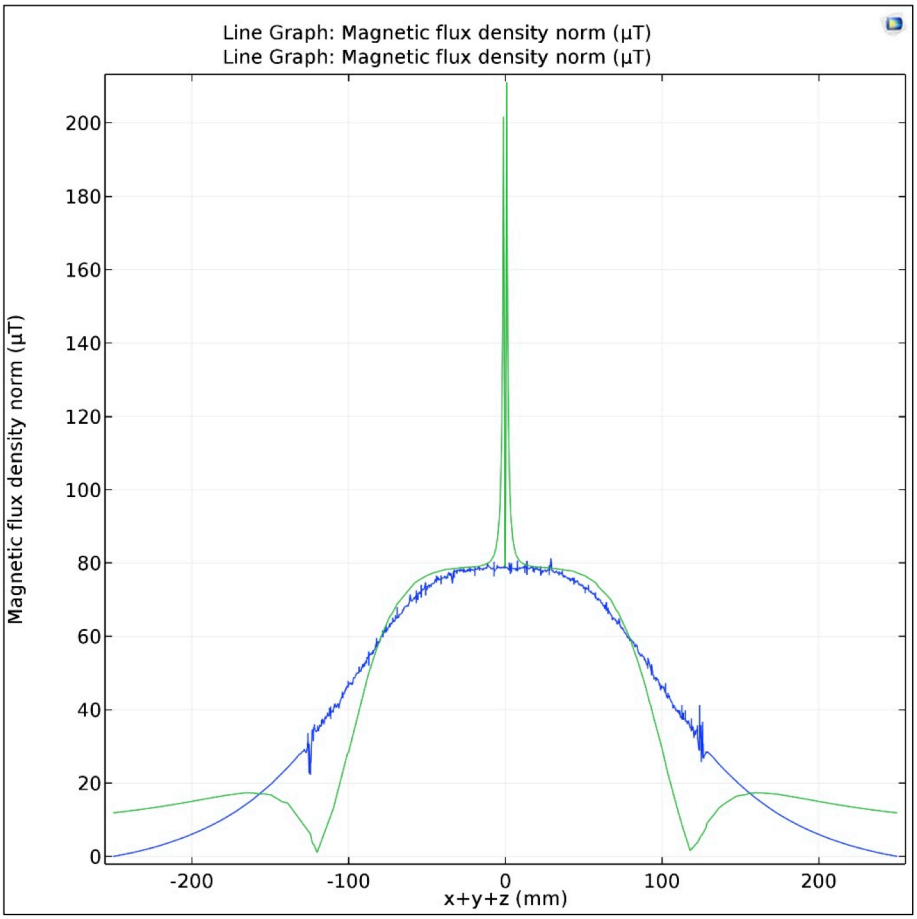

Figure 79: Sum of magnetic fields, second cutting plane

The boundary condition is shown in Figure 80 when the magnetic field is null and the safety condition could be at the distance of 200 mm, the same of Helmholtz coils.

Errors in the simulation could be estimated around 15%, if we sum the error obtained with the simulation of the wire and the error acquired with the simulation of coils.

In the Figure 80 it is also represented the mesh which is fine.

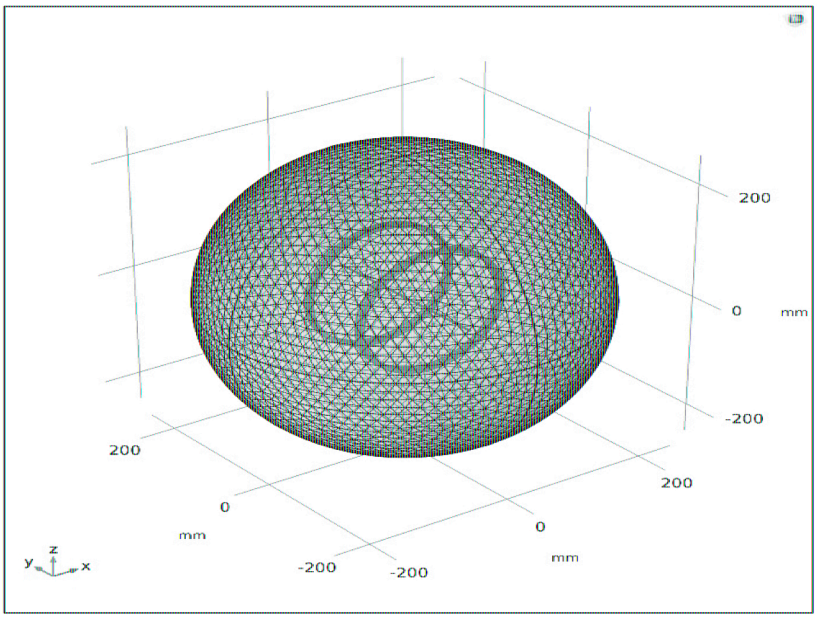

Figure 80: Mesh and boundary condition

6.2 Permanent Magnets and Wire

In this chapter it is looked up how the magnetic field is, if we take account of two
and a wire currying current. As it is said for Helmholtz coils with wire (Cha
procedure is followed. The geometry is in Figure 81 and the input parameters are

Name	Expression	Unit	Description
Permanent Magnets			
M	*500*	*[A/m]*	*Magnetization*
Br	*7*10^(-4)*	*[T]*	*Remanence*
R	*30,00*	*[mm]*	*Outer Radius permanent magn*
r	*3,00*	*[mm]*	*Inner Radius permanent magn*
H	*30,00*	*[mm]*	*Height permanent magnet*
D	*100,00*	*[mm]*	*Distance permanent magnets*
Wire			
i	*1,00*	*[A]*	*Current*
j	*$i/(\pi R^2)$*	*[A/m²]*	*Density current*
R	*1,00*	*[mm]*	*Radius wire*
L	*250,00*	*[mm]*	*Length wire*

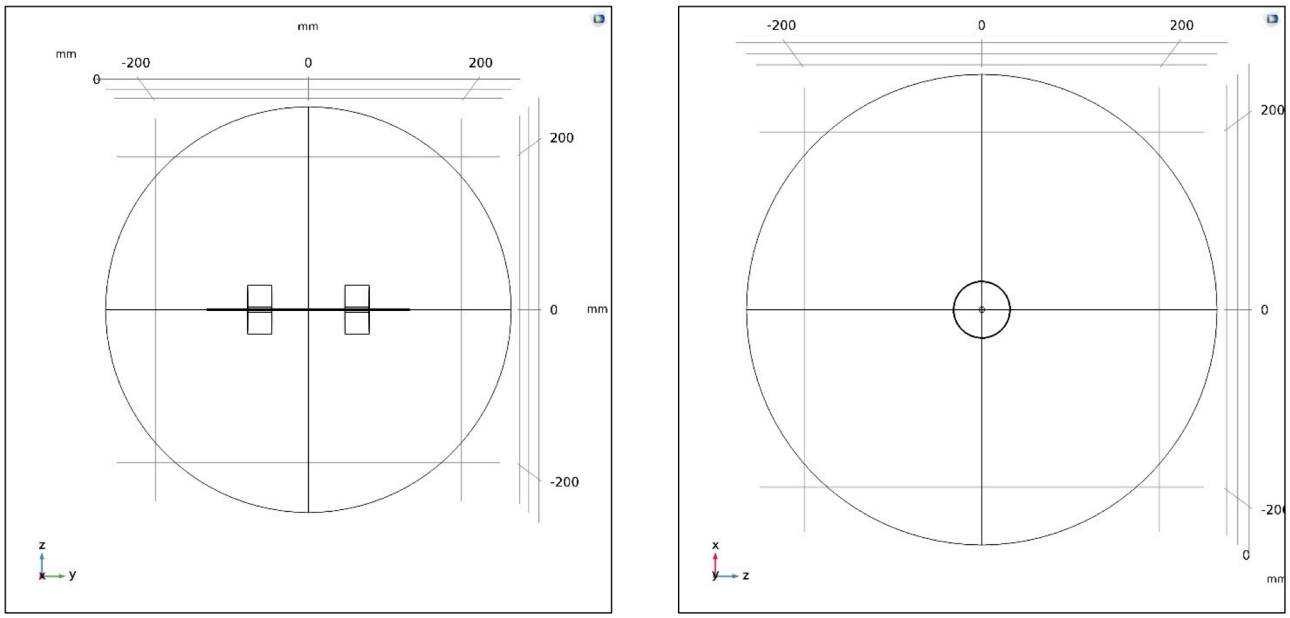

Figure 81: Geometry

Materials used in the simulation are:

- Neodymium for permanent magnets;
- Copper for the wire;
- Air around permanent magnets.

The Figure 82 shows components in coordinate system space. In the Figure 83 there is a global representation with two cutting planes considered.

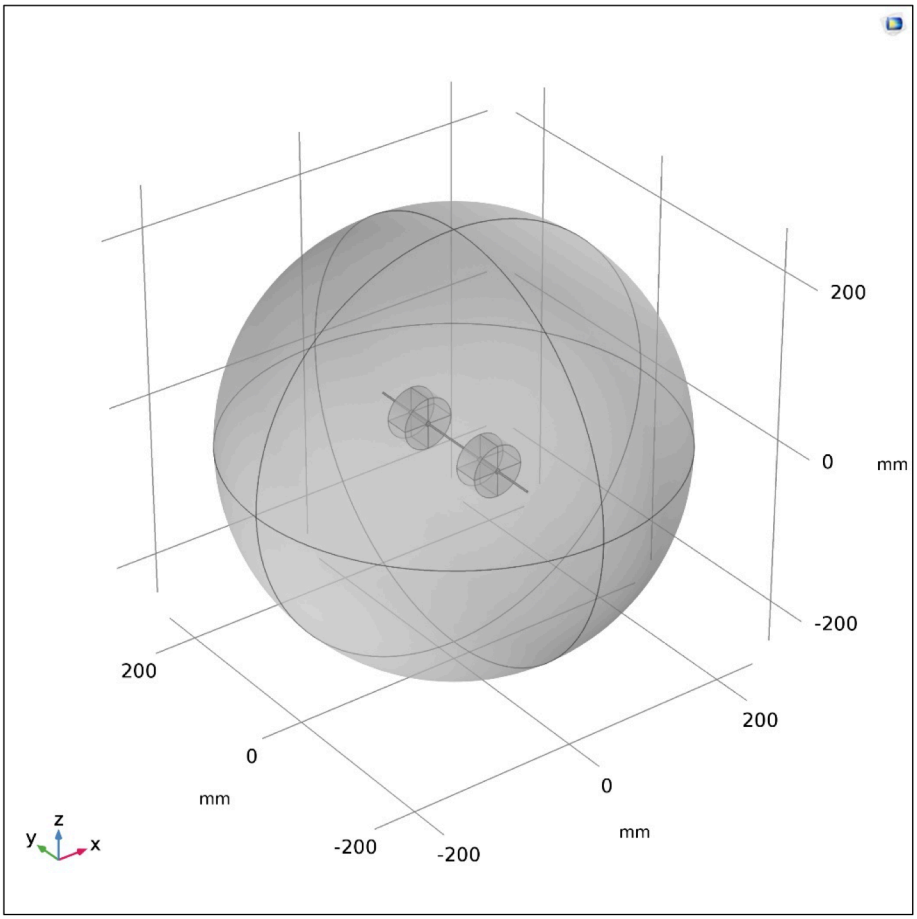

Figure 82: Setup of permanent magnets and wire

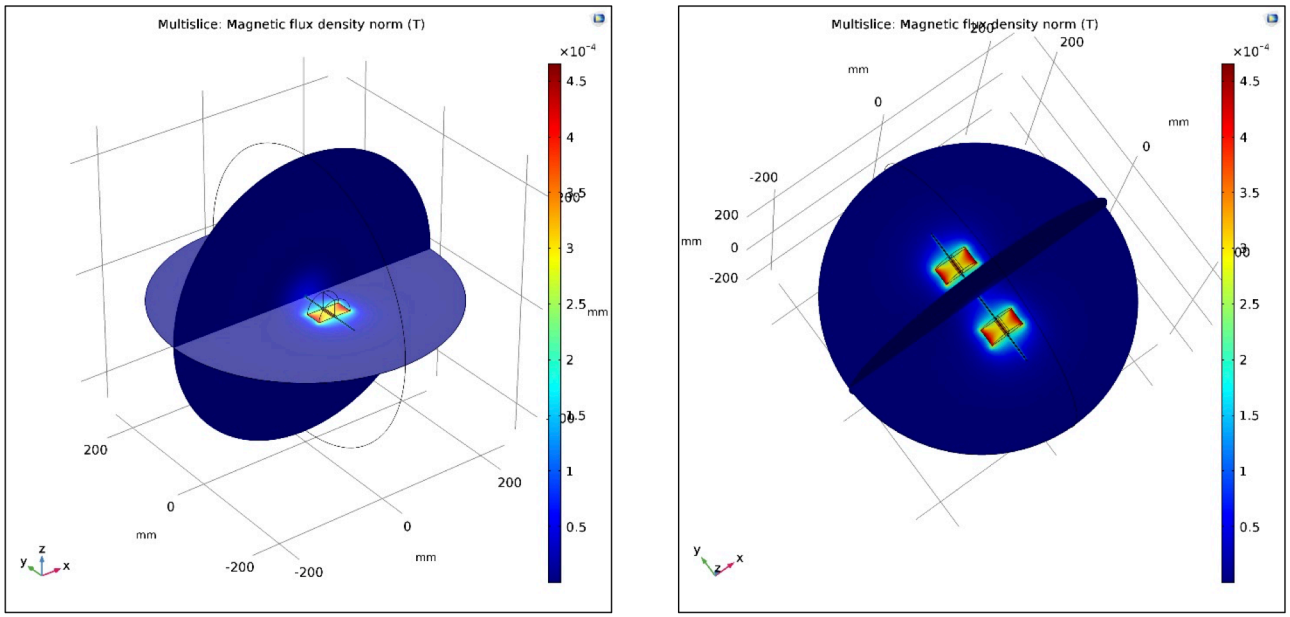

Figure 83: Magnetic field

The magnetic field is studied with the application of two cutting planes:

- the first one is on ZX axis;
- the second one is on XY axis.

The first cutting plane is shown in the figure below with the magnetic flux density in Figure 85 and in Figure 86.

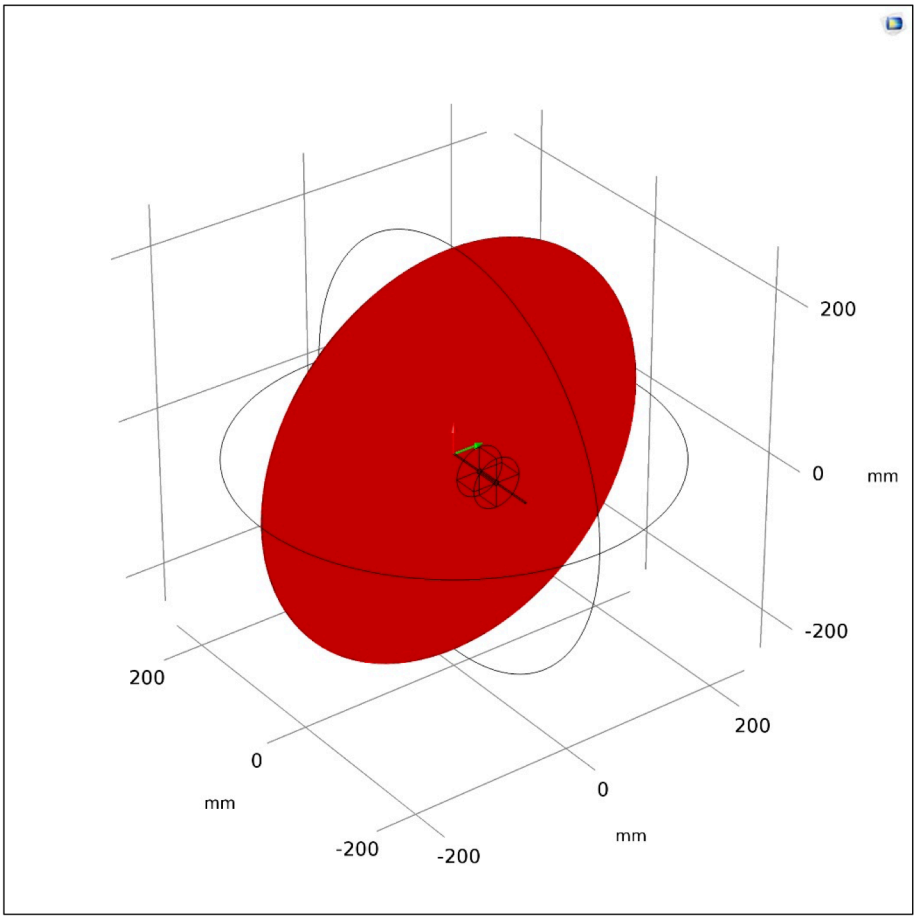

Figure 84: First cutting plane

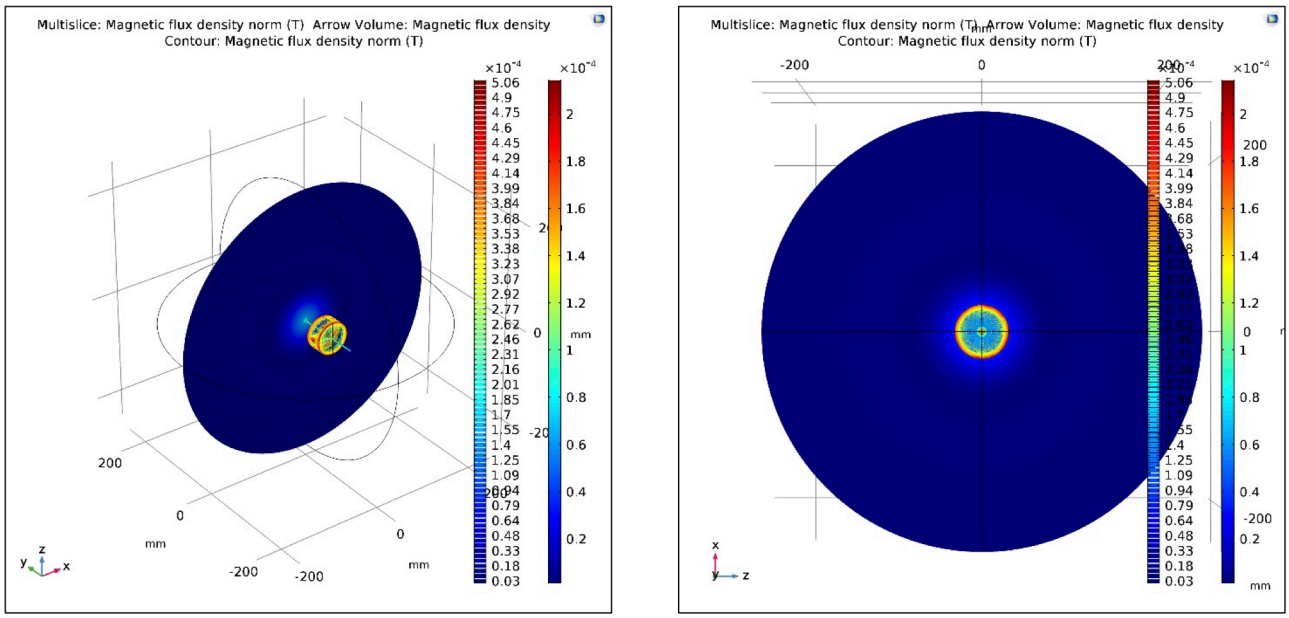

Figure 85: Magnetic flux density, first cutting plane

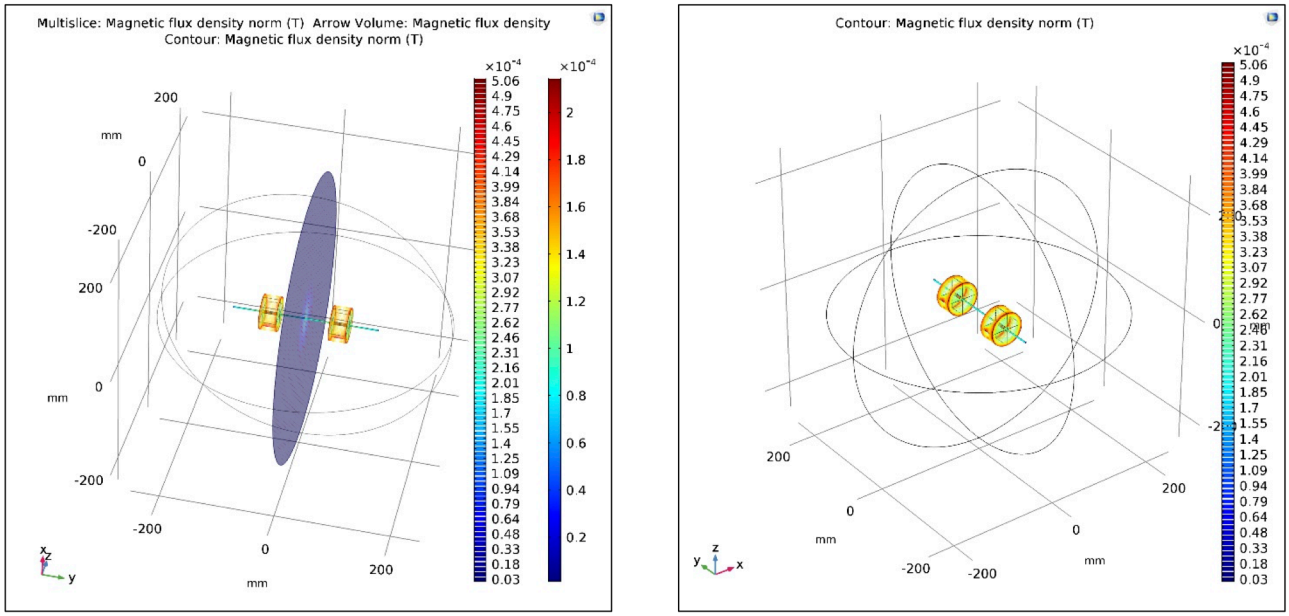

Figure 86: Magnetic flux density, first cutting plane

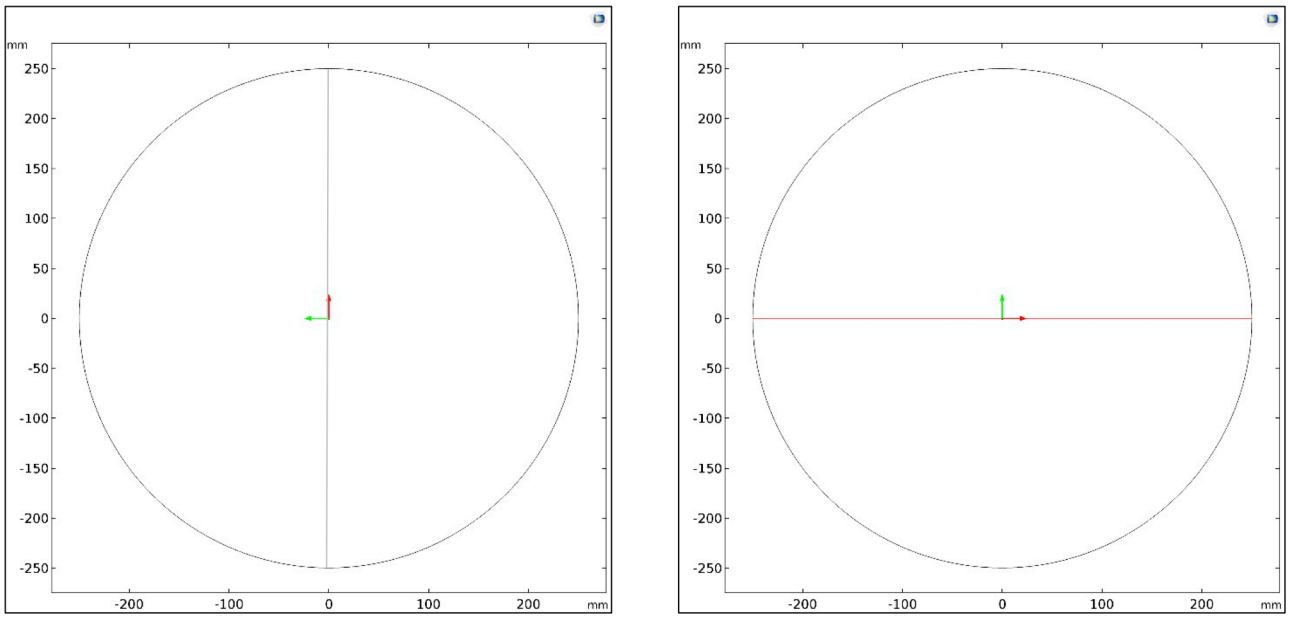

Figure 87: Cutting lines, first cutting plane

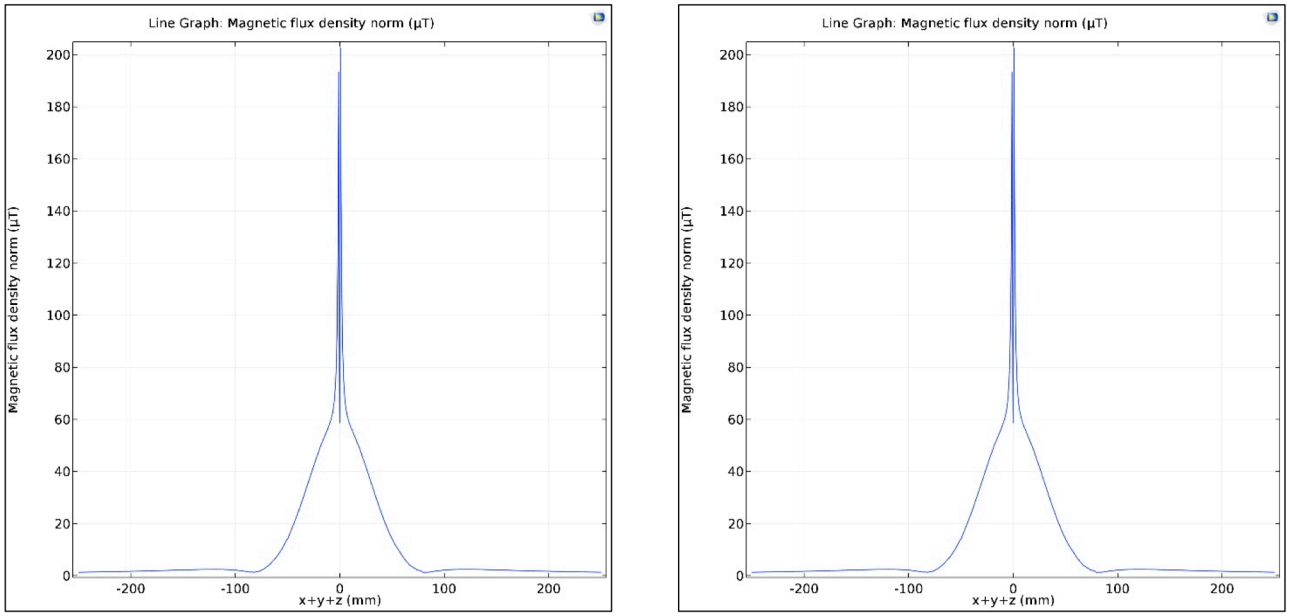

Figure 88: Magnetic field, first cutting plane

As far as the evaluation of magnetic field is concerning, two cutting lines on the first cutting plane are considered, as it is investigated for permanent magnets. It is possible to consider how the magnetic field of the wire with the magnetic field of magnets is.

Using arrows and contour, it is possible to represent the magnetic flux density, as it is shown in the Figure 89 illustrating the second cutting plane which explains clearly how the trend of the magnetic field is. It is also interesting to see that there is not so much uniformity between the two magnets, demonstrating the coherence with the permanent magnets simulation, explained before.

The Figure 91 illustrates that the composition of the magnetic field of magnets with the magnetic field of wire creates Wiedmann's effect. If it is fixed a sample of smart material around the wire, we could see that it twists.

The Figure 92 and the Figure 93 illustrate how is the trend of the magnetic field if are considered two cutting lines.

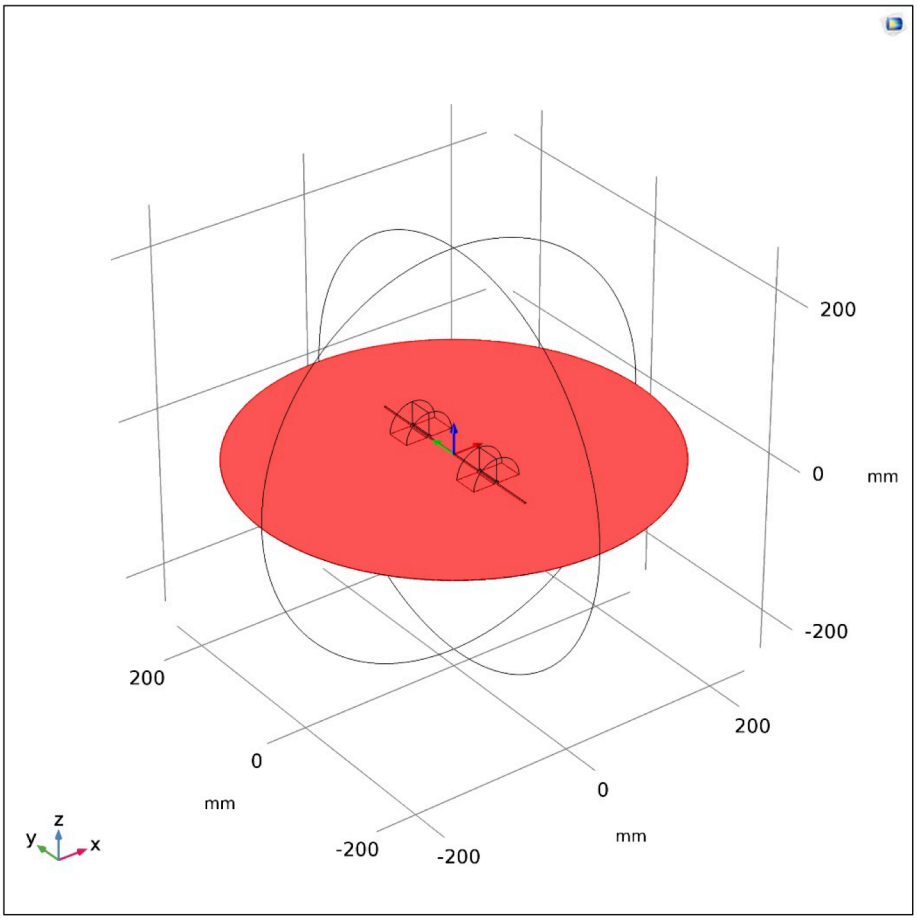

Figure 89: Second cutting plane

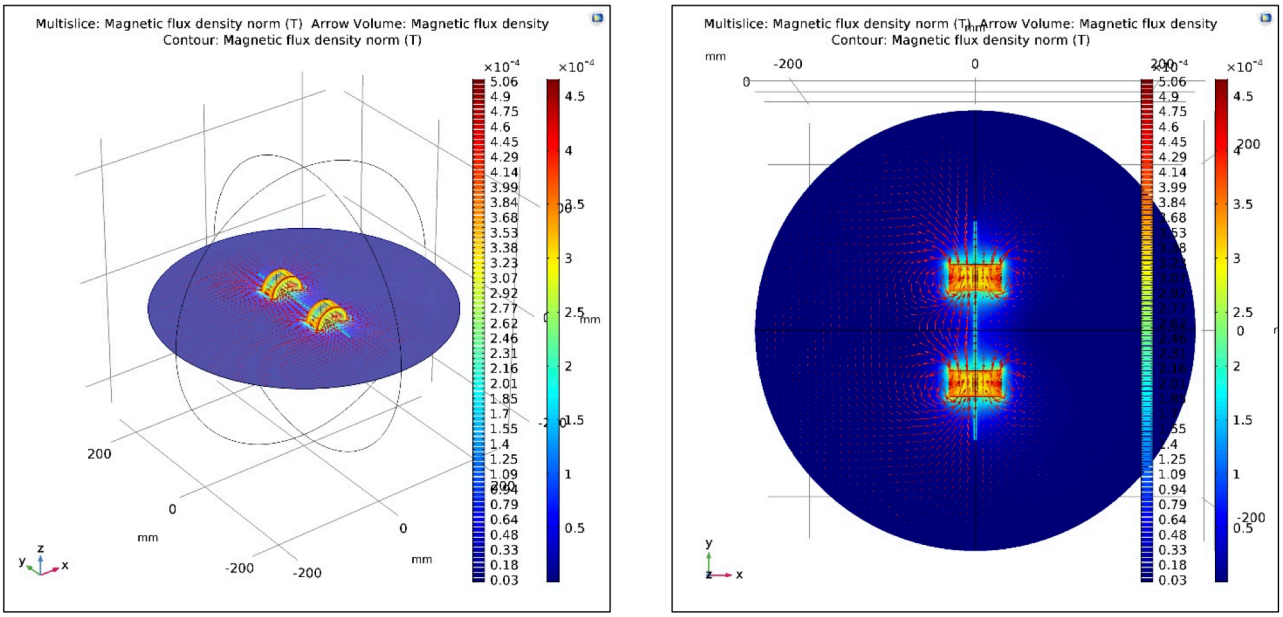

Figure 90: Magnetic flux density, second cutting plane

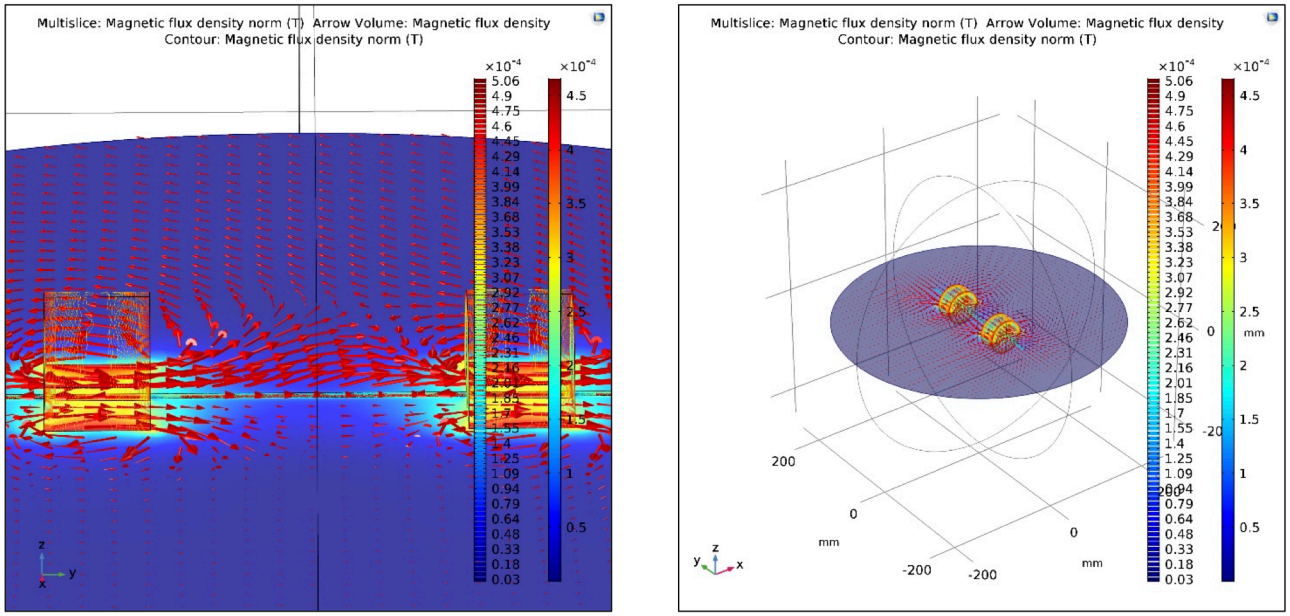

Figure 91: Magnetic flux density, second cutting plane

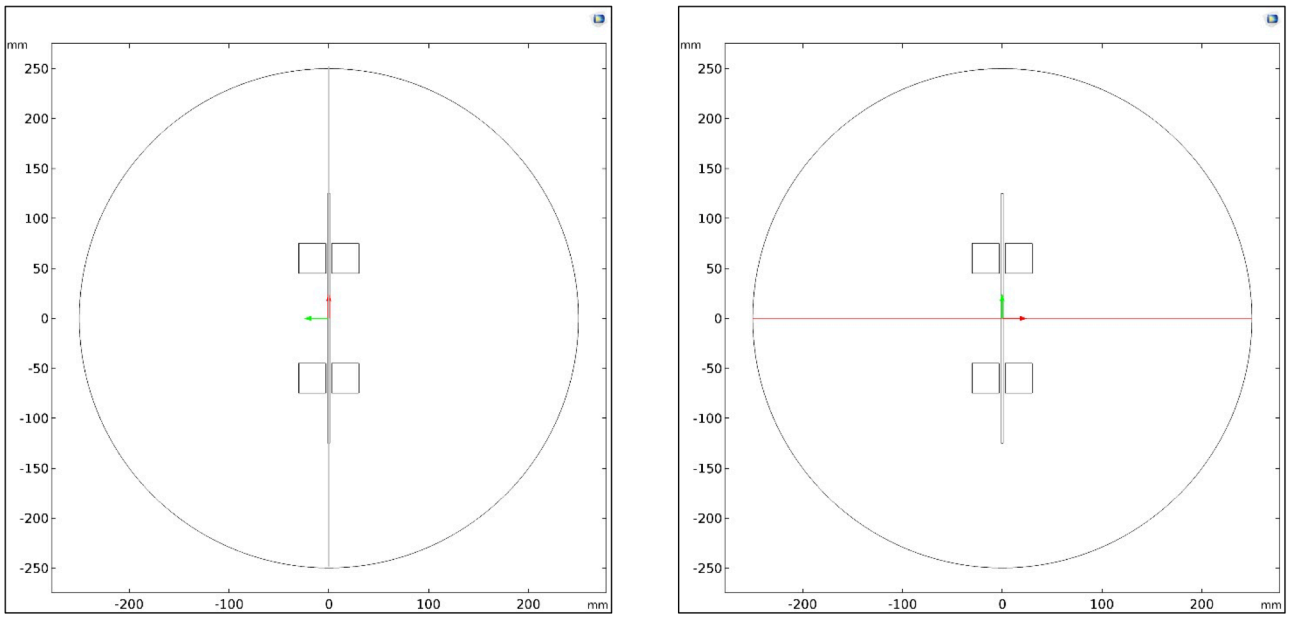

Figure 92: Cutting lines, second cutting plane

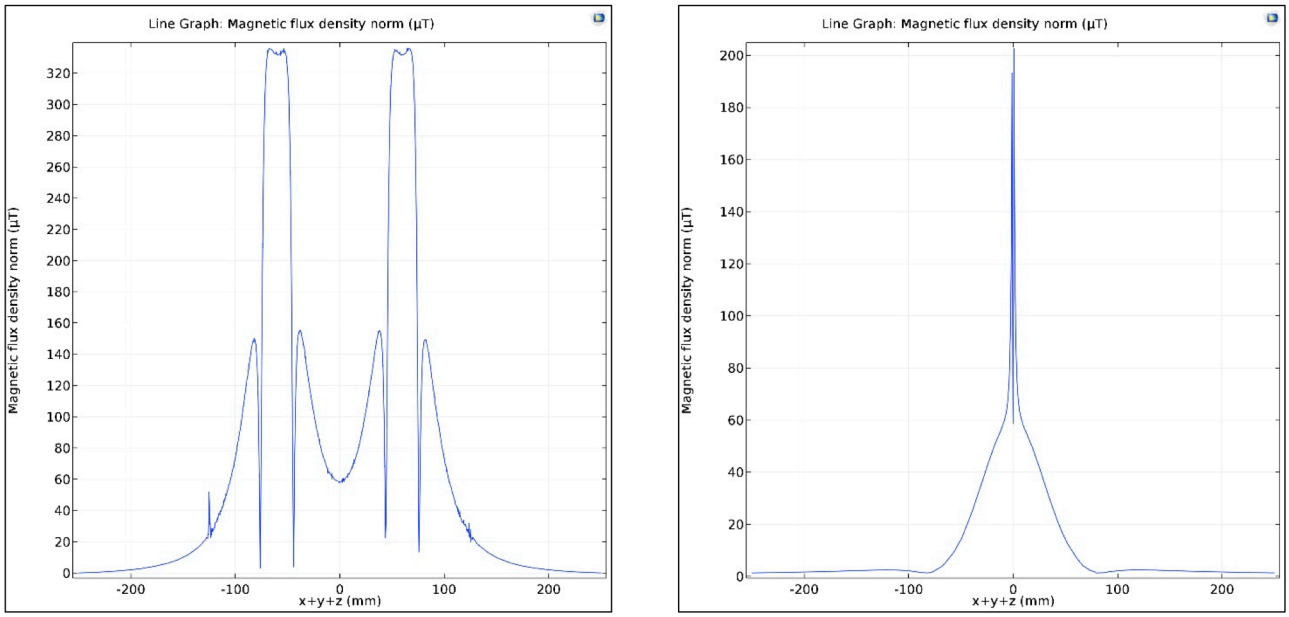

Figure 93: Magnetic field, second cutting plane

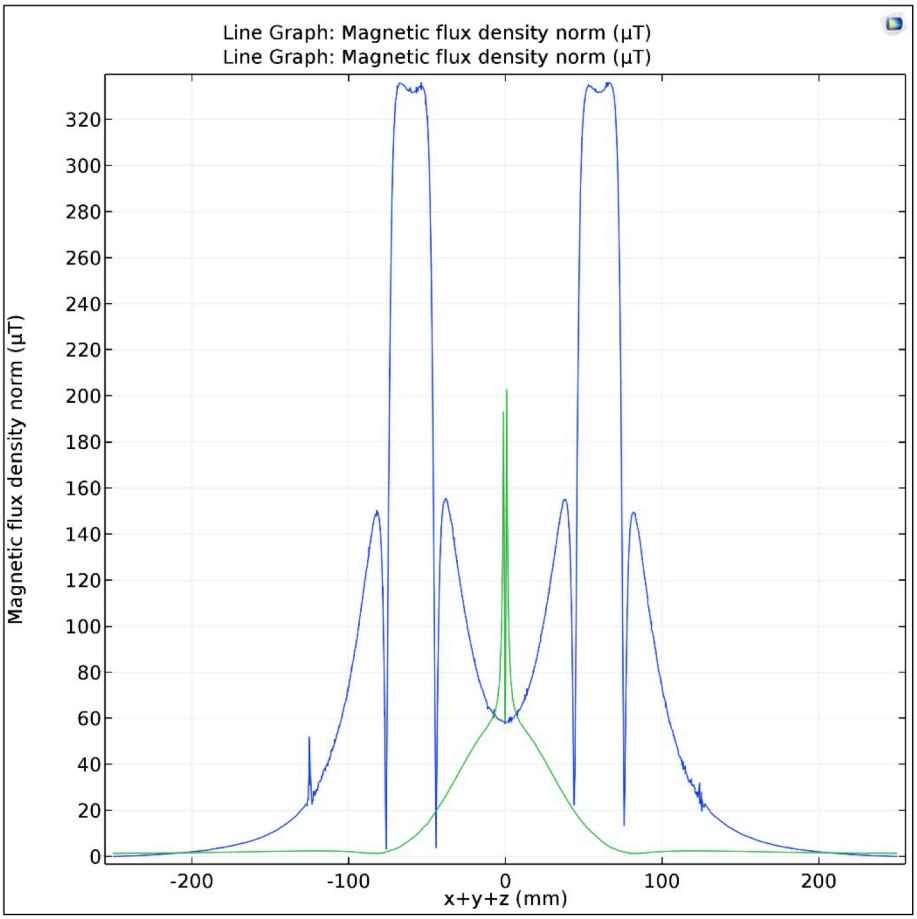

Figure 94: Sum of magnetic fields, second cutting plane

The Figure 94 evaluates composition of the magnetic field whose trend is illustrated in the Figure 93.

The boundary condition is shown in the Figure 95 when the magnetic field is null. The safety condition is the same of permanent magnets, described in the previous chapter.

Errors in the simulation could be estimated around 35% if we sum both the error obtained with the simulation of the wire and the error of the simulation of magnets.

It is reasonable to notice that in the Figure 95 the mesh built is fine.

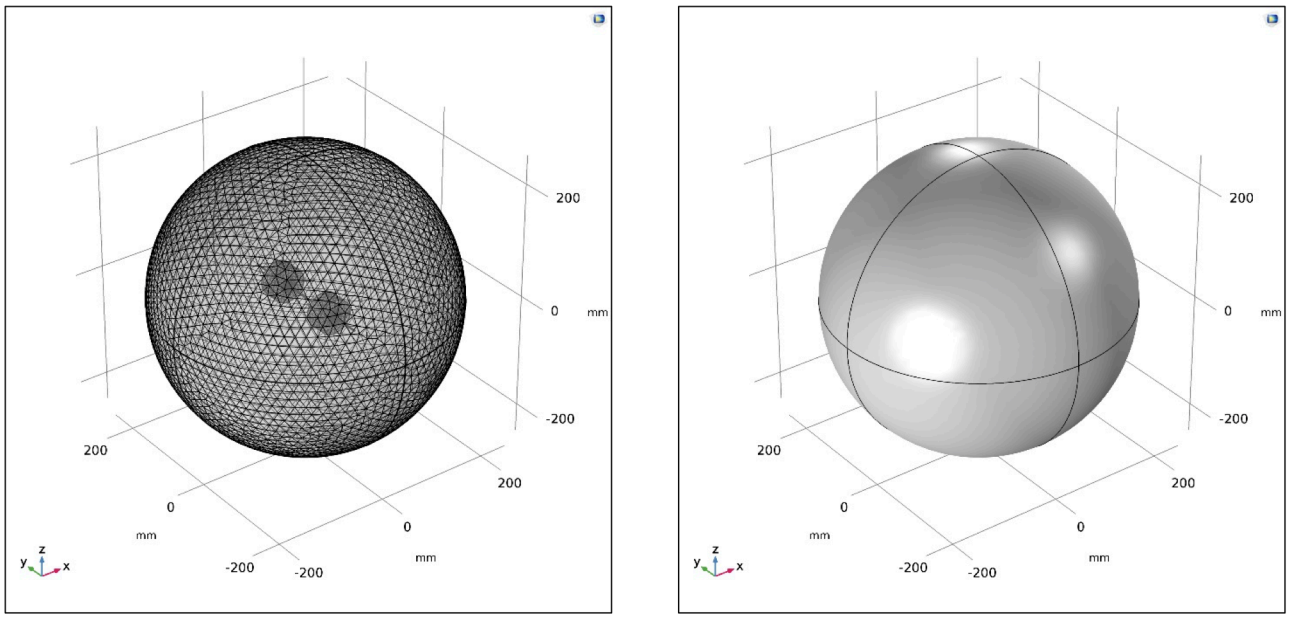

Figure 95: Mesh and boundary condition

7.0 Design of the Experimental Setup

In this chapter it is explained how to design a magneto-mechanical actuator which moves a smart material when:
- the current flows inside the wire and the Helmholtz coils, as a consequence the smart material twists thank to the composition of two magnetic fields;
- the current flows inside the wire and it twists thank to the composition of the magnetic field of the wire and that one of permanent magnets.

Both of these setups produce the same effect, and it is decided to investigate torsion, angle of torsion, displacement, stress and magnetic field, changing these parameters of the smart material:
- relative permeability;
- sizes (outer radius and length).

Graphs values are evaluated after numerous simulations; the aim is to find a relationship between both smart material properties and sizes with torsion, thus clarify Wiedmann's effect.

Two different setups for Helmholtz coils are analyzed and after all, the optimal solution is found, simulated with permanent magnets.

A fundamental question is dealt with the consideration of the torsion: the investigation does not estimate the friction because the experiment takes little time and its effects could be negligible and thus it is as an ideal case.

7.1 Helmholtz Coils and Wire with Smart Material

The setup simulated considers two different conditions about input parameters because it is interesting to know how the trend of the investigation data is. After that, graphs obtained are interpreted and the optimal smart material, which is simulated with the permanent magnets, is chosen. This chapter explains the intermediate step of the work and it is considered the key of the interpretation about Wiedmann's effect.

In the table below the input parameters of the two setups are listed. Both of them reports the same trends but with different order of magnitude. Helmholtz coils are simulated at the same distance of their radius because, as explained in the chapter 1.10, setting the distance between the two coils $D = R$ minimizes the no uniformity of the field at the center of the coils. In our case, it is reasonable to obtain a uniform magnetic field for the sample of the smart material which is fixed around the wire in the middle distance.

The difference between the first and the second setup is
- D which becomes the double;
- N which becomes 20 times bigger than the first.

First setup

Name	Expression	Unit	Description
Helmholtz Coils			
i	*5,00*	*[A]*	*Current*
L	*5,00*	*[mm]*	*Length coil*
H	*10,00*	*[mm]*	*Height coil*
R	*100,00*	*[mm]*	*Radius coil*
D	*100,00*	*[mm]*	*Distance coils*
N	*10*	*/*	*Windings*
i_{tot}	*i*N*	*[A]*	*Current tot*
Wire			
i	*30,00*	*[A]*	*Current*
j	$i/(\pi R^2)$	$[A/m^2]$	*Density current*
R	*1,00*	*[mm]*	*Radius wire*
L	*250,00*	*[mm]*	*Length wire*

Second setup

Name	Expression	Unit	Description
Helmholtz Coils			
i	*5,00*	*[A]*	*Current*
L	*5,00*	*[mm]*	*Length coil*
H	*10,00*	*[mm]*	*Height coil*
R	*200,00*	*[mm]*	*Radius coil*
D	*200,00*	*[mm]*	*Distance coils*
N	*200*	*/*	*Windings*
i_{tot}	*i*N*	*[A]*	*Current tot*
Wire			
i	*30,00*	*[A]*	*Current*
j	$i/(\pi R^2)$	$[A/m^2]$	*Density current*
R	*1,00*	*[mm]*	*Radius wire*
L	*500,00*	*[mm]*	*Length wire*

In Figure 96 it is illustrated the geometry of the setup.

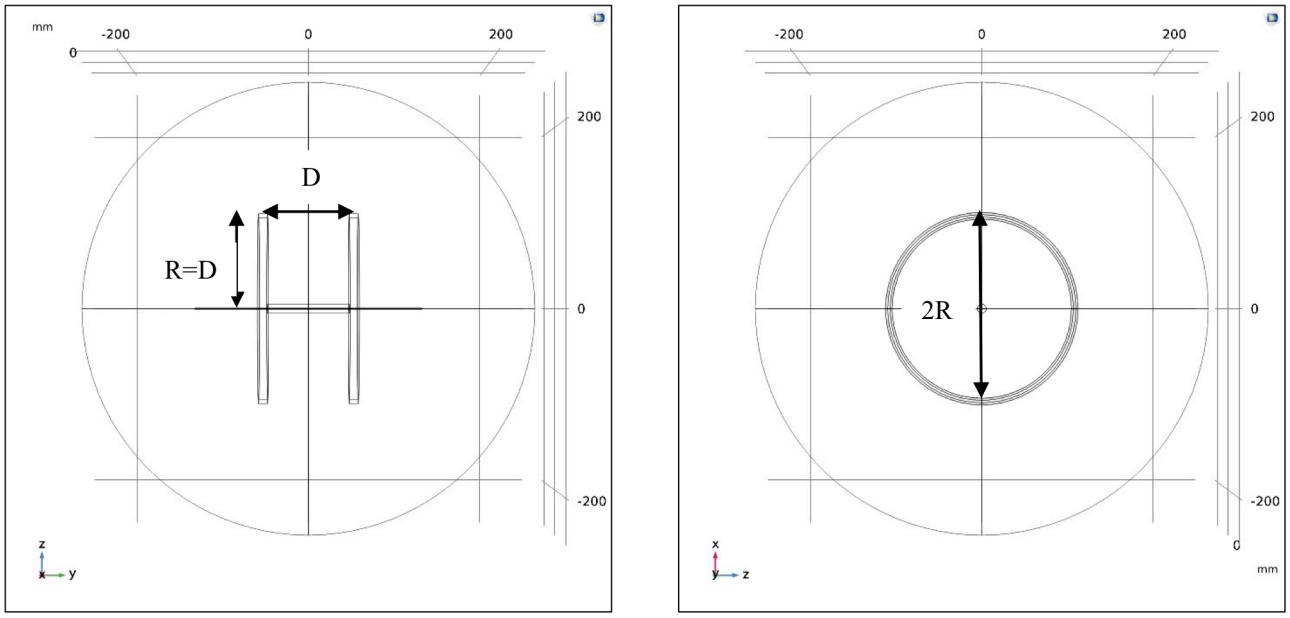

Figure 96: Geometry

Materials used in the simulation:

- Iron Powder SMP1172 for coils ($\mu r = 1$ *[H/m]*);
- Copper for the wire;
- Air around components;
- Smart material for the sample fixed around the wire.

The sample has these initial sizes:

SIZES	
Length [mm]	*60,00*
Inner Radius [mm]	*1,00*
Outer Radius [mm]	*2,00*

and these initial properties:

PROPERTIES	
Density ρ [kg/m³]	*6000,00*
Young's modulus E [Pa]	*40000,00*
Poisson's ratio v	*0,45*
Electric conductivity [S/m]	*0,00*
Relative permittivity ε_r	*10,00*
Permeability μ_0 [H/m]	*4π*10^(-7)*
Relative permeability μr [H/m]	*10,00*
Saturation magnetostriction λ_s	*0,10*
Saturation magnetization M_s [A/m]	*0,45*10^(6)*

As discussed before, the investigation finds a relation between smart material properties:

- relative permeability;
- external radius;
- length;

and these parameters:

- torsion (twisting) with its angle;
- stress;
- displacement;
- magnetic field;

Consequently, it is possible to choose optimal sizes of the sample and relative permeability μ_r to obtain a visible displacement (values around millimeters).

Investigation of the relative permeability

Smart Material parameters

Outer Radius [mm]	Inner Radius [mm]	Length [mm]
2,00	*1,00*	*60,00*

First setup

Rel. Permeability [H/m]	Displacement [µm]	Magnetic Field [T]	Torsion [N*µm]	Stress [N*m²]	Torsion Angle [deg]
1,00	*0,1906*	*0,0185*	*0,0235*	*22,9910*	*45,2237*
5,00	*0,4182*	*0,0550*	*0,0723*	*31,6540*	*45,0481*
10,00	*0,6321*	*0,1003*	*0,0993*	*42,0420*	*44,9928*
50,00	*1,6735*	*0,4536*	*0,1355*	*172,9300*	*44,9383*
100,00	*2,6554*	*0,8156*	*0,1398*	*523,0700*	*44,9316*

Second setup

Rel. Permeability [H/m]	Displacement [µm]	Magnetic Field [T]	Torsion [N*µm]	Stress [N*m²]	Torsion Angle [deg]
1,00	*1,2042*	*0,0758*	*0,0675*	*94,0420*	*44,1495*
5,00	*2,5124*	*0,0899*	*0,1247*	*164,9100*	*43,9303*
10,00	*4,1634*	*0,1765*	*0,2684*	*249,0600*	*43,6681*
50,00	*11,9880*	*0,8395*	*1,4922*	*647,9800*	*43,5263*
100,00	*17,8670*	*1,5629*	*2,7179*	*922,1200*	*43,5890*

Parameters illustrated in tables are:

- the maximum displacement on the smart material;
- the maximum magnetic field on the setup which is localized in the middle space between permanent magnets, instead the minimum value is on the boundary of the setup (approximately null);
- the maximum torsion on the smart material and its maximum angle (Maxwell tensor);
- the maximum stress calculated with Von Mises' law.

The results of the two setups listed in the tables before are reported below, where on the X axis there is the relative permeability [H/m] and on the Y axis there is the parameter studied with the same unit of the table. The left side shows results of the first setup while the right side reports results of the second setup.

Displacement

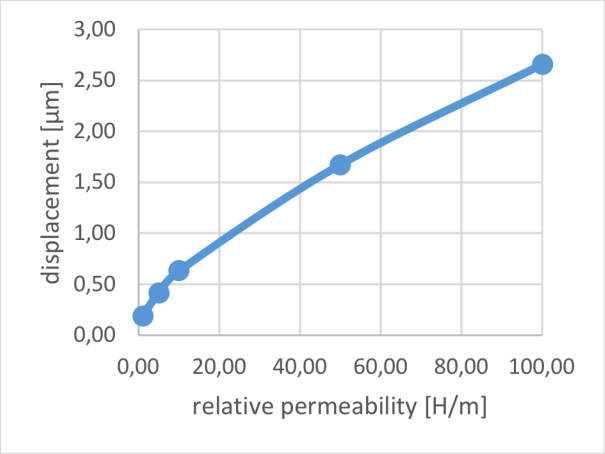

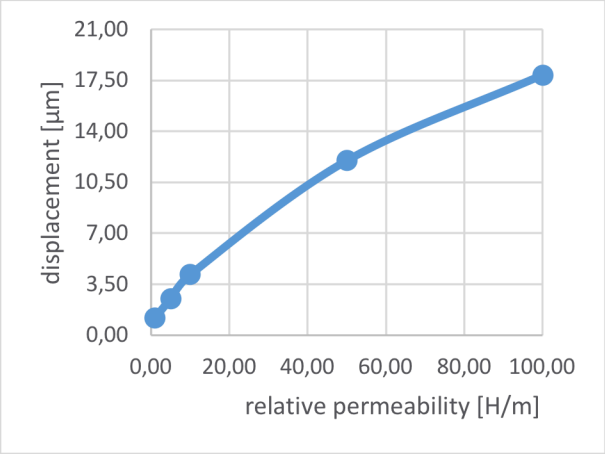

Magnetic Field

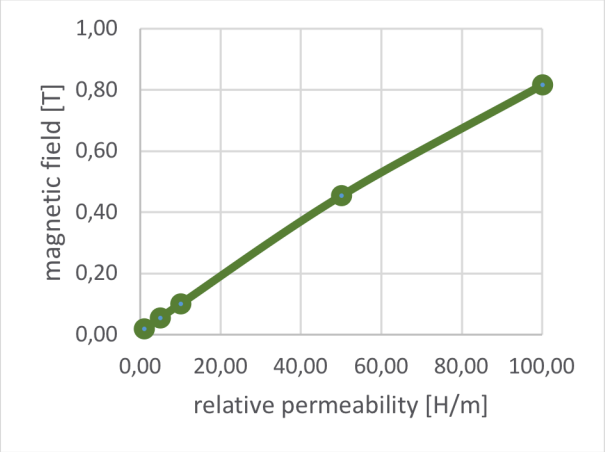

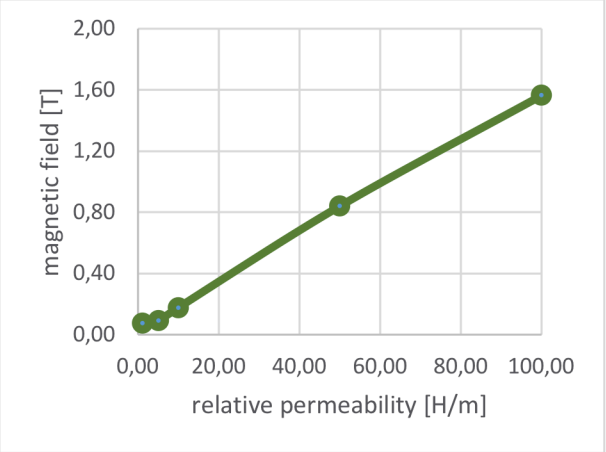

Torsion

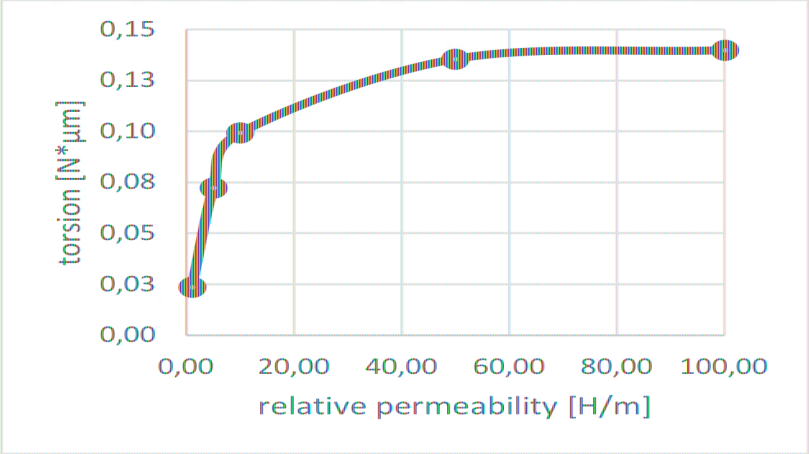

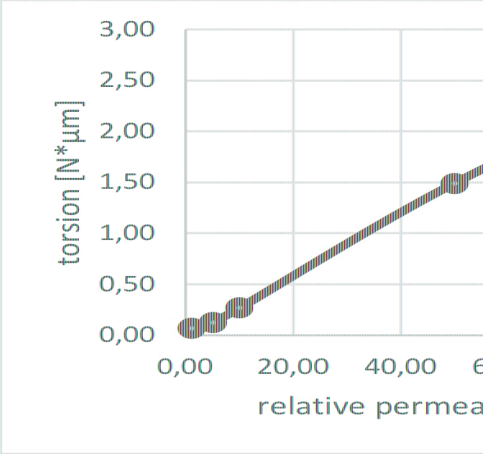

Stress

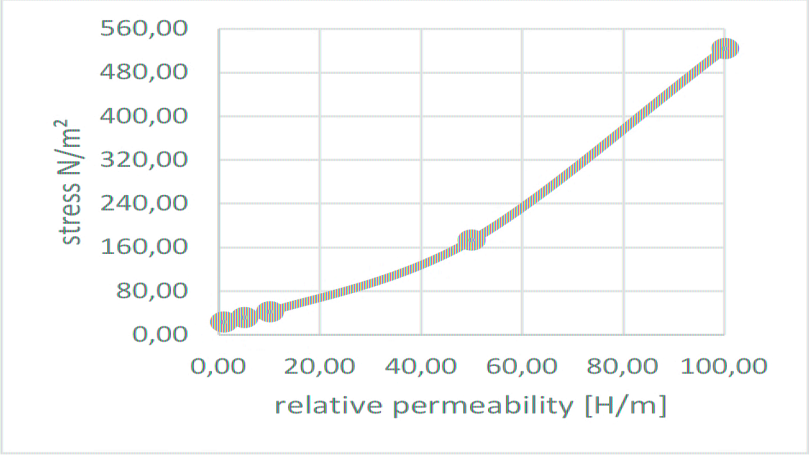

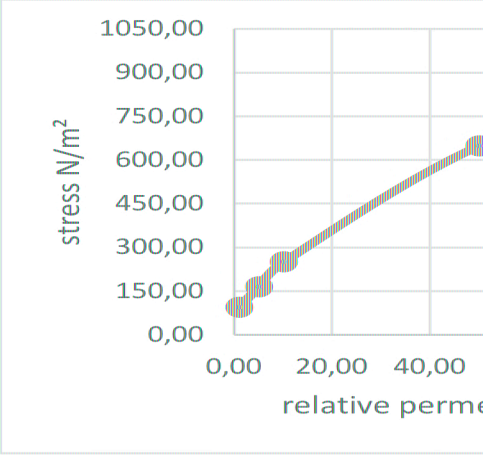

Torsion Angle

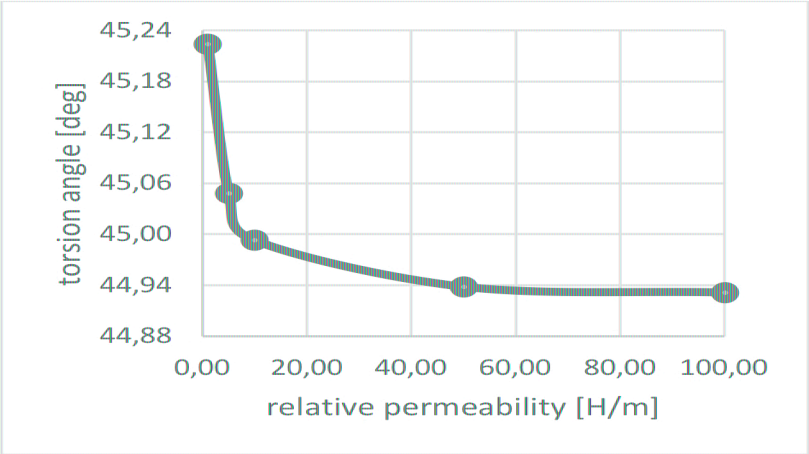

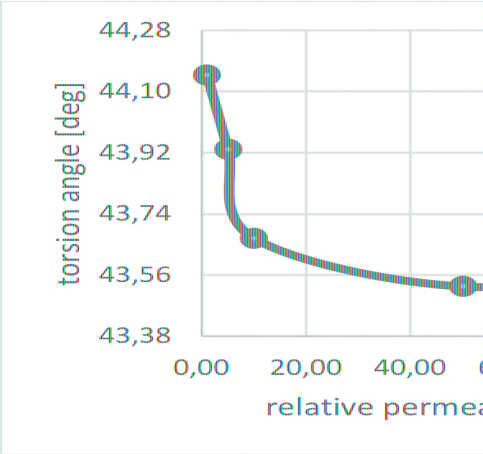

From graphs, it is possible to see the same trend for the same parameter investigat
torsion are different because they depend on the distance between coils and ma
The investigation of the outer radius takes as relative permeability the value of 1
graph of the torsion in the first setup comes to convergence at this value.

Investigation of the outer radius

Smart Material parameters

Rel. Permeability [H/m]	Inner Radius [mm]	Length [mm]
100,00	1,00	60,00

First setup

Outer Radius [mm]	Displacement [µm]	Magnetic Field [T]	Torsion [N*µm]	Stress [N/m²]
2,00	2,6554	0,8156	0,1398	523,070
2,50	3,9211	0,9096	0,1499	546,490
3,00	5,0749	1,2721	0,2221	668,000
3,50	6,1528	1,3244	0,2438	712,650
4,00	7,0398	1,2885	0,0831	654,490
4,50	7,8951	1,5701	0,1155	669,030
5,00	8,6431	1,6794	0,4669	695,290
5,50	9,3240	1,3228	0,1942	605,230
6,00	9,7476	1,6188	0,2831	716,890

Second setup

Outer Radius [mm]	Displacement [µm]	Magnetic Field [T]	Torsion [N*µm]	Stress [N/m²]
2,00	17,8670	1,5629	2,7179	922,120
2,50	26,2130	1,3952	1,9988	1199,800
3,00	33,9690	1,3955	1,5716	1452,000
3,50	39,2970	1,6516	1,4137	1636,300
4,00	47,2770	1,8428	2,3709	1863,500
4,50	49,1220	1,5746	3,1458	1854,300
5,00	51,0690	1,6892	9,2767	1636,800
5,50	52,7980	1,4747	3,1079	1431,200
6,00	55,8100	1,8662	5,6463	1374,500

Results of two setups, listed in the tables before, are reported in following graphs, where on the X axis there is the outer radius [mm] and on the Y axis there is the parameter studied with the same unit of the table.

The left side shows results of the first setup while the right side reports results of the second setup.

Displacement

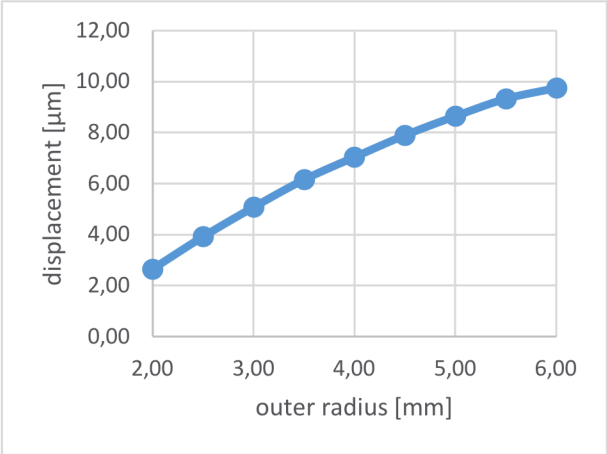

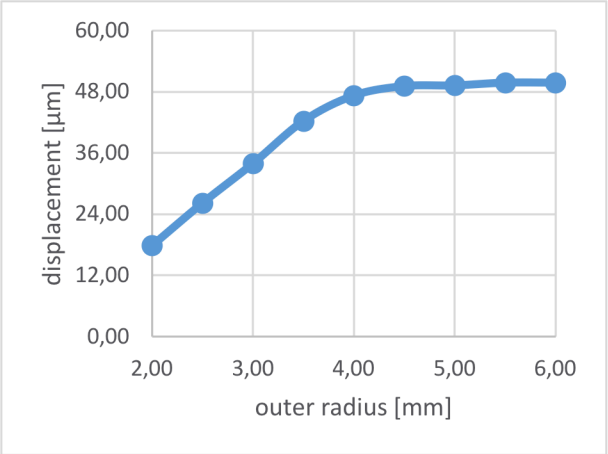

Magnetic Field

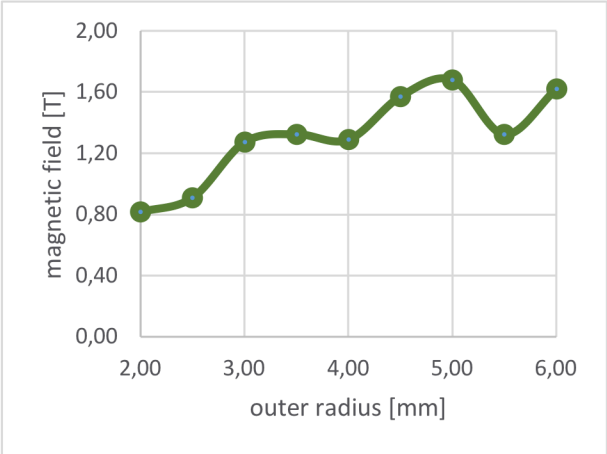

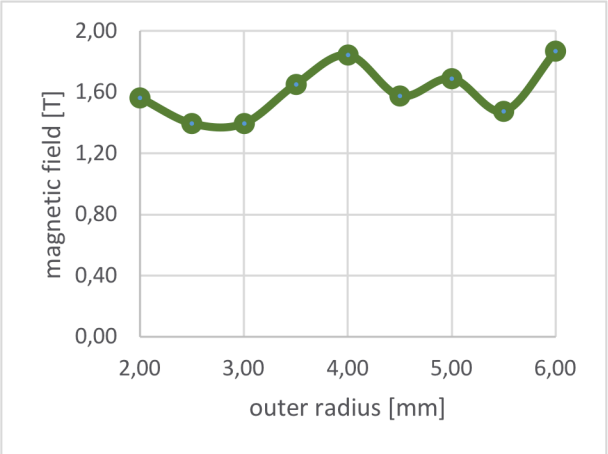

Torsion

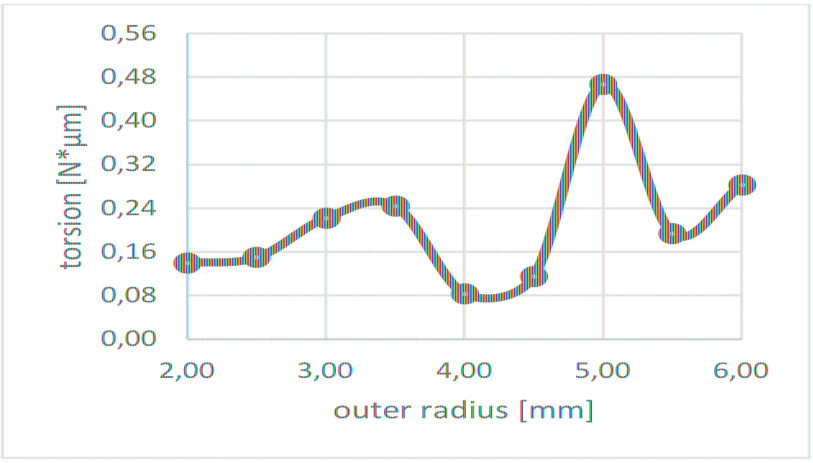

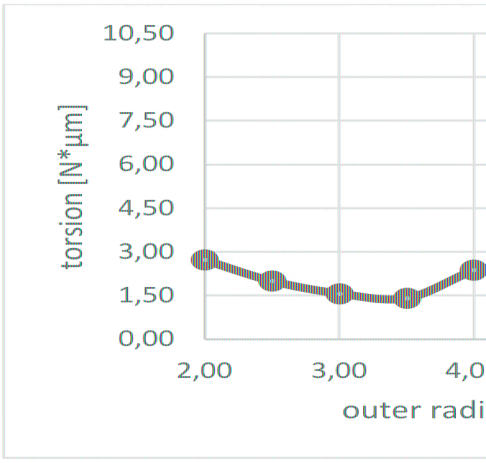

Stress

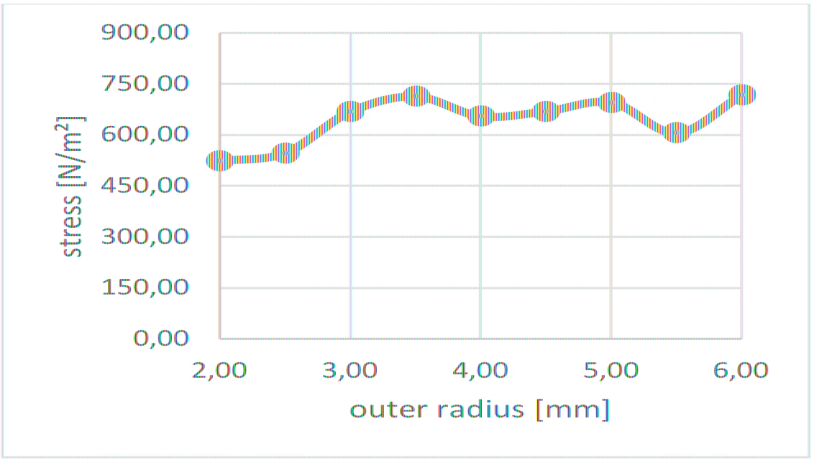

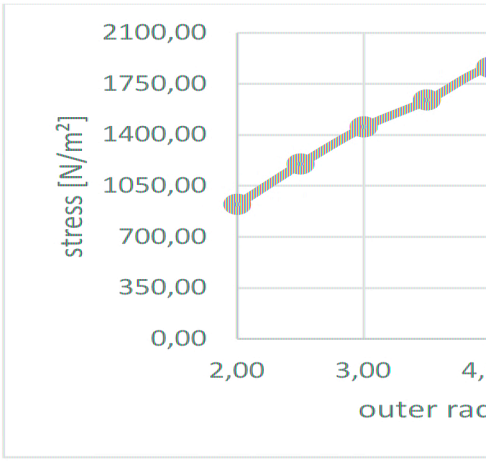

Torsion Angle

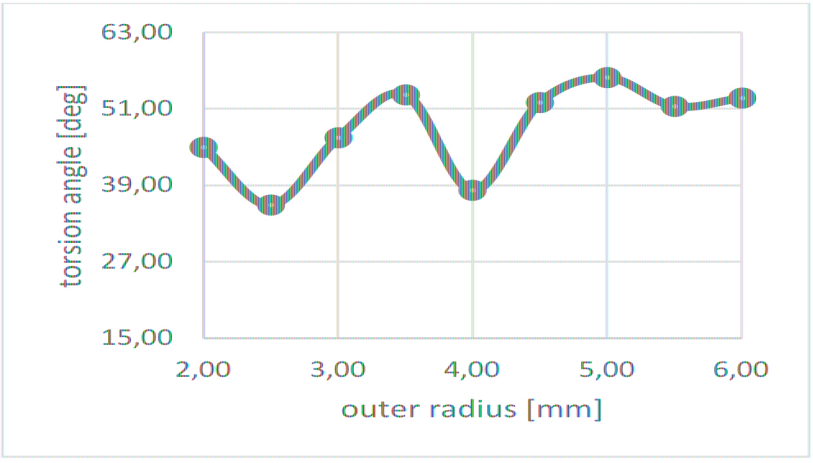

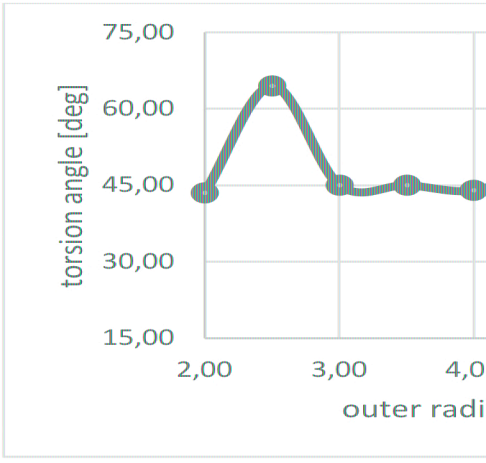

From graphs it is possible to see the same trend for the same parameter exan
displacement indicate that the optimal outer radius is 5 mm because at this value
- the maximum torsion;
- the displacement comes to convergence in the second setup at this value.

The torsion angle is around 45 degrees and it is a valid result because it means
fields are in equilibrium and none prevails on the other.

Investigation of the length

Smart Material parameters

Rel. Permeability [H/m]	Inner Radius [mm]	Outer Radius [mm]
100,00	1,00	5,00

First setup

Length [mm]	Displacement [µm]	Magnetic Field [T]	Torsion [N*µm]	Stress [N/m²]
40,00	5,5868	1,1910	0,0309	607,430
50,00	6,5609	1,6556	0,0886	698,460
60,00	7,3849	1,5717	0,1032	640,800
70,00	8,0677	1,4805	0,3991	684,550
80,00	8,6431	1,6794	0,4669	695,290
90,00	9,0730	1,4453	0,1552	653,410

Second setup

Length [mm]	Displacement [µm]	Magnetic Field [T]	Torsion [N*µm]	Stress [N/m²]
40,00	36,1960	1,2101	2,6334	933,160
60,00	51,0690	1,6892	9,2767	1636,800
80,00	62,5790	1,8030	9,7721	1575,000
100,00	70,5050	2,0305	7,3978	1857,700
140,00	78,4800	1,6517	25,4080	2020,500
180,00	81,5450	1,8553	15,6570	2436,200

Displacement

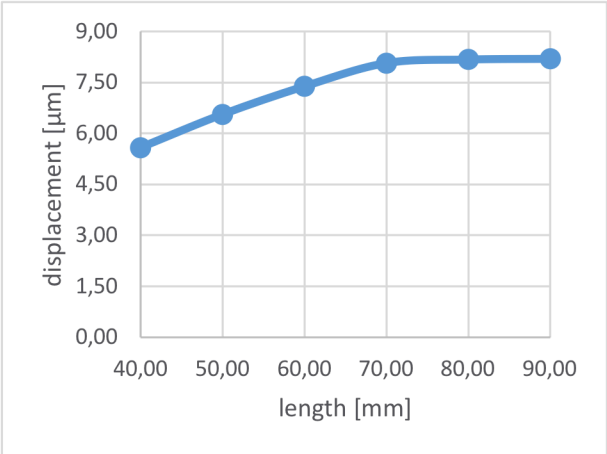

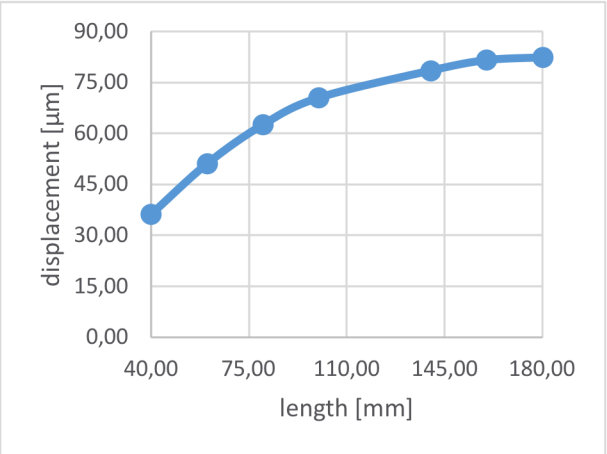

Magnetic Field

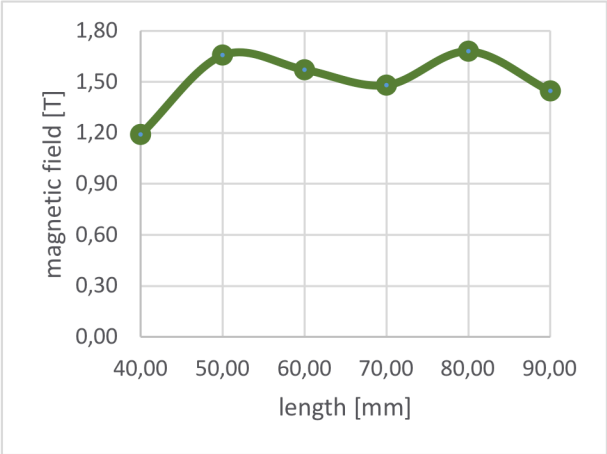

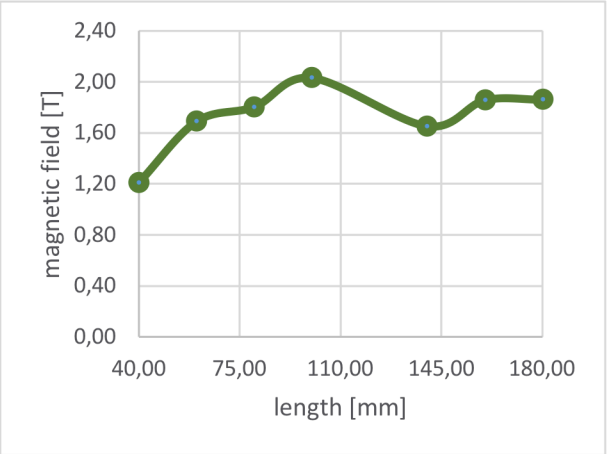

Torsion

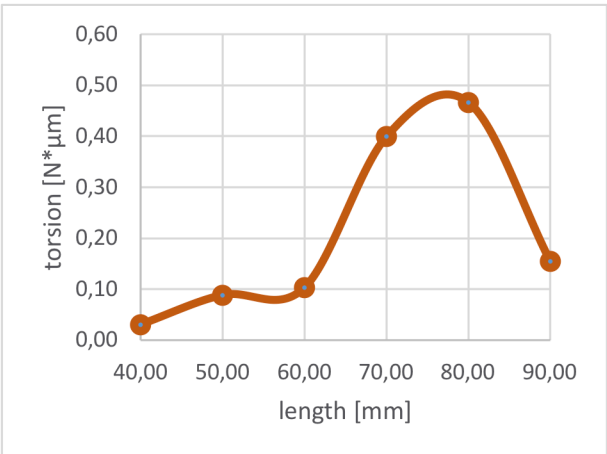

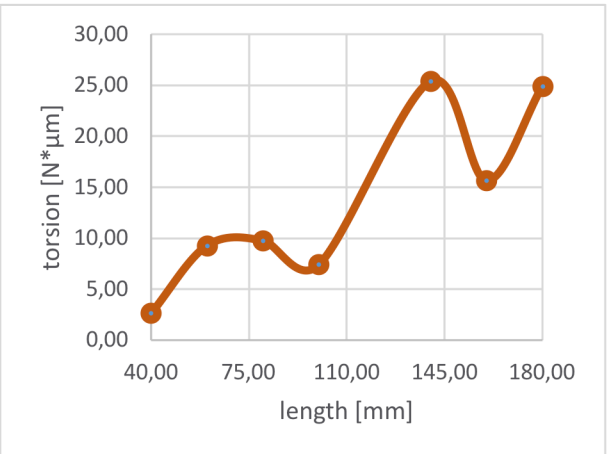

Stress

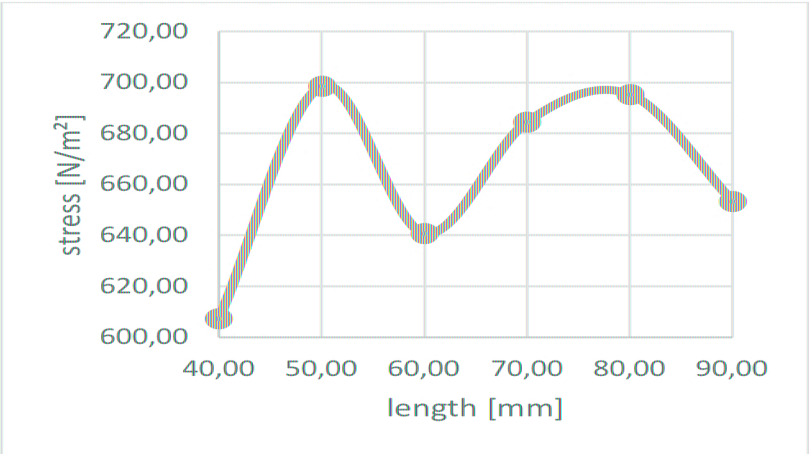

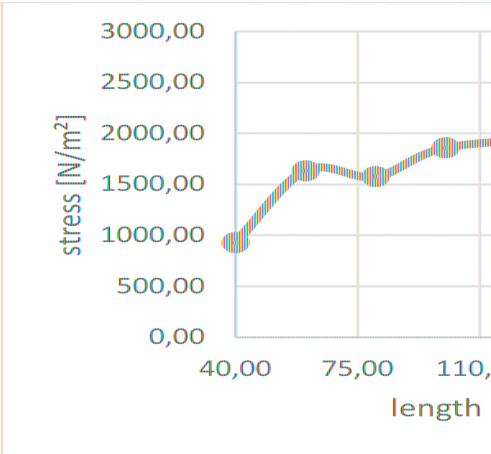

Torsion Angle

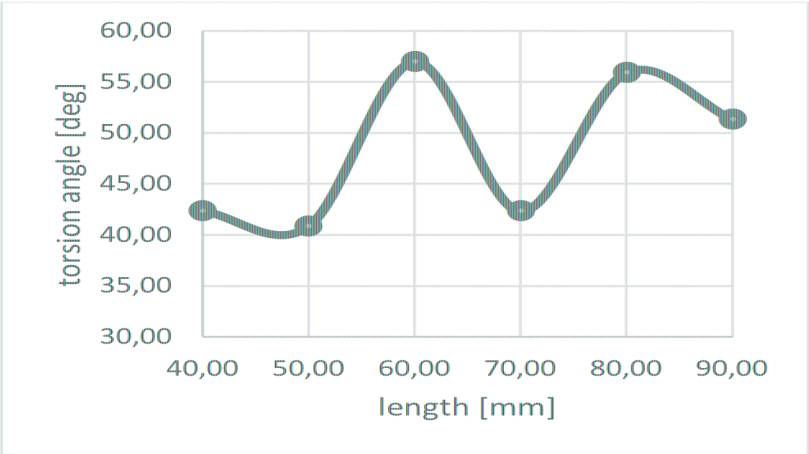

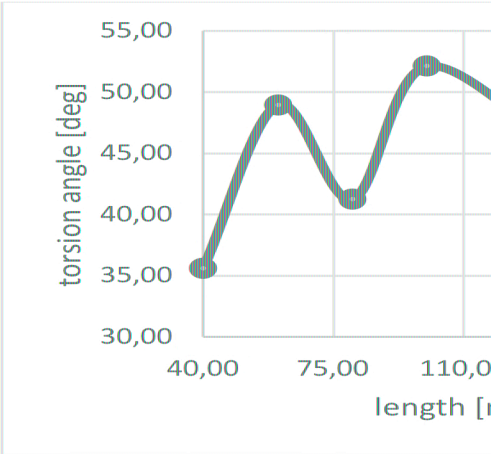

The same trend, connected to the same parameter analyzed, is possible to consider
and displacements indicate that the optimal length is 70 mm for the first setup a
second setup. Length is linked to the distance between coils and it could be in
parameter, but these graphs illustrate that the optimal length become double if th
coils redouble; in fact the first setup has a distance of 100 mm while the second is

In this investigation optimal sizes and properties of the material are:

SIZES	
Length [mm]	*70 <L<140*
Inner Radius [mm]	*1,00*
Outer Radius [mm]	*5,00*

PROPERTIES	
Density ρ [kg/m³]	*6000,00*
Young's modulus E [Pa]	*40000,00*
Poisson's ratio v	*0,45*
Electric conductivity [S/m]	*0,00*
Relative permittivity ε_r	*10,00*
Permeability μ_0 [H/m]	*4π*10^(-7)*
Relative permeability μr [H/m]	*100,00*
Saturation magnetostriction λ_s	*0,10*
Saturation magnetization M_s [A/m]	*0,45*10^(6)*

It is considerable to show to the reader the last simulation with the optimal solution about the first setup.

Smart Material parameters

Rel. Permeability [H/m]	Inner Radius [mm]	Outer Radius [mm]	Length [mm]
100,00	*1,00*	*5,00*	*70,00*

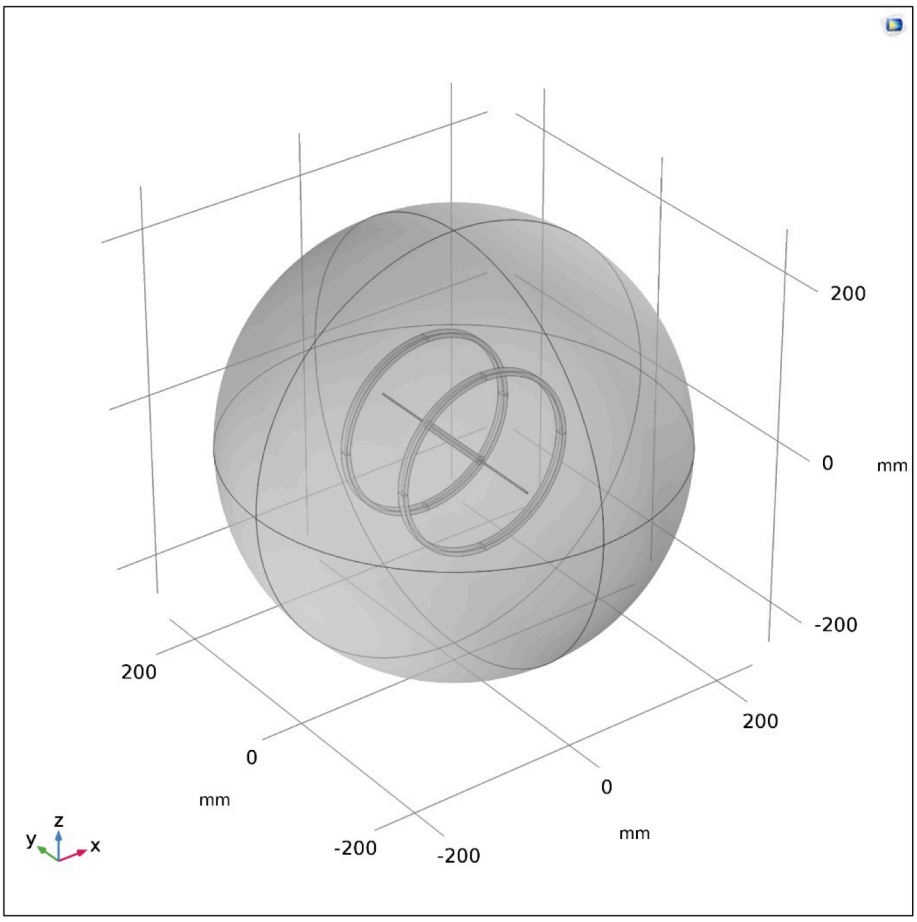

Figure 97: Setup of Helmholtz coils and wire with smart material

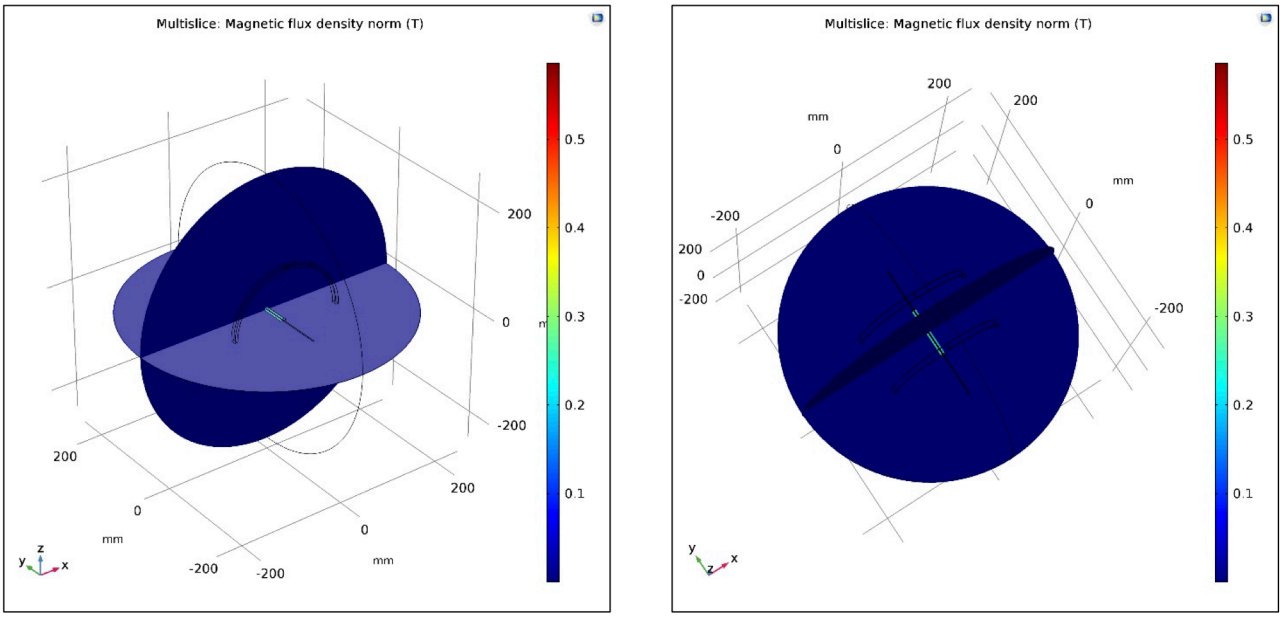

Figure 98: Magnetic field

The magnetic field is studied with the application of two cutting planes:

- the first one is on ZX axis;
- the second one is on XY axis.

The Figure 99 displays the first cutting plane, with the possibility to evaluate the magnetic flux density in different views (Figure 100, Figure 101). Arrows indicate how the behavior of the filed around the system is.

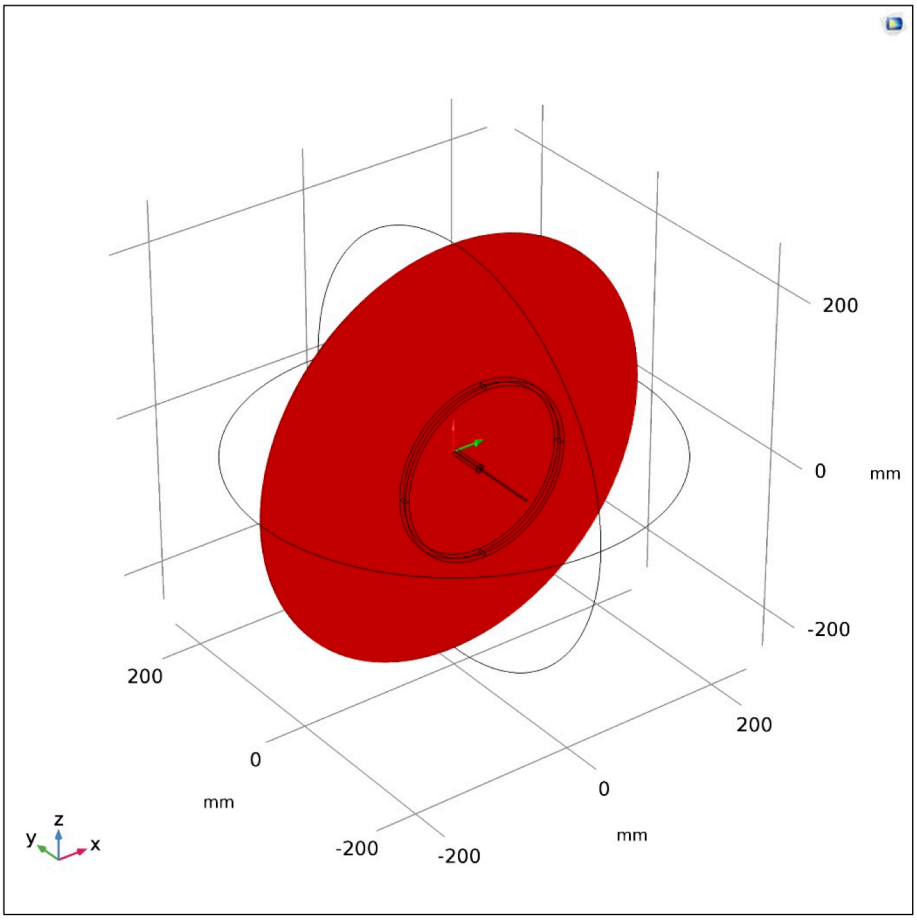

Figure 99: First cutting plane

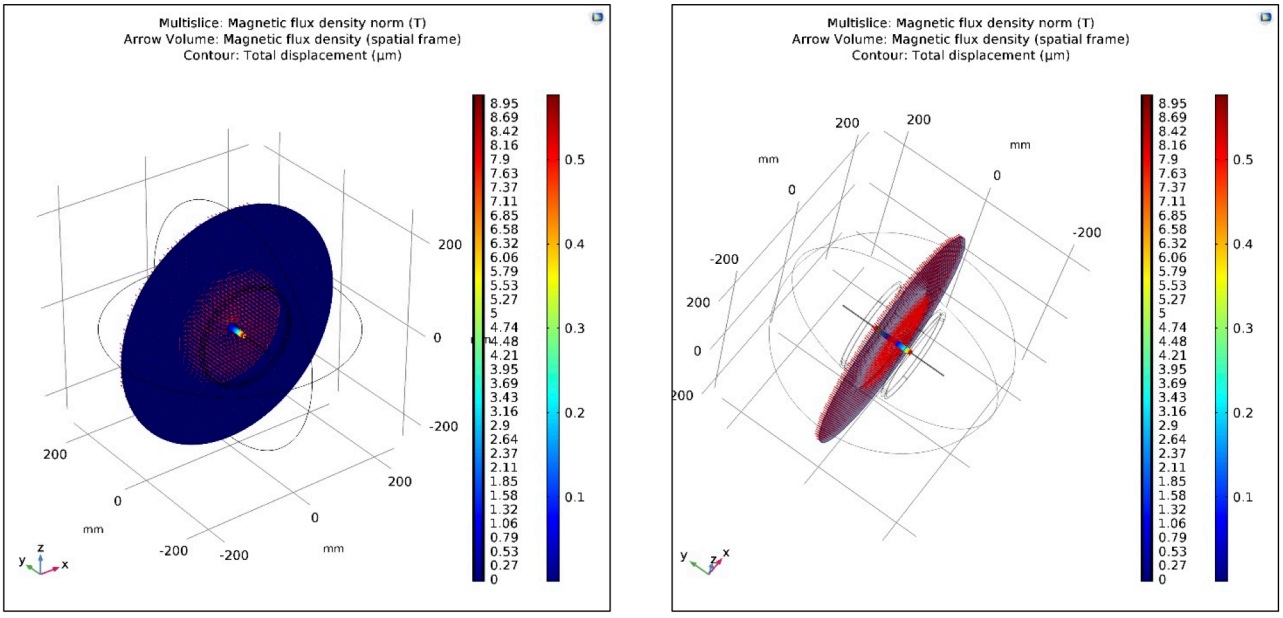

Figure 100: Magnetic flux density, first cutting plane

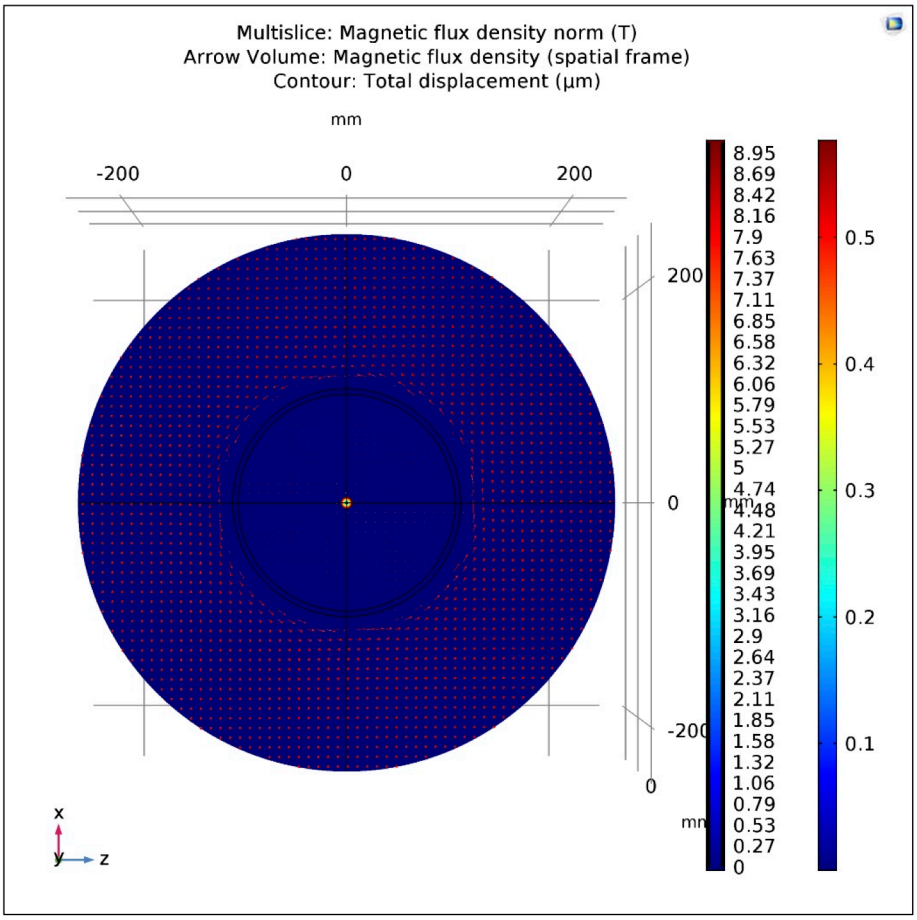

Figure 101: Magnetic flux density, first cutting plane

Figures above show how the magnetic flux trend is and successively two different cutting lines (Figure 102) on this first cut plane are taken into consideration.

As expected, results are the same and are reported in cutting lines figures: the maximum value is in the middle of the line.

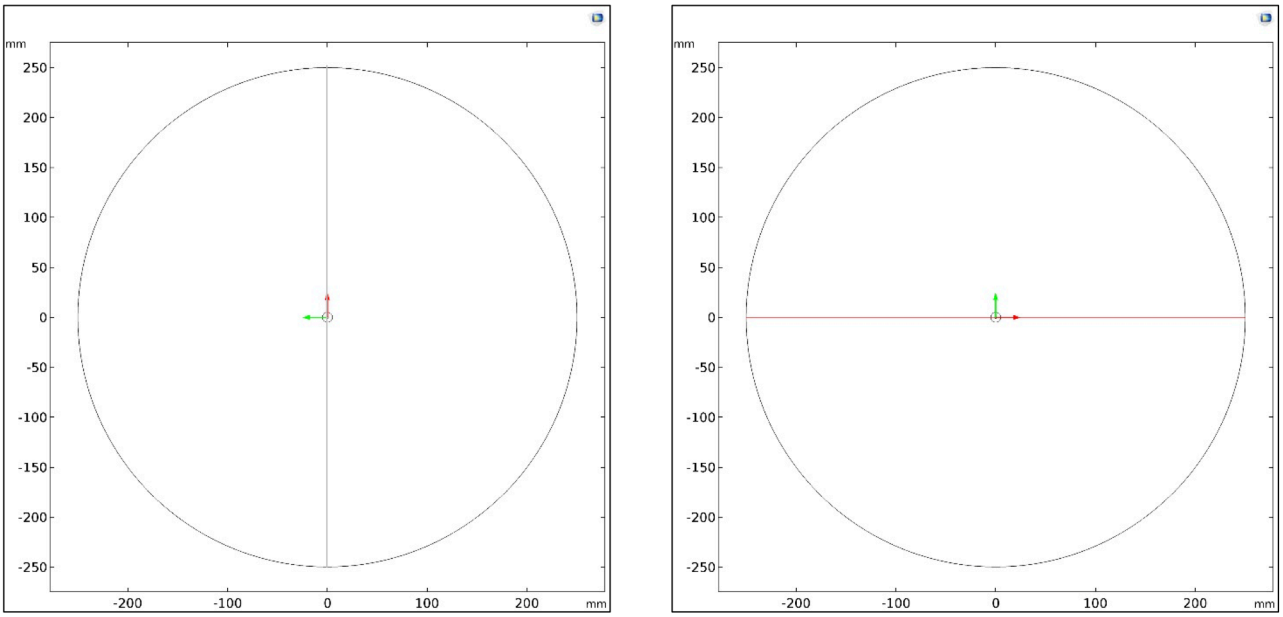

Figure 102: Cutting lines, first cutting plane

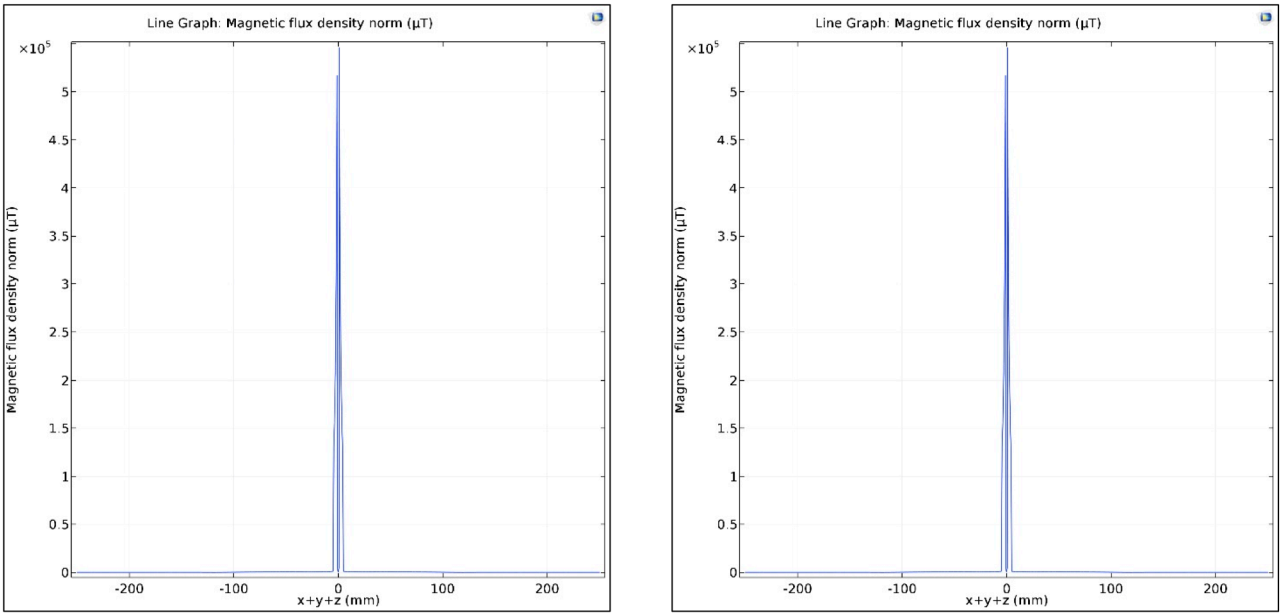

Figure 103: Magnetic field, first cutting plane

In the Figure 104 the second cutting plane is considered with the representation of the magnetic field. Arrows take information about direction, side and intensity. It is useful to understand how the flux is around the smart material (Figure 106), so that arrows give the idea that it is exposed to twist because the magnetic field is not circular but helical with the twist angle, building as composition of two magnetic fields.

In the Figure 107 and the Figure 108 there is the same study executed with the first cutting plane. It could be absorbing to understand how the magnetic field is, if the first cut line is considered, (figures on the left) because it is easy to compare this result with the previous one, demonstrated theoretically.

The Figure 109 shows the composition of two magnetic fields if there is the inclination to understand the order to magnitude.

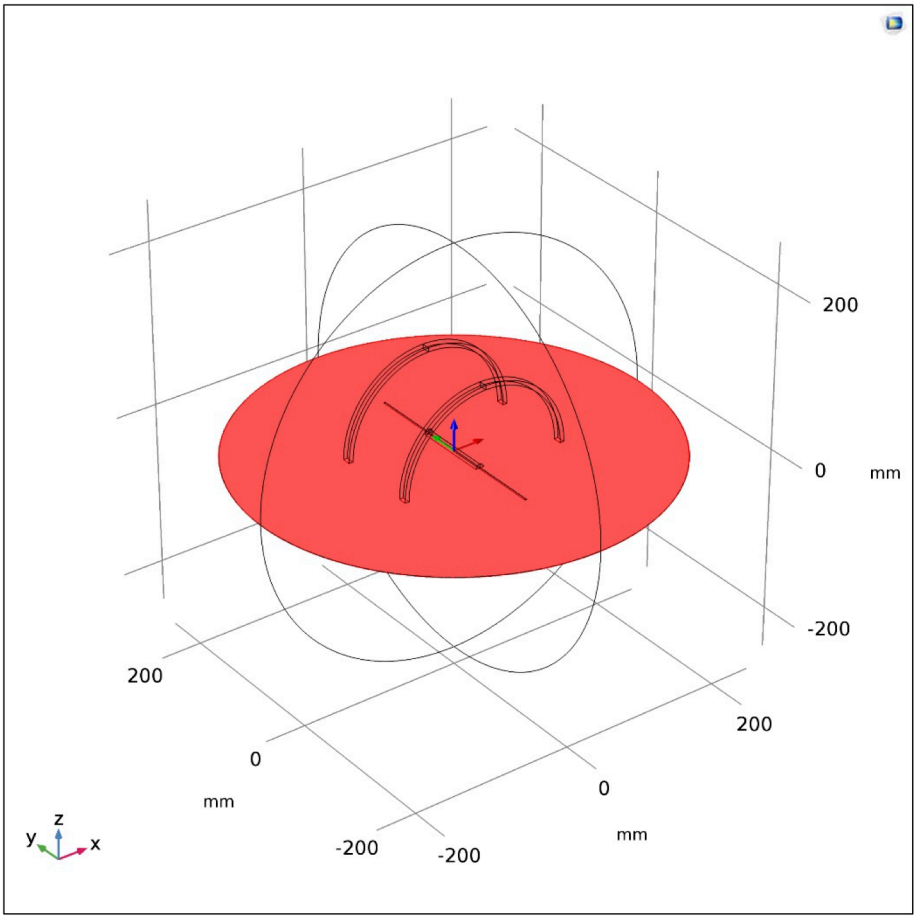

Figure 104: Second cutting plane

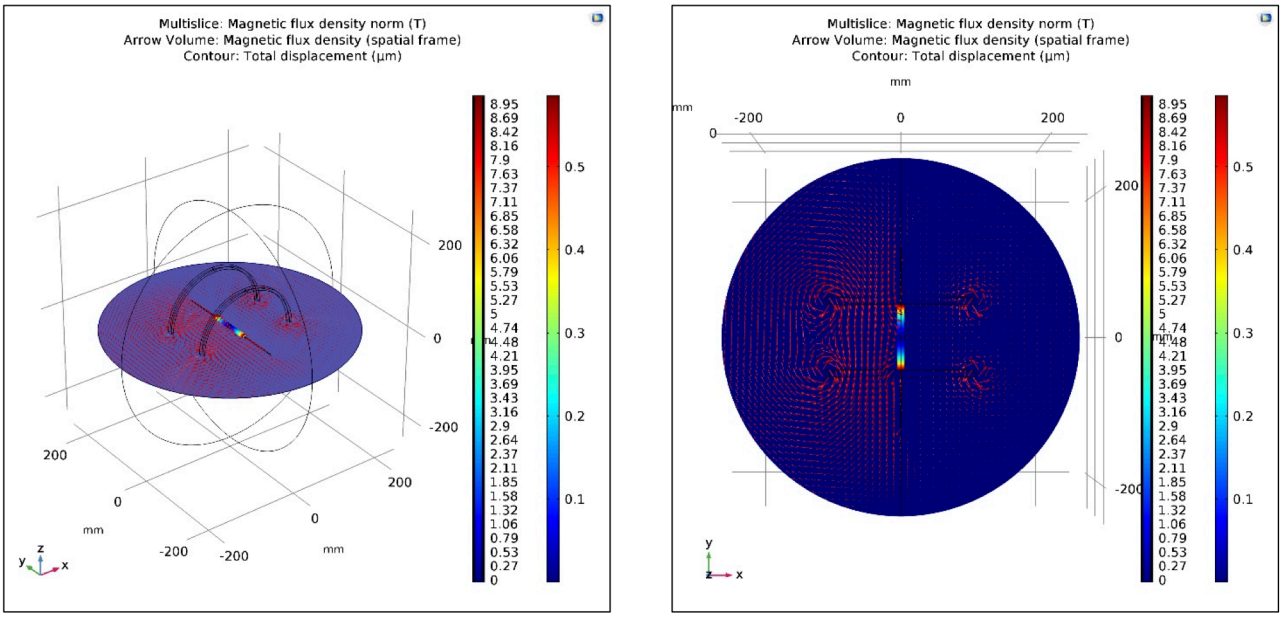

Figure 105: Magnetic flux density, second cutting plane

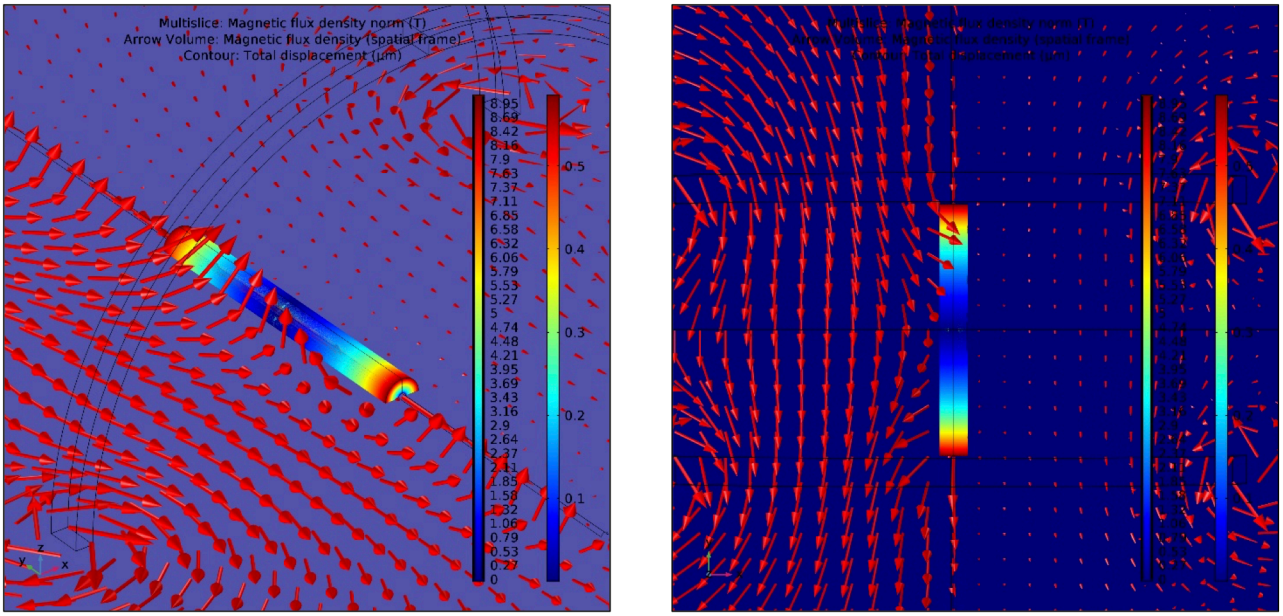

Figure 106: Magnetic flux density of the smart material, second cutting plane

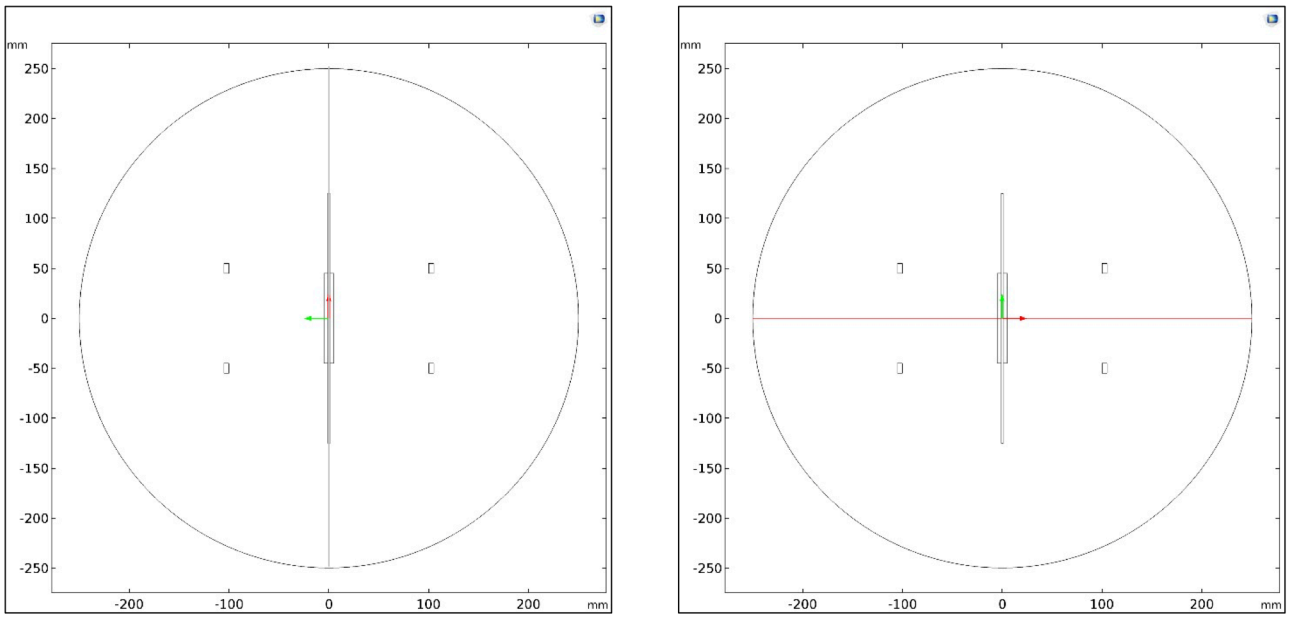

Figure 107: Cutting lines, second cutting plane

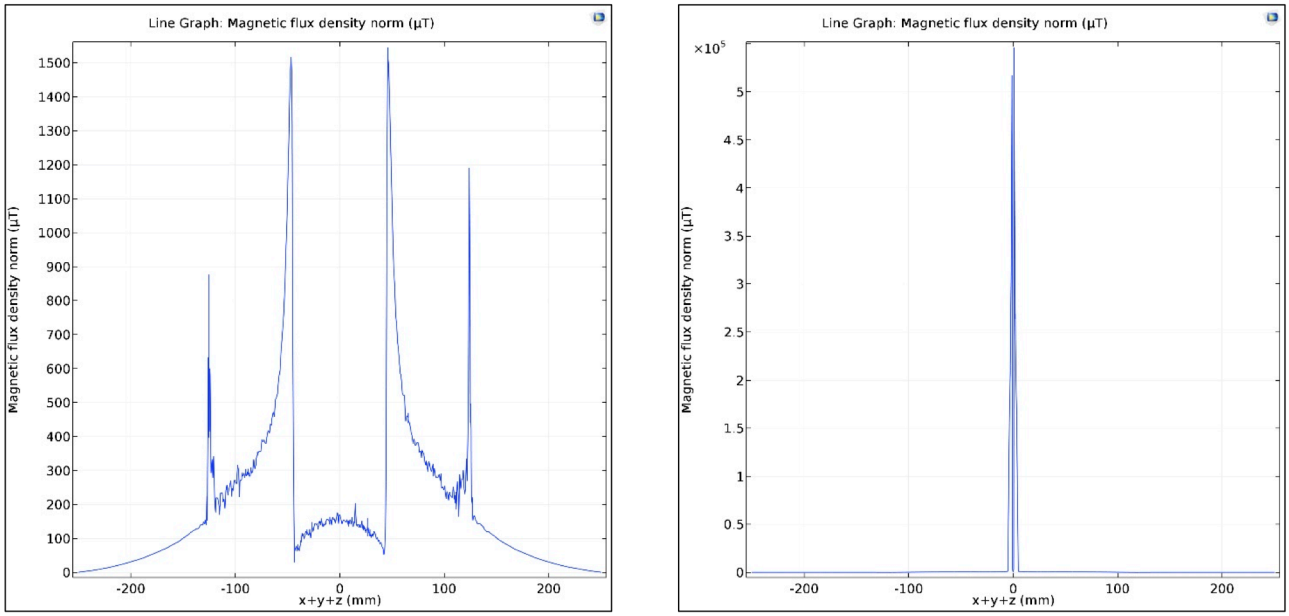

Figure 108: Magnetic field, second cutting plane

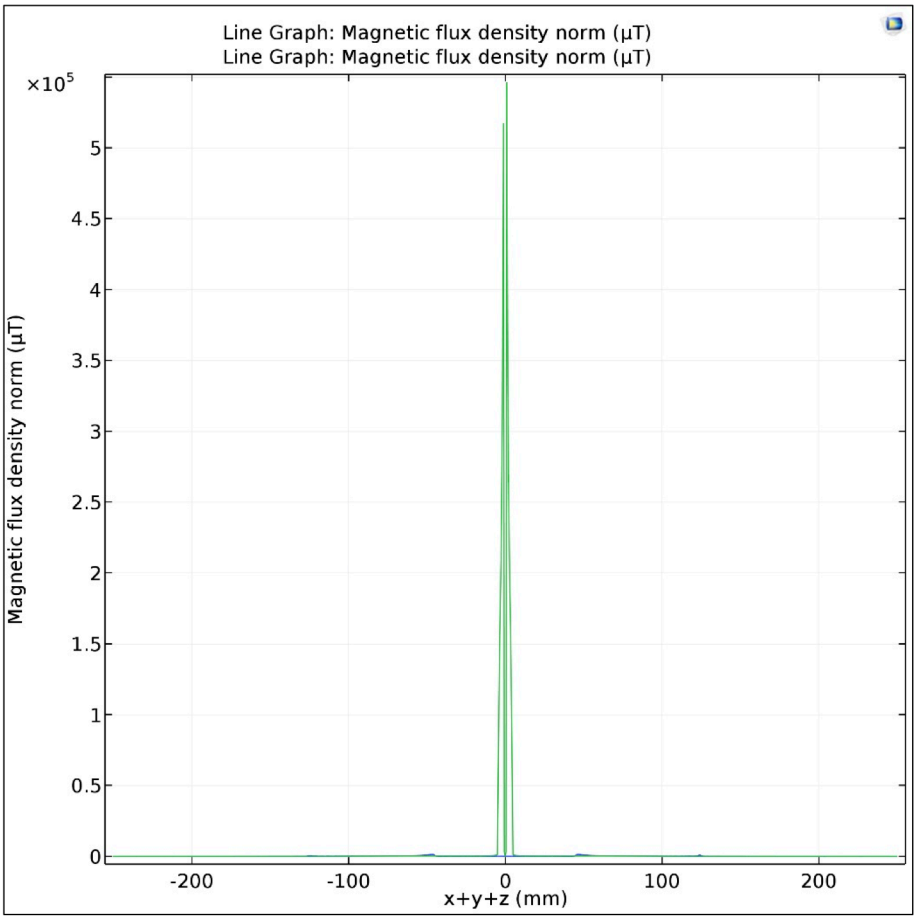

Figure 109: Sum of magnetic fields, second cutting planes

In the Figure 110 the mesh and the boundary condition of the system are illustrated. Mesh is fine and gives small values of errors, which are the sum of both permanent magnets and wire. Boundary conditions are important because the magnetic insulation is considered and at that distance the magnetic field could be approximately null.

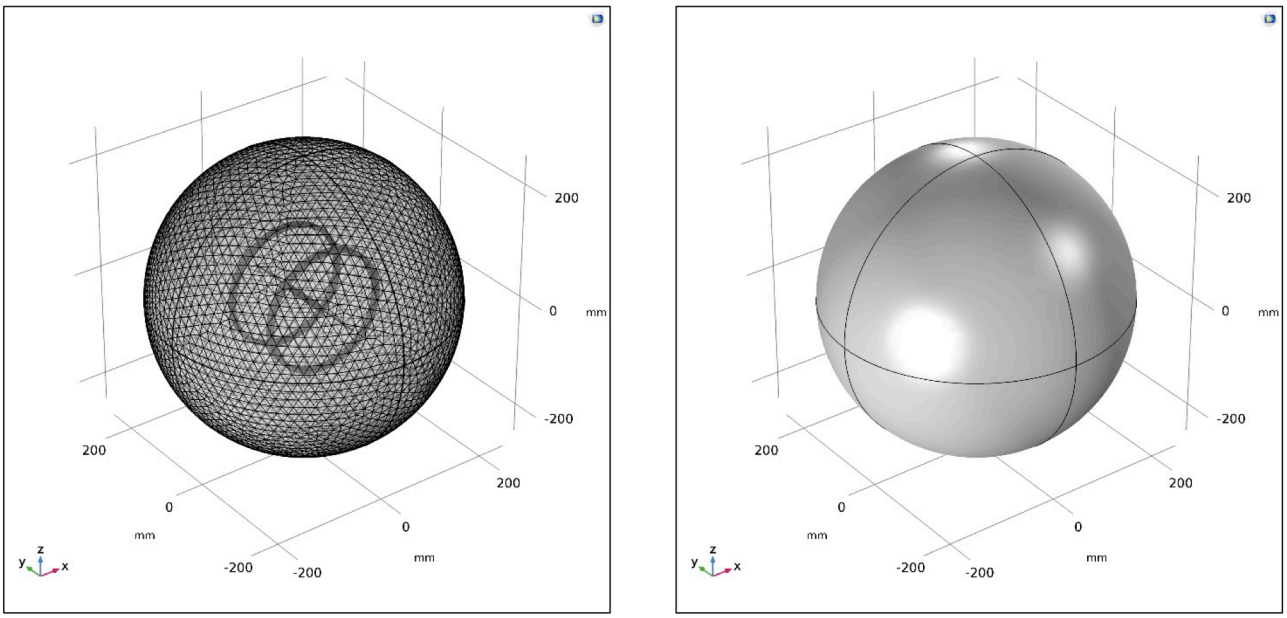

Figure 110: Mesh and boundary condition

Another important question could be to know how the displacement of the wire is, if it is in iron and its relative permeability changes. The table below demonstrates that values obtained are smaller than the simulation data of the smart material, so that it is another point useful to compare our investigation.

The setup verified is composed by wire and two Helmholtz Coils with a radius of 200 mm.
Materials used in the simulation are:
- Iron Powder SMP1172 for coils ($\mu r = 1$ *[H/m]*);
- Iron for the wire;
- Air around components.

The wire has these sizes:

SIZES	
Length [mm]	*500,00*
Inner Radius [mm]	*1,00*
Outer Radius [mm]	*5,00*

and these properties:

PROPERTIES	
Density ρ [kg/m³]	*7080,00*
Young's modulus E [Pa]	*2*10^(11)*
Poisson's ratio v	*0,45*
Electric conductivity [S/m]	*1,12*10^(7)*
Relative permittivity ε_r	*1,00*
Permeability μ_0 [H/m]	*4π*10^(-7)*
Saturation magnetostriction λ_s	*2,00*10^(-4)*
Saturation magnetization M_s [A/m]	*1,50*10^(6)*

The table below shows results if the relative permeability changes.

Rel. Permeability [H/m]	Displacement [µm]	Torsion [N*µm]
1,00	*0,0232*	*1,2407*
5,00	*0,0252*	*1,2374*
10,00	*0,0271*	*1,2523*
50,00	*0,1307*	*1,1557*
100,00	*0,4975*	*0,5167*

There are also graphs linked to the table in which on the X axis there is the relative permeability and on Y axis both displacement and torsion with the same units listed in the table.

Displacement

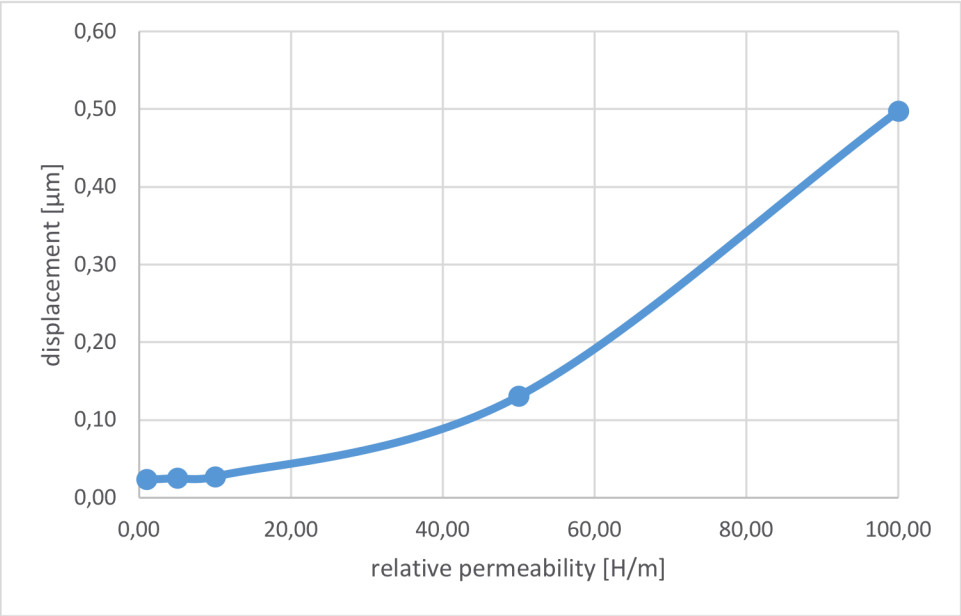

Torsion

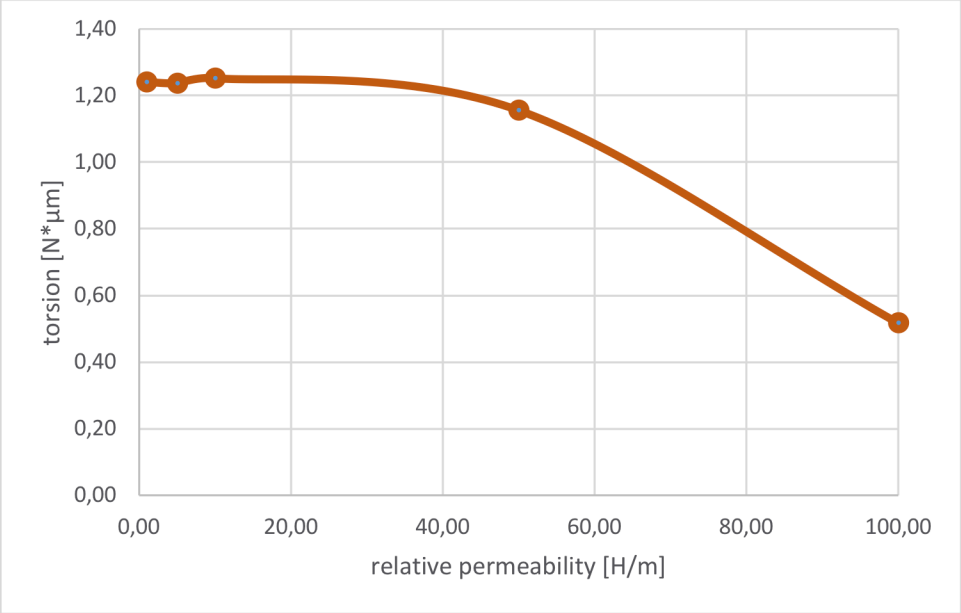

Graphs also illustrate that the trend for the torsion and the displacement is not the same but the opposite than previous results analyzed.

7.2 Permanent Magnets and Wire with Smart Material

In the next chapter it is explained the relation between the smart material prope
the torsion and other parameters. Permanent magnets are simulated and then the
the experimentation. Although permanent magnets replace Helmholtz coils, re
because their physics and application are equal. It is decided to simulate this setu

Name	Expression	Unit	Description
Permanent Magnets			
M	*10^6*	*[A/m]*	*Magnetization*
Br	*1,30*	*[T]*	*Remanence*
R	*30,00*	*[mm]*	*Outer Radius permanent magn*
r	*3,00*	*[mm]*	*Inner Radius permanent magn*
H	*30,00*	*[mm]*	*Height permanent magnet*
D	*200,00*	*[mm]*	*Distance permanent magnets*
Wire			
i	*30,00*	*[A]*	*Current*
j	$i/(\pi R^2)$	$[A/m^2]$	*Density current*
R	*1,00*	*[mm]*	*Radius*
L	*250,00*	*[mm]*	*Length*

The sample of smart material shows these sizes:

SIZES [mm]	
Length	*50,00*
Inner Radius	*1,00*
Outer Radius	*5,00*

and these properties:

PROPERTIES	
Density ρ [kg/m³]	*6000,00*
Young's modulus E [Pa]	*40000,00*
Poisson's ratio v	*0,45*
Electric conductivity [S/m]	*0,00*
Relative permittivity ε_r	*10,00*
Permeability μ_0 [H/m]	*4π*10^(-7)*
Relative permeability μr [H/m]	*100,00*
Saturation magnetostriction λ_s	*0,10*
Saturation magnetization M_s [A/m]	*0,45*10^(6)*

Figures below show the geometry of the setup.

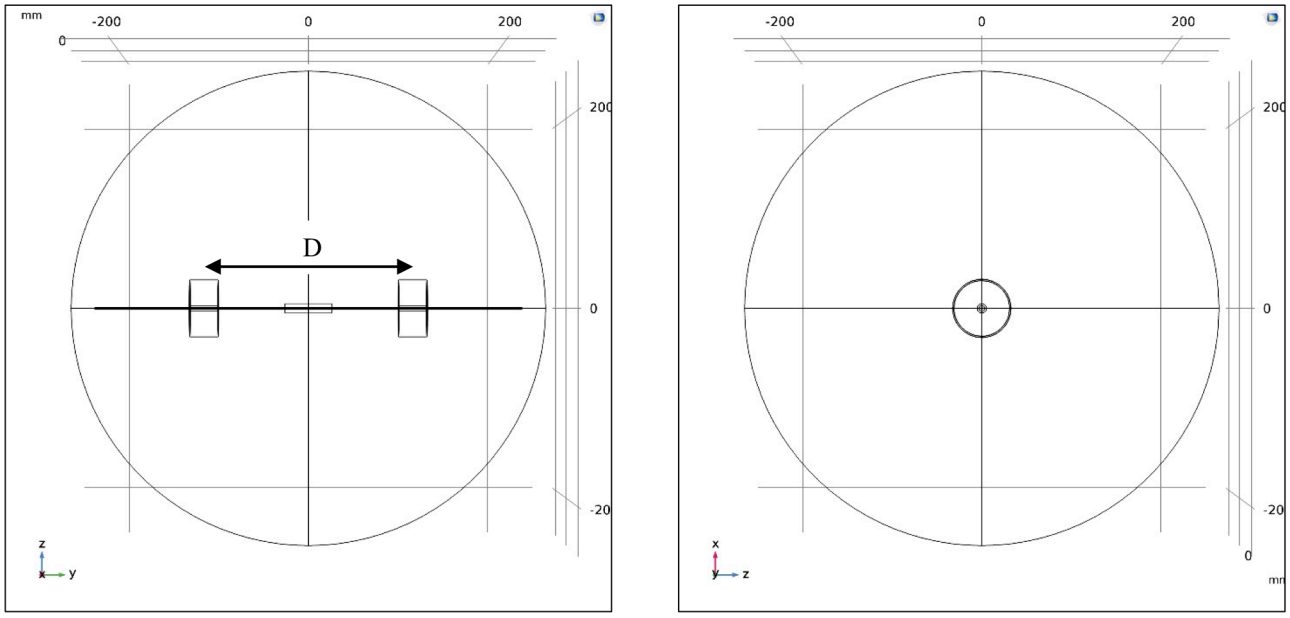

Figure 111: Geometry

Materials used in the simulation are:

- Neodymium for permanent magnets;
- Smart material for the sample around the wire with optimal properties and sizes, dealt with in the chapter before;
- Copper for the wire;
- Air around components.

The Figure 112 shows the setup in coordinate system space. Permanent magnets are fixed with opposite pole faces, therefore the north pole of one permanent magnets is near the south pole of the other.

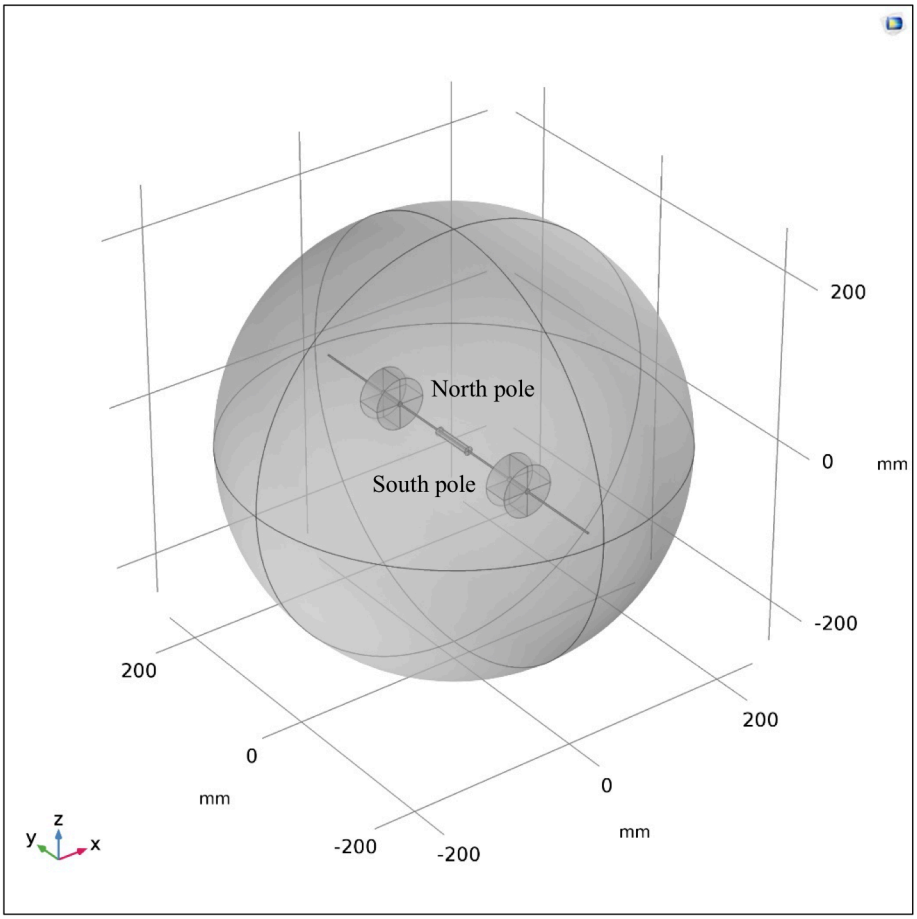

Figure 112: Setup of permanent magnets and wire with smart material

In the table below, it is shown how parameters change with the distance between

Displacement [µm]	Magnetic Field [T]	Torsion [N*µm]	Stress [N/m²]	Torsion [deg
911,4600	1,5057	165,2200	23059,0000	34,90
105,9500	1,5137	6,6037	3539,0000	35,32
46,1390	1,5792	3,1759	1241,2000	44,47
10,8500	1,5818	0,1331	832,0400	47,14
5,1638	1,5974	0,0255	694,4700	54,79

As explained before, parameters illustrated in the table are:

- the maximum displacement on the smart material;
- the maximum magnetic field on the setup which is localized in the middle space
magnets, instead the minimum value is on the boundary of the setup (approximat
- the maximum torsion on the smart material and its maximum angle (Maxwell te
- the maximum stress calculated with Von Mises' law.

Graphs about the table explained are reported following: the distance is on the X
and on the Y axis there is the parameter investigated with the same unit listed in t

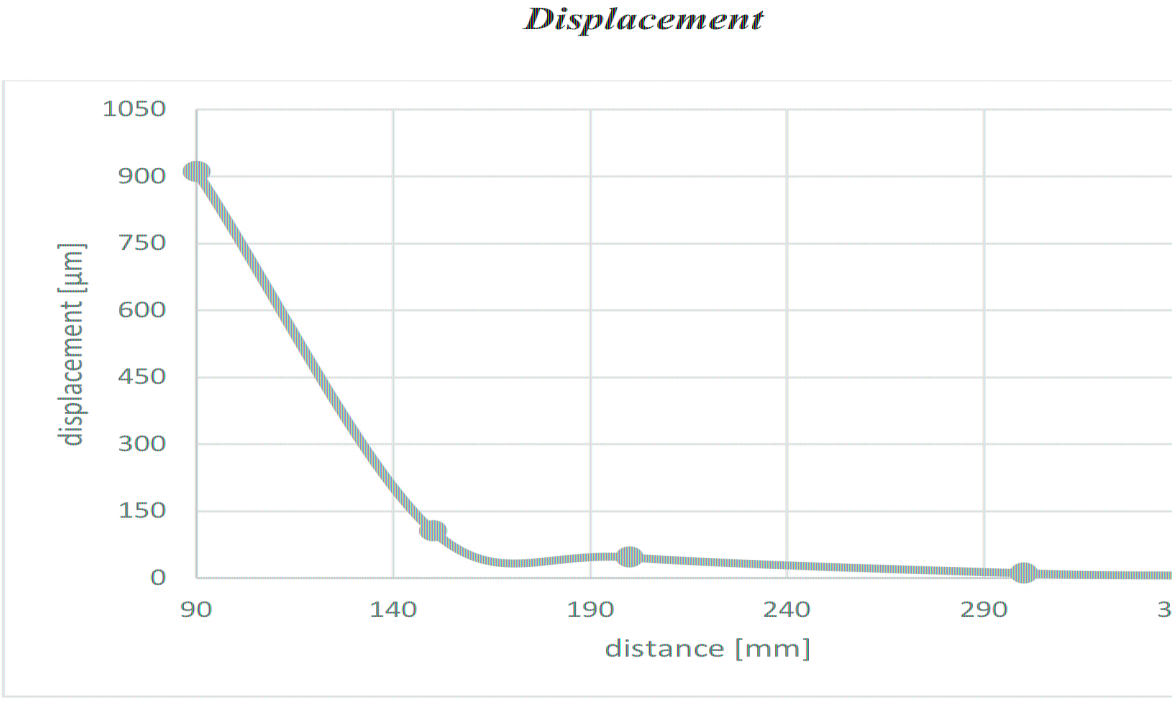

Magnetic Field

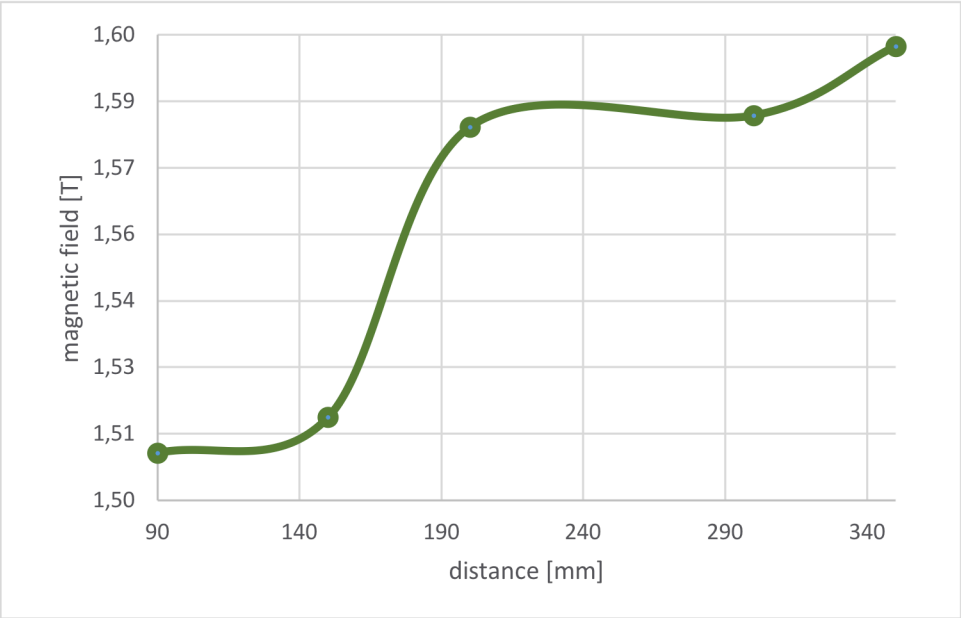

Torsion

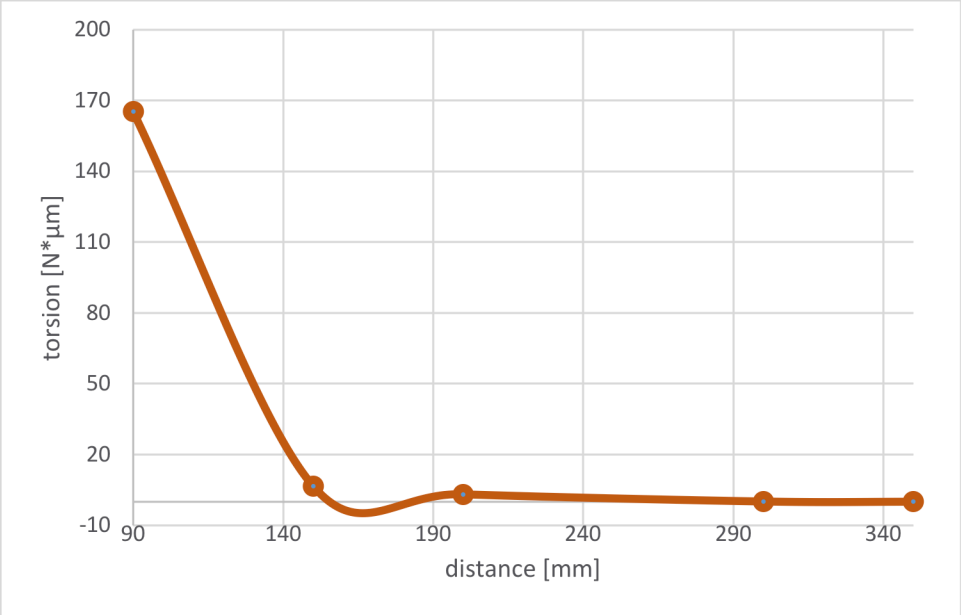

Stress

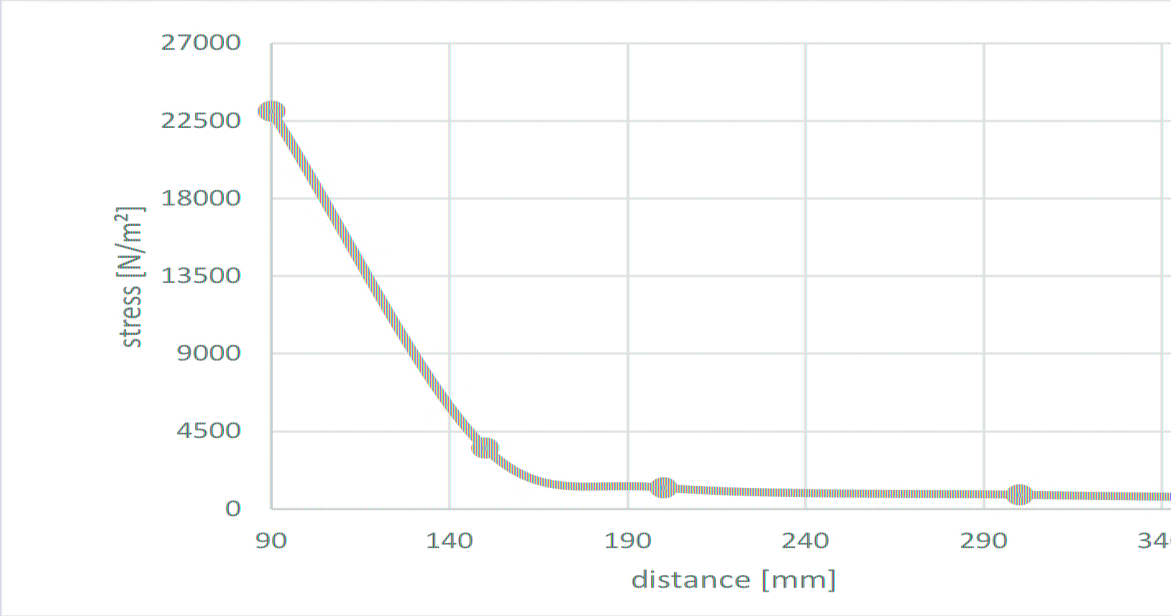

Torsion Angle

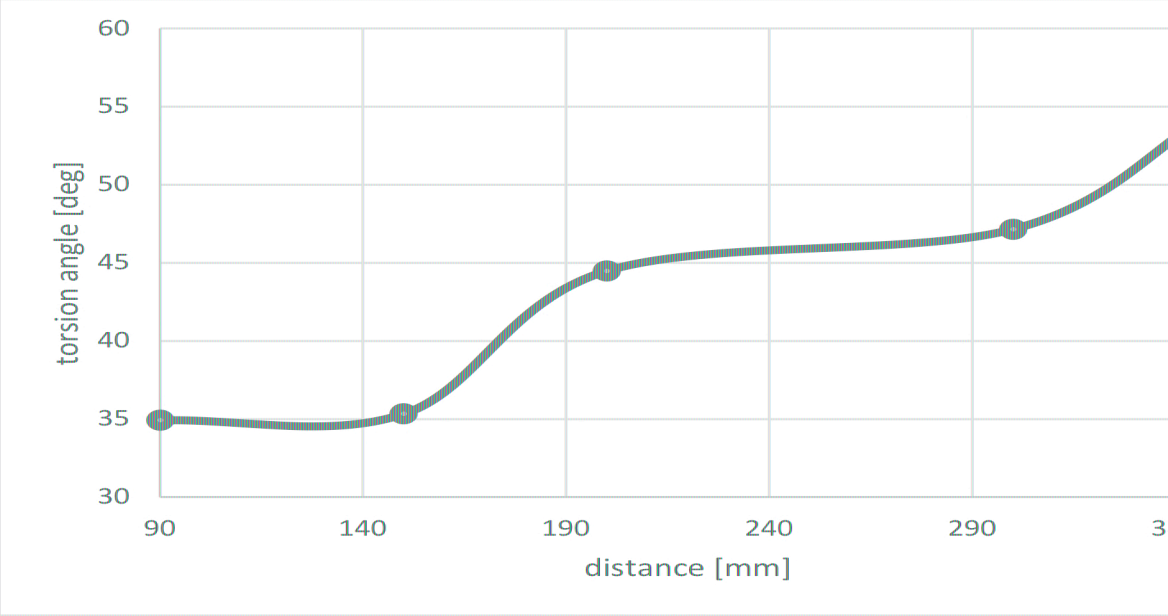

It is chosen to explain the simulation using the distance of 200 mm because the to
by the composition of two magnetic fields: one of the wire and the other of per
the distance is smaller than 200 mm the smart material is influenced so much by

of permanent magnets that it can elongate; instead if the distance is bigger than 200 mm it is affected by the magnetic field of the wire; for these reasons the torsion angle is an important parameter to define the type of influence on the smart material. In this case, the value is around 45 degrees and as a consequence a good equilibrium between the magnetic field of wire and the magnetic field of the permanent magnets is obtained.

When the current flows in the wire, it is possible to evaluate how the magnetic field surrounds the system. In this view, there is a global representation with two cut planes considered.

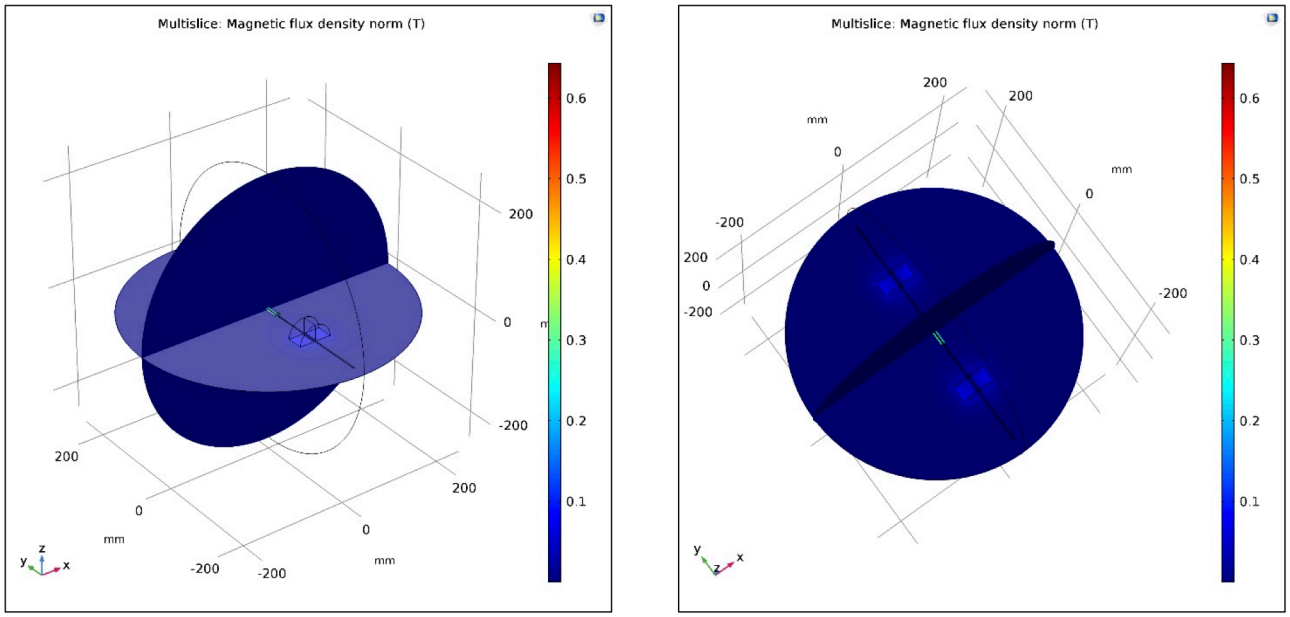

Figure 113: Magnetic field

The magnetic field is studied with the application of two cutting planes:
- the first one is on ZX axis;
- the second one is on XY axis.

The first cutting plane is shown in Figure 114 where it is possible to evaluate the magnetic flux density in different views (Figure 115, Figure 116). Arrows indicate how is the behavior of the field around the system.

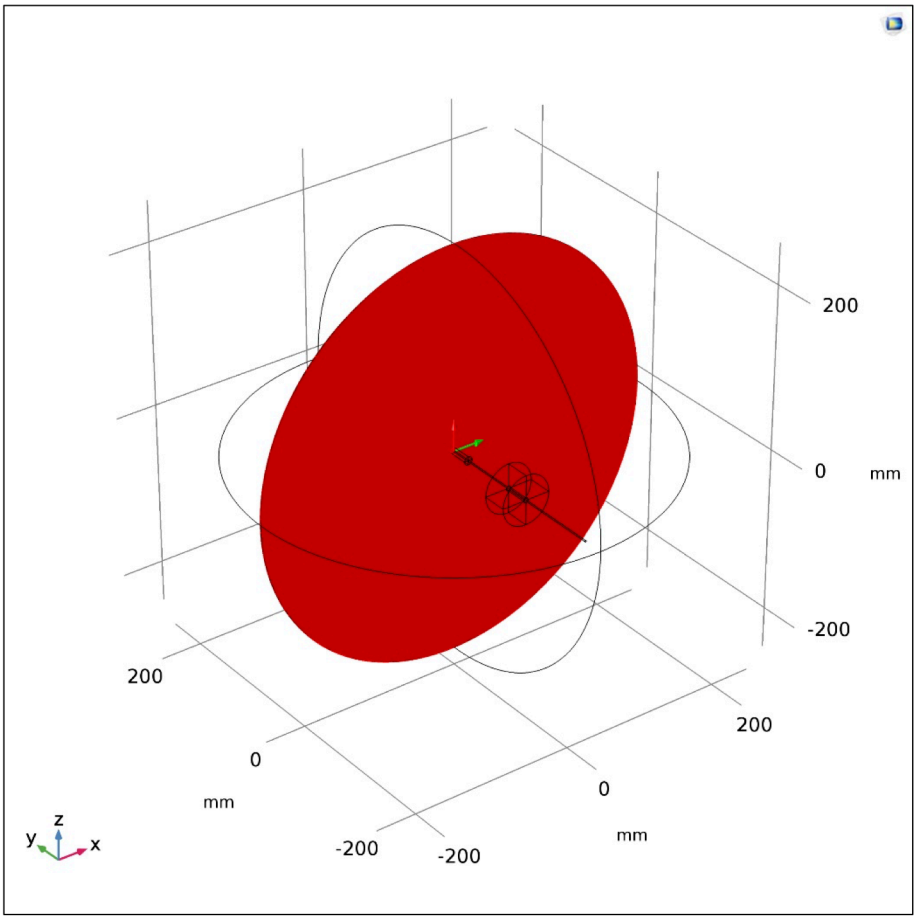

Figure 114: First cutting plane

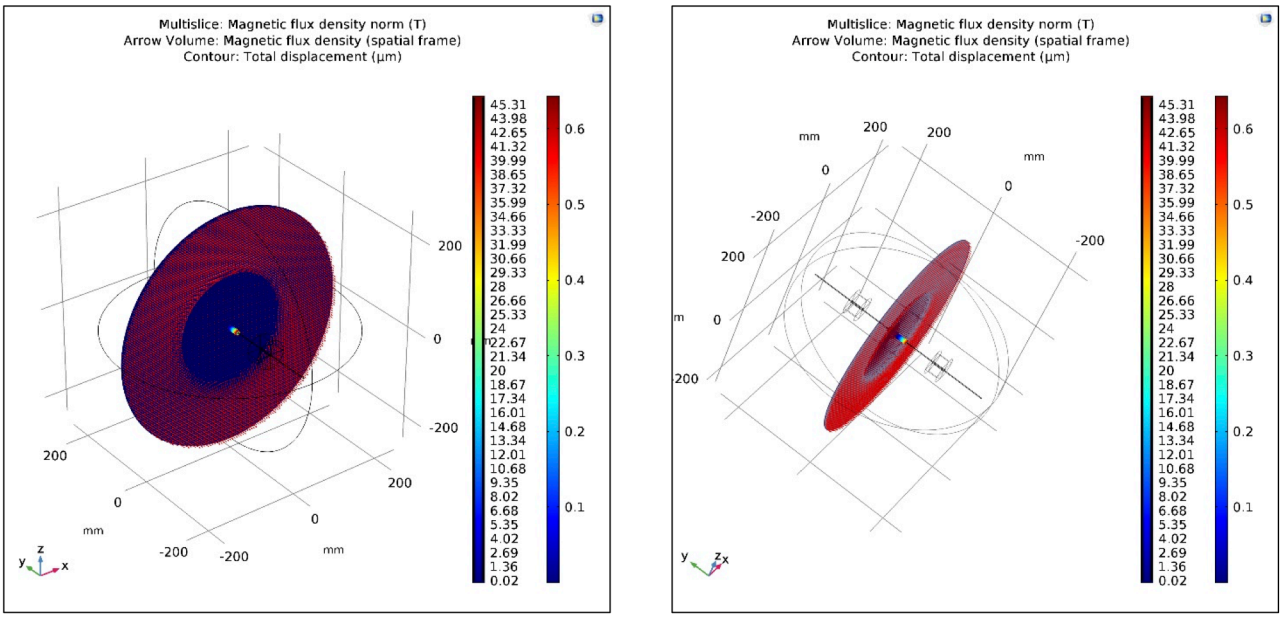

Figure 115: Magnetic flux density, first cutting plane

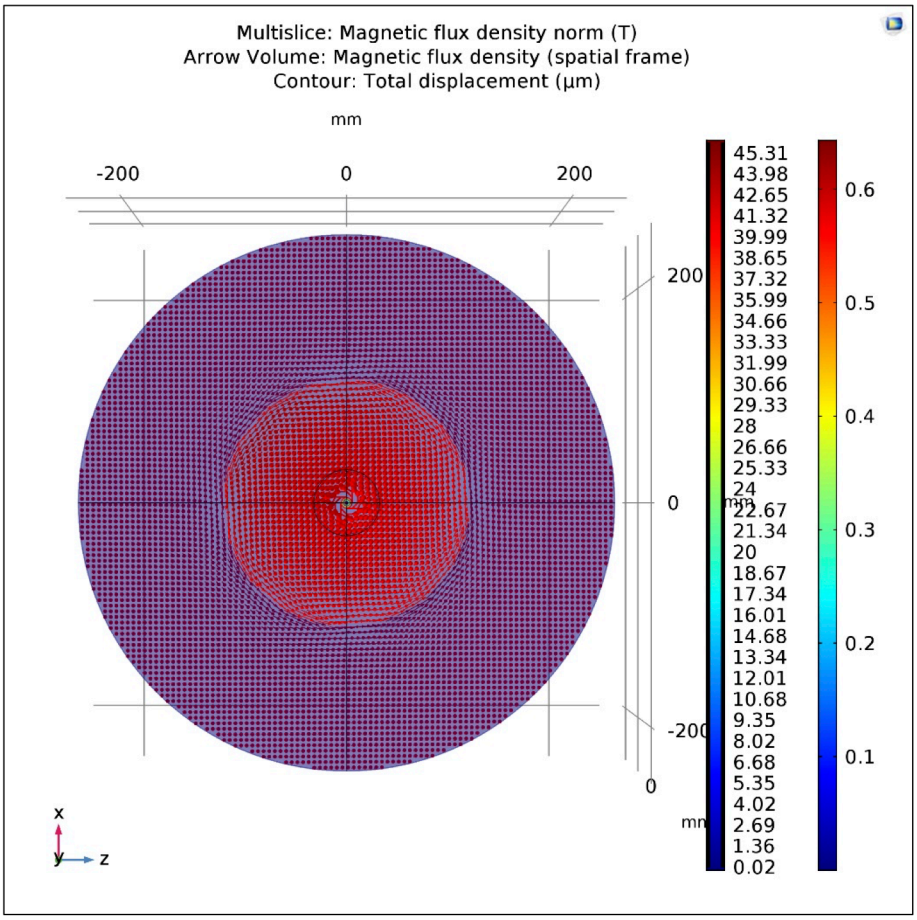

Figure 116: Magnetic flux density, first cutting plane

The figures above show how the magnetic flux trend is and subsequently two different cutting lines (Figure 117) on this first cutting plane are considered.

As expected, results are the same and are reported at the cutting lines figures: the maximum value is in the middle of the line.

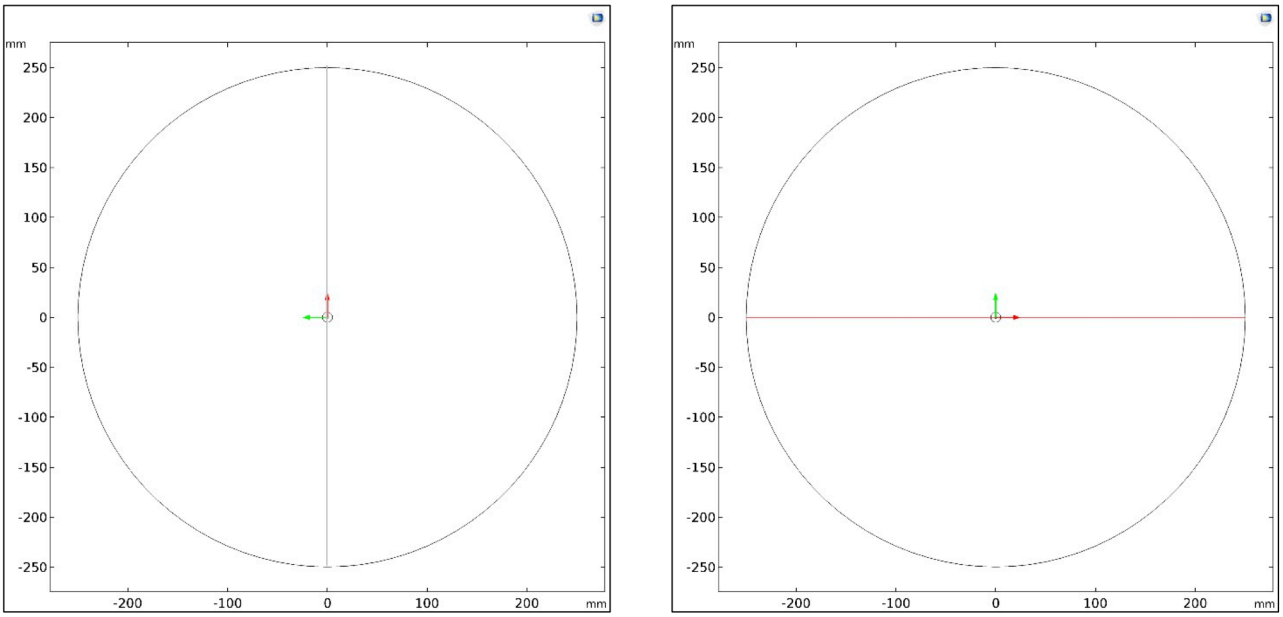

Figure 117: Cutting lines, first cutting plane

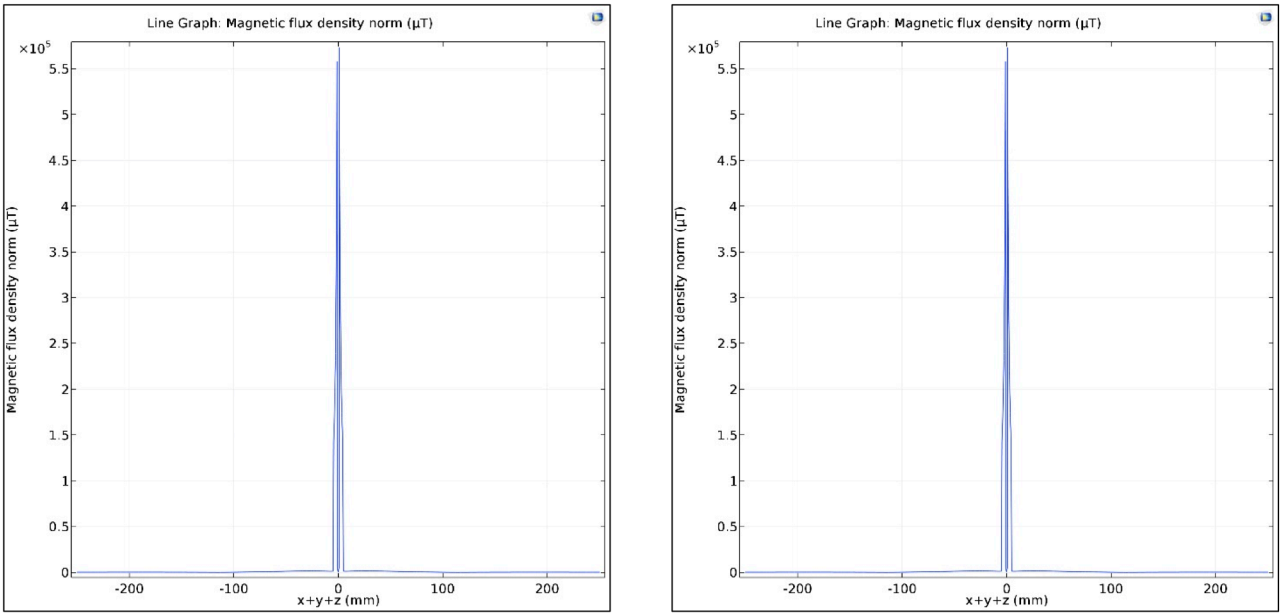

Figure 118: Magnetic field, first cutting plane

In the Figure 119, the second cutting plane is considered with the representation of the magnetic field. Arrows take information about direction, side and intensity. It is useful to understand how the flux around the smart material is (Figure 122), thus arrows give the idea that it is exposed to twist because the magnetic field it is not circular but helical with the twist angle which is the composition of the two magnetic fields.

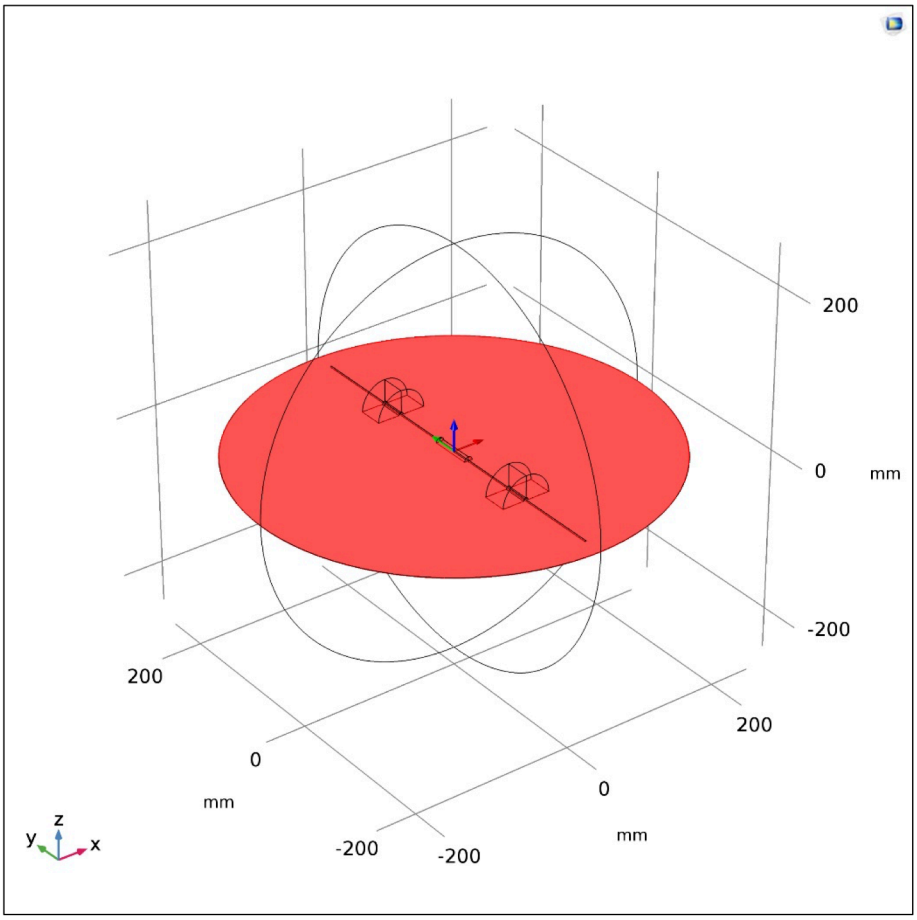

Figure 119: Second cutting plane

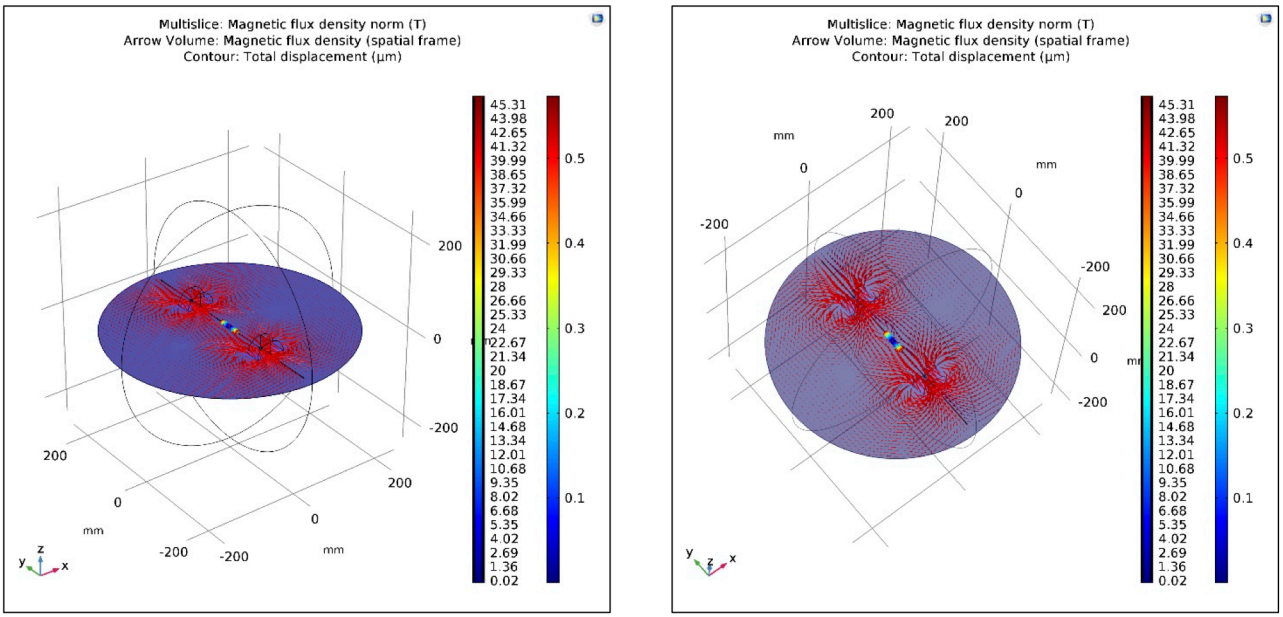

Figure 120: Magnetic flux density, second cutting plane

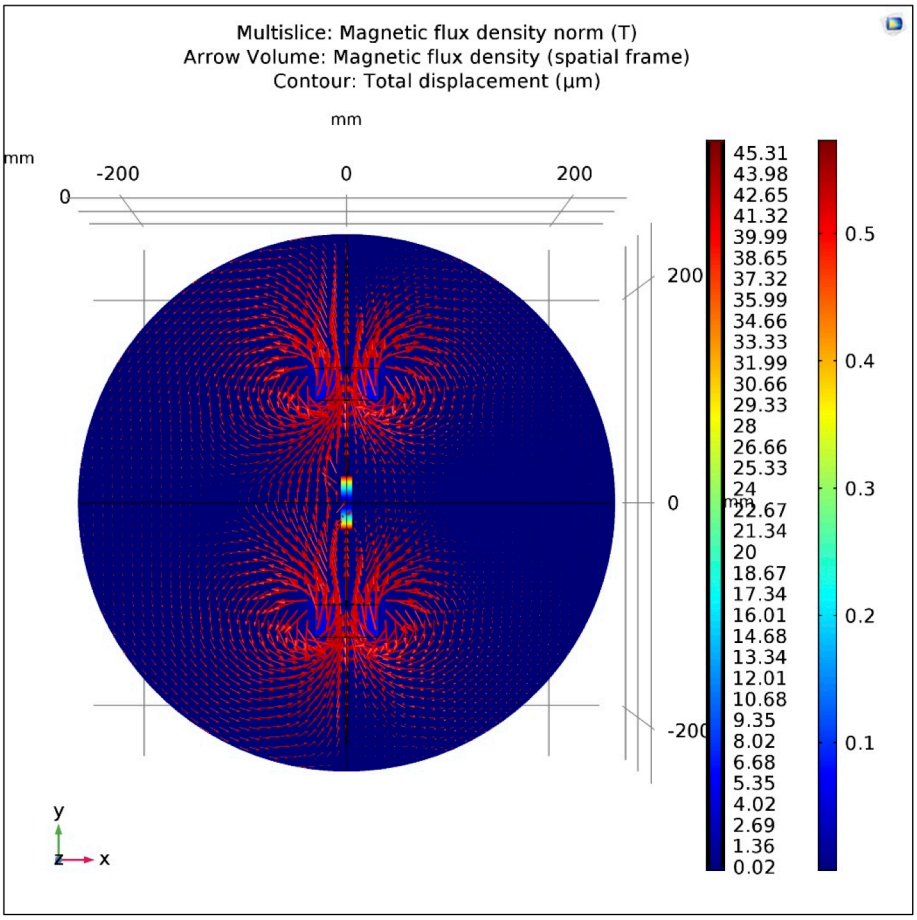

Figure 121: Magnetic flux density, second cutting plane

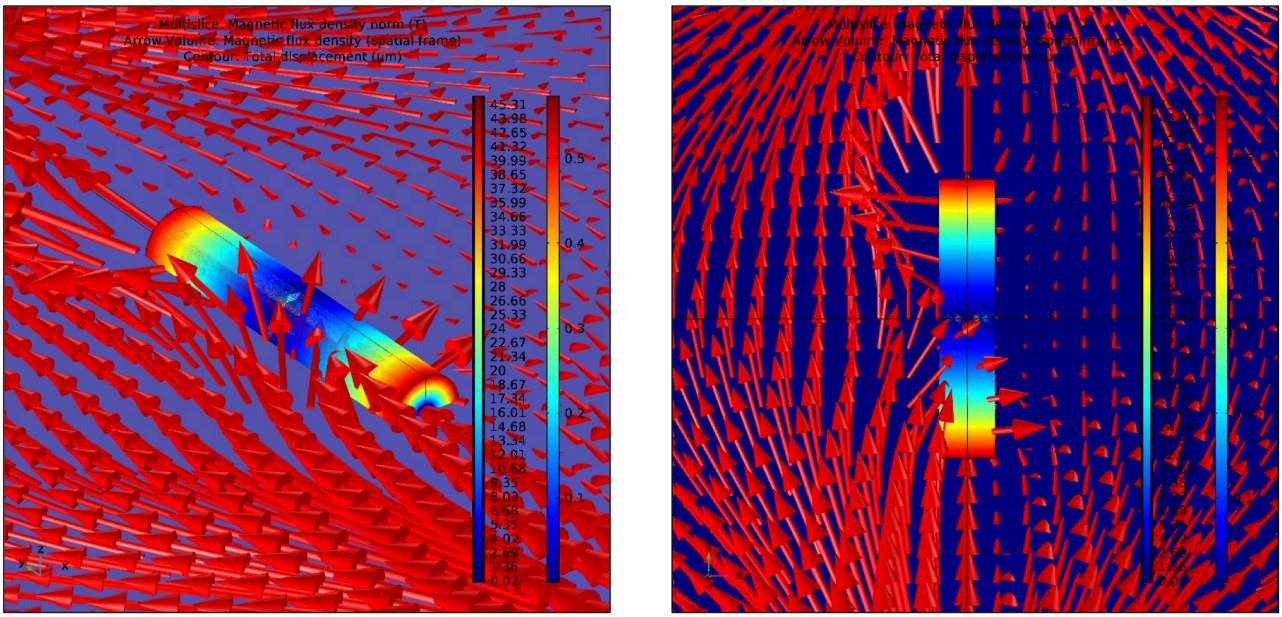

Figure 122: Magnetic flux density of the smart material, second cutting plane

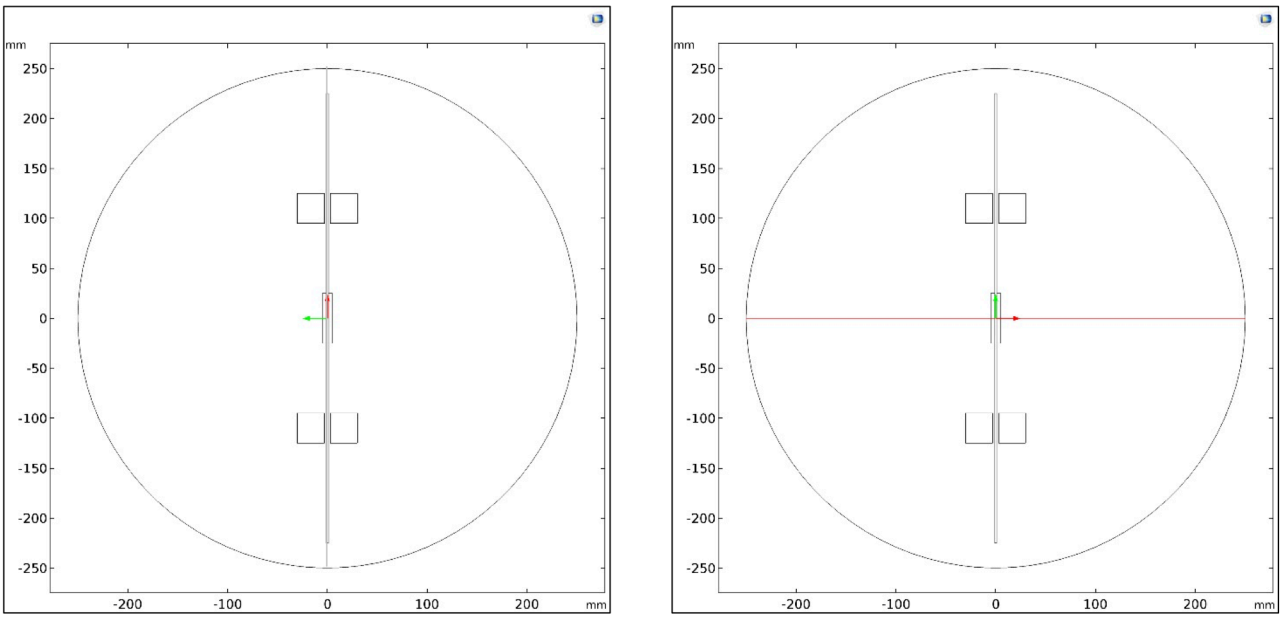

Figure 123: Cutting lines, second cutting plane

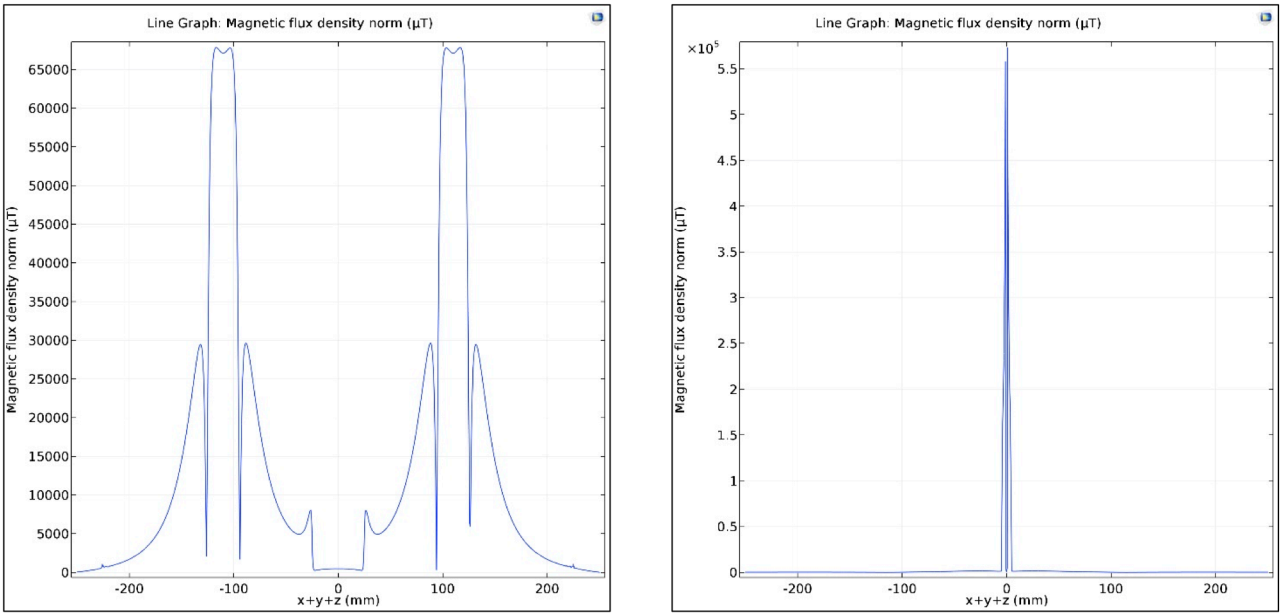

Figure 124: Magnetic field, second cutting plane

In the Figure 123 and the Figure 124 there is the same study carried out with the first cutting plane. It is interesting to notice how the magnetic field is, if the first cut line is considered (figures on the left) because it easy to compare this result with the previous one which is proved theoretically.

The Figure 125 shows the composition of two magnetic fields if there is the intention to understand the order to magnitude.

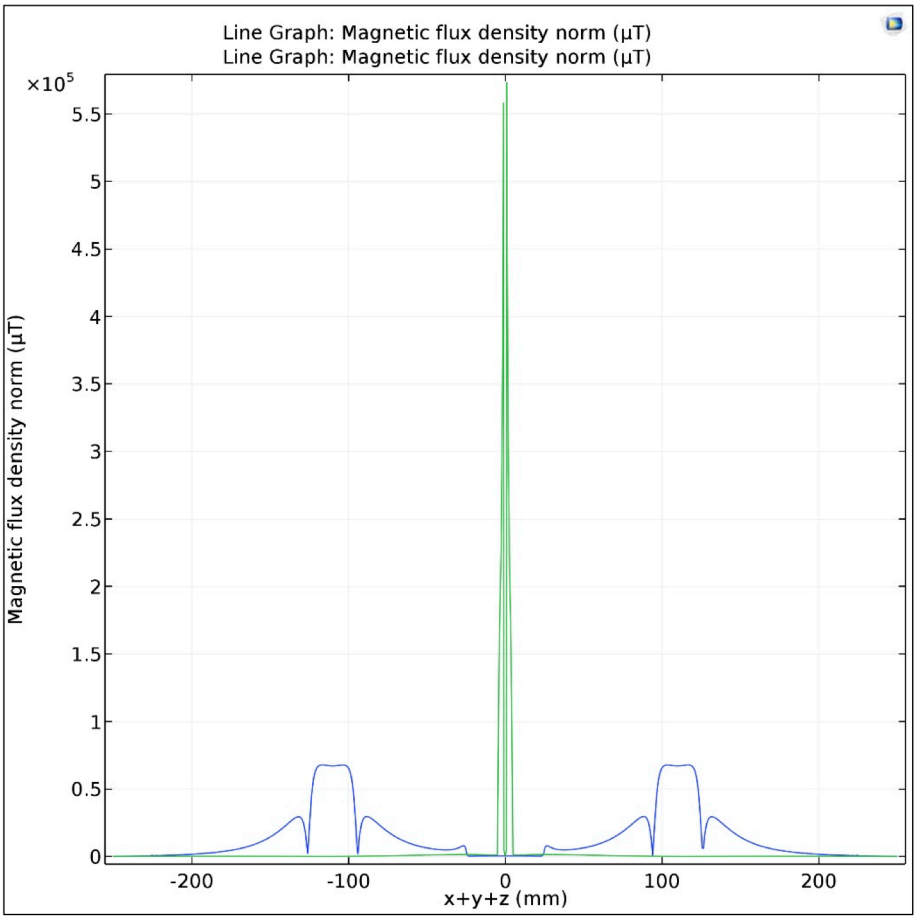

Figure 125: Sum of magnetic fields, second cutting plane

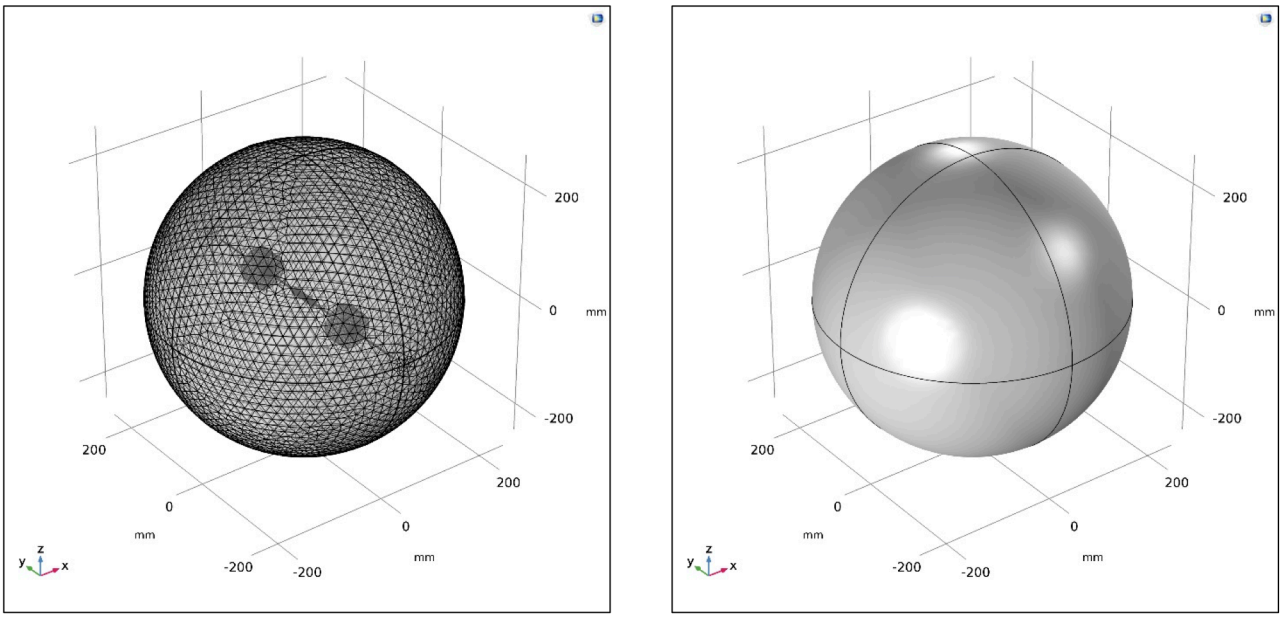

Figure 126: Mesh and boundary condition

In the Figure 126 the mesh and the boundary condition of the system are illustrated. Mesh is fine and gives values of error around the 35%, obtained from previous simulations: it is calculated with the sum of the error both of permanent magnets and of the wire. Boundary conditions are important because the magnetic insulation is considered and at that distance the magnetic field could be approximately null.

Concerning the smart material, the modulus of displacement is taken into account:

$$s = \sqrt{u^2 + v^2 + w^2} \tag{7.0}$$

where:

- u is the displacement on the X axis;
- v is the displacement on the Y axis;
- w is the displacement on the Z axis.

The maximum and minimum modulus are shown, considering the volume of the smart material.

Obviously figures report the maximum in the area around the outer radius, instead the minimum (which is null) is admitted where mechanics constraints are established between the sample of smart material and the wire.

In the Figure 129 and the Figure 130 there are also streamlines which give the idea about the trend of displacement. Surely there is a helical behavior and the torsion is verified. As it is possible to read from the legend, the material has the maximum twist on its sides and decreases in the middle also why the torsion has two different rotation ways.

The maximum modulus of torsion is considered on smart material in this way:

$$T = \sqrt{{T_x}^2 + {T_y}^2 + {T_z}^2} \tag{7.1}$$

where:

- T_x is the torsion on the X axis;
- T_y is the torsion on the Y axis;
- T_z is the torsion on the Z axis.

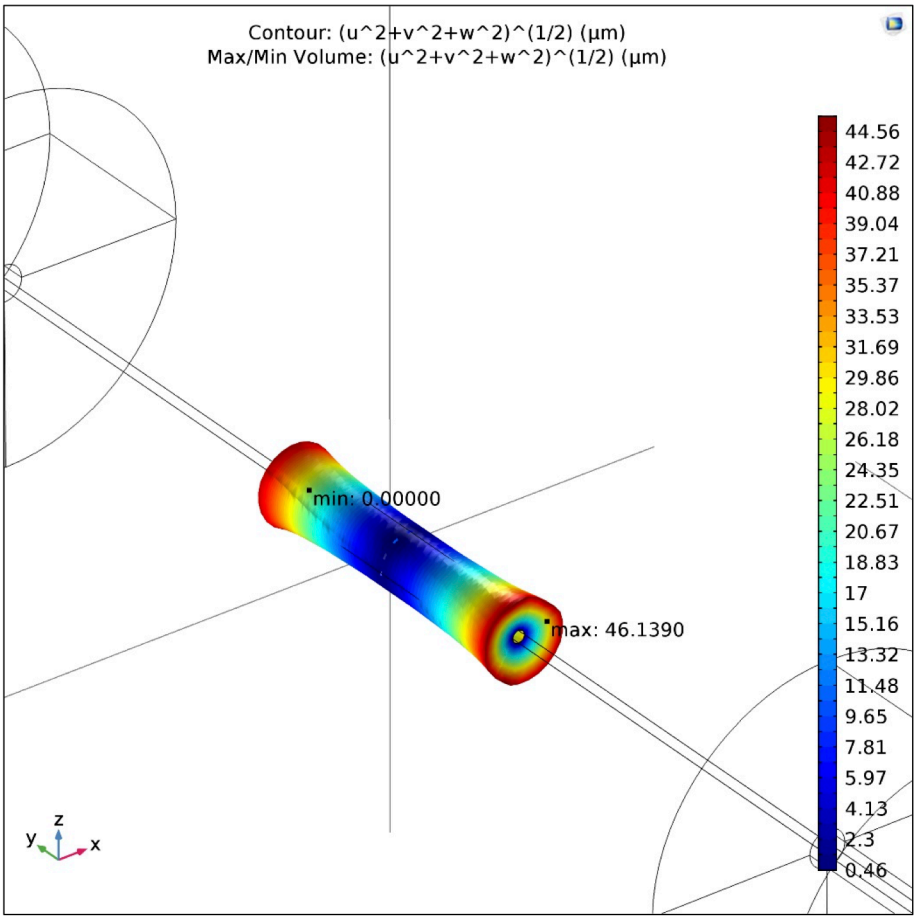

Figure 127: Smart material

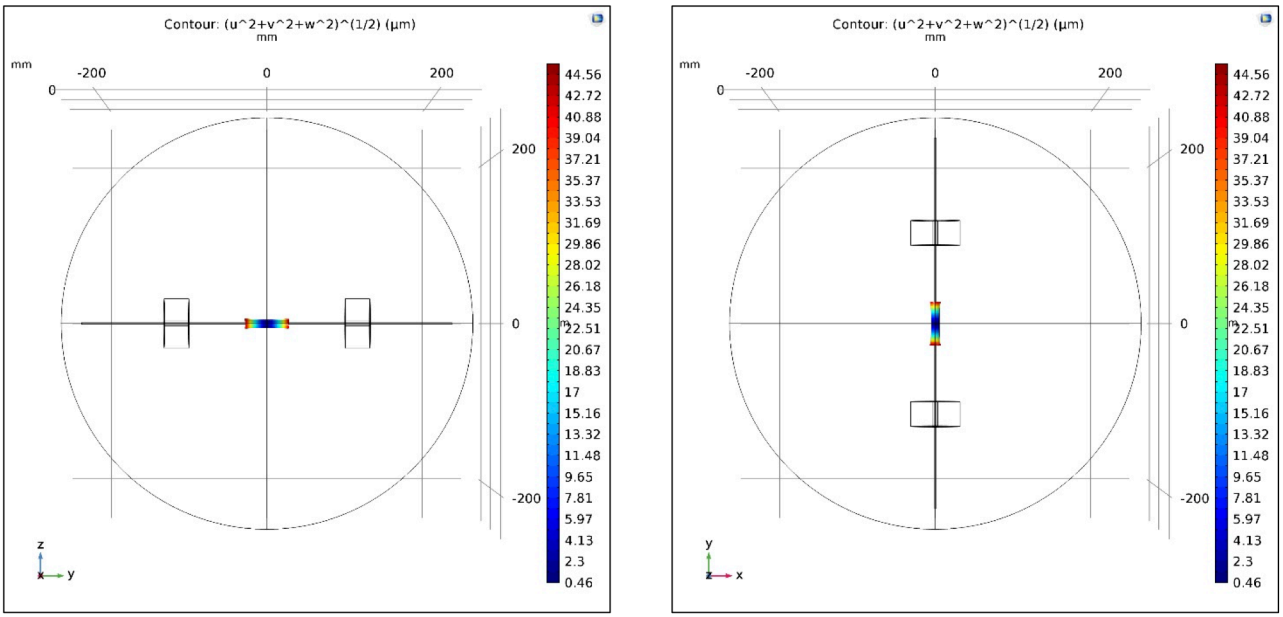

Figure 128: Smart material, views

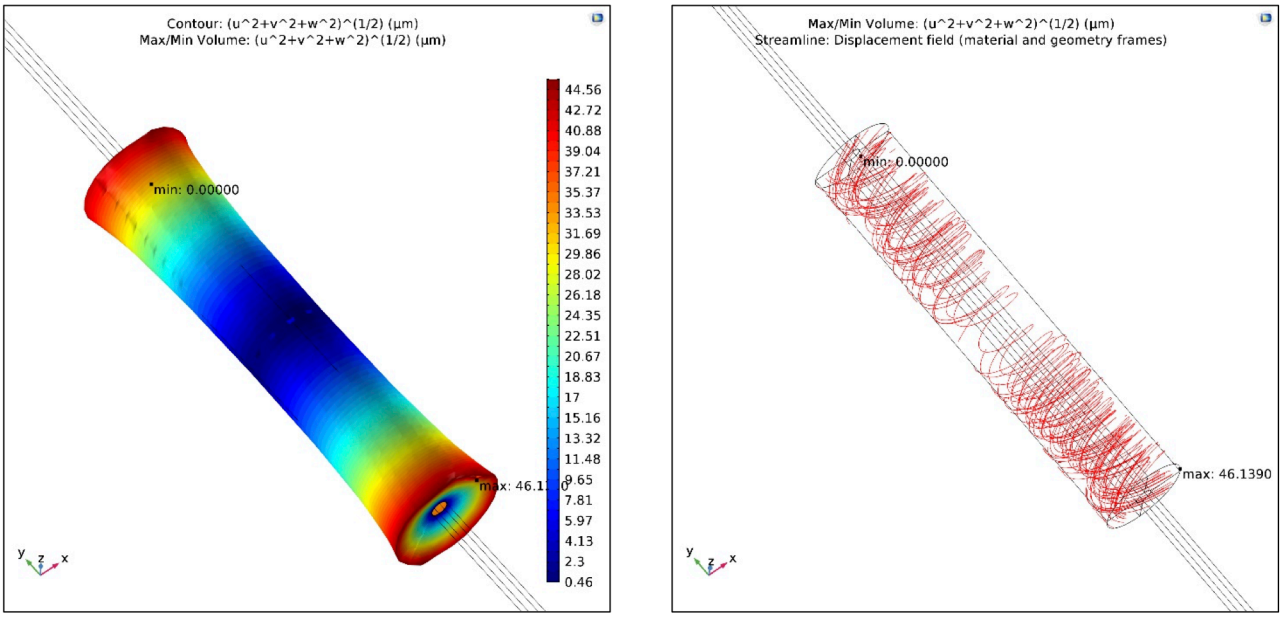

Figure 129: Smart material, views

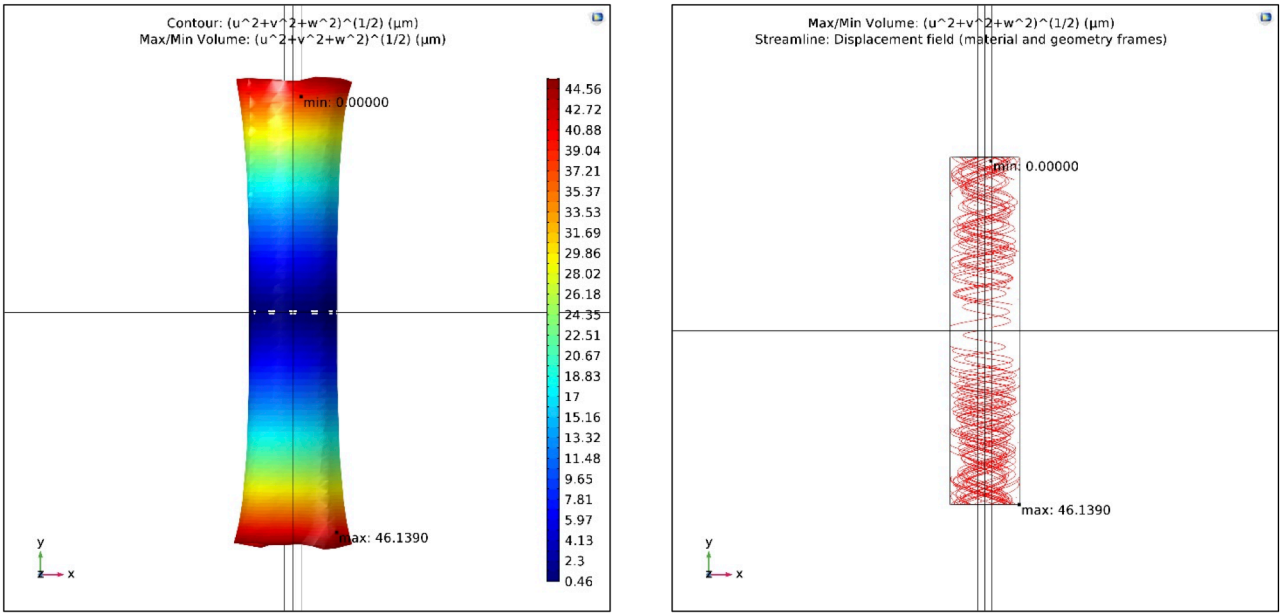

Figure 130: Smart material, views

7.3 Feasibility Studies

This work tries to find a relation between theoretical aspects, explained in previous chapters, and its applications. These last ones are final results of a planning which admits firstly a simulation part and secondly the experimentation. Both of these steps must be in coherence with the theory which proves the concept.
The contribution of the student in this thesis is to demonstrate Wiedmann's effect on a smart magnetostrictive material, considering these three main steps:
- theory;
- simulations;
- experimentation.

Simulation data demonstrate that the aim established is achieved and there is a relation between parameters investigated and smart material properties. Theory confirms that simulation data are verified, considering value of errors caused by mesh and other aspects linked to software and calculator.

Theory and reality are two extremities which consider in the middle a mathematical model. Simulation software uses these models to predict the performance of something, in our case is the smart material. Surely the prediction of performances should be confirmed with the experimentation because it is known that mathematical models introduce input parameters and return output parameters. Moreover, models simplify the reality with their hypothesis and introduce an error on final results, also influenced by other errors caused by the software (calculator) and the instrumentation. Therefore, they could be kept under control by the user, but it is impossible to delate them. This explains how reality results are similar to theory data; this is important to verify the right way of investigation.

In our case, previous studies allow to assert that it is possible to make the experimentation and produce the smart material, prepared with different sizes but with the same initial properties because from a specific chemical aspect it could lost its mechanical properties. Surely if the composition changes a higher relative permeability can be considered, for example 100 H/m.

The sample of smart material produced is shown in the Figure 131. It has same properties listed in chapter 4.1 but these new sizes:

SIZES [mm]	
Length	*50,00*
Inner Radius	*1,00*
Outer Radius	*5,00*

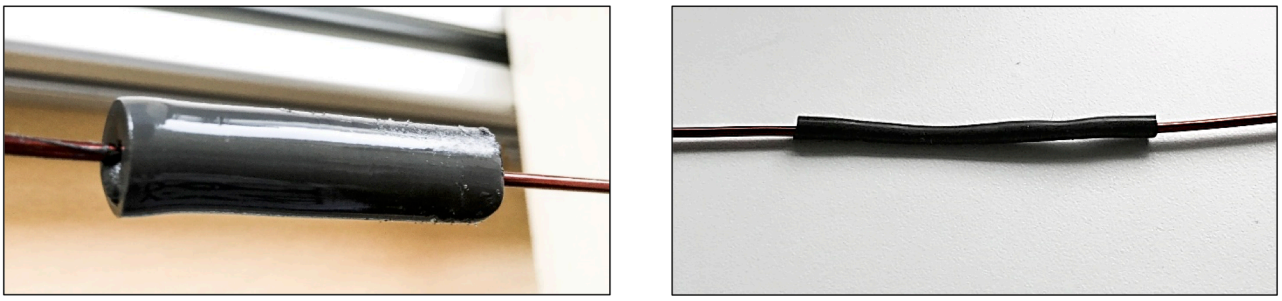

Figure 131: Samples of smart material

8.0 Comsol Multiphysics Simulations

This study includes a simulation part which is carried out with the aid of the software Comsol Multiphysics [10]. The simulation of Helmholtz coils and wire with smart material is reported below. The software follows two important steps:

- preprocessor;
- postprocessor.

In the first one it is set:

- geometry;
- materials;
- physics;
- study.

and in the last one:

results.

In the preprocessor is important to define the physics and in particular forces and mechanics constraints so that the software con simulate the right system solution.

The interpretation of results is permitted in many ways, as it was possible to read in the previous chapters. It is allowed to evaluate:

- graphs;
- plots;
- specific values;
- arrows;
- isolines (contour);
- streamlines;

and so many other options which can be useful to get the right interpretation of the simulation.

In the next chapters is explained in detail how the simulation was built because it could be interesting to understand what is concealed behind the software.

8.1 Preprocessor: Geometry, Materials, Physics, Mesh, Study

The main window of the software is shown in the Figure 132 where on the right side there is the model and on the left side there is the model builder. On the top bar there are three bottoms highlighted:

- add material;
- add physics;
- add study.

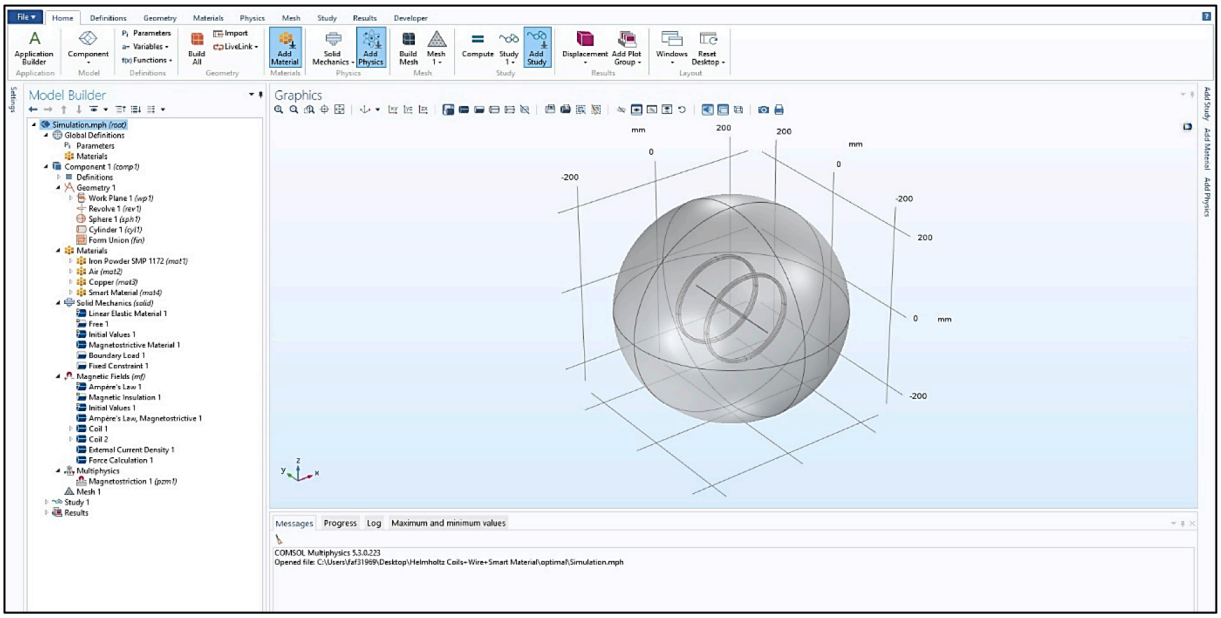

Figure 132: Main window with model builder preprocessor

The first step is to create the geometry and to define some important parameters in global definitions. In our model it is important to set these input values:

- the current inside the wire and its density current;
- sizes of the wire;
- the current inside coils;
- sizes of coils.

The simulation of permanent magnets model is the same of Helmholtz coils with the difference that it is not considered the current inside coils but the magnetization.

When the geometry is solved, the material of every component is added. There is a material library in which it is possible to choose the right material or a blank model if there is a new one, like the smart material.

Material properties are linked to physics that we added and in our case it is fundamental the relative permeability and other magnetic properties of materials.

Every time it is chosen an option, it is possible to select the part of the component that could be:
- domain
- boundary.

In the next step, as it is shown in the Figure 133, is added the physics of the system:
- solid mechanics;
- magnetic fields.

In the solid mechanics is admitted the smart material fixed around the wire, considering surfaces in contact with each other and it is considered the electromagnetic tensor (Maxwell tensor) applied to the sample.

In magnetic fields it is considered:
- Ampere's law for every component;
- the setup of coils;
- the density current of the wire;
- the magnetic insulation;
- the force calculation.

The force calculation, which is set for the smart material, is interesting for the investigation of the twisting. Surely the magnetostriction is the right way to take on.

The last step is the mesh of the model and it is possible to evaluate these points:

- extra-fine mesh;
- fine mesh.

Errors in the simulation are surely due to mesh: if it is extra-fine, errors will be smaller than a mesh coarse. In simulations it is used a fine mesh and tetrahedral shape, which could invalidate results, is avoided.

Obviously, an extra-fine mesh increases computational times with similar results to fine mesh model. This choice permits to obtain approximately 25 minutes to simulation and it is acceptable.

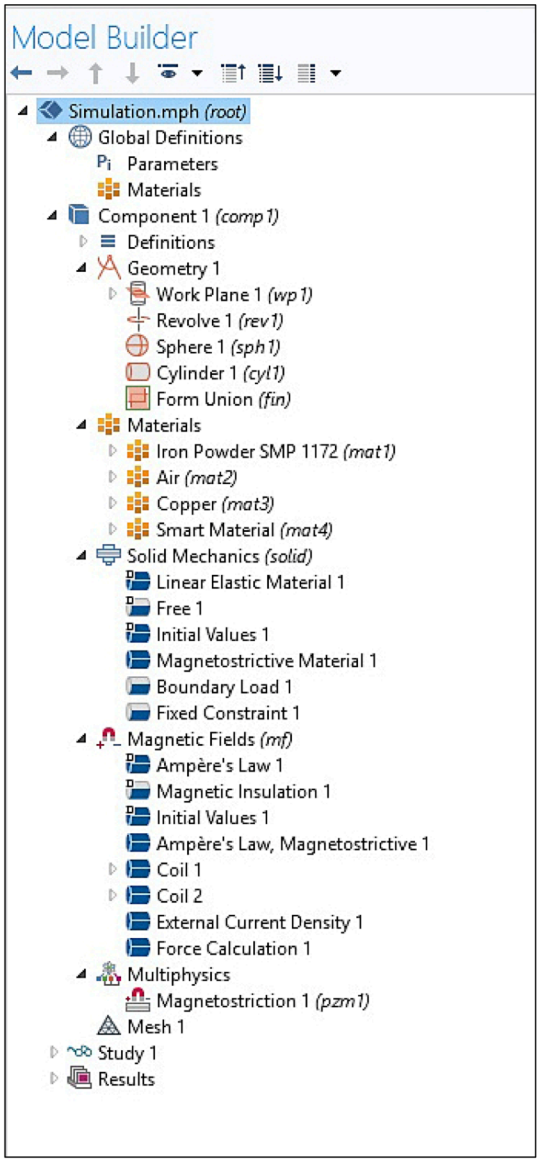

Figure 133: Model builder preprocessor

8.2 Postprocessor: Results

The postprocessor is the part of the software in which it is possible to evaluate results about investigation parameters.

The Figure 134 shows the main window with the model builder postprocessor.

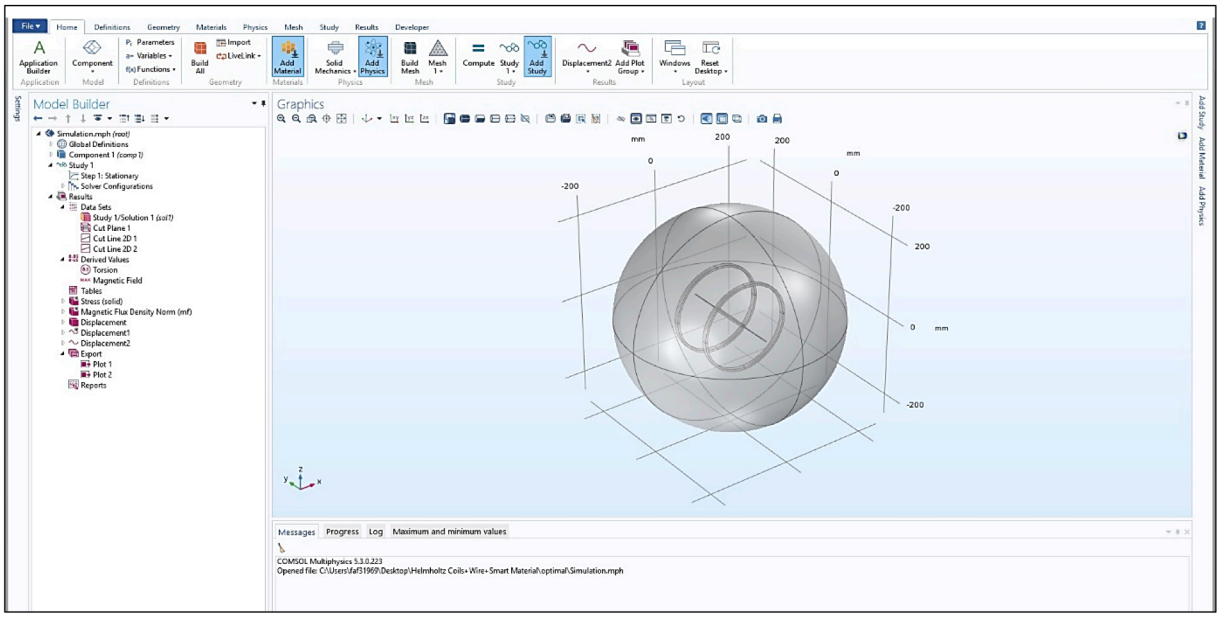

Figure 134: Main window with model builder postprocessor

The aim of our work is to investigate:

- torsion (twisting) with its angle;
- stress (Von Mises' law);
- displacements;
- magnetic field.

The Figure 135 illustrates the analysis of parameters listed before is set and it is also possible to applicate cut planes and lines.

Results obtained are verified with the theory and with the experimentation which is the last step for the study validation.

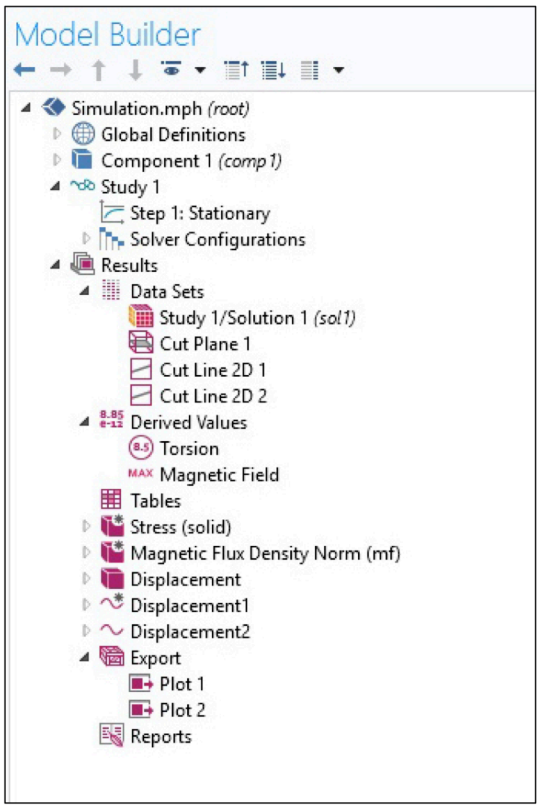

Figure 135: Model builder postprocessor

9.0 Fabrication of the Experimental Setup

The experimental setup is the last step in the study about twisting of the smart material. In the previous chapter the relationship between the smart material properties and its torsion is described. Simulation data confirm that it is possible to see without any instrument the torsion of the smart material if it is prepared with a relative permeability of 100 H/m. This last one is the main parameter which regulate with sizes, in particular the outer radius, the behavior of the material.

It was not possible to produce a smart material with properties and sizes discovered, because from a chemical aspect an excessive increase of CIP defines a material anisotropic, not homogenous, thus little chemical bounded. However, the experiment was made to demonstrate the right way of the investigation and to confirm that it was not possible to obtain a displacement around millimeters with a relative permeability of 10 H/m.

The first step was to design in CAD with the software Autodesk Inventor Professional 2017 two wooden boxes to arrange permanent magnets inside, because they were powerful (Remanence of 1,3 T) (Figure 136) [11]. For safety reasons they were fixed with screws to two aluminum profiles and everything was collocated inside a cube box to isolate the high magnetic field of the system. Between two wooden boxes there was a wire with the smart material which had these sizes:

SIZES	
Length [mm]	*50,00*
Inner Radius [mm]	*1,00*
Outer Radius [mm]	*5,00*

and these properties:

PROPERTIES	
Density ρ [kg/m³]	*6000,00*
Young's modulus E [Pa]	*40000,00*
Poisson's ratio v	*0,45*
Electric conductivity [S/m]	*0,00*
Relative permittivity ε_r	*10,00*
Permeability μ_0 [H/m]	*4π*10^(-7)*
Relative permeability μr [H/m]	*10,00*
Saturation magnetostriction λ_s	*0,10*
Saturation magnetization M_s [A/m]	*0,45*10^(6)*

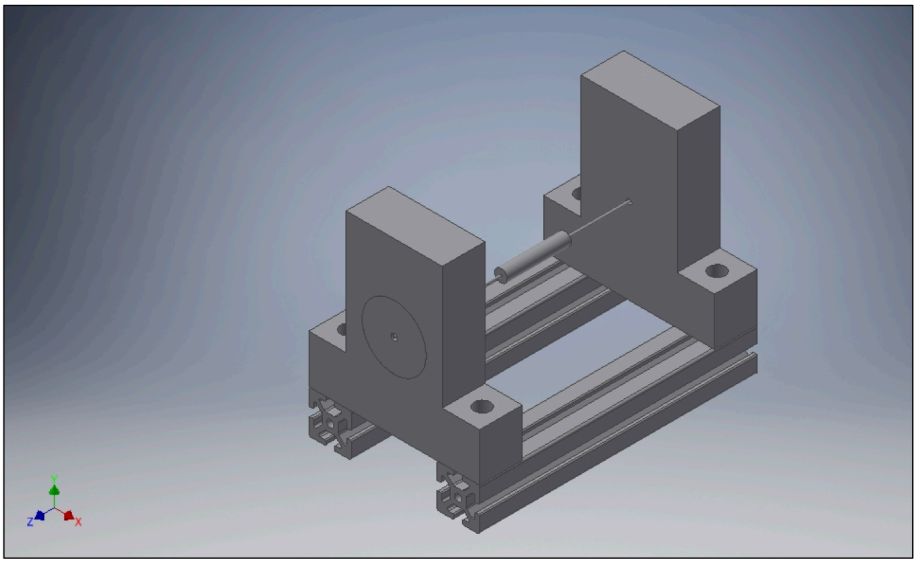

Figure 136: CAD design setup

In figures (Figure 137, Figure 138) below it is shown how the experimental setups looks. It was important the choice of the material because the permanent magnets must interact only with the smart material. [12]

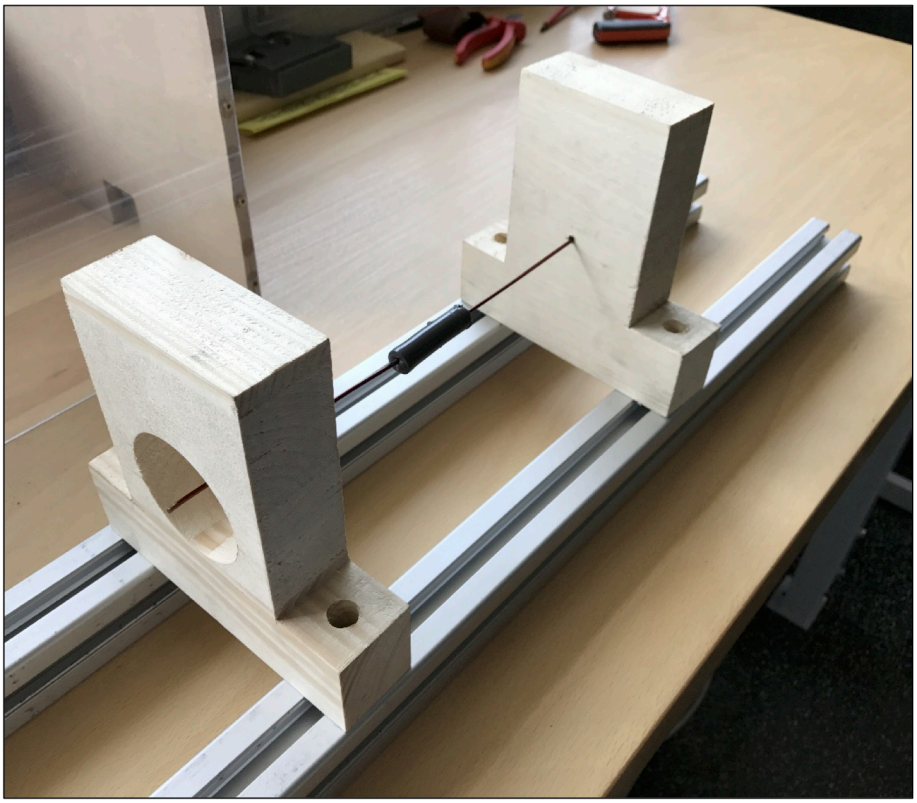

Figure 137: Experimental setup

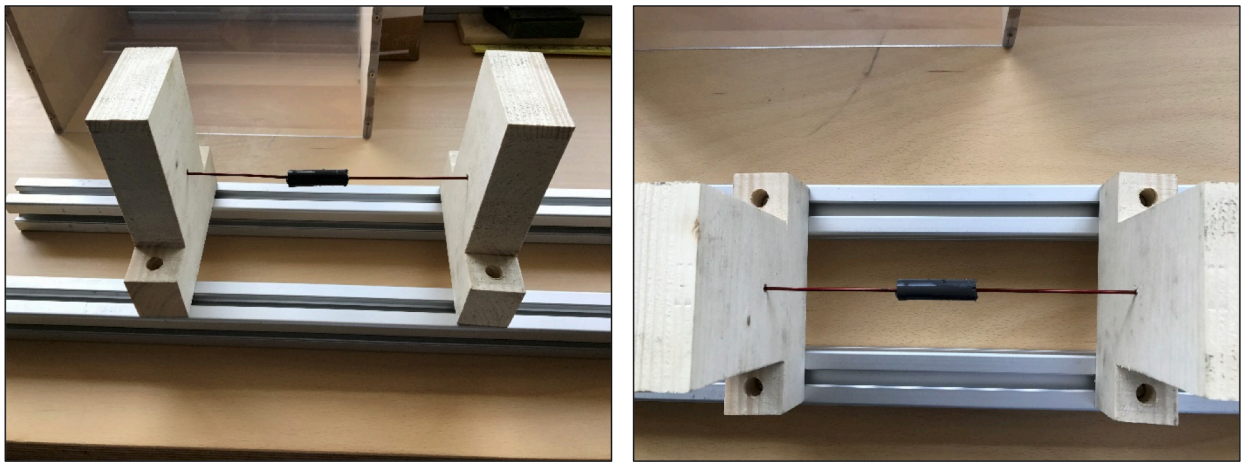

Figure 138: Experimental setup, views

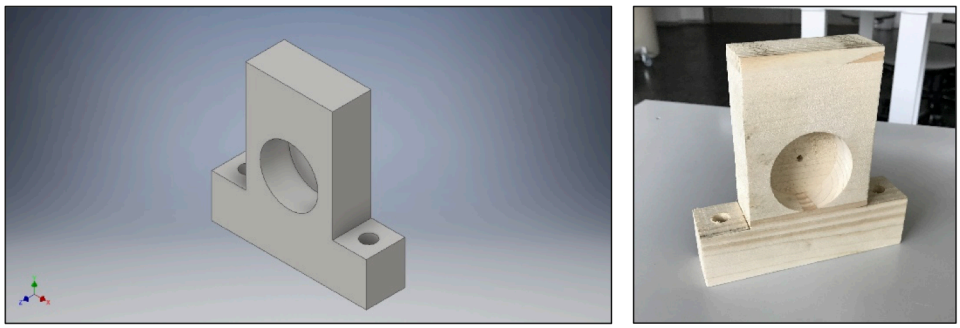

Figure 139: Box

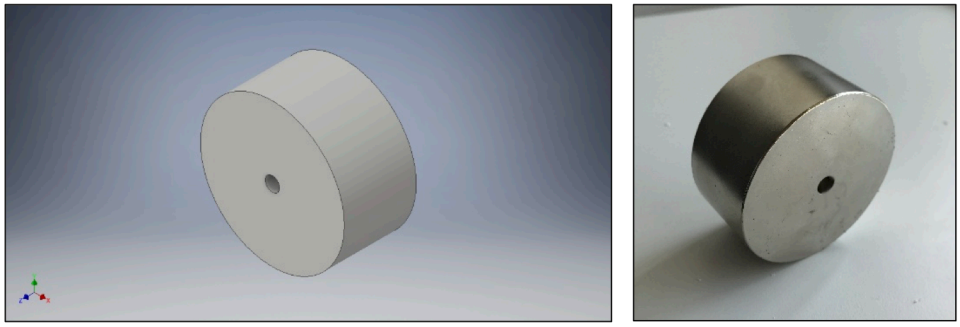

Figure 140: Permanent magnet

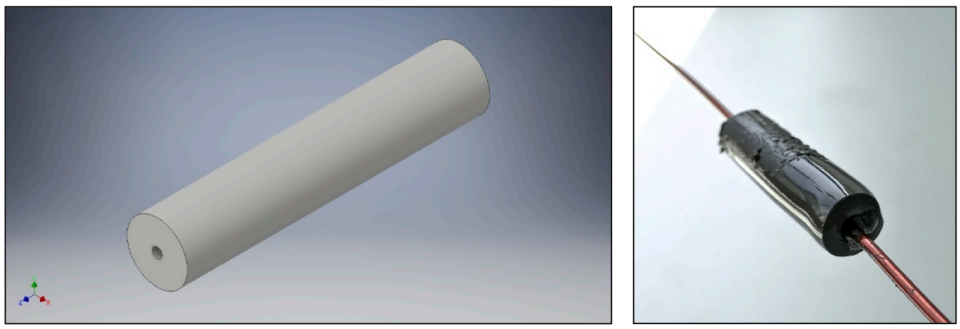

Figure 141: Smart material

Figure 142: Wire

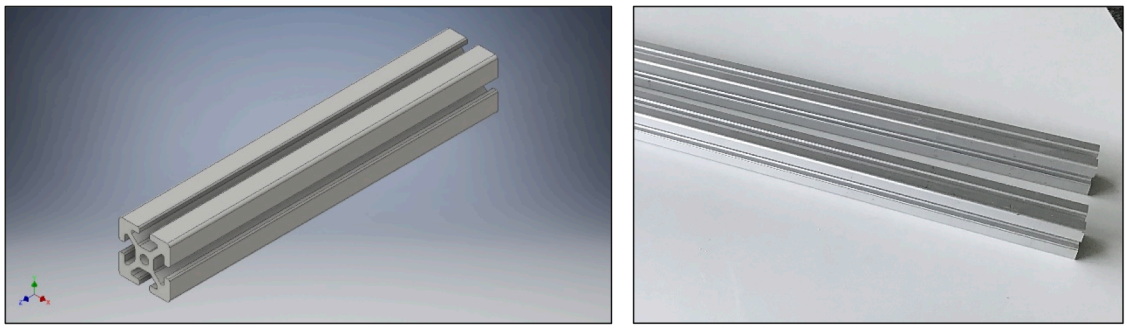

Figure 143: Profile

Materials used in the experimentation:

- Neodymium for permanent magnets;
- Smart material for the sample around the wire with properties and sizes described before;
- Copper for the wire;
- Aluminum for profiles;
- Wooden box to fix the permanent magnets to profiles with steel screws;
- Air around components at the temperature T = 20°C (room temperature).

As illustrated before, it was reasonable to study the interaction between permanent magnets and smart material, and in our case it was possible because profiles and screws had a low impact on the final results of the experiment.

The technical design of the wooden box and the technical information of permanent magnets are added below, if there is the interest to prove a different setup or to verify what this study demonstrated.

The technical design in Figure 144 shows real measures in millimeters but it is not in scale. In Figure 145 and in Figure 146 it is useful to know which is the remanence of permanent magnets and which is the attraction force in relation of the distance between them. In the technical information the remanence is linked to Magnetization N45 and the value is 1,3 T. [13]

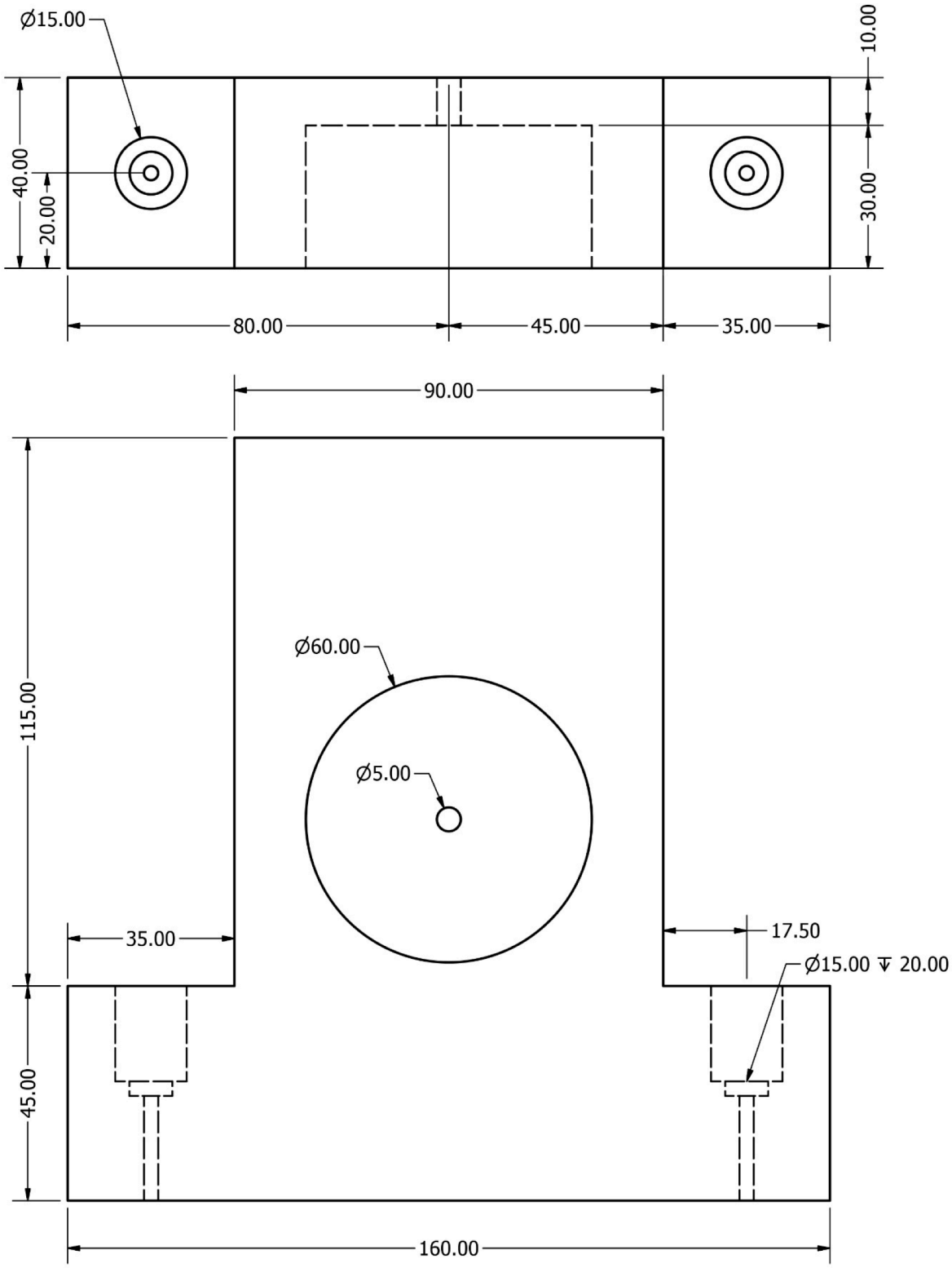

Figure 144: Technical design

Technical information

Article ID	R-60-06-30-N
Material	NdFeB
Shape	Ring
Outer diameter	60 mm
Inner diameter	6 mm
Height	30 mm
Tolerance	+/- 0,1 mm
Direction of magnetisation	axial (parallel to height)
Coating	Nickel-plated (Ni-Cu-Ni)
Manufacturing method	sintered
Magnetisation	N45
strength	approx. 120 kg (approx. 1180 N)
Max. working temperature	80°C
Weight	638,2077 g
Curie temperature	310 °C
Residual magnetism Br	13200-13700 G, 1.32-1.37 T
Coercive field strength bHc	10.8-12.5 kOe, 860-995 kA/m
Coercive field strength iHc	≥12 kOe, ≥955 kA/m
Energy product (BxH)max	43-45 MGOe, 342-358 kJ/m³

Pollutant-free according to RoHS Directive 2011/65/EU.

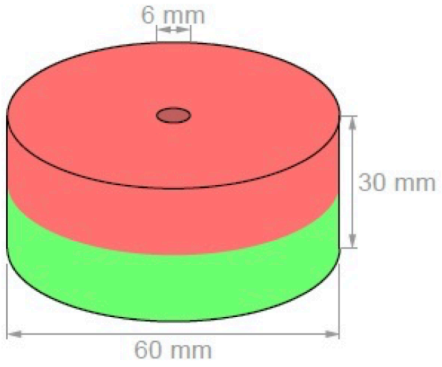

Figure 145: Technical information

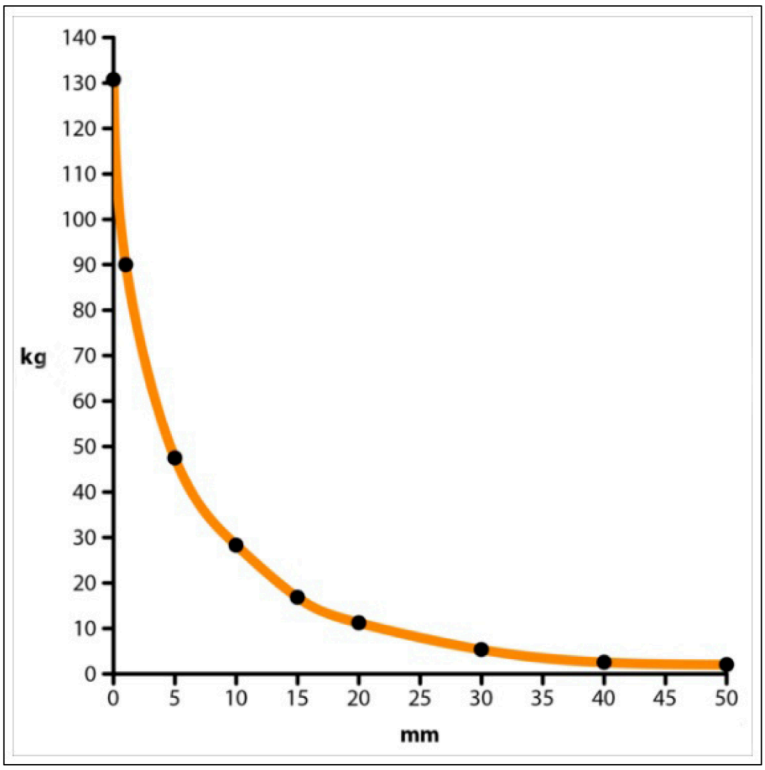

Figure 146: Graph Force-Distance

9.1 Measurements

As expected, the experiment did not report visible results about the smart material, thus it was not possible to measure and compare our investigation results. It was only seen a small elongation of the material due to permanent magnets, because it was clear that they had the magnetic field stronger than the one of the wire and that the smart material had also a low relative permeability. This last one, is the main concept linked to torsion, in fact if the current which flowed in the wire had been high, results would not have changed significant. Instead, if the relative permeability had changed it would have been possible to obtain a visible torsion.

It is possible to study the torsion, which is in micrometers, taking some instrument like microscope or using laser and optical fiber. Surely, it could be the following step of this investigation and it is the next start to confirm what it is at the basis of this general method.

In figures below, it is show the experiment and how is the setup before taking the current. [12]

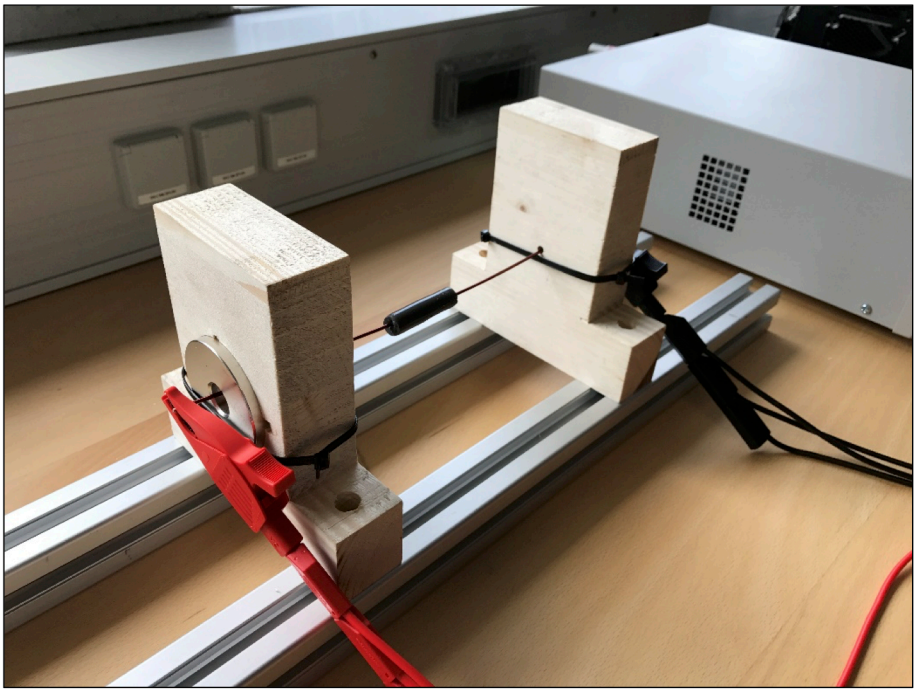

Figure 147: Measurements

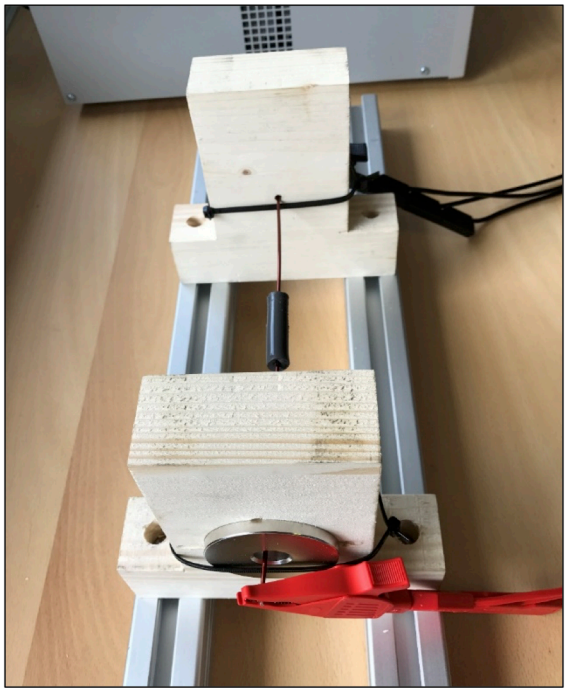

Figure 148: Measurements, view

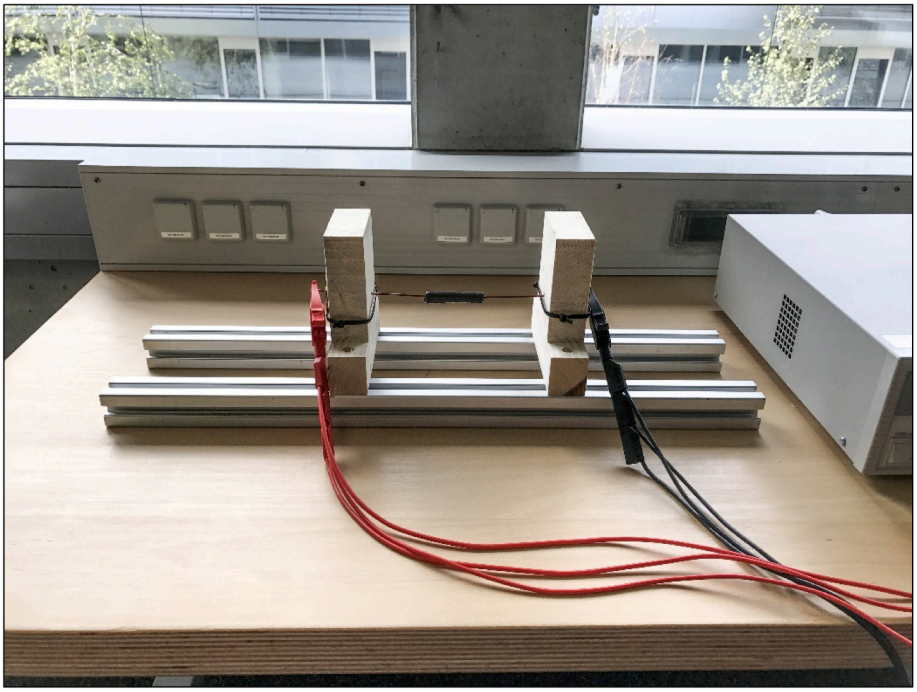

Figure 149: Measurements, view

It was also, as discussed before, used a safety Plexiglas box which could reduce the magnetic flux and protect from the high current (Figure 150). In the next chapter, safety is explained in detail with rules to follow when somebody works with the magnetic fields and currents.

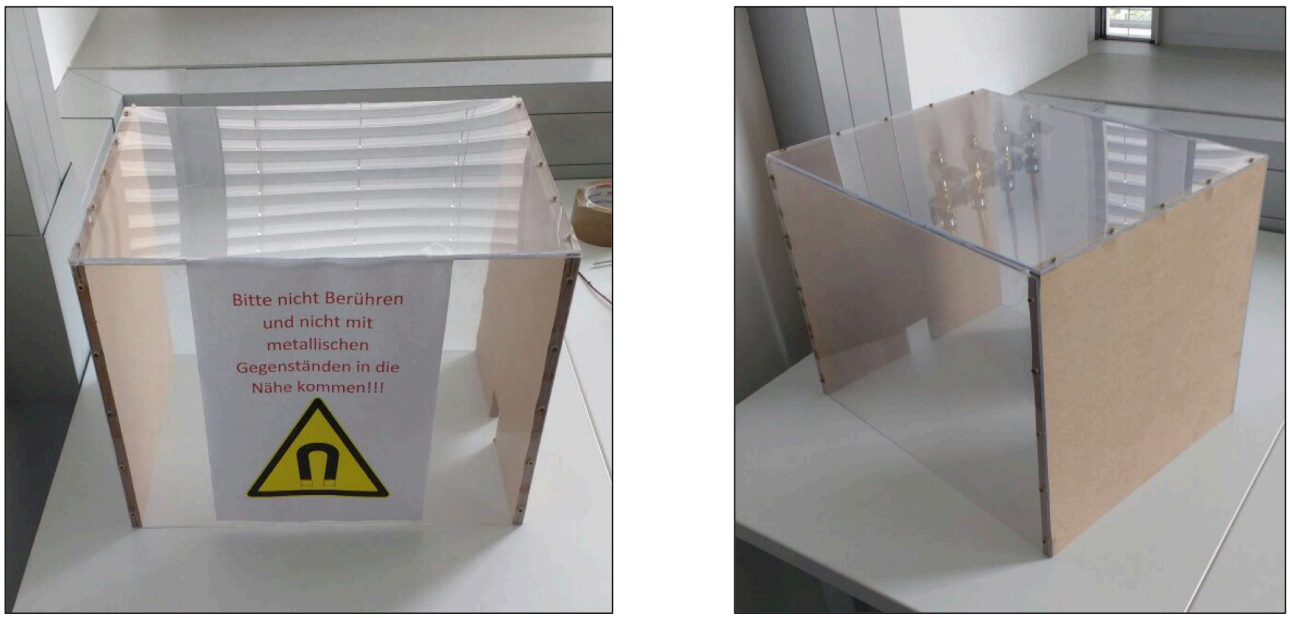

Figure 150: Safety box

9.2 Proof of the Concept: Choice of the Material

The experimentation way is a useful step to predict which are properties and sizes of the smart material.

The choice of the material depends on what application is considered. Wiedmann's effect moves the material with different values of torsion and this could be interesting because there are many application fields. Maybe if it is probable to prepare a smart material with a relative permeability around 100 H/m, it could be a useful material, controllable without instruments (using only sight).

Nowadays the biomedical field is evolving considerably in studies about artificial limbs and the investigation dealt with in this thesis could be applied. Obviously, it is important to understand the

biocompatibility and other information which must be analyzed with more attention because the healthcare is a complex but fundamental field.

Another way to apply our material is robotics field or simply in mechanical field to check or to evaluate some information in complex devices.

In any case, if a visible displacement is expected, the smart material must have these properties:

PROPERTIES	
Density ρ [kg/m³]	*6000,00*
Young's modulus E [Pa]	*40000,00*
Poisson's ratio v	*0,45*
Electric conductivity [S/m]	*0,00*
Relative permittivity ε_r	*10,00*
Permeability μ_0 [H/m]	*4π*10^(-7)*
Relative permeability μr [H/m]	*100,00*
Saturation magnetostriction λ_s	*0,10*
Saturation magnetization M_s [A/m]	*0,45*10^(6)*

10.0 Working Setting: Safety

Safety takes an important role when some studies must be verified as in this thesis. When somebody works with current and magnetic fields it is important to follow some rules, written below. [13] [14].

Fields involved in this safety extract are:
- magnetic;
- electrical;
- chemical;
- mechanical.

The most important field is the first one because an inappropriate use of permanent magnets could be dangerous during the experimentation.

MAGNETIC FIELD

In this case, permanent magnets are used and it is reasonable to follow these tips:

Contusions

Big magnets have a very strong attractive force.

• Unsafe handling could cause jamming of fingers or skin in between magnets. This may lead to contusions and bruises.

• Powerful, very large magnets could cause bone fractures.

Wear heavy protective gloves when handling larger magnets.

Pacemaker

Magnets could affect the functioning of pacemakers and implanted heart defibrillators.

• A pacemaker could switch into test mode and cause illness.

• A heart defibrillator may stop working.

• If you wear these devices keep sufficient distance to magnets.

• Warn others who wear these devices from getting too close to magnets.

Heavy objects

Too heavy loads, symptoms of fatigue as well as material defect could cause a magnet or magnetic hook to loosen from the surface that is was attached to.

Falling objects could lead to serious injuries.

• The indicated adhesive force applies only to ideal conditions. Allow for a high safety cushion.

• Don't use magnets in places where people could sustain injuries in case of material failure.

Metal splinters

Neodymium magnets are brittle. Colliding magnets could crack.

Sharp splinters could be catapulted away for several meters and injure your eyes.

• Avoid the collision of magnets.

• Wear safety glasses when handling larger magnets.

• Make sure that nearby people are also protected or keep their distance.

Magnetic Field

Magnets produce a far-reaching, strong magnetic field. They could damage TVs and laptops, computer hard drives, credit and ATM cards, data storage media, mechanical watches, hearing aids and speakers.

• Keep magnets away from devices and objects that could be damaged by strong magnetic fields.

• Please refer to the table of recommended distances (Figure 146: Graph Force-Distance).

Combustibility

When machining magnets, the drilling dust could easily ignite.

Stay away from machining magnets or use appropriate tools and sufficient cooling water.

Nickel allergy

Many of our magnets contain nickel, also those without nickel coating.

• Some people have an allergic reaction when they come into contact with nickel.

• Nickel allergies could develop from perpetual contact with nickel-plated objects.

• Avoid perpetual skin contact with magnets.

• Avoid contact with magnets if you already have a nickel allergy.

Influence on people

According to the current level of knowledge, magnetic fields of permanent magnets do not have a measurable positive or negative influence on people. It is unlikely that permanent magnets constitute a health risk, but it cannot be ruled out entirely.

• For your own safety, avoid constant contact with magnets.

• Store large magnets at least one meter away from your body.

Splintering of coating

Most of our neodymium magnets have a thin nickel-copper-nickel coating to protect them from erosion. This coating could splinter or crack due to collision or large pressure. This makes them vulnerable to environmental influences like moisture and they could oxidize.

• Separate big magnets, especially spheres, with a piece of cardboard.

• Avoid collisions of magnets as well as repeated mechanical exposure (e.g. blows, bashes).

Oxidation, corrosion, rust

Untreated neodymium magnets oxidize quickly and disintegrate.

Most of our magnets have a nickel-copper-nickel coating to protect them from corrosion. This coating provides some protection against corrosion, but it is not robust enough for continuous outdoor use.

• Use magnets only in the dry indoors or protect them against environmental influences.

• Avoid damages to the coating.

Temperature resistance

Neodymium magnets have a maximum working temperature of 80 to 200 °C.

Most neodymium magnets lose part of their adhesive force permanently at a temperature of 80 °C.

• Don't use magnets in places where they are exposed to extreme heat.

• If you use an adhesive, don't harden it with hot air.

Mechanical treatment

Neodymium magnets are brittle, heat-sensitive and oxidize easily.

• When drilling or sawing a magnet with improper tools, the magnet may break.

• The emerging heat may demagnetize the magnet.

• The magnet will oxidize and disintegrate due to the damaged coating.

Stay away from mechanical treatment of magnets if you do not possess the necessary equipment and experience.

Airfreight

Magnetic fields of improperly packaged magnets could influence airplane navigation devices.

In the worst case it could lead to an accident.

• Airfreight magnets only in packaging with sufficient magnetic shielding.

Postage

Magnetic fields of improperly packaged magnets could cause disturbances in sorting machines and damage fragile goods in other packages.

• Use a large box and place the magnet in the middle surrounded by lots of padding material.

• Arrange magnets in a package in a way that the magnetic fields neutralize each other.

• If necessary, use sheet iron to shield the magnetic field.

ELECTRICAL FIELD

When working in the area of the protective low voltage (up to 50 volts AC and 120 volts DC), the test assemblies are only allowed to be changed, removed or replaced if the voltage source is switched off and other hazards are also excluded. Work must always be carried out at least if two people with visual contact are in the room. In case of danger, the circuit must be immediately disconnected from the power supply by switching it off.

CHEMICAL FIELD

The use of the chemical area is permitted with the use of necessity protective measures (protective goggles, respiratory protective masks, protective gloves and protective shoes) and particular safety instructions which must be followed by qualified personnel.

MECHANICAL FIELD

The use of mechanical area is permitted with the use of the safety equipment (protective goggles, respiratory protective masks, protective gloves and protective shoes) and it is permitted to take part only by people who provide proof of training in mechanical engineering.

CONCLUSION

This study could be an important step in order to evolve it in application fields. It was explained the evolution from the theoretical approach to simulation which was verified with the experimentation. These three important points demonstrate that it is possible to use a smart magnetostrictive material which twists thanks to Wiedmann's effect. Surely, this investigation started from the known theory, therefore magnetism laws, and the effect linked to magnetic properties of materials. This last aspect permitted to investigate how a magneto-mechanical actuation system works and which is the behavior of a smart material prepared. Therefore, was possible to achieve a relation between the physics and its applications through engineering. Surely, smart materials are increasingly used because every device must work with specific conditions, in fact a material which performs as we want, with properties established, is the result that nowadays everything is optimized in order to obtain the maximum performance.

In this study it was possible to follow these points:
- simulation of smart material performances with different setup;
- preparation of smart material sample;
- fabrication of the experimental setup;
- validation of simulation data and choice of the smart material.

Simulations were handled in various chapters because it is reasonable that before the fabrication we must be certain about results which we expect.

It is clear that simulation software, if used correctly, reducing time and costs, shows how our investigation is real. Obviously, the experimentation is the final step useful to proof the concept explained. In the same way this investigation can show and prove how the behavior of the smart material with magnetic properties is when there are magnetic fields. The aim proposed is reached and it was possible to explain how magnetic properties influence the mechanical behavior of the smart material. Therefore, the magneto-mechanical phenomenon was described and this study could be the start of new way of applications.

APPENDIX

Table 1

r [mm]	B [μT] simulation	B [μT] theory	Error [%]
0,00	0,00	0,00	0,00%
0,06	12,54	12,56	0,12%
0,17	34,39	34,46	0,19%
0,21	42,85	42,85	0,01%
0,24	46,78	47,44	1,38%
0,26	51,71	52,31	1,15%
0,28	54,98	55,55	1,01%
0,30	58,72	59,23	0,88%
0,32	63,60	64,42	1,27%
0,48	95,94	96,68	0,76%
0,55	107,56	109,02	1,34%
0,56	110,86	112,46	1,42%
0,67	132,54	134,41	1,39%
0,75	147,62	149,08	0,98%
1,00	196,60	200,00	1,70%
1,31	149,65	152,31	1,75%
1,39	140,99	143,75	1,92%
1,51	127,78	132,41	3,49%
1,55	123,02	128,73	4,44%
1,63	116,34	122,98	5,40%
1,80	106,15	111,34	4,66%
1,86	103,52	107,60	3,79%
2,00	92,93	99,84	6,92%
2,02	92,35	98,99	6,71%
2,04	91,62	97,95	6,46%
2,44	78,15	82,00	4,70%
2,61	72,22	76,52	5,62%
2,81	67,59	71,26	5,15%
2,87	65,70	69,60	5,60%
2,99	63,53	66,98	5,14%
3,11	59,72	64,33	7,18%
3,15	58,92	63,43	7,11%
3,27	56,76	61,11	7,12%
3,32	55,83	60,16	7,20%
3,47	53,18	57,61	7,69%
3,54	51,70	56,44	8,39%
3,66	49,79	54,61	8,83%
3,67	49,44	54,51	9,30%

4,01	*45,26*	*49,82*	*9,15%*
4,28	*42,00*	*46,68*	*10,02%*
4,46	*39,91*	*44,87*	*11,05%*
4,48	*40,03*	*44,61*	*10,27%*
4,52	*39,31*	*44,28*	*11,23%*
4,56	*38,95*	*43,83*	*11,11%*
4,62	*38,56*	*43,33*	*11,01%*
4,67	*38,16*	*42,84*	*10,93%*
4,72	*37,78*	*42,38*	*10,87%*
5,07	*35,15*	*39,48*	*10,97%*
5,21	*33,08*	*38,37*	*13,79%*
5,24	*32,93*	*38,16*	*13,69%*
5,26	*32,84*	*38,01*	*13,62%*
5,59	*31,18*	*35,75*	*12,77%*
5,86	*29,87*	*34,13*	*12,48%*
6,03	*29,02*	*33,16*	*12,49%*
6,15	*28,43*	*32,52*	*12,57%*
6,33	*27,68*	*31,59*	*12,40%*
6,41	*26,98*	*31,22*	*13,58%*
6,52	*26,42*	*30,66*	*13,81%*
6,93	*24,41*	*28,85*	*15,38%*
7,41	*22,78*	*26,99*	*15,60%*
7,73	*21,85*	*25,86*	*15,52%*
8,60	*19,47*	*23,26*	*16,30%*
8,75	*19,09*	*22,85*	*16,46%*
8,88	*18,77*	*22,52*	*16,63%*
9,07	*18,32*	*22,06*	*16,96%*
9,18	*18,05*	*21,80*	*17,19%*
9,27	*17,65*	*21,58*	*18,20%*
9,47	*17,38*	*21,12*	*17,73%*
9,56	*17,25*	*20,92*	*17,53%*
9,87	*16,83*	*20,27*	*16,96%*
9,88	*16,82*	*20,25*	*16,93%*
10,00	*16,34*	*20,00*	*18,31%*

Table 2

r [mm]	B [μT] theory	B [μT] simulation	Error [%]
-50,01	81,62	73,44	10,02%
-49,02	81,95	73,77	9,98%
-45,67	83,06	74,88	9,85%
-45,02	83,28	75,10	9,82%
-44,87	83,03	74,85	9,85%
-44,77	83,14	74,96	9,84%
-44,59	83,18	75,00	9,83%
-44,16	83,28	75,10	9,82%
-43,89	83,35	75,17	9,81%
-43,53	83,43	75,25	9,80%
-40,72	84,09	75,91	9,73%
-40,59	84,12	75,94	9,72%
-40,39	84,14	75,96	9,72%
-37,84	84,56	76,38	9,67%
-37,65	84,60	76,42	9,67%
-36,76	84,75	76,57	9,65%
-35,82	84,90	76,72	9,63%
-34,04	85,20	77,02	9,60%
-33,18	85,29	77,11	9,59%
-33,04	85,32	77,14	9,59%
-32,41	85,42	77,24	9,58%
-32,27	85,45	77,27	9,57%
-31,97	85,50	77,32	9,57%
-29,28	85,76	77,58	9,54%
-29,15	85,77	77,59	9,54%
-28,58	85,86	77,68	9,53%
-28,05	85,90	77,72	9,52%
-27,44	85,95	77,77	9,52%
-26,39	86,06	77,88	9,50%
-24,81	86,24	78,06	9,49%
-24,59	86,25	78,07	9,48%
-24,29	86,27	78,09	9,48%
-24,23	86,27	78,09	9,48%
-21,86	86,38	78,20	9,47%
-19,91	86,47	78,29	9,46%
-19,80	86,47	78,29	9,46%
-18,15	86,55	78,37	9,45%
-17,31	86,59	78,41	9,45%
-17,01	86,58	78,40	9,45%
-15,82	86,61	78,43	9,44%

-15,38	86,62	78,44	9,44%
-15,01	86,63	78,45	9,44%
-14,92	86,63	78,45	9,44%
-10,66	86,69	78,51	9,44%
-10,25	86,69	78,51	9,44%
-9,87	86,70	78,52	9,44%
-9,76	86,70	78,52	9,44%
-7,78	86,72	78,54	9,43%
-7,68	86,72	78,54	9,43%
-5,13	86,76	78,58	9,43%
0,00	86,82	78,64	9,42%
0,00	86,78	78,60	9,43%
0,00	86,76	78,58	9,43%
0,00	86,76	78,58	9,43%
0,00	86,77	78,59	9,43%
0,00	86,78	78,60	9,43%
3,66	86,75	78,57	9,43%
4,10	86,75	78,57	9,43%
4,51	86,75	78,57	9,43%
5,19	86,74	78,56	9,43%
5,38	86,74	78,56	9,43%
7,32	86,73	78,55	9,43%
8,19	86,72	78,54	9,43%
9,03	86,72	78,54	9,43%
10,39	86,71	78,53	9,43%
10,98	86,70	78,52	9,43%
11,70	86,70	78,52	9,44%
12,03	86,69	78,51	9,44%
13,09	86,68	78,50	9,44%
13,29	86,67	78,49	9,44%
13,78	86,67	78,49	9,44%
14,44	86,66	78,48	9,44%
15,31	86,62	78,44	9,44%
16,57	86,59	78,41	9,45%
17,16	86,57	78,39	9,45%
17,59	86,56	78,38	9,45%
20,41	86,45	78,27	9,46%
20,49	86,45	78,27	9,46%
20,59	86,45	78,27	9,46%
20,94	86,42	78,24	9,47%
21,20	86,40	78,22	9,47%
22,00	86,36	78,18	9,47%

22,67	*86,39*	*78,21*	*9,47%*
24,69	*86,22*	*78,04*	*9,49%*
25,48	*86,15*	*77,97*	*9,50%*
25,74	*86,13*	*77,95*	*9,50%*
28,92	*85,86*	*77,68*	*9,53%*
28,94	*85,85*	*77,67*	*9,53%*
31,08	*85,67*	*77,49*	*9,55%*
31,22	*85,66*	*77,48*	*9,55%*
32,14	*85,53*	*77,35*	*9,56%*
33,21	*85,37*	*77,19*	*9,58%*
34,48	*85,15*	*76,97*	*9,61%*
35,42	*85,03*	*76,85*	*9,62%*
35,75	*84,97*	*76,79*	*9,63%*
36,29	*84,88*	*76,70*	*9,64%*
37,01	*84,74*	*76,56*	*9,65%*
37,35	*84,81*	*76,63*	*9,65%*
39,59	*84,29*	*76,11*	*9,71%*
40,16	*84,15*	*75,97*	*9,72%*
41,64	*83,81*	*75,63*	*9,76%*
42,13	*83,69*	*75,51*	*9,77%*
42,39	*83,63*	*75,45*	*9,78%*
42,52	*83,60*	*75,42*	*9,78%*
45,22	*82,97*	*74,79*	*9,86%*
47,00	*82,54*	*74,36*	*9,91%*
47,19	*82,49*	*74,31*	*9,92%*
47,83	*82,29*	*74,11*	*9,94%*
48,36	*82,13*	*73,95*	*9,96%*
50,27	*81,52*	*73,34*	*10,03%*

Table 3

r [mm]	B [μT] theory	B [μT] simulation	Error [%]
-50,44	650000,00	657460,00	1,15%
-49,41	650000,00	657020,00	1,08%
-48,23	650000,00	657330,00	1,13%
-47,21	650000,00	658040,00	1,24%
-47,04	650000,00	658230,00	1,27%
-47,00	650000,00	658270,00	1,27%
-46,90	650000,00	658360,00	1,29%
-46,02	650000,00	659390,00	1,44%
-44,50	650000,00	660920,00	1,68%
-44,46	650000,00	660970,00	1,69%
-44,38	650000,00	660990,00	1,69%
-44,32	650000,00	661110,00	1,71%
-44,28	650000,00	661130,00	1,71%
-43,35	650000,00	661210,00	1,72%
-42,47	650000,00	659950,00	1,53%
-40,92	650000,00	650550,00	0,08%
-39,37	650000,00	623820,00	4,03%
-38,44	605565,82	590410,00	2,50%
-37,84	568741,80	557590,00	1,96%
-37,84	571893,08	557580,00	2,50%
-37,84	581126,88	555040,00	4,49%
-37,84	558419,40	553000,00	0,97%
-37,84	553194,58	552930,00	0,05%
-36,30	432231,77	416850,00	3,56%
-36,30	397262,16	396350,00	0,23%
-36,30	392492,98	383410,00	2,31%
-36,30	393195,87	383400,00	2,49%
-36,30	390358,85	389040,00	0,34%
-36,30	391751,61	389040,00	0,69%
-36,30	391249,97	391240,00	0,00%
-36,29	401234,49	401090,00	0,04%
-36,21	395515,46	385540,00	2,52%
-34,76	112546,74	109590,00	2,63%
-34,75	107924,64	107530,00	0,37%
-34,74	109596,78	108000,00	1,46%
-34,64	89198,55	88870,00	0,37%
-33,82	50471,61	48672,00	3,57%
-33,56	96438,21	93000,00	3,57%
-33,47	108794,74	105220,00	3,29%
-33,38	120740,92	120260,00	0,40%

-33,27	139504,06	134430,00	3,64%
-33,18	144576,99	142470,00	1,46%
-33,03	166758,86	165850,00	0,55%
-32,06	224865,15	243550,00	8,31%
-31,67	247051,92	265520,00	7,48%
-31,49	255493,58	272960,00	6,84%
-30,71	282465,33	296930,00	5,12%
-30,29	291551,88	308830,00	5,93%
-30,03	295960,15	312620,00	5,63%
-29,46	302582,97	320650,00	5,97%
-29,27	303995,21	321790,00	5,85%
-28,80	306261,26	323950,00	5,78%
-28,34	306980,18	324690,00	5,77%
-27,87	306541,52	325620,00	6,22%
-27,35	304925,97	324020,00	6,26%
-27,14	304011,11	323190,00	6,31%
-25,78	295293,65	315930,00	6,99%
-25,77	295262,64	315560,00	6,87%
-25,76	295161,69	315470,00	6,88%
-25,68	294542,61	315440,00	7,09%
-24,95	288402,04	310340,00	7,61%
-24,84	287469,76	309420,00	7,64%
-24,73	286481,34	309180,00	7,92%
-22,74	267096,94	292680,00	9,58%
-21,56	255001,61	282490,00	10,78%
-21,51	254526,72	282090,00	10,83%
-21,18	251097,89	279230,00	11,20%
-17,98	218625,44	252620,00	15,55%
-16,96	208808,25	245220,00	17,44%
-15,19	192508,93	233300,00	21,19%
-14,84	189349,65	231480,00	22,25%
-13,73	179765,97	224590,00	24,93%
-11,58	162524,17	210690,00	29,64%
-10,50	154438,94	205560,00	33,10%
-10,07	151360,00	204050,00	34,81%
-9,87	149936,54	203290,00	35,58%
-8,63	141440,00	197890,00	39,91%
-7,65	135023,65	195350,00	44,68%
-4,91	282272,28	186220,00	34,03%
-3,79	271336,56	183140,00	32,50%
-0,80	292314,38	180910,00	38,11%
1,22	249455,07	183210,00	26,56%

2,24	285428,66	183960,00	35,55%
5,85	336754,25	189020,00	43,87%
7,33	133022,08	193500,00	45,46%
8,03	137470,06	195310,00	42,07%
8,40	139919,51	194890,00	39,29%
11,53	162103,29	210650,00	29,95%
13,09	174456,41	218530,00	25,26%
14,91	189967,40	230190,00	21,17%
18,12	220000,91	254550,00	15,70%
19,31	231896,18	263280,00	13,53%
19,72	236090,77	267370,00	13,25%
19,90	237927,94	268760,00	12,96%
20,28	241862,65	271580,00	12,29%
20,49	244032,12	273340,00	12,01%
20,64	245576,93	274580,00	11,81%
20,78	246979,04	275830,00	11,68%
20,92	248423,55	277070,00	11,53%
21,59	255352,55	282770,00	10,74%
22,78	267492,68	292670,00	9,41%
23,08	270602,36	295230,00	9,10%
24,58	285041,88	307620,00	7,92%
25,04	289218,12	311140,00	7,58%
25,52	293292,78	314270,00	7,15%
26,65	301349,71	320140,00	6,24%
27,29	304677,71	323460,00	6,16%
27,41	305165,98	324080,00	6,20%
27,68	306068,45	325000,00	6,19%
28,89	305938,51	324830,00	6,17%
29,21	304381,86	322850,00	6,07%
29,35	303400,63	322220,00	6,20%
30,84	278702,82	300350,00	7,77%
30,96	275351,70	291950,00	6,03%
31,21	266767,82	286330,00	7,33%
31,35	261353,62	278250,00	6,46%
31,40	259501,74	277390,00	6,89%
31,56	252356,18	270250,00	7,09%
31,60	250327,86	267480,00	6,85%
31,65	247847,24	269230,00	8,63%
32,26	211032,55	219420,00	3,97%
33,22	118967,77	137110,00	15,25%
33,32	106623,65	128560,00	20,57%
33,50	81425,59	105080,00	29,05%

33,61	66765,15	86939,00	30,22%
33,70	52683,65	70039,00	32,94%
34,03	20127,95	20097,00	0,15%
34,19	6390,90	6381,60	0,15%
34,62	85790,08	85474,00	0,37%
35,08	175420,96	175150,00	0,15%
35,11	183913,29	181240,00	1,45%
35,15	189938,85	189330,00	0,32%
35,26	209483,57	209160,00	0,15%
35,27	211985,47	211980,00	0,00%
36,12	368752,46	363000,00	1,56%
36,62	494108,72	450700,00	8,79%
36,64	430632,77	430540,00	0,02%
36,67	435165,30	435000,00	0,04%
36,70	452660,42	443850,00	1,95%
36,73	491435,64	446910,00	9,06%
36,75	461655,47	452520,00	1,98%
36,78	506498,87	465190,00	8,16%
37,04	502196,14	484290,00	3,57%
37,15	511823,71	493590,00	3,56%
38,09	588854,66	575250,00	2,31%
38,23	584402,54	580580,00	0,65%
38,27	581686,93	580830,00	0,15%
38,29	622832,06	583750,00	6,27%
39,66	650000,00	631340,00	2,87%
39,66	650000,00	631340,00	2,87%
39,66	650000,00	631340,00	2,87%
39,66	650000,00	631740,00	2,81%
39,66	650000,00	631740,00	2,81%
39,66	650000,00	636500,00	2,08%
41,14	650000,00	652720,00	0,42%
42,35	650000,00	659670,00	1,49%
43,36	650000,00	661030,00	1,70%
44,23	650000,00	661160,00	1,72%
45,57	650000,00	659900,00	1,52%
47,01	650000,00	658290,00	1,28%
48,45	650000,00	657230,00	1,11%
49,89	650000,00	657170,00	1,10%

BIBLIOGRAPHY

[1] Fundamentals of Physics - Halliday, Resnick

[2] https://www.comsol.it/model/magnetic-field-of-a-helmholtz-coil-15

[3] https://en.wikipedia.org/wiki/Helmholtz_coil

[4] https://www.supermagnete.it/eng/faq/How-do-you-calculate-the-magnetic-flux-density

[5] Massachusetts Institute of Technology, Department of Physics, Lecture 23: Magnetic materials - Scott Hughes

[6] https://en.wikipedia.org/wiki/Magnetostriction

[7] http://www.sensorland.com/HowPage024.html

[8] Magnetostriction, Document Part Number 550947 Revision A - Temposonic MTS Sensors

[9] Chemical Extract, Laboratory Sensor System in OTH Regensburg University (Germany)

[10] Data and Figures for the simulations are taken by the software:
Comsol Multiphysics version 5.3 License Number: 6078741, licensed to Laboratory Sensor System in OTH Regensburg University (Germany)

[11] Figures CAD are taken by the software:
Autodesk Inventor Professional 2017 Education License for Student, Politecnico di Torino (Italy)

[12] Figures for the experimentation are taken by the student Fabio Facente in the Laboratory Sensor System in OTH Regensburg University (Germany)

[13] https://www.supermagnete.it/eng/ring-magnets-neodymium/ring-magnet-60mm-x-6mm-x-30mm-neodymium-n45-nickel-plated_R-60-06-30-N

[14] Laboratory Regulation, Laboratory Sensor System in OTH Regensburg University (Germany)

FIGURES

To Professor Chamonine and To all team of the Laboratory…

To Professor Tonoli…

Thanks for supporting me !!!

Danke

To me that I never give up…

To my parents Arturo and Giuseppina, my strength and important guide of my life… my past, my present and my future!!!

To my sister Flavia, my hope and my friend of challenge…

To my girlfriend Adriana, light of my eyes and my happiness…

To all people who believe in me…

Thanks to exist !!!

Proud to be a future mechanical engineer